Investigating the role of caspase cleavage of ROCK1 in tissue homeostasis and tumour development

Linda Julian

Submitted in fulfilment of the requirements for the degree of Doctor of Philosophy

October 2015

The Beatson Institute for Cancer Research

University of Glasgow

Abstract

During apoptosis, caspase cleavage of ROCK1 removes an auto-inhibitory region yielding a constitutively active kinase fragment. This results in phosphorylation of downstream targets that promote contractile force generation leading to cell shrinkage, membrane blebbing and nuclear disintegration. To address fundamental questions regarding the purpose of ROCK1 cleavage and consequent apoptotic morphological features, a novel mouse model was generated that carries a single amino acid substitution in the caspase cleavage site (D1113A) that converts ROCK1 to a caspase-resistant non-cleavable (ROCK1nc) form. When apoptosis was induced in ROCK1nc cells, morphological features were significantly impaired, although the biochemical apoptotic program itself was unaffected.

To understand the biological role of apoptotic morphological features in the maintenance of tissue homeostasis, acute liver damage was induced in mice with the liver-selective genotoxic compound diethylnitrosamine (DEN). Following DEN treatment, there were increased TUNEL-positive apoptotic cells and increased neutrophil infiltration in ROCK1nc mice. Histologically, ROCK1nc livers were more damaged, paralleled by higher serum alanine transaminase levels. We hypothesized that uncleared apoptotic debris undergoing secondary necrosis may release damage associated molecular patterns (DAMPs) that may aggravate liver damage by recruiting neutrophils to the liver. Indeed, inhibiting the cytokine activities of HMGB1 reduced neutrophil infiltration as well as liver damage in ROCK1nc mice. Furthermore, to determine whether defects in tissue damage responses in ROCK1nc mice would affect tumour development, the ROCK1nc mutation was introduced into two different cancer models, specifically the DEN-induced hepatocellular carcinoma and Eμ-myc lymphoma mouse models. Defective caspase cleavage of ROCK1 promoted increased infiltration of CD8+ T-cells in ROCK1nc liver tumours and had a protective effect against tumour development in both tumour models. Taken together, our results indicate that apoptotic morphological features suppress inflammation which helps to maintain tissue homeostasis but enables tumourigenesis.

Table of Contents

List of Tables

List of Figures

Dedication

I dedicate this thesis to my late grandparents, Mr. P. Stencilas and Mrs. Susanna Stencilas.

In mind, a constant thought
In heart, a silent tear
They are not lost, but gone before.

Acknowledgements

Working towards a PhD has definitely been a gratifying experience and I am indebted to many for making this journey memorable. Firstly, I would like to thank my supervisor Professor Michael Olson for his guidance and I sincerely appreciate his patience and encouragement whilst allowing me the room to work in my own way. Special thanks to my advisor, Professor Owen Sansom, for the helpful discussions we have had during our meetings.

I would like to extent my sincere gratitude to The Beatson Institute for Cancer Research, its director, Professor Karen Vousden and Cancer Research UK for funding my PhD and also for giving me the opportunity to present my research at national and international meetings.

My sincere thanks goes to pathologists Dr. Ayala King, Dr. Francesco Marchesi and Joshua Leach for the long discussions, which helped me immensely. I extend my gratitude to Dr. Karen Blyth for her valuable suggestions regarding animal work. Heartfelt thanks goes to all the research services at Beatson, especially histology services as well as the BSU/BRU team.

I would like to thank all members of our group (R17), past and present, for making the last four years really enjoyable. Life outside work had been a veritable source of delight and I am grateful to all my friends for the good times we spent together.

I owe a great debt of gratitude to my schoolteachers who laid the foundation stone to my education and to my university professors who inspired my love for science.

Finally, I would like to thank my family for their love and encouragement. I am deeply grateful to my grandparents and my parents for supporting me in all my pursuits. I would especially like to thank my mother for being my driving force and inspiration throughout my life. Above all, I thank God for his unparalleled grace and blessings.

Author's Declaration

I am the sole author of this thesis. The work presented in this thesis is entirely my own unless otherwise stated.

Linda Julian

Abbreviations

3D	Three-dimensional
ADP	Adenosine diphosphate
ALT	Alanine aminotransferase
AMT	Amoeboid to mesenchymal transition
Arg	Arginine
ATP	Adenosine triphosphate
ATP11C	Adenosine triphosphate type 11C
BCA	Bicinchoninic acid
BrdU	5-bromo-2'-deoxyuridine
Ca^{2+}	Calcium
CD	Cluster of differentiation
CDC50A	Cell division cycle protein 50 A
CHX	Cycloheximide
CRD	Cysteine-rich zinc finger-like motif domain
CTLs	Cytotoxic T lymphocytes
DAB	3, 3'-diaminobenzidene tetrahydrochloride
DAMPs	Damage-associated molecular patterns
DAPI	4', 6-diamidino-2-phenylindole
DEN	Diethylnitrosamine
dH_2O	Distilled water
dl	Decilitre
DMEM	Dulbecco's Modified Eagle Medium
DMPK	Myotonic dystrophy protein kinase
DMSO	Dimethyl sulfoxide
DNA	Deoxyribonucleic acid
DTT	Dithiothreitol
dUTP	Deoxyuridine triphosphate
ECM	Extracellular matrix
EDTA	Ethylenediaminetetraacetic acid
EGF	Epidermal growth factor
ELISA	Enzyme-linked immunosorbent assay
EMT	Epithelial to mesenchymal transition
F-actin	Filamentous actin
FACS	Fluorescence activated cell sorting
FBS	Foetal bovine serum
FFPE	Formalin-fixed paraffin-embedded
FGF	Fibroblast growth factor
Foxp3	Forkhead box P3
g	Gram
G-actin	Globular actin
GFP	Green fluorescent protein
GM	Genetically modified
H&E	Haematoxylin and Eosin

Hb	Haemoglobin
HCC	Hepatocellular Carcinoma
HCT	Haematocrit
HMGB1	High-mobility group box 1
HN	Hepatic Nodule
HRP	Horse radish peroxidase
IFN-gamma	Interferon gamma
IHC	Immunohistochemistry
IL	Interleukin
kg	Kilogram
l	Litre
LC-MS	Liquid chromatography-mass spectrometry
LPC	Lysophosphatidylcholine
Lys	Lysine
M	Molar
MEFs	Mouse embryonic fibroblasts
MCH	Mean corpuscular haemoglobin
MCHC	Mean corpuscular haemoglobin concentration
MCP-1	Monocyte chemoattractant protein-1
MCV	Mean corpuscule volume
MFG-E8	Milk fat globule epidermal growth factor-8
mg	Milligram
MIG	Monokine induced gamma interferon
MIP-1alpha	Macrophage inflammatory protein-1alpha
ml	Millilitre
MLC	Myosin II regulatory light chain
MLCK	MLC kinase
mm	Millimetre
MPV	Mean platelet volume
MRCK	Myotonic dystrophy kinase-related Cdc42-binding kinase
N	Normal
NK	Natural killer cells
NKT	Natural killer T cells
NAFLD	Non-alcoholic fatty liver disease
NASH	Non-alcoholic steatohepatitis
OCT	Optimal cutting temperature
PARP	Poly (ADP ribose) polymerase
PC	Phosphatidylcholine
PCT	Plateletcrit
PDW	Platelet distribution width
PE	Phosphatidylethanolamine
PH	Pleckstrin homology
PI	Phosphatidylinositol
PLT	Platelet
PS	Phosphatidylserine
RBCs	Red blood cells

RBD	Rho binding domain
rcf	Relative centrifugal force
RDW	Red cell distribution width
RNA	Ribonucleic acid
ROCK	Rho-associated coiled-coil containing kinase
ROCK1nc	ROCK1 non-cleavable
ROCK1wt	ROCK1 wild-type
ROS	Reactive oxygen species
rpm	Revolutions per minute
RSK	Ribosomal S6 kinase
S1P	Sphingosine-1-phosphate
SD	Standard deviation
SEM	Standard error of mean
SILAC	Stable isotope labelling of amino acids in cell culture
SLE	Systemic lupus erythematosus
SM	Sphingomyelin
TG	Transglutaminase
TGF-β	Transforming growth factor beta
TiGER	Tissue-specific Gene Expression and Regulation
TLRs	Toll-like receptors
TMEM16F	Transmembrane protein 16F
TNFα	Tumour necrosis factor alpha
Tregs	Regulatory T cells
TUNEL	Terminal deoxynucleotidyl transferase dUTP nick-end labelling
U	Units
WB	Water bath
WBCs	White blood cells
WT	Wild-type
µg	Microgram
µl	Microlitre
UV	Ultraviolet
V	Volts

1 Introduction

[Text extracted from JULIAN, L. & OLSON, M. F. 2014. Rho-associated coiled-coil containing kinases (ROCK): structure, regulation, and functions. Small GTPases, 5, e29846 (Julian and Olson, 2014) and JULIAN, L. & OLSON, M. F. 2015. Apoptotic membrane dynamics in health and disease Cell Health and Cytoskeleton, 7, 133-142 (Julian and Olson, 2015)]

1.1 Rho Associated Coiled-Coil Kinases

Rho associated coiled-coil kinases (ROCK) are serine/threonine kinases which were originally identified as prominent downstream effectors of the Rho GTPases (Leung et al., 1995, Matsui et al., 1996, Leung et al., 1996, Nakagawa et al., 1996, Ishizaki et al., 1996). ROCK proteins primarily regulate and modulate the cytoskeleton by promoting the stabilization and bundling of actin filaments and the subsequent generation of actin-myosin contractility via phosphorylation of downstream targets. ROCK proteins have been extensively studied over the years and have been found to be indispensable for many cellular processes that are dependent on the actin-myosin cytoskeleton including, but not limited to: cell contraction, migration, adhesion, apoptosis, survival and proliferation. In this section, I will focus on the structure, regulation, downstream substrates and functions of ROCK.

Two mammalian ROCK homologs have been identified, ROCK1 (also known as ROKβ, Rho-kinase β, ROCK I or p160ROCK) and ROCK2 (also known as ROKα, Rho kinase and ROCK II). In humans, the two isoforms ROCK1 and ROCK2 both contain 33 exons and are located on chromosome 18 (18q11.1) and 2 (2p24), respectively. The ROCK1 open reading frame encodes 1354 amino acids, whereas ROCK2 encodes 1388 amino acids. A pseudogene derived by partial duplication and inversion of ROCK1, called *Little ROCK*, is located on chromosome 18p11.32 of vascular smooth muscle cell lines and organs rich in vascular smooth muscle cells (Montefusco et al., 2010). ROCK2 has a reported splice variant termed ROCK2m, preferentially expressed in skeletal muscle, which is characterized by the inclusion of an extra exon between exon 27 and exon 28 (Pelosi et al., 2007).

1.1.1 Structure

The two ROCK homologues share 64% identity in their primary amino acid sequences, with the highest homology (92%) within the kinase domains and the coiled-coil domains being the most diverse (55%) (Nakagawa et al., 1996). The kinase domains of ROCK are closely related to many homologous domains in this family, including myotonic dystrophy kinase (DMPK), myotonic dystrophy kinase related-Cdc42 related kinases (MRCK) α and ß, and citron Rho-interacting kinase (CRIK). To date, the crystal structures of the kinase domains from ROCK1 (Jacobs et al., 2006), ROCK2 (Yamaguchi et al., 2006), MRCKα MRCKß (Heikkila et al., 2011) and DMPK (Elkins et al., 2009) have been determined, which has highlighted the high degree of tertiary as well as primary similarity. The ROCK kinase domains are located in the amino-terminal region, followed by a central ~600 amino acid long amphipathic α-helix forming a coiled-coil region (Samuel and Olson, 2010). At the carboxyl-terminal region, there is a split pleckstrin homology (PH) domain, which is bisected by an internal cysteine-rich zinc finger-like motif domain (CRD) (Figure 1-1). The two separate PH portions assemble together to form a typical PH domain that is attached by two short linkers to a separate CRD (Wen et al., 2008). Distinct from most other kinase proteins, the amino-terminal and carboxyl-terminal extensions of the ROCK kinase domains are essential for its catalytic activity (Leung et al., 1996, Jacobs et al., 2006, Yamaguchi et al., 2006).

Crystal structure studies have provided deeper insight into the different domains of the protein. The canonical Rho binding domain (RBD) forms a parallel coiled-coil dimer as revealed by crystal structure determinations and binds exclusively to the switch I and switch II regions of GTP-bound active RhoA and RhoC (Shimizu et al., 2003, Dvorsky et al., 2004). Two additional Rho-interacting domains were identified that can tightly interact with RhoA and which may cooperatively contribute to binding (Blumenstein and Ahmadian, 2004). Recent crystal structure studies on the coiled-coil domain of ROCK1 revealed a unique sequence feature that creates an irregularity in the domain and possible conformational flexibility (Tu et al., 2011).

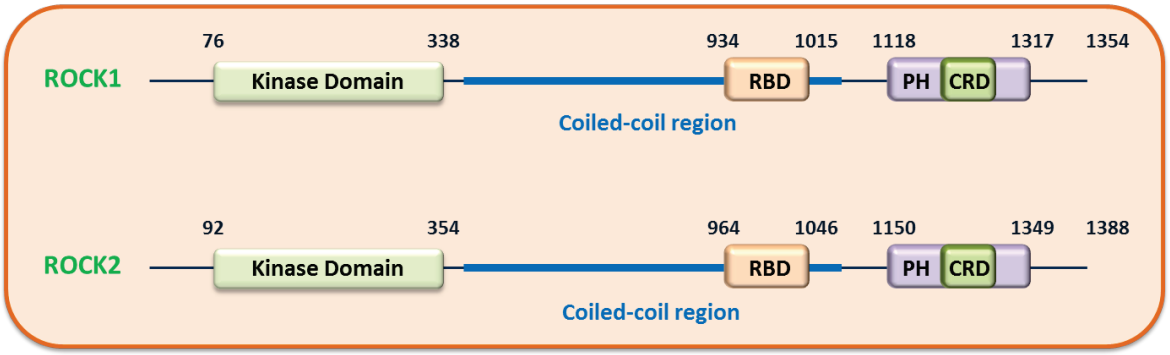

Figure 1-1 Molecular organization of ROCK isoforms
Diagram shows a schematic representation of ROCK1 and ROCK2 protein domains. The kinase domain is situated at the N terminus followed by a coiled-coil region with Rho-binding domain (RBD) in the middle and a pleckstrin homology (PH) domain with an internal cysteine-rich region (CRD) at the C-terminus. Protein domains and their indicated positions were taken from the National Center for Biotechnology Information. Figure adapted from (Julian and Olson, 2014)

ROCK has two dimerization domains: the ~70 residue amino terminal dimerization region and the coiled-coil helical regions (Jacobs et al., 2006, Yamaguchi et al., 2006). Dimerization is essential for its kinase activity and regulation (Dvorsky et al., 2004, Jacobs et al., 2006, Yamaguchi et al., 2006, Garg et al., 2008). Charged residues in the coiled-coil region might function as a hinge that allows the N terminal kinase domains to interact with C-terminal inhibitory regions. Structural determination of full-length ROCK protein crystals will ultimately reveal how the various domains interact and the mechanism of auto-inhibition.

1.1.2 Regulation

Although ROCK1 and ROCK2 have highly related functional domains and significant amino acid identity, they are regulated both by common means as well as mechanisms unique to ROCK1 or ROCK2.

1.1.2.1 Conventional Activation

The carboxyl-terminal region of ROCK which contains the Rho binding domain and the pleckstrin homology domain acts as an auto-inhibitory region of the kinase domain, since deletion of this portion results in constitutive activation of either kinase in vitro and in vivo (Amano et al., 1999, Ishizaki et al., 1997) (Figure 1-2). Inhibition may occur either because the active site of the kinase domain is blocked by interaction with portions of the carboxyl terminal region or due to stabilization of a catalytically incompetent conformation (Jacobs et al., 2006). The Ras superfamily includes the Rho-GTPase proteins RhoA and RhoC, which are the most well characterized ROCK regulators. Several lines of evidence show that interaction of activated, GTP-bound Rho proteins with the RBD elevate the kinase specific activity of ROCK by inducing conformational changes that disrupt the negative regulatory interactions between the kinase domain and the auto-inhibitory carboxyl terminal region(Leung et al., 1996, Ishizaki et al., 1996, Nakagawa et al., 1996). However, structural studies of the holoenzyme, either in isolation or associated with active Rho proteins have not been reported to confirm this model.

However, during apoptosis, ROCK1 is activated by cleavage and removal of the auto-inhibitory domain by caspases (Coleman et al., 2001, Sebbagh et al., 2001). Similarly, ROCK2 can be activated by Granzyme B-mediated cleavage, which also leads to concomitant caspase activation and ROCK1 activation (Sebbagh et al., 2005) (Figure 1-2). In a non-apoptotic scenario in endothelial cells, thrombin was reported to activate caspase 2 and increase ROCK2 expression, resulting in increased levels of caspase 2-mediated proteolytic cleavage and consequent activation of ROCK2 (Sapet et al., 2006). Several other mechanisms of ROCK regulation have also been described over the years including stimulation of ROCK activity by lipids messengers like arachidonic acid and sphingophosphocholine (Feng et al., 1999, Shirao et al., 2002).

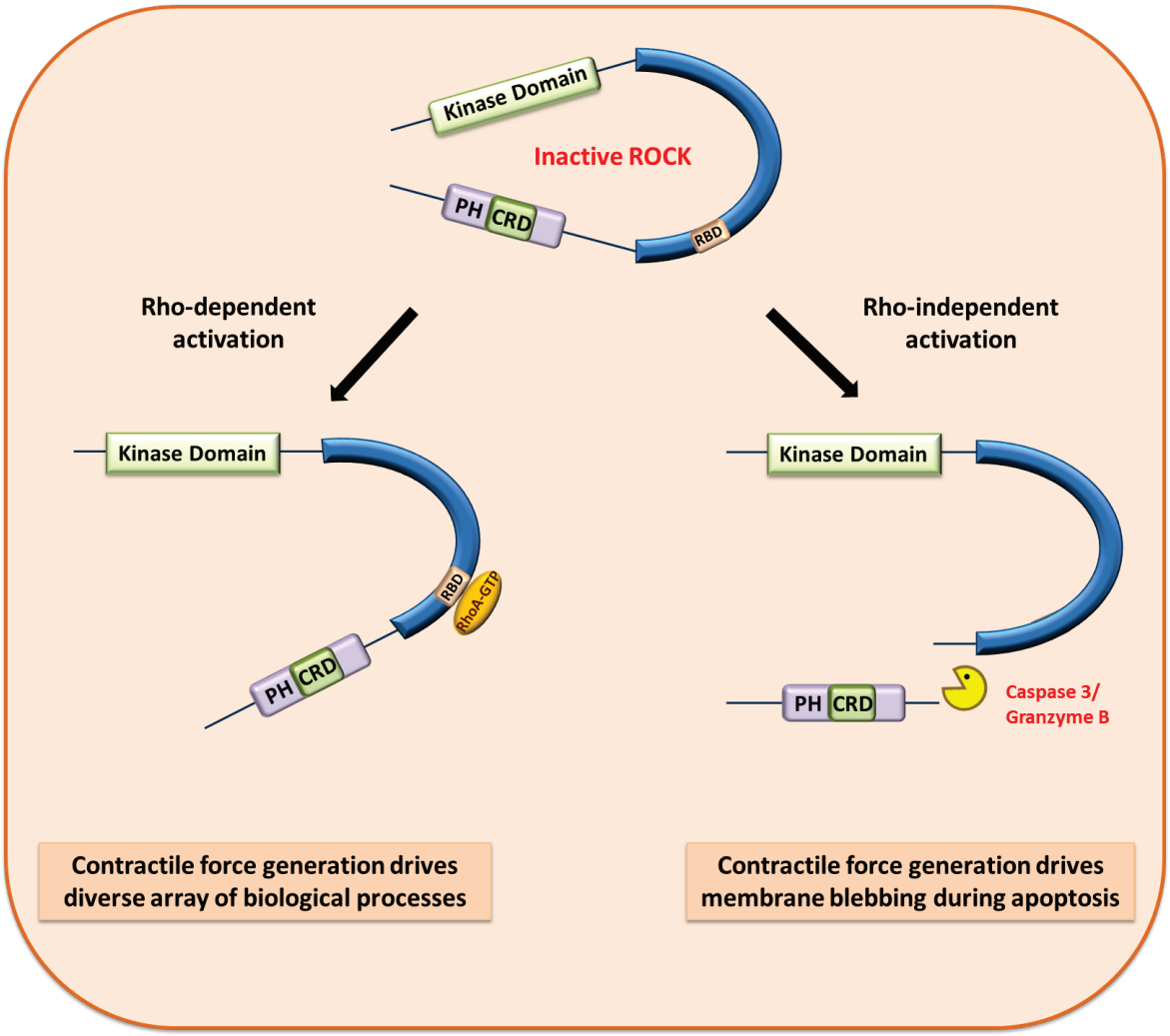

Figure 1-2 Conventional modes of ROCK activation

Diagram shows schematic representation of modes of ROCK activation. In the inactive state, the carboxyl terminal of ROCK acts as an auto-inhibitory region. Binding of active RhoA to the Rho binding domain (RBD) disrupts the negative regulation, thus rendering the kinase active. ROCK protein can also be activated in a Rho-independent manner by removal of the inhibitory carboxyl terminal of ROCK1 and ROCK2 by caspase 3 and granzyme B mediated cleavage, respectively. Figure adapted from (Julian and Olson, 2014).

1.1.2.2 Phosphorylation

Crystal structure analyses revealed that the unphosphorylated ROCK1 kinase domain had a catalytically competent conformation without phosphorylation or conformational input from RhoA binding to the RBD (Jacobs et al., 2006). Unlike other AGC family kinases that require activation loop phosphorylation (Schackmann et al., 2011), the ROCK kinase domains do not appear to require phosphorylation for activity. However, additional kinases may regulate ROCK signalling by phosphorylating other regions. For example, Polo-like kinase-1 works synergistically with RhoA to maximally activate ROCK2 by phosphorylating at any one of four conserved sites Thr-967, Ser-1099, Ser-1133 and Ser- 1374 (Lowery et al., 2007). Phosphorylation of ROCK2 on Tyr-722 inhibits activity by decreasing RhoA binding (Sinning et al., 2011), while Shp-2 mediated dephosphorylation increases RhoA responsiveness (Lee and Chang, 2008). Auto-phosphorylation by ROCK2 on S1366 (Rautou et al., 2011) and by ROCK1 on S1333 (Chuang et al., 2013) is a reflection of the kinase activation, although these sites do not regulate catalytic activity. However, phosphorylation on these sites might contribute to protein subcellular localization (Ishiuchi and Takeichi, 2011). Large scale phosphoproteomics studies have identified numerous phosphorylations on human ROCK1 (45 sites reported on www.phosphosite.org) and ROCK2 (43 sites), although the majority of them have not been confirmed by independent means. The frequency of some observed phosphorylations (e.g. ROCK1 Tyr-913 and Ser-1341, or ROCK2 Ser-1379) suggests that they have physiological significance, which will likely be determined in the future.

1.1.2.3 Negative Regulation

Although Rho proteins generally activate ROCK, other GTP-binding proteins have been found to negatively regulate ROCK signalling. Gem was shown to interact with ROCK1 in the coiled-coil region adjacent to the RBD, thereby inhibiting phosphorylation of MLC and the MYPT1 subunit of MLC phosphatase (Ward et al., 2002). Rad1, another small GTP-binding protein was also reported to mimic Gem in inhibiting actin-myosin contractility by blocking ROCK2, resulting in reduced cell rounding and neurite retraction (Ward et al., 2002). In contrast to the highly related RhoA, B and C proteins that can stimulate stress fibre formation through ROCK, RhoE decreases stress fibre formation (Guasch et al., 1998, Nobes et al.,

1998) by binding to the amino-terminal region of ROCK1, but not ROCK2, thus physically interfering with ROCK1 kinase activity (Riento et al., 2003, Riento and Ridley, 2003, Riento et al., 2005). Interestingly, protein kinase PDK1 competitively binds to a similar region of ROCK1 as RhoE, thereby antagonizing the negative regulation of ROCK1 by Rho E (Pinner and Sahai, 2008). Recently, Coronin1B was identified as an attenuator of ROCK2 signalling by directly binding to the PH domain (Rana and Worthylake, 2012). Identification of additional interactions with similar ROCK regulators may highlight mechanisms that modulate ROCK activity locally without global effects on this signalling pathway.

1.1.3 Expression and Localization

Initial studies revealed a uniform expression of ROCKs during embryogenesis and in adult tissues (Leung et al., 1996, Nakagawa et al., 1996). Analysis of ROCK1 and ROCK2 expressed sequence tag distribution using the Tissue-specific Gene Expression and Regulation (TiGER) database (Liu et al., 2008b) revealed that their distribution patterns were similar and that there were few specific organ/tissues with expression levels that were dramatically higher than another (Julian and Olson, 2014). Notably, there was significant ROCK1 expression in the thymus and blood, with little to no ROCK2 expression detected.

Several studies examined the subcellular localization of the two ROCK isoforms. Early studies on ROCK2 localization reported a predominantly cytosolic distribution (Leung et al., 1995, Matsui et al., 1996). Overexpression of an active RhoA mutant resulted in the recruitment of ROCK2 to both internal and peripheral cell membranes, where it was observed to be largely associated with actin microfilaments (Vandenabeele et al., 2010, Leung et al., 1995). Further studies on ROCK2 subcellular distribution revealed accumulation at the cleavage furrow, implicating its role in the formation of contractile ring during cytokinesis (Kosako et al., 1999, Inada et al., 1999). In addition, ROCK2 has been reported to localize in the nucleus of growing cells (Tanaka et al., 2006), stress fibres (Katoh et al., 2001, Kawabata et al., 2004), filamentous vimentin network in serum-starved cells (Sin et al., 1998) as well as to the centrosomes (Ma et al., 2006). Interestingly, Shroom, a key player in apical cell constriction in neurulation, binds to ROCK2 and regulates its distribution to apical cell junctions to achieve a localized activation (Flynn and Helfman, 2010, Ehrenschwender et

al., 2010). Subcellular localization of ROCK1 has not been as well characterized, but some studies point to ROCK1 association with the plasma membrane (Glyn et al., 2003, Stroeken et al., 2006) and centrosomes (Chevrier et al., 2002). In rat embryonic fibroblasts, ROCK1 and ROCK2 had distinct distribution pattern with ROCK1 concentrated in the perinuclear regions and sometimes associated with stress fibres whereas ROCK2 was characteristically distributed at the cell membrane ruffles along with perinuclear distribution (Yoneda et al., 2005).

1.1.4 Downstream Targets

Activated ROCK proteins phosphorylate a number of downstream targets involved in different biological processes, and given the high similarity in their kinase domains, it is likely that the two isoform would phosphorylate numerous common substrates. From the several studies aimed at identifying ROCK substrates, a consensus amino acid motif for phosphorylation in most cases was found to be R/KXXS/T or R/KXS/T (R- Arginine, K- Lysine, S- Serine, T- Threonine, X- any amino acid), although some non-canonical sites have also been identified by peptide phosphorylation screening (Kang et al., 2007).

One of the primary roles defined for ROCK is the regulation of actin-myosin cytoskeletal organization. Phosphorylated myosin II regulatory light chains (MLC) promote actin-myosin contractility by activating myosin ATPase, thus enabling its interaction with F-actin to generate a contractile force (Vicente-Manzanares et al., 2009). ROCKs can phosphorylate MLC at Ser-19 and Thr-18 and this occurs at the same sites that are phosphorylated by MLC kinase (Amano et al., 1996). However, depletion of Ca2+ to block activation of MLC kinase (MLCK) resulted in decreased MLC phosphorylation in response to G-protein activation in airway smooth muscle cells, indicating that ROCK may largely contribute to elevating MLC phosphorylation indirectly by inhibiting dephosphorylation (Iizuka et al., 1999, Sward et al., 2000). MLC dephosphorylation is mediated by a phosphatase complex (PP1M) that is composed of a PP1cδ catalytic subunit, the myosin binding subunit MYPT1 that modulates the targeting of myosin to the phosphatase, and a small regulatory subunit M20 (Hartshorne and Hirano, 1999). Phosphorylation of MYPT1 by ROCK on Thr-695 and Thr-850 leads to the inhibition of MLC dephosphorylation by dissociating myosin from the phosphatase, thereby allowing for increased net MLC phosphorylation and

subsequent activation of myosin ATPase (Kimura et al., 1996, Feng et al., 1999a, Kawano et al., 1999, Velasco et al., 2002). Moreover, MLC phosphorylation to induce stress fibre and focal adhesion assembly is spatially regulated by MLCK, MRCK and ROCK, where ROCK is involved in the formation of stress fibres in the centre of fibroblasts, while MLCK and MRCK function at the periphery (Totsukawa et al., 2000, Ando et al., 2013). In addition, ROCK kinases also regulate actin filament dynamics by phosphorylating LIM kinases 1 and 2 (Scott and Olson, 2007) on activation loop Thr-508 (Ohashi et al., 2000) and Thr-505 (Katoh et al., 2001, Sumi et al., 2001) respectively. Activated LIM kinases phosphorylate and inactivate the actin severing protein cofilin, resulting in a net increase in the number of actin filaments within cells (Arber et al., 1998, Adams et al., 1996). Collectively, ROCK activation leads to a concerted series of events that promote actin-myosin mediated contractile force generation and consequent morphological changes.

1.1.5 ROCK Functions

At the time when the two isoforms of ROCK were identified, nearly 20 years ago, they were proposed to be regulators of the actin cytoskeleton. Since then the role of ROCKs has been studied comprehensively in many different contexts. Some of the major functions will be discussed here. But, its role in apoptosis will be addressed in the next section.

1.1.5.1 Actin Organization

Formation of stress fibres and focal adhesion complexes by MLC phosphorylation was one of the first functions identified for ROCK (Amano et al., 1997). Stress fibres are contractile apparatus in cells that are composed of bundles of F-actin and myosin II which are especially prominent in cultured cells, but have also been shown to be manifested in cells *in vivo* (Sugimoto et al., 1991, Murakami and Ishikawa, 1991). These actin-myosin fibres are linked to discrete points on the inner plasma membrane called focal adhesions, where dynamic protein complexes that contribute to cell adhesion to the extracellular matrix are localized (Schiller et al., 2013). Expression of constitutively active ROCK consistently induced the formation of stress fibres and focal adhesions, whereas kinase dead and the N terminal truncated ROCK mutants induced disassembly of

stress fibres and focal adhesion complexes, accompanied by cell spreading (Leung et al., 1996, Amano et al., 1997, Ishizaki et al., 1997). Although both ROCK isoforms appear to contribute to focal adhesion formation and microfilament bundling, siRNA knockdown experiments have revealed some differences in their functions. In fibroblasts, ROCK1 and ROCK2 play distinct roles in the subcellular sites of MLC phosphorylation and in the assembly of fibronectin matrices at the cell surface during actin cytoskeleton mediated extracellular matrix assembly (Yoneda et al., 2005, Yoneda et al., 2007). Knockdown of ROCK1 in keratinocytes blocked focal adhesion maturation, which decreased cell adhesion to fibronectin, while ROCK2 knockdown reduced turnover, leading to the formation of large focal adhesions with increased stability that promoted fibronectin adhesion (Surma et al., 2011, Hohenberger et al., 2011). Using mouse embryo fibroblasts (MEFs) deleted for ROCK1 or ROCK2, it was observed that ROCK1 regulates peripheral actin-myosin ring formation through MLC phosphorylation and ROCK2 stabilizes the cytoskeleton through cofilin phosphorylation following treatment with the chemotherapeutic drug doxorubicin (Shi et al., 2013). These results indicate that ROCK1 and ROCK2 may have different functions in cells, likely due to differences in the way that there are regulated and subtle differences in localization that result from non-overlapping patterns of lipid and/or protein binding.

Although ROCK signalling can recapitulate the effects of Rho activation, this may not hold true in all instances and may require additional Rho effector proteins to work cooperatively with ROCK. This has been well demonstrated in the context of stress fibre assembly where ROCK induced stress fibres are thicker than those induced by RhoA (Leung et al., 1996, Amano et al., 1997, Ishizaki et al., 1997). Rho activates one of its effectors mDia1 (mammalian homologue of *Drosophila* Diaphanous 1), which interacts with profilin, thus transforming the condensed stress fibres to thinner actin fibres, which remains disorganized in the absence of ROCK activity (Watanabe et al., 1999). These studies indicate the necessity for mDia to act in concert with ROCKs following Rho activation in stress fibre assembly.

1.1.5.2 Cell Migration

One of the crucial events that enable cellular motion is actin-myosin-mediated contraction that allows anterograde motion of the cell and rear cell retraction. Given the importance of ROCK in the regulation of actin cytoskeleton dynamics, it is not surprising that this enzyme has been implicated in cell migration. There are two predominant modes of single cell migration, that have been described as mesenchymal and amoeboid, which are interconvertible in tumour cells depending on the microenvironment. An elongated, spindle like morphology that requires the activation of small GTPase Rac as well as presence of protease activity characterizes the mesenchymal migration mode. In amoeboid migration, cells exhibit a rounded morphology as well as formation of bleb like protrusions that deforms the collagen thus allowing them to squeeze through extracellular matrix without the need for proteolysis (Wolf et al., 2003, Wilkinson et al., 2005, Wyckoff et al., 2006). ROCK signalling is a requirement for amoeboid migration as it generates actin-myosin contractility and protrusion of blebs in all directions. Interestingly, low adhesion cells like lymphocytes and neutrophils appear to take on the amoeboid mode, thus conferring them a high degree of mobility even in the absence of proteolysis which is well suited for their function (Friedl and Wolf, 2003). On the other hand, mesenchymal invasion seems to have limited dependence on ROCK, as the ROCK inhibitor Y-27632 can inhibit invasion of several amoeboid cell lines in 3D matrices but not mesenchymal invasion (Sahai and Marshall, 2003). In accordance, expression of an active ROCK resulted in rounded morphology with several membrane blebs (Sahai and Marshall, 2003). A recent study reported that FilGAP, a Rac GTPase activating protein, acts downstream of ROCK during amoeboid migration and can also regulate mesenchymal to amoeboid transition by inactivating Rac (Saito et al., 2012). As mentioned above, tumour cells display a high degree of plasticity as inhibition of ROCK converts their morphology from amoeboid to transitional (Sanz-Moreno et al., 2008). On the other hand, inhibition of Rac or in the presence of protease inhibitors, there is transition from proteolysis dependent mesenchymal mode to amoeboid (Sahai and Marshall, 2003, Wolf et al., 2003, Sanz-Moreno et al., 2008). These studies can have a deep impact on the development of anti-metastatic drug therapies.

1.1.5.3 Cell Proliferation and Cytokinesis

Numerous studies have highlighted the importance of ROCK in the regulation of cell proliferation, which may be due to a role in mediating cytoskeletal tension or may be mediated by cytoskeleton-independent pathways. In accordance with this, ROCK inhibitors have been shown to have anti-proliferative effects in some cell types including airway and prostatic smooth muscle cells and cardiac myocytes (Takeda et al., 2006, Zhao and Rivkees, 2003, Yahiaoui et al., 2006). Conversely, active ROCK can induce proliferation in some cell types including fibroblasts, in which modulation of the levels of specific cell cycle regulators appears to play an important role (Croft and Olson, 2006). The influence of ROCK activity on the levels of cell cycle regulatory proteins also has been implicated in the proliferation of corneal epithelial cells (Chen et al., 2008) and gastric cells (Zhang et al., 2009).

Although ROCK activity may promote proliferation in some cells types, in other contexts ROCK appears to have anti-proliferative functions. For example, inhibition of ROCK activity in human keratinocytes resulted in increased proliferation and decreased terminal differentiation, while conditional ROCK2 activation had the opposite effects, suggesting a role for ROCK in the regulation of keratinocyte fate (McMullan et al., 2003).

During cytokinesis, cells undergo dramatic reorganization of the cytoskeleton and are divided in two daughters through the actions of the actin-myosin rich contractile ring. Shortly after the identification of ROCK kinases, it was observed that dominant negative ROCK2 inhibited cleavage furrow formation in *Xenopus* embryos and in mammalian cells, resulting in multinucleation (Yasui et al., 1998). Further studies revealed the accumulation of ROCK2 at the cleavage furrow during cytokinesis, where it was an important contributor to MLC phosphorylation (Kosako et al., 1999, Kosako et al., 2000). However, although ROCK2 inhibition did not completely arrest cytokinesis, it did result in prolonged cleavage furrow ingression, suggesting that ROCK2 makes indispensable contributions to the normal progression of cytokinesis (Kosako et al., 2000). Interestingly, ROCK kinases do not appear to be responsible for the phosphorylation of ezrin/radixin/moesin (ERM) proteins localized at the cleavage furrow, suggesting that there must be other cleavage furrow kinases that may

play complementary and/or redundant roles in cytokinesis (Kosako et al., 2000, Yokoyama et al., 2005). Taken together, ROCK may have a general positive role as a promoter of cell proliferation in many cell types, with some exceptions in specialized contexts.

1.1.5.4 Embryonic Development

ROCK1 and ROCK2 have been reported to have overlapping expression patterns in developing embryos and are highly enriched in the cardiac mesoderm, lateral plate mesoderm, and the neural plate in chick and mouse embryos where they play vital roles in various embryonic morphogenetic events, including cell migration, differentiation and axis formation (Shi et al., 2011). Earlier experiments that sought to elucidate the roles of ROCK signalling in development have been performed with small molecule inhibitors that block both kinases with equal potency (Wei et al., 2001); therefore these studies do not provide any information on the specific functions of each ROCK protein. Genetic deletion of ROCK1 or ROCK2 in mice made it possible to dissect the roles of these proteins in development (Table 1-1). A consistent abnormality in ROCK1 and ROCK2 knockout mice on a C57BL/6N strain background was failure of closure of eyelids and ventral body wall giving rise to eyes open at birth and omphalocele phenotypes (Shimizu et al., 2005, Thumkeo et al., 2005). Formation of organized actin-myosin cables in the eyelid epithelial sheets and the actin-myosin-mediated closure of umbilical rings were impaired in both knockout models (Shimizu et al., 2005, Thumkeo et al., 2005). Despite the two isoforms having highly conserved kinase domains, they apparently cannot compensate for each other in these tissues. ROCK1 and ROCK2 double heterozygous mice also displayed the same phenotype, albeit at a lower frequency, suggesting that the observed phenotypes are the result of insufficient gene dosage with both isoforms cooperatively regulating the movement of epithelial sheets for eyelid and ventral body wall closure (Thumkeo et al., 2005). Yet, ROCK1 or ROCK2 knockout mice and double heterozygous mice that survived continued to develop normally, and were fertile and apparently healthy, suggesting that ROCK1 and ROCK2 are particularly important during development when cell movement is required for the formation of tissues and organs (Shimizu et al., 2005, Thumkeo et al., 2005).

Interestingly, ROCK2 deletion on a mixed genetic background of C57BL/6N and 129/SvJ strains exhibited placental dysfunction, intrauterine growth retardation and 90% embryonic death in utero (Thumkeo et al., 2003). On the same C57BL/6N strain background, the survival rate of ROCK2 knockouts was less than was observed for ROCK1 deletion, due to an additional defect in the placental labyrinth layer (Thumkeo et al., 2005). Similarly, differences in strain background also had an effect in ROCK1 knockouts, as the eyelids open at birth and omphalocele phenotypes were not observed in mice with mixed C57BL/6N and 129/SvJ or FVB backgrounds (Zhang et al., 2006). These studies indicate that strain differences, and by inference additional genetic modifiers that have yet to be identified, affect the manifestation of these phenotypes in ROCK1 or ROCK2 deleted mice. The lack of phenotypes in other tissues suggests that both homologues can functionally compensate for each other during development or that there is a lower requirement for total ROCK protein.

Genotype	Strain	Genetic Modification	Lethality, Developmental Phenotype	Phenotype of Survivors	Refs
ROCK1-/-	C57BL/6	Deletion of exon 3 and 4	Perinatal (~90%) EOB and omphalocele	Fertile and healthy, 50% had eye lesions	(Shimizu et al., 2005)
	C57BL/6	Deletion of exon 1b	In utero or perinatal (~95%) EOB and omphalocele	Not recorded	Rikitake et al, 2005
	FVB	Disruption of exon 5	Embryonic (~60%) Not recorded	Fertile and healthy	Zhang et al, 2006
ROCK2-/-	C57BL/6 - 129/SvJ	Deletion of most of exon 3	Embryonic (~92%), Perinatal (~95%) Placental dysfunction, intrauterine growth retardation	Runted, fertile	Thumkeo et al, 2003
	C57BL/6	Deletion of most of exon 3	Embryonic (~88%), Perinatal (>99%) Placental dysfunction, EOB and omphalocele	Not recorded	Thumkeo et al, 2005
	CD-1	Deletion of most of exon 3	None	Impaired motor function	Duffy et al, 2009
ROCK1+/-	C57BL/6	Deletion of exon 1b	None	Fertile and healthy	Rikitake et al, 2005
ROCK1+/-	FVB	Disruption of exon 5	Embryonic (~30%) Not recorded	Fertile and healthy	Zhang et al, 2006
ROCK1+/- ROCK2+/-	C57BL/6	Deletion of exon 3 and 4 (ROCK1); most of exon 3 (ROCK2)	Perinatal (~30%) EOB and omphalocele	Fertile and healthy	Thumkeo et al, 2005

Table 1-1: Genetic mouse models of ROCK knockout

1.1.6 Current Status of ROCK Inhibitors

Existing information about many of the cellular functions of ROCKs was aided by the availability of several commercial inhibitors. Most of these inhibitors work by competing with the ATP for binding to their catalytic site. The implication of the ROCK isoforms in several pathological conditions (Julian and Olson, 2014) has promoted the therapeutic use of these inhibitors in various animal and human disease models, a major one being cardiovascular diseases.

Among the different inhibitors, Y-27632 (Uehata et al., 1997) and fasudil (Asano et al., 1987) have been extensively used for experiments. Y-27632 belongs to the pyridine class of chemicals and is a non- selective inhibitor of both ROCK1 and ROCK2. Fasudil (HA-1077), belonging to the isoquinoline group, although being a moderate inhibitor of ROCK, is the only one that has been approved for clinical use in Japan since 1995 for the treatment of cerebral vasospasm and ischemia (Olson, 2008). Various clinical studies have been undertaken to test the efficacy of fasudil, for example in pulmonary arterial hypertension (Ishikura et al., 2006), atherosclerosis (Nohria et al., 2006) and aortic stiffness (Noma et al., 2007). Other inhibitors which are commonly used include Y-32885 (Uehata et al., 1997), hydroxyfasudil (HA-1100) (Arai et al., 1993), and H-1152 (Ikenoya et al., 2002). In addition to fasudil, more inhibitors are gaining access to clinical trials (phase 2) including Y-39983 for glaucoma (Tokushige et al., 2007), BA-210 for spinal cord injury (Lord-Fontaine et al., 2008)and SAR407899 for erectile dysfunction (Lohn et al., 2009). Despite the development of so many inhibitors, none of them is absolutely ROCK specific. Most of these inhibitors also inhibit protein kinase C-related kinase (PRK) as well as ribosomal S6 kinase (RSK), cyclic AMP dependent protein kinase (PKA) and mitogen and stress activated protein kinase (MSK1) (Bain et al., 2007). Whether the effect of ROCK inhibitors in clinical trials is a result of inhibition of additional kinases is not known and hence evidence gleaned from ROCK inhibitor studies have to be interpretted with caution. Recently, the focus has been shifted to identifying and developing isoform-specific ROCK inhibitors (Boerma et al., 2008). Since these are still in their infancy, mouse models with conditional or tissue specific deletion of ROCK1 and/or ROCK2 still remain crucial for understanding the biological functions of ROCKs.

1.2 ROCK1 in Apoptotic Membrane Blebbing

The role of ROCK isoforms as key regulators of the actin myosin cytoskeleton has been appreciated over many years. Despite the advances in the field of cell death, not much was known about the mediators driving the morphological features of dying cells until the late nineties. Seminal reports implicating the ROCK isoforms in the modulation of actin myosin activity, thus driving the formation of dynamic membrane protrusions called blebs during cell death became the key to unravelling the biological significance of these events. In this section, I will present a brief overview about apoptosis and its features before delving into the role of ROCK during the execution phase of apoptosis.

1.2.1 Apoptosis or Programmed Cell Death

Multicellular organisms need to get rid of excess, unwanted or damaged cells through a dedicated molecular programme called 'apoptosis'. The term 'apoptosis' was first conceived in 1972 by Kerr, Wyllie and Currie to describe a distinct form of programmed cell death (Kerr et al., 1972). Our understanding of the molecular components governing this program, stem largely from genetic studies on the nematode *C. elegans*, mostly from the 1980s and 1990s (Horvitz, 1999). Subsequent characterization led to the identification of three apoptotic pathways, namely extrinsic or death receptor pathway, intrinsic or mitochondrial pathway, and perforin or granzyme pathway. Proteases known as cysteine-dependent aspartate specific proteases or caspases, which can cleave proteins at aspartic acid residues, were identified as central components of the apoptotic program (Cerretti et al., 1992, Nicholson et al., 1995, Alnemri et al., 1996). These proteases are ubiquitously expressed as inactive precursors that are activated during apoptosis. Caspases involved in apoptosis may be divided into initiator or effector caspases. Intracellular and extracellular apoptotic stimuli received via one of the three pathways activate the initiator caspases 2, 8, 9 and 10, which in turn signal via a caspase activation cascade to propagate the death stimulus by activating the downstream effector caspases 3, 6, and 7 (Cohen, 1997). Activated effector caspases orchestrate the destruction of diverse cellular structures by selectively cleaving target proteins to elicit the morphological and biochemical features associated with apoptosis, which will be

dealt in detail below. Here, I will briefly describe how apoptosis plays a key and central role from development to adult life in multicellular organisms.

1.2.1.1 Apoptosis during Developmental Processes

Embryonic development is governed by tight orchestration between cell division and cell death. The role of programmed cell death during development was elucidated using *C. elegans*, *D. melanogaster* and the mouse as model systems.

A striking and obvious function of apoptosis in vertebrate development is digit formation, since impaired apoptosis leads to ineffective removal of cells between developing digits resulting in retention of interdigital webbing (Milligan et al., 1995, Lindsten et al., 2000). Apoptosis during embryonic development is also involved in the conversion of solid structures into hollow tubes thereby giving tissues and organs their form and structure. For example, during gastrulation, the conversion of solid embryonic ectoderm into hollow closed tubes of columnar epithelial cells is made possible by apoptosis of inner ectodermal cells (Coucouvanis and Martin, 1995, Coucouvanis et al., 1995). Apoptosis is also involved in cardiac morphogenesis as it is essential in the development of the four chambered heart (Abdelwahid et al., 2002). Apart from sculpting, another role of apoptosis is the deletion of transient structures that are no longer essential, for example the Mullerian duct in males and the Wolffian duct in females are eliminated during development (Jacobson et al., 1997). In addition, mechanical force generated by apoptotic cells has recently been shown to be vital for generating tension in developing *D. melanogaster* tissues to induce epithelial folding, thus establishing proper topography (Monier et al., 2015).

In other circumstances, cell death mechanisms are also involved in the elimination of superfluous and potentially dangerous cells during development. For example, the immune system uses apoptosis to eliminate developing lymphocytes lacking functional antigen receptors thus eliminating self-reactive cells that could lead to autoimmunity (Opferman and Korsmeyer, 2003, Opferman et al., 2003). The role of apoptosis in nervous system development has also been widely recognized, where superfluous neurons and neurons that fail to establish functional synaptic connections are eliminated (Nijhawan et al.,

2000). These observations clearly demonstrate a decisive role of apoptosis in normal embryonic development.

1.2.1.2 Apoptosis Maintains Tissue Homeostasis

In addition to its roles in development, apoptosis is also crucial for the maintenance of tissue homeostasis throughout adult life. Cell turnover in adult tissues is highly variable across tissue types, and heavily relies on the apoptotic machinery to remove damaged and superfluous cells. In adults, cell death also plays a key role in tissue remodelling, such as mammary gland involution (Lund et al., 1996) and follicular atresia of the postovulatory follicle (Tilly et al., 1991). Along with the tightly controlled apoptotic program, highly efficient phagocytic mechanisms ensure prompt removal of apoptotic debris, thereby reducing the potential for apoptotic cells to lose their membrane integrity and become necrotic (secondary necrosis), resulting in inflammation (Franz et al., 2006). In contrast to the immunologically silent apoptotic process, necrosis may stimulate inflammatory responses that could be harmful to neighbouring cells in the tissue. Despite the large number of cells dying by apoptosis in adult tissues, only a small number of apoptotic cells can be detected even in tissues with high cell turnover such as the thymus (Platt et al., 2000). This is likely to be because the apoptotic cells are rapidly recognized and engulfed by professional phagocytes or adjacent neighbouring cells. Defects in clearance mechanisms have been linked to inflammation and autoimmunity reflecting the importance and efficiency of apoptotic cell clearance under normal circumstances (Nagata et al., 2010).

1.2.2 Cellular Features during Apoptosis

During apoptosis, cells undergo a series of alterations that help in distinguishing them from their healthy counterparts and eventually aid in their efficient recognition and removal. These cellular alterations are broadly divided into two; biochemical and morphological.

1.2.2.1 Biochemical Features

Apoptotic cells undergo several biochemical modifications, of which externalization of phosphatidylserine is the most well-known. Plasma

membranes in eukaryotic cells feature an asymmetric distribution of lipids between the inner and outer leaflets, with phosphatidylcholine (PC) and sphingomyelin (SM) predominantly present on the outer leaflet, whereas phosphatidylserine (PS), phosphatidylinositol (PI) and phosphatidylethanolamine (PE) are confined to the cytoplasmic face of membranes (Leventis and Grinstein, 2010). The maintenance of lipid asymmetry under homeostatic conditions is under the control of transporters called flippases and floppases (Contreras et al., 2010). A third type of enzyme known as scramblases, contributes to the loss of lipid asymmetry and increased PS extracellular exposure when activated (Bevers and Williamson, 2010).

Loss of membrane asymmetry and PS externalization on the outer leaflet of the plasma membrane are common features of apoptotic cells, independent of the form of apoptotic stimulus (Fadok et al., 1992b). During apoptosis, scramblase XK-related protein 8 (Xkr8) gets activated by caspase cleavage, and mediates PS externalization in a Ca^{2+} independent manner (Suzuki et al., 2013). Recent studies identified adenosine triphosphate type 11C (ATP11C) and cell division cycle protein 50A (CDC50A) as being involved in apoptotic PS exposure (Segawa et al., 2014). ATP11C, a flippase responsible for redirecting PS from the outer to the inner leaflet, is inactivated by caspase mediated cleavage (Segawa et al., 2014). CDC50A is required for localization of ATP11C to the plasma membrane, and knockout of CDC50A results in constitutive PS exposure (Segawa et al., 2014). These data strongly indicate that during apoptosis, caspase mediated activation of Xkr8 and caspase mediated inactivation of ATP11C work in a coordinated fashion to permit PS exposure. However, PS exposure is not restricted to apoptotic cells alone, but may also be seen on activated platelets (Lentz, 2003). Transmembrane Protein 16F (TMEM16F), which has a Ca^{2+}-dependent phospholipid scramblase activity, was identified as a mediator of PS externalization in activated platelets (Suzuki et al., 2010, Yang et al., 2012). Studies confirmed that PS externalization was not just an indicator of loss of membrane asymmetry during apoptosis, but has an important active function to play in the clearance of apoptotic cells by acting as a recognition signal for phagocytic cells (Fadok et al., 1992a, Fadok et al., 1992b). Apart from PS externalization, other biochemical features include DNA fragmentation,

degradation of cytoskeletal and nuclear proteins, and extensive protein cross-linking.

1.2.2.2 Morphological Features

Apart from these biochemical changes that occur in apoptotic cells, several dramatic morphological alterations are also key events when cells die by apoptosis (Kerr et al., 1972). Broadly termed as the execution phase of apoptosis, these structural modifications include cell shrinkage, chromatin condensation, nuclear fragmentation, and formation of dynamic plasma membrane protrusions called blebs that eventually detach, culminating in fragmentation into apoptotic bodies. Blebs are formed when cell membrane delaminate from cortical cytoskeletal structures (Figure 1-3). Two phases of plasma membrane blebbing were reported in apoptotic cells, with the first phase occurring concomitant with cell detachment (Lane et al., 2005). Several non-adherent cell lines fail to display this first phase of blebbing, suggesting a role for the initial phase in maintaining detachment from substrate and/or neighbouring cells (Lane et al., 2005). The second phase observed in both adherent and non-adherent cells, results in the formation of blebs that contain chromatin and other cellular contents (Lane et al., 2005). These membrane protrusions and apoptotic bodies serve as concentration sites for phagocytic markers allowing efficient detection and engulfment by patrolling phagocytes and/or neighbouring cells (Korb and Ahearn, 1997, Ogden et al., 2001).

Caspases play major roles both in the commitment phase and in the execution phase of apoptosis through their cleavage of numerous protein substrates. Adherent cells retract from neighbouring cells and from extracellular substrates via caspase cleavage of ß-catenin, a critical regulator of adherens junctions (Brancolini et al., 1997) and focal adhesion proteins like tensin (Kook et al., 2003). Caspase-mediated cleavage and weakening of nuclear structural lamin proteins, as well as contractile force generated by the actin myosin cytoskeleton, results in nuclear fragmentation and redistribution of chromatin to the blebs and apoptotic bodies (Croft et al., 2005). Packaging of intracellular contents into membrane bound apoptotic bodies is believed to be crucial in avoiding unwanted inflammatory responses by preventing the release of potential self-antigens into the surrounding milieu.

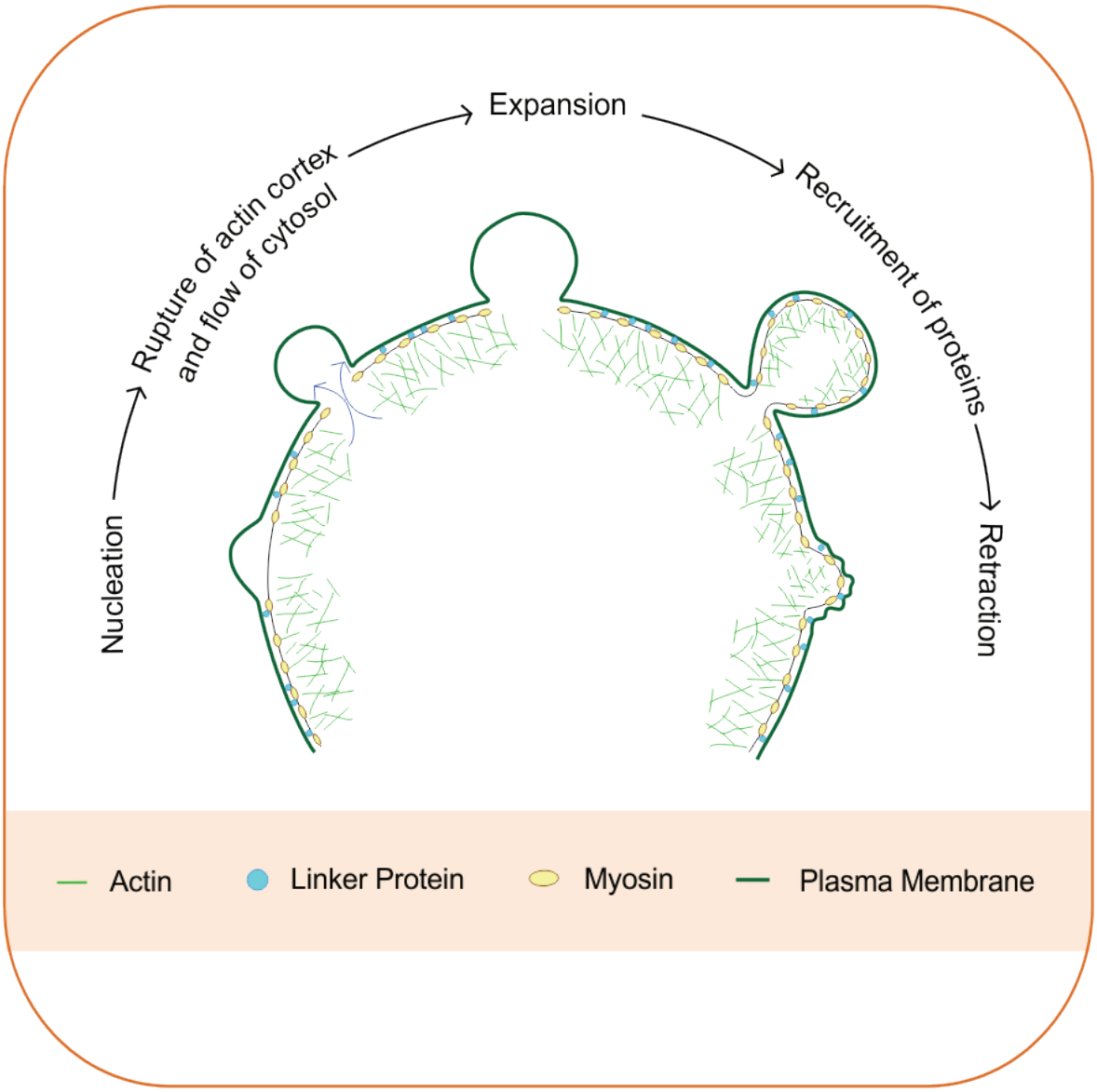

Figure 1-3 Life cycle of a bleb

Life cycle of a bleb can be subdivided into steps: nucleation, expansion and retraction. Blebs are produced when cell membrane delaminates from the cortical cytoskeleton. Pressure generated by actomyosin contraction and flow of cytoplasm expands the newly formed blebs. Proteins recruited into blebs contribute to contractility and subsequent bleb retraction. Figure adapted from (Julian and Olson, 2015).

1.2.3 ROCK1 and Apoptotic Blebbing

Although blebbing may be observed during several cellular processes including cytokinesis, migration and spreading, arguably its most totemic manifestation is during the execution phase of apoptosis (Fadok et al., 1992b). Despite being one of the hallmark features of apoptosis, little was known about the mechanistic drivers underlying this phenomenon until the 1990s. Various studies showed that reorganization of cytoskeletal structures drives the formation of membrane blebs and apoptotic bodies (Mills et al., 1998). Disruption of filamentous actin inhibited the formation of apoptotic bodies without affecting DNA fragmentation, indicating a requirement for polymerized actin during the later stages of apoptosis (Cotter et al., 1992). One early study implicating myosin contraction in bleb formation showed that microinjecting an active form of myosin light chain kinase (MLCK) resulted in active surface blebbing during mitosis (Fishkind et al., 1991). Subsequently, it was shown that blebbing cells had increased levels of myosin II regulatory light chain phosphorylation and that inhibition of MLCK activity decreased blebbing (Mills et al., 1998). Actin-myosin contractile force generation results from the phosphorylation of the regulatory myosin light chains, which promotes myosin binding to filamentous actin, coupling of actin-myosin filaments to linker proteins at the plasma membrane, and ATP-dependent actin-myosin filament contraction (Somlyo and Somlyo, 1994, Somlyo and Somlyo, 2003). Inhibition of myosin contractility with the myosin II ATPase blocker blebbistatin, reduced apoptotic blebbing (Orlando et al., 2006).

Apoptotic membrane blebbing was found to be dependent on ROCK activity and independent of the function of its upstream regulator, RhoA (Coleman et al., 2001, Sebbagh et al., 2001). During apoptosis, activated caspases cleave ROCK1 after a DETD (amino acids 1110-1113) sequence, thus removing the auto-inhibitory C terminal region and generating a truncated kinase fragment with increased intrinsic activity. The ROCK kinase fragment generated can phosphorylate downstream targets including MLC, leading to actin-myosin contractile force generation, cell contractility, and consequent membrane blebbing and apoptotic body formation. The significance of ROCK1 for apoptotic blebbing has been shown in other cell types, including cardiac myocytes, lymphoma cells and non-small cell lung carcinoma cells (Parent et al., 2005,

Chang et al., 2006, Zihni et al., 2007). Of notable importance was the relocalization of fragmented DNA into blebs and apoptotic bodies upon caspase activated ROCK1 cleavage (Coleman et al., 2001). In addition to these morphological responses, ROCK1 activity was also required for nuclear envelope tearing and disintegration (Croft et al., 2005). During the early stages of rapid membrane blebbing and apoptotic body release, there may be leakage of damage associated molecular pattern (DAMP) proteins, such as nucleosomal histones, highlighting a possible role for blebbing cells and apoptotic bodies to alert the immune cells for efficient phagocytic uptake prior to secondary necrosis (Wickman et al., 2013).

However, during cell death induced by natural killer cells, Granzyme B cleaves ROCK2 at a homologous position to the caspase-cleavage site on ROCK1, leading to constitutive ROCK2 activation that is sufficient to promote caspase-independent membrane blebbing (Sebbagh et al., 2001). However, given that Granzyme B also activates caspases leading to ROCK1 activation, the only apparent situation in which ROCK2 would be activated without concomitant ROCK1 activation in apoptotic cells is in cells that selectively express ROCK2 with little to no ROCK1 expression.

1.3 Blebbing and Apoptotic Cell Clearance

1.3.1 The Decisive Phase of Apoptosis: Efferocytosis

Clearance of apoptotic cells, also known as 'efferocytosis' is the ultimate, and arguably the most important step of programmed cell death. Elegant genetic studies in the nematode *C. elegans* suggested a tight coordination between cell death and clearance pathways resulting in removal of apoptotic cells before they were fully dead (Reddien et al., 2001, Hoeppner et al., 2001). Swift removal and degradation of apoptotic corpses is crucial for immune tolerance and for the maintenance of tissue homeostasis. Several significant studies over the years have improved our understanding of this complex and evolutionarily conserved process. Multicellular organisms are bestowed with specialized cells called 'phagocytes' such as macrophages and immature dendritic cells, resident in most tissues and dedicated to the engulfment and prompt removal of apoptotic cells. However in some tissues, neighbouring epithelial and mesenchymal cells are designed to function as 'nonprofessional' phagocytes and engulf nearby apoptotic cells (Wood et al., 2000, Nandrot et al., 2004, Monks et al., 2008). These professional and non-professional phagocytes efficiently remove enormous numbers of unwanted, excess and damaged cells prior to the loss of their plasma membrane integrity. Rapid engulfment would prevent leakage of potentially damaging intracellular contents into the extracellular milieu, thereby mitigating damage.

To date, a wide range of apoptotic cell derived ligands, phagocytic receptors and ligand-receptor bridging molecules involved in corpse removal have been identified. In order to simplify the complex clearance mechanism, the process is broadly divided into several steps, specifically the recruitment of phagocytes to the site of apoptotic cells through 'find me' signals, the recognition by phagocytes through 'eat me' signals displayed by apoptotic cells, and finally the ingestion of apoptotic corpses and post engulfment consequences. As discussed previously, apoptotic cells undergo several distinct morphological changes to facilitate their recognition and clearance. How these typical morphological features may interplay with the different steps of clearance mechanism to expedite the 'safe' removal of apoptotic cells in an immunologically quiescent manner will be discussed here.

1.3.1.1 Recruitment Phase: 'Find me' signals

Locating dying cells prior to the loss of their plasma membrane integrity and the ensuing irrevocable damage is a crucial step for efficient phagocytosis. A growing list of 'find me' signals released by dying cells to attract phagocytes has been reported over the last decade. These include lysophosphatidylcholine (LPC), sphingosine-1-phosphate (S1P), chemokine CX3CL1 (Fractalkine FKN) and nucleotides ATP and UTP (Lauber et al., 2003, Gude et al., 2008, Truman et al., 2008, Elliott et al., 2009). LPC and S1P are lipid signals secreted by apoptotic cells and recognized by G-protein coupled receptors G2A and S1P-R, respectively on phagocytes (Peter et al., 2008, Rosen and Goetzl, 2005). Although these lipid ligands have been shown to stimulate macrophage chemotaxis to the proximity of apoptotic cells, their role in an *in vivo* context is yet to be established (Lauber et al., 2003, Gude et al., 2008). The chemokine CX3CL1 was shown to attract macrophages to apoptotic B cells in germinal centres but knocking out its macrophage receptor CX3CR1 failed to exhibit an increased persistence of apoptotic cells or accumulation of secondary necrotic cells, suggesting that the chemokine was only responsible for recruiting the macrophages but was not required for clearance (Truman et al., 2008). Small amounts of nucleotides ATP and UTP are also released as chemotactic signals by apoptotic cells through the pannexin 1 (PANX1) channels and they mediate phagocyte recruitment via P2γ2 receptors (Elliott et al., 2009, Chekeni et al., 2010). Disruption of this ligand receptor interaction resulted in accumulation of apoptotic cells in the thymus suggesting a clear relationship between 'find me' signals and efficient clearance (Elliott et al., 2009). Release of multiple signals from apoptotic cells to mediate phagocyte attraction suggests plausible molecular redundancy to ensure fast and proficient removal of apoptotic debris.

The range of these 'find me' signals may be quite short (Elliott et al., 2009), but this may suffice for tissues which are granted the luxury of having their very own resident phagocytes, possibly in close proximity to a dying cell. However, attracting distant tissue phagocytes or phagocytes from the circulation may be challenging for these short range signals. Our recent studies showed that limited membrane permeabilization occurs in blebs and apoptotic bodies which allows the release of damage associated molecular pattern proteins (DAMPs) during early apoptosis (Wickman et al., 2013). DAMPs are intracellular contents that

when released by dying or dead cells can interact with immune cells through Toll like receptors (TLRs) and activate them (Chen and Nunez, 2010). One could speculate that these membrane delimited fragments that are produced during cell death would enable long distance dispatching of 'find me' signals (Gregory and Pound, 2010).

1.3.1.2 Recognition Phase: 'Eat me' Signals

For phagocytes to distinguish a dying cell from its healthy viable counterparts, a number of surface markers adorn the apoptotic cell. These 'eat me' signals not only serve as recognition molecules, but also aid in establishing a physical contact between the phagocyte and the apoptotic cell. Of notable importance is the exposure of otherwise confined inner membrane lipid phosphatidylserine (PS) (Fadok et al., 1992b) as discussed in the previous sections. Over the years, many membrane receptors responsible for PS recognition has been identified including BAI1, Stabilin 2 and members of the T cell immunoglobulin domain (TIM) protein family (Park et al., 2007, Park et al., 2008a, Kobayashi et al., 2007, Miyanishi et al., 2007). In addition to these bona fide receptors that bind to PS directly, several bridging molecules that engage with phagocytic receptors and PS simultaneously have been identified. Milk fat globulin EGF factor 8 (MFG-E8) is a bridging molecule secreted by macrophages that binds to PS on apoptotic cells and mediates uptake by engaging with $\alpha_v\beta_3$ integrins on phagocytes (Hanayama et al., 2002). Other bridging molecules including protein S and GAS6 that can also bind to PS and in turn be recognized by phagocytic cell surface receptors such as the Tyro3-Axl-Mer family of receptors (Anderson et al., 2003, Ishimoto et al., 2000). The need for multiple recognition mechanisms for just one 'eat me' signal is possibly a testament of the importance for the efficient clearance of apoptotic debris.

However, externalized PS has also been detected on some viable cells (Lentz, 2003) suggesting that additional signals are necessary to trigger phagocytosis. In addition it was also proposed that the exposure of PS must be above a certain sensitivity threshold to initiate the engulfment phase (Borisenko et al., 2003). This proposal was challenged recently by studies showing that both viable and apoptotic cells exposing PS can be engulfed by macrophages (Segawa et al.,

2014). This suggested the need for other ‘eat me’ signals to act in concert with PS to aid efficient phagocytosis. Other ‘eat me’ signals identified includes Calreticulin and Annexin I (Gardai et al., 2005) (Arur et al., 2003). Calreticulin is translocated from the endoplasmic reticulum to the plasma membrane during apoptosis and acts together with PS and drives optimal efferocytosis (Gardai et al, 2005). Exposed calreticulin is detected by LDL-receptor related protein (LRP) on phagocytes, which stimulates the final engulfment phase (Gardai et al., 2005). Annexin I is another intracellular protein that is externalized during cell death and identified to co-localize with PS and facilitates phagocytic uptake of the apoptotic cell (Arur et al., 2003, Blume et al., 2009).

The role of apoptotic blebbing in the clearance of dying cells could also be envisioned during the recognition phase of efferocytosis. Apoptotic blebs may be able to serve as focal points for the aggregation of ‘eat me’ signals including PS. For example, complement C1q specifically and directly binds to apoptotic blebs on apoptotic keratinocytes, endothelial cells and peripheral blood mononuclear cells and expedites engulfment by phagocytes by engaging with their C1q receptors (Korb and Ahearn, 1997, Navratil et al., 2001). Concentration of ‘eat me’ signals on blebs may orchestrate rapid and efficient efferocytosis (Wickman et al., 2012).

1.3.1.3 Engulfment Phase

Molecular tethering between the phagocyte and the ‘eat me’ signal initiates a signalling cascade within the phagocytes that drives cytoskeletal reorganization to enable engulfment of apoptotic corpses. Deeper insights into the engulfment machinery came from numerous genetic studies on *C.elegans, D.melanogaster* and mammalian models. Two Rac dependent engulfment pathways, which are evolutionarily conserved, were identified. The first pathway involved proteins including Dock180, CrkII and ELMO (Wu and Horvitz, 1998, Reddien and Horvitz, 2000, Gumienny et al., 2001). Upon receiving cues from the receptor-ligand interaction, ELMO functionally co-operates with Dock180 and CrkII, which finally leads to Rac1 activation (Gumienny et al., 2001). The second conserved signalling pathway involves engagement of LRP receptors on phagocytes by ligands like calreticulin causes direct interaction with adaptor protein GULP, resulting in downstream Rac activation (Su et al., 2002). Similarly, Stabilin 2

receptor which binds to PS can also interact with GULP to initiate uptake of PS bound apoptotic cells (Park et al., 2008b). This culminates in cytoskeletal rearrangements in phagocytes, thus facilitating internalization of apoptotic debris. The ingested apoptotic corpse is then processed via the phagolysosomal pathway (Kinchen and Ravichandran, 2010).

The functional significance of blebbing and apoptotic body formation has not been defined yet, but it has been hypothesized that fragmentation of an apoptotic cell into 'bite- sized' apoptotic bodies may have a beneficial effect in phagocytosis (Fadeel, 2004). In vitro studies suggest that ROCK1 mediated fragmentation of apoptotic cells is important for phagocytosis (Orlando et al., 2006). However, it remains to be seen if this holds true in an in vivo context across all cell types, because it is possible that smaller cells like the immune cells may not require fragmentation to be easily engulfed.

1.3.2 Microenvironmental Effects of Apoptotic Cell Clearance

While the effect of apoptotic cells on phagocytes that come in direct contact with them have been extensively studied, recent years have seen an escalating interest in understanding the effect of apoptotic cell clearance on their microenvironment. Conditioning the microenvironment mostly occurs through the release of physiological mediators by apoptotic cells and the participating phagocytes.

Apart from the physical clearance of dying cells that prevents the release of toxic intracellular contents into the surrounding milieu, perhaps the most celebrated effect of efferocytosis is the suppression of an inflammatory response thus facilitating an 'immunologically silent' clearance of apoptotic cells. Various studies have shown that apoptotic cells not only discourage the production of pro-inflammatory cytokines like TNFα, IL-1ß, IL-8 and IL-12 by the phagocytes but also stimulate them to produce anti-inflammatory mediators such as TGF and IL-10 (Voll et al., 1997, Fadok et al., 1998, McDonald et al., 1999). Intuitively, the first step in achieving this feat is recruiting the right kind of phagocyte. In concert with the classical 'find me' signals, 'keep out' signals like lactoferrin, which inhibits granulocyte (pro-inflammatory) recruitment, are also released from apoptotic cells (Bournazou et al., 2009, Bournazou et al., 2010). In addition to inhibiting granulocyte migration, lactoferrin also inhibits pro-inflammatory mediators and promotes the production of anti-inflammatory mediators (Crouch et al., 1992, Togawa et al., 2002). It is interesting to note that anti-inflammatory mediators can also increase the capacity of phagocytes to engulf apoptotic material (Chung et al., 2006). However, the widely accepted notion of apoptotic cell death being immunologically silent has been challenged before by studies showing that apoptotic cells can stimulate the production of pro-inflammatory mediators (Lucas et al., 2003, Kurosaka et al., 2003). This may be due to fact that in some cases the apoptotic cells are progressing to secondary necrosis thus resulting in a shift from 'silent' to an inflammatory state. It is also possible that pro-inflammatory cytokine release precedes anti-inflammatory mediator release (Lucas et al., 2003). This complex interplay and balancing act between the apoptotic cells and phagocytes creates a microenvironment conducive for maintaining tissue homeostasis.

Cellular responses to apoptotic cells and their clearance are not limited to the responding phagocytes. As mentioned earlier, neighbouring epithelial and mesenchymal cells can also act as non-professional phagocytes to dispose apoptotic debris. In fact, eliminating macrophages in the mouse embryo resulted in the phagocytosis duty being taken up by neighbouring mesenchymal cell (Wood et al., 2000). This not only underscores the apparent redundancy in apoptotic cell clearance but also highlights a type of microenvironmental conditioning. In addition to this, apoptotic cells can also directly produce factors or stimulate neighbouring cells to produce factors that promote proliferation and angiogenesis, thus aiding in the repair process (Knies et al., 1998, Morimoto et al., 2001, Golpon et al., 2004, Hristov et al., 2004). Thus it is conclusive that apoptotic cell clearance has the potential to induce major effects on cells in the near vicinity as well as at long distance.

1.3.3 Consequences of Defective Apoptotic Cell Clearance

Considering the fact that apoptotic cell clearance machinery in multicellular organisms is complex and highly efficient, it is not surprising that any defects in this process can have pathological consequences. Uncleared dead cells can have significant implications on the immune system and the neighbouring cells. Here, I will highlight some of the main pathologies linked to defective apoptotic cell clearance (Table 1-2). The link between apoptotic clearance defects and cancer will be discussed in the forthcoming section.

1.3.3.1 Autoimmunity

Apoptotic clearance defects have been associated with autoimmune disorders like systemic lupus erythematosus for a long time (Herrmann et al., 1998, Baumann et al., 2002, Perniok et al., 1998). Persisting dead cells may become necrotic, thus releasing their intracellular contents, which would provoke autoantibody production against the intracellular antigens and DNA. Patients with systemic lupus erythematosus (SLE), a chronic autoimmune disorder affecting multiple organs, have autoantibodies in the sera that are specific for nuclear components (Rumore and Steinman, 1990). There is also an increase in the level of circulating apoptotic cells, and in some SLE patients macrophages exhibit reduced ability to engulf apoptotic cells (Herrmann et al., 1998, Perniok

et al., 1998, Baumann et al., 2002). Several genetic models bearing defects in different components of the clearance pathway have suggested a strong link between apoptotic cell clearance defects and autoimmunity (Table 1-2). Nevertheless, it should be noted that defective clearance does not always result in an autoimmune phenotype as evidenced by studies in CD14 knockout mice and mannose binding lectin deficient mice (Devitt et al., 2004, Stuart et al., 2005). Whether the uncleared apoptotic cells in these mice retain the ability to induce an immunomodulatory environment to curtail autoimmunity still remains to be answered. Also, the existence of panoply of apoptotic signals, receptors and bridging ligands suggests a high level of redundancy proposing a possible explanation for this discrepancy.

1.3.3.2 Atherosclerosis

Atherosclerosis is a life threatening disease, which involves chronic inflammation of the vascular wall. Monocytes and macrophages play a crucial role in the formation of atherosclerotic plaques and a documented characteristic of such plaques is the accumulation of cell debris during progression towards advanced stages (Tabas, 2010). At the onset of plaque formation, macrophages take up lipids, and these lipid-laden macrophages eventually die and get engulfed by surrounding macrophages. However, as the plaque lesion expands, there is increased cell death and reduced engulfment of apoptotic macrophages. These uncleared apoptotic cells ultimately become necrotic, causing plaque rupture thus leading to thrombosis (Tabas, 2010). Intuitively, the persistence of apoptotic cells was linked to plaque progression. Indeed, defects in some components of the clearance pathway caused acceleration of atherogenesis in atherosclerotic mouse models like LDLR-/- and ApoE-/- (Table 1-2). These genetic studies highlighted the importance of clearance of dead cells from atherosclerotic lesions to curb its progression to advanced stages. Contrary to this, Gas6 deficiency on an atherosclerotic background has a favourable outcome in that it formed stable plaques with smaller necrotic cores suggesting the likelihood of other physiological functions for these ligand-receptors interactions apart from engulfment itself (Lutgens et al., 2008).

1.3.3.3 Respiratory Diseases

Persistence of apoptotic cells has been observed in a number of human lung diseases including cystic fibrosis, chronic obstructive pulmonary disease, asthma and acute lung injury (Yun et al., 2008). Although these pathologies have not been directly linked to defects in components of the clearance pathways, alveolar macrophages from patients show decreased ability to phagocytose apoptotic cells (Hodge et al., 2007, Vandivier et al., 2009). In fact, potentially harmful environment like cigarette smoke can hamper the phagocytic ability of alveolar macrophages (Kirkham et al., 2004, Hodge et al., 2007). Although chronic inflammation in the lung seems to be associated with uncleared dead cells, additional investigations are essential to understand whether defects in the clearance mechanism can influence pathogenesis of these lung diseases.

1.3.3.4 Neurological Diseases

In the brain, microglia serves as primary phagocytes that respond to apoptotic cells. Several chronic neurodegenerative disorders like Parkinson's (Mochizuki et al., 1996), Alzheimer's (Su et al., 1994) and Huntington's disease (Thomas et al., 1995) exhibit uncleared apoptotic cells in the brain. Mice deficient in fractalkine receptor, CX3CR1 in the brain microglia resulted in increased accumulation of apoptotic neurons thus suggesting an important role for 'find me' cues from dying neurons (Cardona et al., 2006). Additionally, reduced levels of bridging molecule MFG-E8 was reported in patients with Alzheimer's disease (Boddaert et al., 2007).

Model	Function	Phenotype	References
MFG-E8-/-	Bridging ligand	Autoantibodies, Splenomegaly, Glomerulonephritis	(Hanayama et al., 2004)
αv-/-(conditional knockout)	Phagocyte receptor	Autoantibodies, Ulcerative colitis	(Lacy-Hulbert et al., 2007)
C1q-/-	Bridging ligand	Autoantibodies, Glomerulonephritis	(Botto et al., 1998)
mer^{kd} (functional knockout)	Receptor for Gas6	Autoantibodies, Mild renal pathology	(Cohen et al., 2002)
TIM-4-/-	Receptor for PS	Autoantibodies	(Rodriguez-Manzanet et al., 2010)
TG-/- (LDLR-/-)	Crosslinking enzyme	Increased atherosclerotic lesions	(Boisvert et al., 2006)
mer^{kd} (ApoE-/-)	Receptor for Gas6	Increased plaque necrosis	(Thorp et al., 2008)
GAS6-/-(ApoE-/-)	Bridging ligand	Stable atherosclerotic lesions	(Lutgens et al., 2008)

Table 1-2: Genetic mouse models with apoptotic cell clearance defects and associated phenotypes

1.4 Role of Apoptotic Blebbing in Tumourigenesis

The preceding section had focussed on the complex mechanism of apoptotic cell clearance and how the interplay between apoptotic cells and phagocytes manipulates the microenvironment in an immunological context to maintain tissue homeostasis. In situations where this highly efficient efferocytosis mechanism is disrupted, the apoptotic debris can challenge the otherwise normally ensuing immunological tolerance. High levels of cell death can occur within the tumour microenvironment. Whether efficient apoptotic cell clearance has a beneficial or detrimental effect in neoplastic progression has been a topic of debate over many years. Given the fact that efferocytosis has a significant impact on the immune microenvironment as discussed in the previous section, it seems logical to explore the role of immune system in cancer development and progression. In this section, I will discuss how the immune system sculpts the tumour microenvironment, and finally will consider the consequences of apoptotic cell clearance in a cancer context.

1.4.1 Cancer and Inflammation

A link between the cancer development and chronic inflammation has been appreciated since the 19th century. There is considerable evidence which points towards an association between inflammation and a predisposition for cancer development (Grivennikov et al., 2010). Chronic inflammatory conditions including hepatitis, bronchitis and gastritis precede tumour development. About 18 % of the global cancer burden is attributed to chronic inflammation caused by infectious agents (Parkin, 2006). Classic examples include increased risk of cervical and hepatocellular cancer with human papilloma virus or hepatitis virus infection, respectively. Not only do viral infections contribute to cancer, infections caused by bacteria *Helicobacter pylori* can result in gastric cancer, and parasitic infection with *Schistosomiasis* can cause bladder cancer (Balkwill and Mantovani, 2001). In other cases, conditions associated with chronic irritation and inflammation such as long term exposure to silica, asbestos and cigarette smoke also predispose individuals to cancer (Coussens and Werb, 2002). Figure 1-4 shows the various stages at which inflammation can contribute to tumourigenesis.

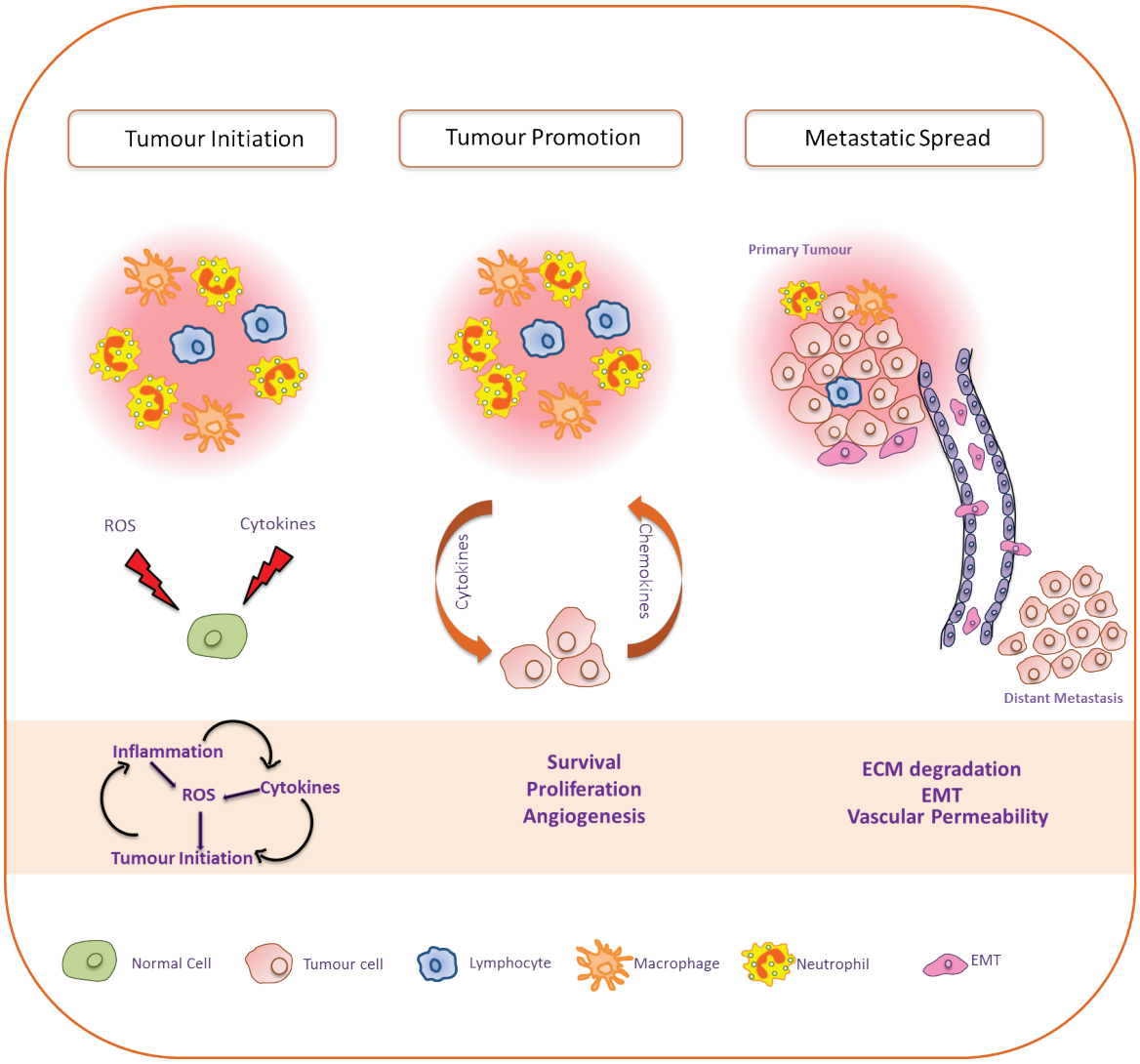

Figure 1-4 Multifaceted role of inflammation in cancer
Inflammation can contribute to tumour initiation, promotion and metastasis. Reactive oxygen species (ROS) produced by inflammatory cells can cause tumour-initiating mutations. Inflammatory cells also secrete cytokines that supports survival, proliferation and angiogenesis during tumour promotion. Tumour cells produce chemokines that attract more inflammatory cells. Eventually, inflammation can also contribute to metastasis by producing mediators that increases vascular permeability. ECM = extracellular matrix; EMT= epithelial to mesenchymal transition. Figure adapted from (Grivennikov et al., 2010).

1.4.2 Immunosurveillance of Tumours

Although a causal relationship between inflammation and cancer is widely accepted, it is necessary to consider a protective effect of inflammation against tumourigenesis. In multicellular organisms, an inflammatory response orchestrates defence against microbial infections as well as mediates tissue repair and regeneration. By protecting the host against microbes, indirectly the host is also protected from pathogen-induced tumours. By the rapid elimination of pathogens, the immune system ensures resolution of inflammation thus preventing the establishment of an inflammatory microenvironment. The immune system can also specifically target and eliminate tumour cells, and this is called cancer immunosurveillance.

In 1909, Paul Ehrlich made the prescient hypothesis that the immune system can protect the host from cancer development (Ehrlich, 1909). This concept was formally introduced in 1957 by Burnet and Thomas as cancer immunosurveillance (Burnet, 1957). Although early experiments failed to establish this hypothesis possibly due to limitations in the mouse models available, by the 1990s, several studies reinstated support for this concept (Dunn et al., 2004). Removal of specific components of the immune system in mouse models resulted in increased tumour incidence and broader tumour spectra suggesting that the immune system can serve as an extrinsic tumour suppressor (Swann and Smyth, 2007). Furthermore, mice immunized with tumours were protected against subsequent challenge by the same tumours, thus suggesting the existence of tumour antigens, which is considered important for cancer immunosurveillance (Old and Boyse, 1966, Klein, 1966). In humans with immunodeficiencies or in patients undergoing immunosuppressive therapy, there was an increased incidence of malignancies (Gatti and Good, 1971, Penn and Starzl, 1970). These studies strongly supported a beneficial role for the immune system in curbing the development of cancer.

1.4.3 Immunoediting: A Refined Model for Cancer Immunosurveillance

Despite the protection offered by immunosurveillance, tumours still develop in the presence of a functioning immune system. To explain this discrepancy, the

concept of immunoediting was introduced in 2002, which offers a better explanation concerning the role of immune system in tumour development (Dunn et al., 2002). The concept of immunoediting is divided into three phases namely elimination, equilibrium and escape (Figure 1-5).

1.4.3.1 Elimination

The elimination phase is based on the original concept of immunosurveillance, in which the innate and adaptive immune systems work in concert to detect and destroy cancer cells to limit tumour development. Although still not comprehensive, the mechanism by which immune cells are summoned to a neoplastic site is thought to be through the release of danger signals like HMGB1 by the damaged tumour cells (Sims et al., 2010). The immune cells can distinguish the tumour from normal cells by the presence of tumour specific antigens. A number of tumour antigens have been identified in humans including mutational antigens (aberrant p53), differentiation antigens (melanocyte differentiation antigen), viral antigens, overexpressed antigens (HER2) and Cancer-Testis (CT) antigens (Boon and van der Bruggen, 1996, Old and Chen, 1998, Rosenberg, 1999). Of course, if a tumour is successfully eradicated during this phase, the immunoediting process has been completed. With the next two phases, the discrepancy in the immunosurveillance model was addressed.

1.4.3.2 Equilibrium

The tumour cells that manage to survive the elimination phase may then enter the equilibrium phase and are maintained in a functional state of dormancy. The survivors would be variants of the tumour cells with several genetic and epigenetic changes thus giving them increased resistance to immune attack (Mittal et al., 2014). Although the molecular mechanisms for this phase remain poorly understood, indications of the existence of an equilibrium phase came from experiments showing that immunocompetent mice treated with low dose carcinogen harboured tumour cells for an extended period of time (Koebel et al., 2007, Teng et al., 2012). Experiments to provide conclusive evidence for the existence of this phase are awaited.

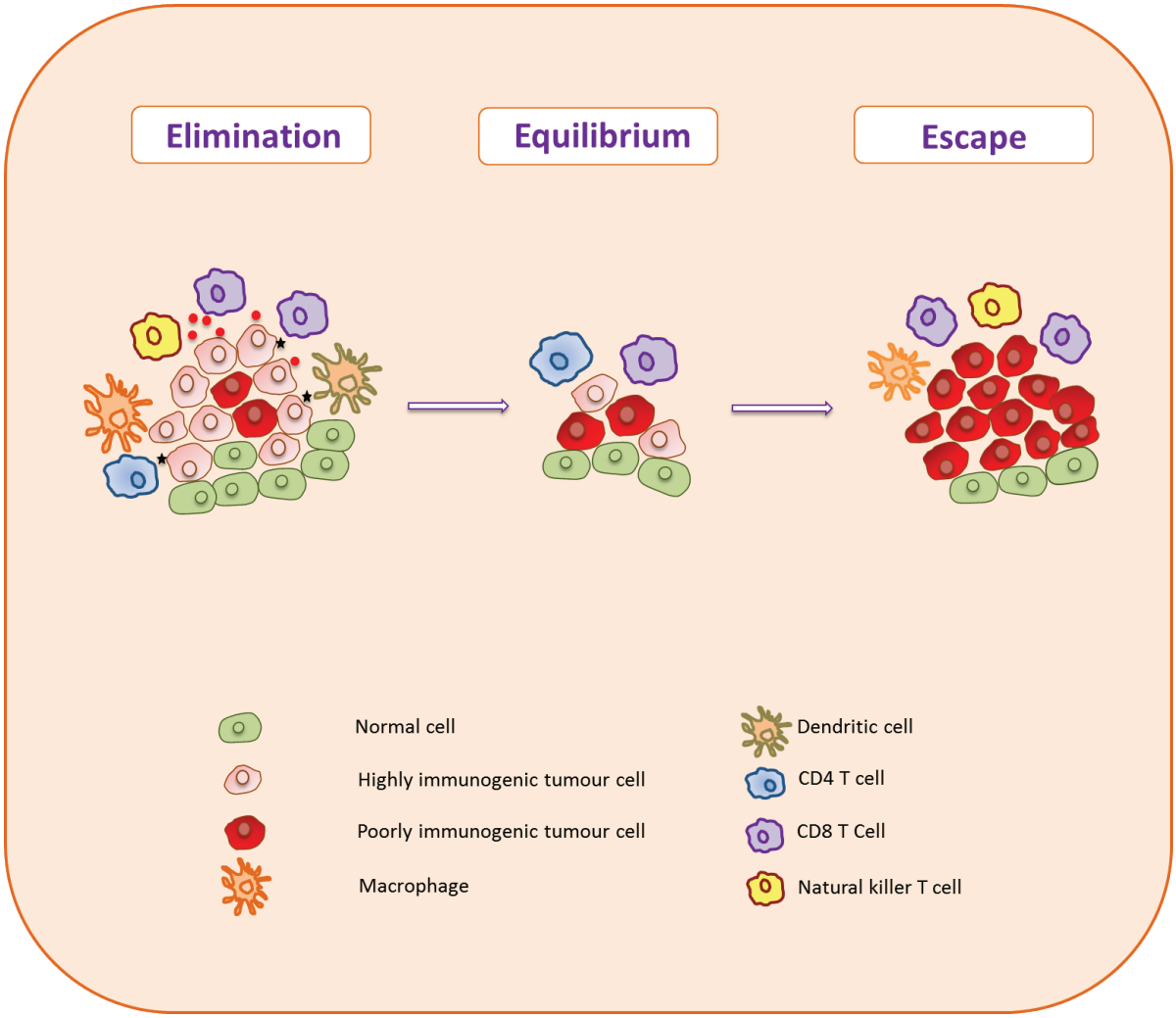

Figure 1-5 Three phases of cancer immunoediting
During the 'elimination' phase, the innate and adaptive immune systems work in concert to detect and destroy cancer cells. Immune cells are summoned by the release of danger signals (red dots) like HMGB1 by the damaged tumour cells. Immune cells distinguish tumour cells by the presence of tumour antigens (black stars) and destroy them. However, some tumour variants manage to survive the 'elimination' phase to then enter the 'equilibrium' phase. In this phase, tumour remains dormant since its growth is prevented by immunologic mechanisms. Tumour cell variants may escape the dormant stage possibly as a consequence of constant immune selection pressure. These cells soon enter the 'escape' phase, where their growth is no longer blocked by immune system. Figure adapted from (Schreiber et al., 2011).

1.4.3.3 Escape

During this phase, tumour cell variants selected during the equilibrium phase escape the dormant stage and commence expansion to form detectable tumours. Reduced recognition by immune cells, increased resistance to the cytotoxic effects of the immune system or both, are properties that have been attributed to tumour cells escaping the equilibrium phase. Tumour cells eventually may impede the establishment of anti-tumour immune response through immunosuppressive cytokines like TGF-β and IL-10 or through regulatory T cells (Khong and Restifo, 2002, Sakaguchi, 2002). Another way of escaping the immune sentinels is by losing expression of tumour specific antigens thus allowing tumour cells to hide from the immune system (Marincola et al., 2000). Additional mechanisms of escape may exist, which will help in sculpting the immunogenicity of a tumour to favour its progression.

1.4.4 Apoptotic Cell Clearance and Tumourigenesis

Given the double role of inflammation in cancer, it would be interesting to discover the role of apoptotic blebbing and apoptotic cell clearance in the development and progression of cancer. As discussed above regarding chronic inflammation driving tumourigenesis, it is easy to envisage a beneficial role for apoptotic cell clearance in limiting tumourigenesis by maintaining an immunosuppressive environment. However, considering the possibility of protection offered by the immune cells against tumours, it is possible that the immunosuppressive effect of apoptotic cell clearance could have an unwanted effect of suppressing anti-tumour immune responses.

Several studies have hinted at a plausible scenario in which efficient apoptotic cell clearance might have an untoward effect on neoplastic progression. Inhibiting PS mediated recognition of apoptotic cells by masking the receptors with Annexin V resulted in increased immunogenicity of lymphoma cells (Bondanza et al., 2004). Additionally, blocking PS mediated uptake of apoptotic cells using monoclonal antibodies also enhanced anti-tumour effects in mice (Ran et al., 2005, He et al., 2009). Blocking the bridging ligand MFG-E8 was also shown to retard the growth of tumours (Jinushi et al., 2008, Jinushi et al., 2009). Still, one needs to be careful while implicating efferocytosis in tumour

development, as it is a complex mechanism primarily designed to maintain tissue homeostasis. In fact ‘find me’ signals like ATP released by apoptotic cells can activate dendritic cells to mount an anti-tumour immune response (Ghiringhelli et al., 2009). However, apoptotic blebbing defects in the context of cancer have not been explored. It is possible that the type of immune sentinels that respond to apoptotic cells with defective blebbing as well as the differential expression of immune mediators in the tumour microenvironment might eventually dictate the direction in which the balance is tipped, namely tumour promoting or anti-tumour immunity.

2 Materials and Methods

2.1 Materials

2.1.1 Antibodies

Table 2-1 List of primary antibodies

Antigen (Clone)	Species	Supplier	Catalogue Number
BrdU (B44)	Mouse	BD Bioscience	347580
C1q (9A7)	Mouse	Abcam	ab71089
CD3 (SP7)	Rabbit	Vector	VP-RM01
CD95 (Jo2)	Mouse	BD Bioscience	554254
F4/80 (CI:A3-1)	Rat	Abcam	ab6640
Foxp3 (FJK-16s)	Rat	eBioscience	14-5773-80
HMGB1	Rabbit	Abcam	ab18256
Ki-67 (MIB-1)	Mouse	Dako	M7240
MLC	Rabbit	Cell Signalling	3672
PARP (C2-10)	Mouse	BD Bioscience	556362
pMLC	Rabbit	Cell Signalling	3674
ROCK1 (46/ROCK-1)	Mouse	BD Transduction	611136
S100A9 (M-19)	Goat	Santa Cruz	sc-8115
Tubulin-α (B-7)	Mouse	Santa Cruz	sc5286
NFKBIA (6A920)	Mouse	Abnova	MAB0057
pNFKBIA (39A1413)	Mouse	Abnova	MAB0056

Table 2-2 List of secondary antibodies

Antibody	Supplier	Catalogue Number
Alexa Fluor 594 goat anti- mouse	Invitrogen	A11032
Alexa Fluor 594 goat anti- rabbit	Invitrogen	A11037
Alexa Fluor 488 goat anti- mouse	Invitrogen	A11029
Alexa Fluor 488 goat anti- rabbit	Invitrogen	A11034

2.1.2 Buffers and solutions

Table 2-3 List of buffers and solutions

Buffer/Solution	Recipe
Citrate Buffer (pH 6)	10 mM Sodium citrate, 0.05 % Tween 20
FACS Buffer	PBS with 5% FBS
Loading Buffer (6x)	3ml 1M Tris, pH 6.8, 1.47 g SDS, 0.85 g DTT, 7.35 ml of Glycerol, 14.2 ml dH_2O and bromophenol blue (few grains)
PBS	170 mM NaCl, 3.3 mM KCl, 1.8 mM Na2HPO4, 10.6 mM H_2PO_4
PBS-T	PBS, 0.1 % Triton x-100
Phosphate Buffer (0.1 M; pH 7.2)	36 ml of $Na_2HPO_4.2H_2O$ (17.8 g in 500 ml), 14 ml of Na_2HPO_4.H20, 50 ml dH_2O (13.6 g in 500 ml)
SDS Lysis Buffer	50mM Tris, 1% SDS, pH 7.5
Sodium Cacodylate (0.1 M; pH 7.4)	4.28 g Sodium Cacodylate, 25 g Calcium chloride, 2.5 ml 0.2 N hydrochloric acid, make up to 200 ml with dH_2O
TBS	20mM Tris-HCL pH 7.5, 136 mM NaCl
TBS-T	20mM Tris-HCL pH 7.5, 136 mM NaCl, 0.1% Tween 20
Tris-EDTA Buffer	10 mM Tris base, 1 mM EDTA, 0.05 % Tween 20

2.1.3 Kits

Table 2-4 List of kits

Kit	Supplier	Catalogue Number
FITC Annexin V Apoptosis Detection Kit	BD Pharmingen	556547
Mouse Cytokine/ Chemokine Magnetic Bead Panel Kit (96-well plate assay)	Milliplex	MCYTOMAG-70K
In situ Cell Death Detection Kit, Fluorescein	Roche	11 684 795 910
ImmPRESS Anti-Goat Kit	Vector	MP-7405
ImmPRESS Anti-Rat Kit	Vector	MP-7444
M.O.M Immunodetection Kit	Vector	PK-2200
Vectastain ABC kit (Anti- Rat)	Vector	PK-6104
TNFα ELISA Kit	R & D System	MTA00B
Caspase-Glo 3/7 Assay	Promega	G8091

2.1.4 Reagents and chemicals

Table 2-5 List of reagents and chemicals

Reagent/ Chemical	Supplier	Catalogue No.
12-O-Tetradecanoylphorbol 13-acetate (TPA)	Sigma	P1585
2- Mercaptoethanol	Sigma	M3148
3,3'-Diaminobenzidine Tetrahydrochloride	Dako	K3467
ABT-199	Selleckchem	S8048
Accutase Solution	Sigma	A6964
Bafilomycin A1	Sigma	B1793
Bicinchoninic Acid	Sigma	B9643
Blebbistatin	Sigma	
Bovine Serum Albumin	Thermo	23209
C1q Protein	Abcam	ab96363
Cell Proliferation Labelling Reagent	GE Healthcare	RPN201
Collagen I	Corning	354249
Copper Sulphate	Sigma	C2284
Cycloheximide	Sigma	C4859
Diethylnitrosamine	Sigma	N0258
Dimethyl Sulfoxide	Sigma	D2650
Donor Bovine Serum	Gibco	16030-074
Dulbecco's Modified Eagle Medium (No glutamine)	Gibco	21969-035
Dulbecco's Modified Eagle Medium (No pyruvate)	Gibco	41965-039
EnVision+ System-HRP Labelled Polymer (Mouse)	Dako	K4001
EnVision+ System-HRP Labelled Polymer (Rabbit)	Dako	K4002
F-12	Gibco	21765-029
Fetal Bovine Serum	Gibco	10270
Ficoll-Paque Plus	GE Healthcare	17-1440-02
Glutaraldehyde	Sigma	G5882
Glycyrrhizin	Sigma	50531
Haematoxylin Z	CellPath	RBA-4201-00A
Hydrogen Peroxide (30% w/v)	Fisher	10687022
Liver Digest Media	Gibco	17703034

Liver Perfusion Media	Gibco	17701038
LY-294002	Cell Signalling	9901
Matrigel	Corning	354234
L-Glutamine (200 mM)	Gibco	25030-032
MEM Non-Essential Amino Acids	Gibco	11140-035
NuPAGE 4-12% Bis-Tris Gel	Life Technologies	NP0321BOX
NuPAGE MES SDS Running Buffer (20x)	Life Technologies	NP0002
NuPAGE MOPS SDS Running Buffer (20x)	Life Technologies	NP0001
NuPAGE Transfer Buffer (20x)	Life Technologies	NP0006-1
Paraformaldehyde (16%)	EMS	15710
Penicillin Streptomycin	Gibco	15140-122
Percoll	Sigma	P1644
Peroxidase Block	Dako	S2023
Ponceau S solution	Sigma	P7170
Prestained Protein Ladder	Thermo	SM0671
Primary Antibody Diluent	Dako	S2022
Proteinase K	Dako	S2032
Recombinant Mouse TNFα	R & D Systems	410-MT-050
RPMI 1640	Gibco	31870-025
RPMI 1640 (no phenol red)	Gibco	32404-014
Triton X-100	Thermo	28314
Trypsin-EDTA (0.05%)	Gibco	25300-054
Tween-20	Sigma	P1379
Vectashield DAPI (hard set)	Vector	H-1500
Vybrant DiO Cell Labelling Solution	Molecular Probes	V-22886
William's E Media	Gibco	22551-022
Y-27632	R & D Systems	1254

2.2 Methods

2.2.1 Animals

2.2.1.1 Mouse Models

ROCK1nc mice were generated at the Beatson Institute (Chapter 3). 129-Trp53tm1Tyj/J and 129/Sv were obtained from Charles River, UK. Eμ-myc mice and Tyr-Cre mice were kindly provided by Dr. Karen Blyth and Prof. Laura Machesky, respectively.

2.2.1.2 Maintenance and Breeding

All animal work was carried out in accordance with UK Home Office regulations in line with Animals (Scientific Procedures) Act 1986 and the European Directive 2010/63/EU. Mice were bred and maintained at the Beatson Institute Animal Facility. Ear notching and general maintenance (food, water and housing) was carried out by the Biological Services Unit at the Beatson Institute. Experimental cohorts and breeding stocks were routinely checked for health concerns. Animals were humanely culled using Schedule 1 techniques as stipulated in our project licence.

2.2.1.3 Animal Genotyping

For routine genotyping, all animals were ear notched at weaning and samples sent to Transnetyx (Cordova, TN, US) genotyping service for analysis.

2.2.1.4 Preparation and administration of substances

2.2.1.4.1 Diethylnitrosamine for acute studies

To prepare Diethylnitrosamine (DEN) for administering into mice, 100 ml of sterile PBS was injected into the bottle containing 1 g of DEN to give a final concentration of 10 mg/ml. The procedure was performed in the fume hood. For short-term studies assessing DEN-induced hepatic injury, mice were treated with a single dose of DEN at 100 mg/kg body weight by intraperitoneal injection and culled at 24, 48, 72 and 96 hours after DEN administration.

2.2.1.4.2 Diethylnitrosamine for tumour studies

For long-term studies of liver tumour development and survival, 14-day old mice were treated with a single dose (40 µl/ 400 µg) of DEN by intraperitoneal injection.

2.2.1.4.3 Glycyrrhizin and Diethylnitrosamine

To prepare Glycyrrhizin (GLZ), sterile PBS was used to dissolve GLZ to a final concentration of 5 mg/ml. The solution was filtered using a 70 µm filter prior to administration by intraperitoneal injection. For Glycyrrhizin (GLZ) and DEN combination treatment, 6 doses of 200 mg/kg each of GLZ were given along with a single dose of DEN (100 mg/kg). Briefly, two doses of GLZ were given before DEN treatment and following DEN treatment, GLZ was injected twice daily for two more days. The following day, mice were sacrificed.

2.2.1.4.4 BrdU

Mice were injected intraperitoneally with 250 µl of BrdU two hours prior to sacrifice.

2.2.1.5 Tissue collection and fixation

Animals were euthanized by a Schedule 1 method using carbon dioxide inhalation, weights were recorded and blood collected for haematology or biochemistry analysis. Necropsy was performed immediately to prevent tissue autolysis. Tissues collected were fixed for at least 24 hours by immersing in 10% neutral buffered formalin. For acute liver studies, left lobe of the liver was routinely used for histological analysis and fixed in 10% neutral buffered formalin. Small pieces from the median lobe were frozen using dry ice or collected in RNALater for RNA analysis. The caudate lobe was frozen using dry ice for making cryosections.

For tumour studies, mice were examined for visible lesions in all organs. For DEN-induced hepatocellular carcinoma studies, liver weights were recorded and the number of tumours counted. Tumour foci were measured using digitised vernier callipers. Lungs were also collected to analyse metastatic lesions. All lymphoid organs including the thymus, spleen and lymph nodes were harvested and weights recorded from Eµ-myc mice. Tissue were either fixed in 10% neutral buffered formalin for histological analysis or maintained in PBS until analysis.

For p53-deficient mice, tumours were harvested and in addition heart, lungs thymus, spleen, pancreas, liver, kidneys, reproductive organs and brain were also collected routinely for histological evaluation. Fixed tissues were then processed, paraffin embedded and sectioned by the Histology Service at the Beatson Institute.

2.2.1.6 Clinical Pathology

2.2.1.6.1 Haematology

Mice were euthanized by carbon dioxide inhalation and blood samples were collected via cardiac puncture in potassium-EDTA tubes. Samples were immediately sent to Clinical Pathology Lab at University of Glasgow Veterinary School for complete haematology analysis.

2.2.1.6.2 Biochemistry: Liver Function Test

Mice were euthanized by carbon dioxide inhalation and blood samples were collected via cardiac puncture in 1.5 ml eppendorf tubes. The blood was allowed to clot at room temperature for at least 30 minutes and then centrifuged at 1500 rcf for 15 minutes at 4° C. The resulting supernatant (serum) was transferred to a fresh tube for analysis. If the serum was not analysed immediately, it was aliquoted and stored at -20° C until ready for analysis. Liver function tests were kindly performed by the Clinical Pathology Lab at the Veterinary School (University of Glasgow), where serum concentrations of ALT, total bilirubin, alkaline phosphatase, total protein, albumin and globulin were determined using an automated analyser.

2.2.2 Histology

Paraffin-embedded tissue sections of 4 µm thickness were cut and routinely stained with haematoxylin and eosin (H&E) by the Beatson Histology Service. Other standard stains performed by the Histology Service include Sirius Red, Perls Prussian Blue and Periodic Acid-Schiff. Blank paraffin sections were cut at 4 µm thickness and stored at 4° C until ready for use. Frozen liver tissue was embedded in OCT and cut at 12 µm thickness and mounted on super-frost slides. Cryosections were stored at -80°C until ready to be used.

2.2.2.1 Immunohistochemistry on FFPE Sections

Immunohistochemistry (IHC) was routinely performed on 4 µm thick formalin-fixed paraffin-embedded (FFPE) sections. IHC for F4/80, S100A9, CD3, Ki-67 and BrdU was performed by the histology service. Primary antibody dilutions are given in Table 2-6. For secondary antibody staining, either ImmPRESS kits or Envision Reagents were used by the histology service.

All other IHC stainings were performed by me. Briefly, sections were deparaffinised in xylene (3 washes of 5 minutes each) and rehydrated through decreasing concentrations of ethanol (2 washes for 3 minutes each in 100% ethanol, 1 wash for 3 minutes in 70% ethanol). Slides were then washed in distilled water (dH_2O). To unmask antigens, slides were boiled at 98° C in a water bath for the specified time in antigen retrieval buffer. The buffer used varied with the antibody in use (Table 2-6). If Proteinase K was used as the retrieval agent, then the slides where incubated at room temperature for the specified time (Table 2-6). Slides were left to cool down to room temperature for at least 30 minutes and then rinsed in distilled water. Endogenous peroxidase activity was quenched by incubating sections in 3 % H_2O_2 in PBS for 10 minutes. After slides were rinsed once in distilled water and once in TBST, the sections were blocked using blocking solution containing 5% serum (depending on the species in which the secondary antibody was raised) in TBST for 30 minutes at room temperature. Primary antibody diluted in blocking solution was added to the slides and kept in a humidified chamber for the specified time. Primary antibody dilutions and incubation times is mentioned in (Table 2-6). Slides were rinsed three times in TBST to remove excess/unbound primary antibody. HRP-labelled secondary antibody was added to the slides and incubated at room temperature for a stipulated time period at room temperature (Table 2-7). Slides were rinsed again three times in TBST before staining with 3, 3'-diaminobenzidine tetrahydrochloride (DAB), as chromogen. Sections were incubated with DAB solution until brown colour develops and the slides were immediately transferred to TBST to stop the reaction.

For counterstaining, slides were rinsed in distilled water and then stained with haematoxylin for 1 minute. After rinsing in distilled water, the slides were then transferred to Scots tap water for 1 minute or until blue colour develops to the

desired intensity. Slides were rinsed in distilled water and the sections were dehydrated using increasing concentrations of ethanol (1 wash for 3 minutes in 70% ethanol, 2 washes for 3 minutes each in 100% ethanol). Slides were then cleared by three washes in xylene for 3-minutes each, before mounting with DPX. In all staining experiments, omitting the primary antibody on one slide served as the negative control. Sections were analysed using bright field microscope (Olympus BX51) and representative images were obtained at different magnifications.

Table 2-6 Primary antibodies with dilutions, incubation conditions and antigen retrieval methods for IHC

Antigen	Dilution; Conditions	Antigen Retrieval Solution	Retrieval Method
BrdU	1:200;35 min, RT	Citrate buffer pH 6	WB; 98°C; 25 min
CD3	1:75; 35 min, RT	Citrate buffer pH 6	WB; 98°C; 25 min
F4/80	1:400; 35 min; RT	Proteinase K	10 min at RT
Foxp3	1:50; O/N; 4°C	Tris-EDTA buffer pH 9	WB; 98°C; 20 min
HMGB1	1:100; O/N; 4°C	Citrate buffer pH 6	WB; 98°C; 20 min
Ki-67	1:100; 35 min; RT	Tris-EDTA buffer pH8	WB; 98°C; 25 min
S100A9	1:1000; 35 min; RT	Citrate buffer pH 6	WB; 98°C; 25 min

Table 2-7 Secondary antibodies with dilutions and incubation conditions for IHC

Secondary antibody	Product	Dilution; Conditions
Anti-Rabbit	K4002; Dako	No dilution; 45 min, RT
Anti-Rat	PK-6104; Vectastain Kit	1:66; 30 min, RT
Anti-Mouse	PK-2200; M.O.M Kit	1:250; 10 min, RT

2.2.2.2 Immunofluorescence on Frozen Sections

Immunofluorescent staining on cryosections was performed on 12 µm thick cryosections of liver. Tissue sections were fixed by immersing the slides in pre-cooled acetone (-20°C) for 10 minutes. Slides were removed from fixative and acetone was allowed to evaporate from the tissue sections for 20 minutes. After slides were rinsed in PBS, cryosections were blocked in blocking buffer (5 % serum in PBS) for 1 hour at room temperature. Primary antibodies diluted in blocking buffer (1:100) was added to the slides and kept in a humidified chamber for 2 hours at room temperature. Slides were rinsed twice in PBS before adding secondary antibodies (1:500 in blocking buffer) and incubated for 1 hour at room temperature. Slides were then rinsed three times in PBS before mounting with Vectashield DAPI (hard set). Cryosections were analysed using fluorescence microscope (Olympus BX51) and images were obtained at 20x magnification.

2.2.2.3 TUNEL Staining

TUNEL staining was performed using the In situ cell death detection kit. Formalin fixed paraffin embedded tissue sections were deparaffinised and rehydrated. The sections were then incubated in Proteinase K solution for 15 minutes at room temperature. TUNEL reaction mixture was prepared according to manufacturer's instructions by mixing 50 µl of Enzyme solution and 450 µl of Label solution. The slides were rinsed twice in PBS and 50-100 µl (depending on the size of the section) of TUNEL reaction mixture was added to the sections. Label solution alone was added to the negative control slide. The slides were incubated in a humidified chamber for 60 minutes at 37°C in the dark. Slides were then rinsed three times in PBS before mounting with Vectashield DAPI (hard set). Sections were analysed using fluorescence microscope (Olympus BX51) and images were obtained at 20x magnification.

2.2.2.4Quantification of Staining

Quantification of staining was performed using ImageJ software (version 1.41). 3 to 5 representative images were captured using Olympus BX51 and cell counter plugin was utilized for analysis of TUNEL, F4/80, S100A9, BrdU, CD3, HMGB1,

Foxp3, CD8 staining. Quantification of Sirius Red staining was done using SlidePath TissueIA image analysis software.

2.2.2.5 Grading

Steatosis was graded on H&E-stained sections based on semi-quantitative estimation of percentage of steatotic hepatocytes, according to the following criteria: grade 0- less than 5 %, grade 1- 5 to 25 %, grade 2- 26 to 50 %, grade 3- 51 to 75 % and grade 4- more than 75 %.

For grading lung metastasis in DEN-induced HCC studies, each slide was given a score from 0 to 5 based on the extent of metastasis, taking into consideration the number and size of metastatic lesions.

2.2.3 *Ex vivo* Imaging of Melanoblasts

Apoptotic morphological features was analysed in skin explants from E15.5 embryos resulting from homozygous Tyr-Cre:Lifeact-GFP:ROCK1wt and Tyr-Cre:Lifeact-GFP:ROCK1nc breeding pairs. The appearance of the mating plug indicated embryonic day 0.5 (E0.5) and 15 days later, pregnant females were euthanized and uterine horns containing embryos were extracted. Embryos were separated from the placenta and embryonic sac and washed in PBS. Lifeact positive embryos were identified by looking for GFP expression in the retina using Olympus CX41 Inverted Microscope. A small piece of embryonic tissue was sent to Transnetyx for genotyping. Embryonic trunk skin was carefully dissected and the sample was sandwiched between a Nucleopore membrane (Whatman) and a gas permeable Lumox membrane in Greiner Lumox 35 mm culture dish. The assembly was arranged with the epidermal side of skin in contact with Lumox membrane to allow time-lapse confocal imaging. Around 50-70 µl of Matrigel was added on top of the Nucleopore membrane in order to immobilize the sample. The dishes were incubated at 37°C for 10 min to allow the matrigel to set. Culture medium (Phenol red free RPMI-1640 containing 10 % FBS, 5 mM L-Glutamine and Pen/Strep) was added after the matrigel had set. Prior to imaging, media was replaced with fresh media contain 100 µM PI3-Kinase inhibitor (LY-294002). Time-lapse images were captured using Nikon A1R

confocal microscope in a 37°C chamber with 5% CO2 at 20× magnification for 19 hours.

2.2.4 Cell Culture Techniques

All cell cultures were incubated at 37°C in a humidified 5% CO2 incubator. Composition of culture media used for different cells is listed in table below.

Table 2-8 Media composition for different cell lines

Cells	Media Components
Hepatocytes	William's E media with 3 % FBS, 100 U/ml penicillin, 100 µg/ml streptomycin and 2 mM L-glutamine
Lymphocytes	RPMI 1640 with 10 % FBS, 5 x 10^{-5} M 2-Mercaptoethanol, 100 U/ml penicillin, 100 µg/ml streptomycin and 2 mM L-glutamine
MEFs	DMEM (w/o L-Glutamine) with 10 % FBS, 100 U/ml penicillin, 100 µg/ml streptomycin and 2 mM L-glutamine
Melanocytes	F-12 with 10 % FBS, 200 nM TPA, 100 U/ml penicillin and 100 µg/ml streptomycin
NIH-3T3	DMEM (w/o Sodium Pyruvate) with 10 % DBS, 100 U/ml penicillin and 100µg/ml streptomycin
RAW 264.7	DMEM (w/o L-Glutamine) with 10 % FBS, 100 U/ml penicillin, 100µg/ml streptomycin and 2 mM L-glutamine

2.2.4.1 Isolation and Culture of Primary Cells

2.2.4.1.1 Mouse Embryonic Fibroblasts (MEFs)

MEFs were generated from E13.5 embryos resulting from homozygous ROCK1wt and ROCK1nc breeding pairs. The appearance of the mating plug indicated embryonic day 0.5 (E0.5) and 13 days later the pregnant females were euthanized and uterine horns containing embryos were extracted. Embryos were dissected from the uterus and washed in PBS. Embryonic heads and livers were removed and a part of the head was sent for genotyping. The remaining tissue from all embryos was pooled and roughly chopped before incubation in 0.05% trypsin-EDTA (1ml/embryo) for 10 min at 37°C. Embryos were then further

dissociated by trituration in serological pipettes, starting with 25 ml pipette and then re-incubated in trypsin-EDTA for another 10 minutes at 37 °C. Cells clumps were further dissociated using 10 ml, 5 ml and finally 1 ml pipette. The cell suspension was plated in pre-warmed MEF media in 15 cm petri dish (around 6 plates for 8-9 embryos). Cells were split at 1:2 ratio the next day (Day 2) when they reached ~80% confluency. On Day 3, cells from each plate was trypsinized and resuspended in 2 ml of freeze medium (10% DMSO in FBS) for cryopreservation. Typically ROCK1wt and ROCK1nc MEFs thawed back to culture proliferated to passage 4-5 before senescing.

2.2.4.1.2 Hepatocytes

Hepatocytes were isolated from mice by collagenase digestion and Percoll gradient method. Isolated cells were seeded on collagen-coated plates. For collagen coating, 50 mg/ml collagen was prepared in water containing glacial acetic acid (6 µl in 5ml water). Plates were coated for 1 hour after which excess liquid was aspirated and plates were left to dry in the hood. For hepatocyte isolation, mice were anesthetized before opening the thoracic cavity and peritoneal cavity. Livers were perfused with Liver Perfusion Media (37°C) via the right atrium and out through the portal vein. Once the liver became pale, Perfusion Media was switched to Liver Digest Media. Digested livers were excised, gall bladder removed and then transferred to a dish containing Liver Perfusion Media. Livers were gently teased with forceps to release the cells into solution. Cell suspensions were then filtered through 70 µm cell strainer to remove undigested tissue and connective tissue. Cells were centrifuged at 135 x g for 1 minute and resuspended in 6 ml of hepatocyte media.

Hepatocytes were separated using a three-layer discontinuous Percoll gradient. Three different Percoll density solutions used were 1.12 g/ml, 1.08 g/ml and 1.06 g/ml. For 1.12 g/ml solution: 2.63 ml of Percoll, 0.3 ml of PBS and 64.6 µl of water; for 1.08 g/ml solution: 2.86 ml of Percoll, 0.5 ml of PBS and for 1.63 ml of water and for 1.06 g/ml solution: 2.085 ml of Percoll, 0.5 ml of PBS and 2.42 ml of water. Percoll gradient was generated by layering 3 ml of 1.12 g/ml solution at the bottom over which 5 ml of 1.08 g/ml solution was carefully layered followed by 5 ml of 1.06 g/ml solution. Over this, 6 ml of cell suspension was carefully layered while avoiding gradient disturbance. The cell suspension

was fractionated by centrifugation without brakes at 750 x g for 20 minutes. After centrifugation, the layer of cells between 1.06 and 1.08 that contained live hepatocytes were collected and added to 10 ml of hepatocyte media. Cell suspension was centrifuged at 135 rcf for 1 minute. Cell pellet was then resuspended in hepatocyte media and seeded in collagen coated plates for analysis.

2.2.4.1.3 Lymphocytes from Tumours

Tumours (thymus, spleen or lymph nodes) were disaggregated aseptically in 4-5 ml of PBS by pushing through a 70 µm cell strainer into a 50 ml centrifuge tube. Lymphocytes were isolated on a Ficoll-Paque density gradient. For this, the disaggregated cell suspension was carefully layered on 5 ml of Ficoll-Paque PLUS in a 15 ml centrifuge tube. The tubes were centrifuged at 3000 rpm for 10 minutes (brake 5). The interphase layer containing live lymphocytes was extracted and washed in 5-10 ml of RPMI medium and centrifuged at 1500 rpm for 5 minutes. The supernatant was discarded and the cells were resuspended in 5-10 ml of RPMI medium. A viable cell count was carried out either on a Coulter Counter or by trypan blue exclusion on a haemocytometer. Cells were frozen at a concentration of 5-10 x 10^6 cells/ vial in freeze medium (10% DMSO and 30% FBS in RPMI medium) for immunophenotyping. For tumour cell line establishment, cells were cultured in 25 cm^2 tissue culture flasks or 12 well plates at a concentration of 2.5 x 10^6 cells/ ml in lymphocyte medium. Cells are normally split at either 1:2 or 1:3. Cell lines were frozen down at passage 6 or 12 at a concentration of 5-10 x10^6 cells/ vial.

2.2.4.2 Induction of Apoptosis

Apoptosis induction was usually preceded by overnight incubation (~ 16 hours) in starve medium (media without serum). For MEFs and NIH 3T3 cell line, apoptosis was generally induced using 50 ng/ml of TNFα and 10 µg/ml of Cycloheximide (CHX) diluted in starve media. For some experiments, other apoptosis inducers including a combination of 2 µg/ml of anti-CD95 and 10 µg/ml of CHX or ultraviolet radiation (0.1 J/cm^2) was used. For primary hepatocytes, 1 µM ABT-199 was used and for melanocytes, 100 µM LY-294002 was used.

2.2.4.3C1q binding on Apoptotic MEFs

ROCK1wt and ROCK1nc MEFs were seeded on collagen-coated coverslips in 6-well dishes at a density of 5 x 10^4 cells per well. Cells were serum-starved overnight prior to induction of apoptosis with 50 ng/ml of TNFα and 10 µg/ml of CHX diluted in starve media. After 1 hour, media was aspirated and cells were fixed in 4 % PFA for 5 minutes. Cells were washed carefully with PBS. 10 µg/ml of C1q diluted in PBS was added to the cells and incubated for 1 hour at room temperature. Cells were washed carefully with PBS. For C1q detection, mouse anti-human C1q, diluted in PBS (1:1000) was added and incubated for 30 minutes at room temperature. After washing cells with PBS, anti-mouse secondary antibody, diluted in PBS (1:3000) was added and incubated for 10 minutes at room temperature. Cells were washed with PBS. To visualize cell membranes, cells were incubated with Vybrant DiO Cell Labelling Solution for 5 minutes. Cells were washed before mounting them with Vectashield DAPI (hardset). Confocal images were captured with Nikon A1R microscope. 3D reconstruction and volumetric rendering of Z-stacks were done using Imaris software.

2.2.4.4 Caspase Activity Assay

Cells were seeded on 96-well plates. Following treatment with appropriate apoptosis inducers, cells were subjected to caspase 3/7 activity measurement using Caspase-Glo assay kit. Briefly, plates containing cells were removed from the incubator and allowed to equilibrate to room temperature for at least 30 minutes. 100 µl of Caspase-Glo reagent was added to each well, contents mixed gently and then incubated for 30 minutes at room temperature. The luminescence for each sample was measured in a plate-reading luminometer.

2.2.5 Microscopy

2.2.5.1Time-lapse Microscopy for MEFs

ROCK1wt and ROCK1nc MEFs were plated on 6-well glass bottom dishes at a density of 2 x 10^6 cells per well. Cells were serum-starved overnight prior to induction of apoptosis with 50 ng/ml of TNFα and 10 µg/ml of CHX diluted in starve media. Bright field time-lapse microscopy images were acquired with a 10x objective using Nikon TE 2000 microscope with a heated stage and 5% CO_2

gas line. Immediately after induction of apoptosis, the dishes were transferred to the microscope, 3-4 random positions were chosen from each well and time lapse images were taken every 3 minutes for 15-17 hours.

2.2.5.2 Time-lapse Microscopy for Hepatocytes

ROCK1wt and ROCK1nc primary hepatocytes were plated on 6-well glass bottom dishes pre-coated with collagen. Cells were serum-starved overnight prior to induction of apoptosis with 1 μM of ABT-199 diluted in starve media. Bright field time-lapse microscopy images were acquired with a 10x objective using Nikon TE 2000 microscope with a heated stage and 5% CO_2 gas line. Immediately after induction of apoptosis, the dishes were transferred to the microscope, 3-4 random positions were chosen from each well and time lapse images were taken every 3 minutes for 18 hours.

2.2.5.3 Electron Microscopy

For scanning electron microscopy (SEM) studies, MEFs from ROCK1wt and ROCK1nc mice were seeded on coverslips pre-coated with collagen in a 12-well plate. Cells were serum starved overnight prior to induction of apoptosis with 50 ng/ml of TNFα and 10 μg/ml of CHX diluted in starve media. After 2 hours of incubation, cells were fixed with 2.5 % glutaraldehyde in 0.1 M phosphate buffer for 1 hour at room temperature. After fixation, cells were washed with phosphate buffer (3 washes for 10 minutes each). Samples were then further processed for SEM analysis by Electron Microscopy Facility at University of Glasgow. Images of apoptotic MEFs were taken at different magnifications.

For transmission electron microscopy (TEM) studies, very small pieces (around 1 mm thickness) of kidney from ROCK1wt and ROCK1nc mice was fixed with 2.5 % glutaraldehyde in 0.1 M sodium cacodylate buffer for 1 hour at room temperature. After fixation, samples were rinsed in sodium cacodylate buffer (3 times for 5 minutes each). Samples were stored at 4°C until ready for processing. Samples were processed at the Electron Microscopy Facility at University of Glasgow. TEM images of kidneys were taken at different magnification.

2.2.6 Flow Cytometry

2.2.6.1 Flow Cytometric Determination of PS Externalization

MEFs were plated on 10 cm plates at a density of 1.5 x 10^6 cells/ plate. Cells were serum-starved overnight prior to induction of apoptosis with 50 ng/ml of TNFα and 10 µg/ml of CHX diluted in starve media. Starve medium alone was added to control cells. After 4 hours of treatment, conditioned media was collected. Cells were washed with PBS before detaching cells with Accutase. Detached cells were collected and added to the tube containing conditioned media. Cell suspension was centrifuged at 1000 rpm for 5 minutes and supernatant was aspirated. Cells were resuspended in 1 ml of ice-cold 1% BSA in PBS. The cell suspension was centrifuged at 1800 rpm for 3 minutes and resuspended in 1% BSA. After another centrifugation at 1800 rpm for 3 minutes, supernatant was aspirated and cells were resuspended in 400 µl of 1X Binding Buffer (FITC Annexin V Apoptosis Detection Kit). To 100 µl of cell suspension, 5µl of FITC Annexin V and 5µl of PI was added, mixed well by vortexing and incubated in the dark for 15 minutes. After incubation 400 µl of 1X Binding Buffer was added and analysed by flow cytometry.

2.2.6.2 Immunophenotyping of Lymphocytes

Frozen vials of lymphocytes isolated from Eµ-myc tumours were thawed and resuspended in 5 ml of RPMI (with 10 % FBS). This was centrifuged at 1500 rpm for 5 minutes at 4°C. Pellet was resuspended in 5 ml of FACS buffer (PBS with 5-10 % FBS) and centrifuged at 1500 rpm for 5 minutes at 4°C. Cell pellet was resuspended in FACS buffer (volume depended on the size of the pellet). Cells were counted and divided for different staining combinations. Around 5 x 10^5 or less cells were used for staining (96 well plate or eppendorfs). Cells were centrifuged at 1500 rpm for 5 minutes at 4°C. Pellet was resuspended in 100 µl of FACS buffer with Fc block (1:250) and incubated for 15 min at 4°C. Meanwhile primary antibody master-mixes were made in FACS buffer (1:500 for Biotinylated Antibodies and 1:100 for FITC/APC antibodies). After Fc block, cells were centrifuged at 1500 rpm for 5 minutes and cell pellet was resuspended in 100 µl of the relevant antibody mastermix and incubated for 30 min at 4°C in the dark. Unstained and single-stained sample controls were also included. Cells were

washed twice with FACS buffer. Samples containing biotinylated antibodies were resuspended in 100µl of Streptavidin (1:500 in FACS buffer) and incubated for 30 min at 4°C in the dark. Cells were washed again and finally resuspended in FACS buffer containing 7AAD (1:1000) for FACS analysis.

2.2.7 Cellular protein extraction and analysis

2.2.7.1 Preparation of cell lysates

After cells had been grown to the desired confluence and treated with apoptotic inducers for the required period of time, they were lysed to extract proteins. For this, culture dishes were placed on ice and the conditioned medium containing apoptotic bodies was collected in cold eppendorf tubes. 10 ml of ice-cold PBS was added to the dishes and using a cell scraper, cell lysates were collected and transferred to the corresponding cold eppendorf tubes. This was centrifuged at 3000 rpm for 5 minutes at 4°C. Supernatant was discarded and the pellet was washed in 1 ml of PBS followed by another centrifugation at 3000 rpm for 5 min at 4°C. Supernatant was discarded and the pellet was resuspended in 200-250 µl of SDS lysis buffer. This was then transferred to QIAshredder tubes and centrifuged for 1 min at 14,000 rpm. The flow-through was transferred to fresh eppendorf tubes and frozen (either rapid freezing or overnight freezing at -80°C). Lysates were then thawed on ice before being centrifuged at 14,000 rpm for 15 minutes at 4°C. The supernatant was transferred to a fresh centrifuge tube, protein concentration determined and samples stored at -20°C or -80°C.

For macrophages treated with histone H2A for 2 hours, cells were washed with PBS twice and collected by scraping. The cell suspension was then centrifuged at 3000 rpm for 5 minutes. Cells were lysed using 8 M Urea and passed through QIAshredder. The flow through was collected for western blotting.

2.2.7.2 Determination of protein concentration

Protein concentration of cell lysates was determined using the bicinchoninic acid (BCA) assay. Briefly, standards (0.08, 0.1, 0.2, 0.4, 1 and 2 mg/ml) were prepared in SDS lysis buffer using a 2 mg/ml albumin standard stock solution. 10 µl of blank (buffer alone), standards and samples were added to a Greiner Bio-One 96-well plate. 1:2 dilutions of protein samples were also included. 200 µl of

developing solution (50:1, bicinchoninic acid: copper sulphate solution) was added to each well, mixed well. Plate was sealed with microplate sealing film and incubated at 37ºC for 30 minutes. Absorbance was measured using Molecular Devices Microplate Reader and sample concentrations were determined from the standard curve generated.

2.2.7.3 SDS-polyacrylamide gel electrophoresis

SDS-polyacrylamide gel electrophoresis (PAGE) was used to separate protein samples based on their molecular weight. Protein samples were first diluted in 6x loading buffer and heated at 95°C for 5 minutes. After heating, samples were briefly centrifuged and loaded on 4-12 % NuPAGE Bis-tris gels alongside Prestained Protein ladder molecular weight marker. Gels were run in tanks containing 1X MOPS/MED SDS running buffer at 100 V for the first 10 minutes and then increased to 160 V and run until the tracking dye front reaches the lower end of the gel. Afterwards, gels were either stained or used for western blotting.

2.2.7.4 Gel Staining

Following protein separation, some gels were stained to detect protein bands as follows. Gels were washed three times in distilled water (dH2O) for 5 minutes each. Gels were then incubated in SimplyBlueTM SafeStain for 1 hour at room temperature. Following this, gels were washed in dH2O for 1 hour and then overnight. Images of stained gels were acquired on a LI-COR Odyssey® system.

2.2.7.5 Western Blotting

Following protein separation, some gels were used for western blotting. Proteins were transferred to PVDF membrane in transfer buffer containing 20 % methanol using a Bio-Rad Mini Trans-Blot® Cell. Briefly, prior to transfer, PVDF membrane was pre-wet in methanol for 15 seconds and then washed in transfer buffer. Sponges and Whatman papers were also pre-wet and then stacked with the gel and membrane. All transfers were run at 100 V for 1 hour using an ice pack in the apparatus. Successful transfer and equal loading of proteins was confirmed by staining the membrane with Ponceau staining solution. After the Ponceau stain was washed off using TBS-T, the membrane was blocked with 5% (w/v) milk

powder or 3% BSA in TBS-T for 1 hour. Primary antibodies were diluted to the required concentration in TBS-T and membranes incubated with these solutions for 2 hours at room temperature or 4^{o}C overnight. This was followed by three washes in TBS-T for 10 minutes each. The membrane was then incubated with the secondary antibody that had been diluted to the required concentration in TBS-T for 45 minutes at room temperature. After the blot was washed in TBS-T three times for 10 minutes each, protein bands were visualised on the LI-COR Odyssey® system. Protein bands were quantified using Image Studio Version 2.1.

2.2.8 Multiplex Cytokine Analysis

Milliplex System (Millipore) allows the simultaneous measurement of different cytokines from the same sample. For my experiment, I custom tailored 15 cytokines (INF-γ, IL-1α, IL-1ß, IL-2, IL-4, IL-5, IL-6, IL-10, IL12p40, IL12p70, IL-17, MCP-1, MIP-1α, MIG, TNFα) to be analysed. The serum levels (pg/ml) of these cytokines were analysed using the Mouse Cytokine/Chemokine Magnetic Bead Panel Kit following manufacturer's instructions. Briefly, 200 µl of wash buffer was added to each well of the 96-well plate, sealed and mixed on a plate shaker for 10 minutes at room temperature after which the wash buffer was decanted. Inverting the plate and tapping it onto absorbent towels removed any residual amount of wash buffer. 25 µl of standards or controls was added to the appropriate wells and 25 µl of assay buffer was added to the sample wells. 25 µl of serum matrix was added to the background, control and standard wells. 25 µl of serum samples diluted 1:2 in assay buffer was added to the sample wells. All serum samples were measured in duplicates. 25 µl of premixed magnetic beads conjugated to antibodies for all 15 analytes were added to each well. Plate was sealed, protected from light and incubated overnight at 4° C on a plate shaker. This was followed by a wash step (two times with 200 µl of wash buffer) on a magnetic plate washer. 25 µl of detection antibodies was added to each well, and plate was sealed and incubated with agitation for 1 hour at room temperature. Streptavidin-phycoerythrin (25 µl) was added to each well, and plates was sealed and incubated with agitation for another 30 minutes at room temperature, followed by a final wash step. Magnetic beads were then re-suspended in sheath fluid and assayed on a Luminex 200 analyser using xPOTENT software.

2.2.9 SILAC

2.2.9.1 SILAC Labelling of NIH 3T3 cells

NIH 3T3 cells were grown in DMEM supplemented with dialysed FBS (10 kDa cut off), 4 mM L-glutamine and labelled arginine (Arg) and lysine (Lys) amino acids for 5 passages. Cells were labelled with light/unlabelled (Lys-0, Arg-0), medium (Lys4, Arg6), and heavy (Lys8, Arg10) medium. Amino acids are labelled with the following isotopes: Lys4- $^{2}H_4$; Lys8- $^{13}C_6$, $^{15}N_2$; Arg6- $^{13}C_6$; Arg10- $^{13}C_6$, $^{15}N_4$. Label incorporation was checked on cell pellets suspended in 8M Urea and confirmed to be >95% by mass spectrometry before cells were used for further experiments.

2.2.9.2 Treatment of SILAC Labelled Cells

Apoptosis was induced with a combination of 50 ng/ml of TNFα and 10 µg/ml of CHX and further supplemented with 10 µM Y-27632 or 50 µM Blebbistatin. Control cells left in starve medium. Briefly, each labelled populations of NIH 3T3 were assigned the following treatments: Light, control; Medium, TNFα + CHX; Heavy, TNFα + CHX + Y-27632. Each labelled population of NIH 3T3 was used in each treatment condition, with Blebbistatin substituting for Y-27632 in one set of replicates, for a total of six replicates. After 4 hours, conditioned media was collected and concentrated.

2.2.9.3 Concentration of Conditioned Media using Strataclean

Conditioned media was collected in falcon tubes and centrifuged at 300 rcf for 10 minutes at 4°C. Supernatant was collected and centrifuged at 2000 rcf for 10 minutes at 4°C. Supernatant was collected in polypropylene tubes (snap on caps) and centrifuged at 10,000 rcf for 30 minutes at 4°C. Supernatant collected was maintained on ice. The pH of the solution was adjusted to 5 with 10 % trifluoroacetic acid. 100 µl of Strataclean Beads was added to the solution, vortexed thoroughly and incubated for 30-60 minutes in the rotor wheel at 4°C. The solution was centrifuged at 872 rcf for 1 minute at 4°C to pellet the beads. Supernatant was removed and 120 µl of 6X loading buffer was added to the beads and mixed thoroughly. Samples were boiled at 95°C for 5 minutes and

then centrifuged at 400 rcf for 1 minute. Supernatant was either run on gel immediately or frozen for later use.

2.2.9.4 Macrophage Uptake of SILAC Labelled Proteins

Heavy labelled population of NIH 3T3 cells were induced with apoptosis with UV (0.1 J/cm^2). After 4 hours of incubation, conditioned media was collected and added to culture dishes containing RAW 264.7 macrophages which were pre-treated with Bafilomycin A1. Macrophages were incubated with conditioned media for 2 hours at 37°C. After incubation, RAW 264.7 cells were washed twice with media and once with PBS. Cells were collected by scraping and centrifuged at 3000 rpm for 5 minutes. Cells were lysed with 8M Urea and the lysate was passed through QIAshredder. Three independent experiments were performed.

2.2.9.5 Mass Spectrometry Analysis

Protein concentration of macrophage cell lysate was determined. 20 µL of supernatant obtained after concentration using Strataclean beads was run on 10 % SDS-PAGE. The gel was stained with Coomassie. Macrophage cell lysate and Coomassie-stained gel was subjected to mass spectrometry and database search was performed by Mass Spectrometry Service Staff, David Sumpton and Sergio Lilla.

2.2.10 TNFα Secretion by Macrophages

RAW 264.7 cells were treated with varying amounts of purified recombinant histone proteins (H2A, H2B, H3 and H4) for 2 hours. The media was collected and assayed for TNFα secretion by using TNFα ELISA kit by following manufacturer's instructions.

2.2.11 Statistical Analysis

Statistical significance ($p<0.05$) of differential findings between experimental groups was determined by performing appropriate tests using GraphPad 6 software. The test used for analysis is stated in the corresponding figure legends.

Results

ROCK1nc Mouse Model

3 Non-cleavable ROCK1 (ROCK1nc) mouse model

3.1 Introduction

The importance of apoptosis in maintaining tissue homeostasis is well documented. Morphological features of cells undergoing apoptosis (cell contraction, membrane blebbing and apoptotic body formation) have been appreciated for more than 40 years, but the biological importance of these dramatic events has yet to be determined. Previously, our lab had identified that during apoptosis, caspase cleavage and activation of ROCK1 is important for formation of blebs (Coleman et al., 2001). Elucidation of the importance of caspase cleavage of ROCK1 and its biological significance has been limited to *in vitro* studies, often using pharmacological inhibitors. As previously discussed, currently available inhibitors are not isoform selective and can have off-target effects. Although these inhibitor-based studies provided invaluable insights into ROCK1-mediated apoptotic membrane blebbing, they still failed to provide proof that caspase cleavage of ROCK1 is necessary for the distinct morphological features of apoptotic cells. In order to understand the fundamental role of cleavage and activation of ROCK1 during apoptosis and also to investigate the biological significance of apoptotic blebbing, a genetically modified (GM) knock-in mouse model was generated by the Transgenic Facility at the Beatson Institute, in which a non-cleavable form of ROCK1 (ROCK1nc) was created by mutating the terminal amino acid D1113 in the caspase cleavage site to alanine. This model is the first of its kind that would allow for the purpose of morphological changes during apoptosis to be determined *in vivo*.

3.1.1 Generation of ROCK1nc mouse model

Briefly, a targeting vector bearing two mutations in exon 27 (3338A>C and 3339T>A) was generated with a floxed neomycin selection cassette in the preceding intron. The targeting vector was generated with 3.1 kb 5' and 5.1 kb 3' homology arms, respectively. When translated, the mutant ROCK1 bears a single missense substitution (D1113A). This modifies the caspase cleavage site and renders the protein insensitive to caspase cleavage. The targeting vector was transfected into 129/Sv mouse embryonic stem cells and the cells were selected by neomycin resistance. Surviving clones were screened and correctly

modified cells were injected into fertilized mouse blastocysts and then implanted into pseudopregnant mice. The resulting chimeric male mice were then crossed with wild-type C57Bl/6 females. Thus, the offspring were of mixed background (129/Sv and C57Bl/6). Mice heterozygous for the mutant ROCK1nc gene retained the floxed neomycin selection cassette and hence were crossed with a Cre deleter strain (on a C57BL/6 background) to remove the cassette. The resulting mice were crossed with wild-type C57Bl/6 mice to remove the Cre transgene. Homozygous mice (ROCK1nc) generated from heterozygous breeding were born in expected Mendelian ratios and did not display any overt phenotype. ROCK1nc mice were then interbred to generate a homozygous strain for use in our studies. Similarly, mice not carrying the ROCK1nc mutation that were generated from heterozygous breeding were also interbred to generate wild-type mice (ROCK1wt) for comparative studies. The caspase cleavage site mutation had no effect on viability and fertility of these mice.

3.1.2 Experimental Aims

The ROCK1nc mouse strain generated at the Beatson Institute is the first genetic model that would enable us to answer fundamental questions regarding apoptotic membrane blebbing *in vivo*. The aim of this study was to characterize the ROCK1nc model by using a combination of *in vitro* and *in vivo* techniques.

3.2 Results

3.2.1 ROCK1nc cleavage is required for apoptotic blebbing and cell contraction

Caspase cleavage of ROCK1 removes an auto-inhibitory domain, which yields a constitutively active kinase fragment that drives actomyosin contractility. The force thus generated drives the morphological features that are typically seen in cells undergoing apoptosis (Coleman et al., 2001). To characterize the requirement for cleavage of ROCK1 for membrane blebbing during apoptosis, I utilized mouse embryonic fibroblasts (MEFs) from ROCK1wt and ROCK1nc mice. MEFs isolated from E13.5 embryos were expanded in culture and seeded on coverslips. Once attached, cells were starved overnight (MEF media without FBS) and then exposed to the apoptosis inducing agents, TNFα and Cycloheximide (CHX) for 4 hours. The samples were then processed for scanning electron microscopy at the University of Glasgow. Scanning electron micrographs of treated cells revealed that the morphology of membrane blebbing was significantly altered in ROCK1nc fibroblasts when compared to the wild-type fibroblasts (Figure 3-1). The cells displayed an inability to contract and bleb properly, thereby verifying previous *in vitro* studies on ROCK1 activity in membrane blebbing using ROCK inhibitors like Y-27632.

To further confirm the defective apoptotic morphology, MEFs were seeded on 6-well glass bottom dishes, starved overnight and treated with TNFα and CHX. Morphological features of apoptosis were observed using time-lapse microscopy. Images were taken at 3 minute time intervals for a maximum of 15 hours. Analysis of time-lapse images clearly demonstrated a profound defect in apoptotic morphology in ROCK1nc fibroblasts compared to wild-type fibroblasts (Figure 3-2). ROCK1wt fibroblasts underwent classic apoptotic morphological features including, membrane blebbing and forceful contraction of the cell to form apoptotic bodies. However, ROCK1nc MEFs showed an obvious inability to contract and bleb properly. They failed to retract and cellular processes remained adhered to the plate surface.

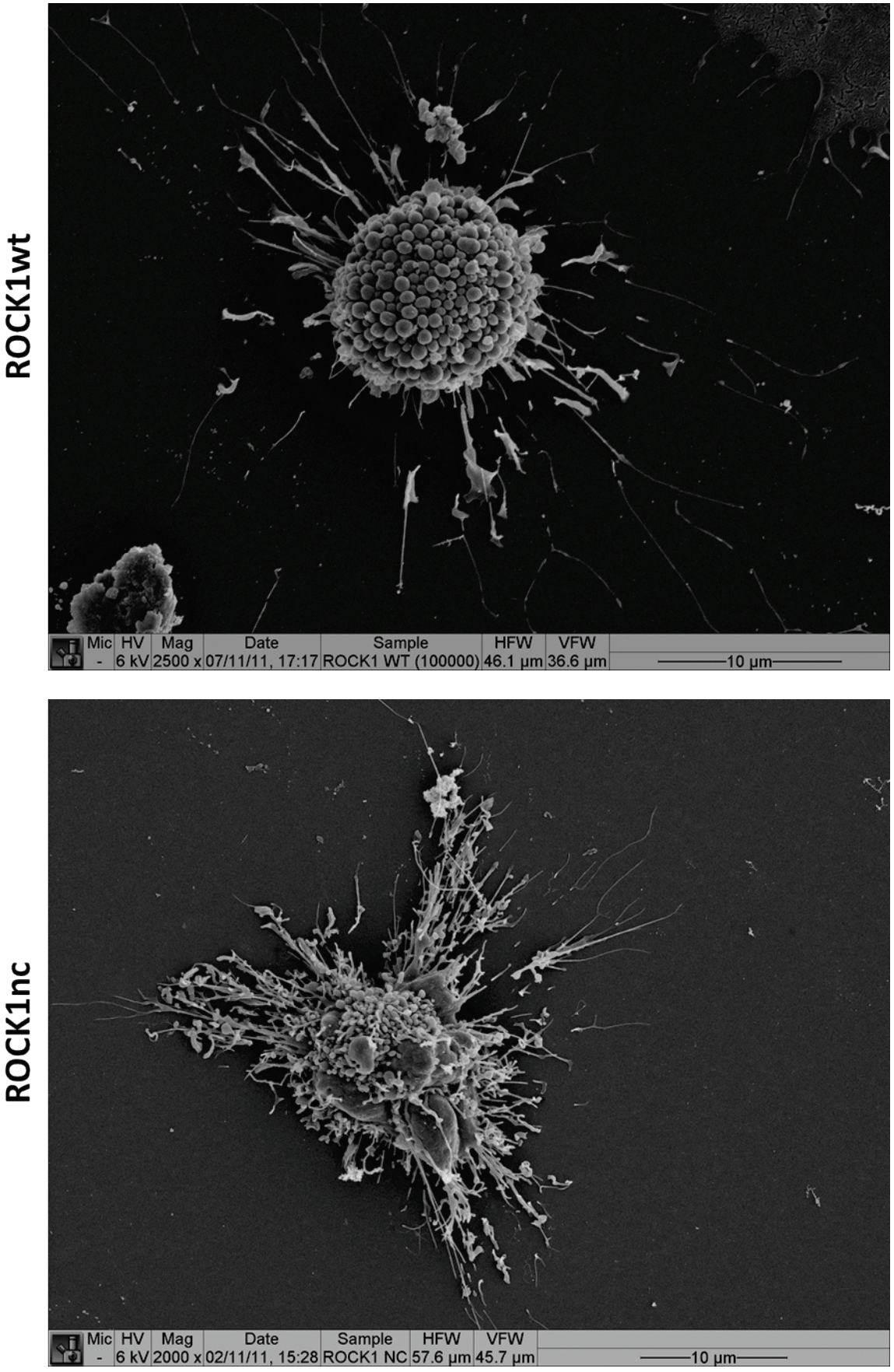

Figure 3-1 ROCK1 cleavage is required for apoptotic blebbing and cell contraction
Scanning electron micrographs of MEFs from ROCK1wt and ROCK1nc mice treated with TNFα and CHX for 4 hours. Scale bars represent 10µm.

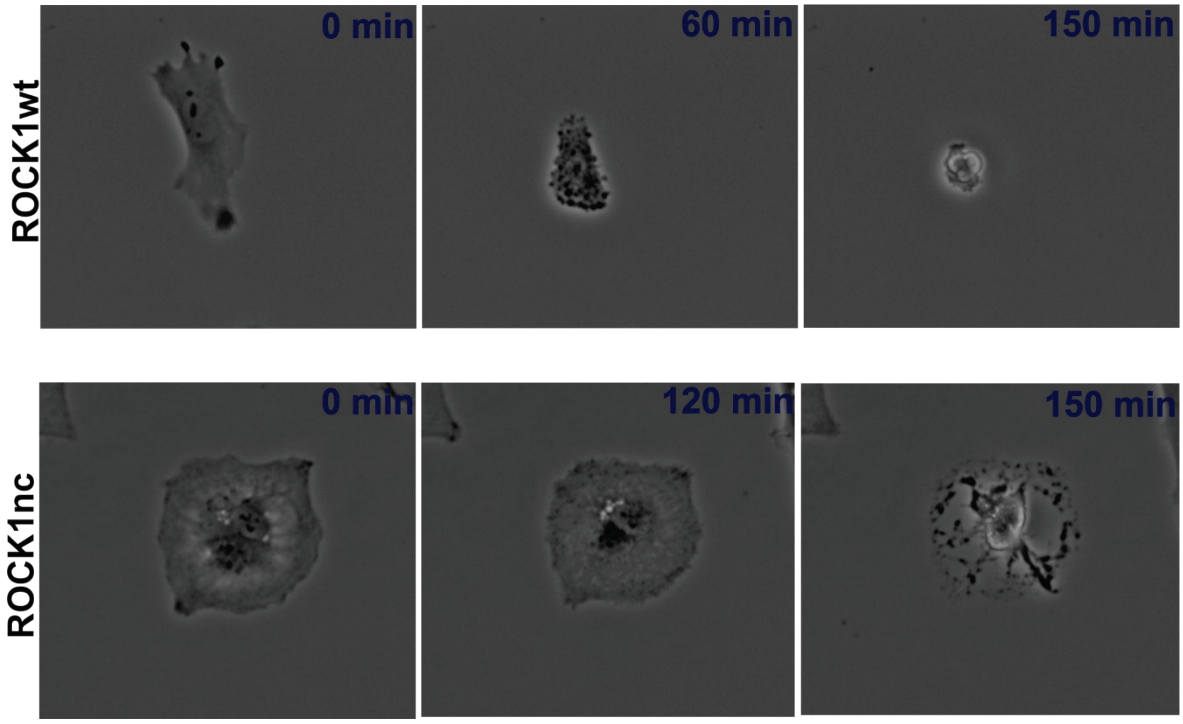

Figure 3-2 Apoptotic ROCK1nc MEFs demonstrate an inability to contract and bleb
Representative time lapse images at indicated times of ROCK1wt and ROCK1nc MEFs induced for apoptosis with TNFα and CHX that were taken at 3 minute time intervals for 150 minutes.

3.2.2 ROCK1 cleavage is not required for cell death

The knock-in mutation that was introduced in the caspase cleavage site of ROCK1 was not expected to hinder caspase activity in these fibroblasts. To validate this, both ROCK1wt and ROCK1nc MEFs were treated with different inducers of apoptosis which included TNFα+CHX, CD95+CHX or UV treatment. Caspase 3/7 activity in untreated MEFs and MEFs treated with apoptosis inducers for 4 hours was evaluated with Caspase-Glo assay kit in a 96-well format. Initially, ROCK1wt and ROCK1nc MEFs were induced with apoptosis and the caspase activity was checked at 1, 2, 3 and 4 hours. The experiment was performed in triplicate. As expected, caspase activity in both ROCK1wt and ROCK1nc MEFs increased with time for all three treatments (Figure 3-3a).

Since apoptotic morphologies were analysed using scanning electron microscopy at 4-hour time point, MEFs were treated with apoptotic inducers for 4 hours and caspase 3/7 activity was analysed. The experiment was done in triplicate and repeated four times. As compared to untreated controls, induction of apoptosis resulted in an increase in caspase activity with all three treatments (Figure 3-3b). The increase in caspase activity was the lowest in cells treated with CD95+CHX. Importantly, there was no significant difference in the caspase activity between the two genotypes with any of the three tested treatments (Figure 3-3b). This confirmed that the caspase activity was not affected by the knock-in mutation in ROCK1 and that cleavage of ROCK1 was not required for cell death.

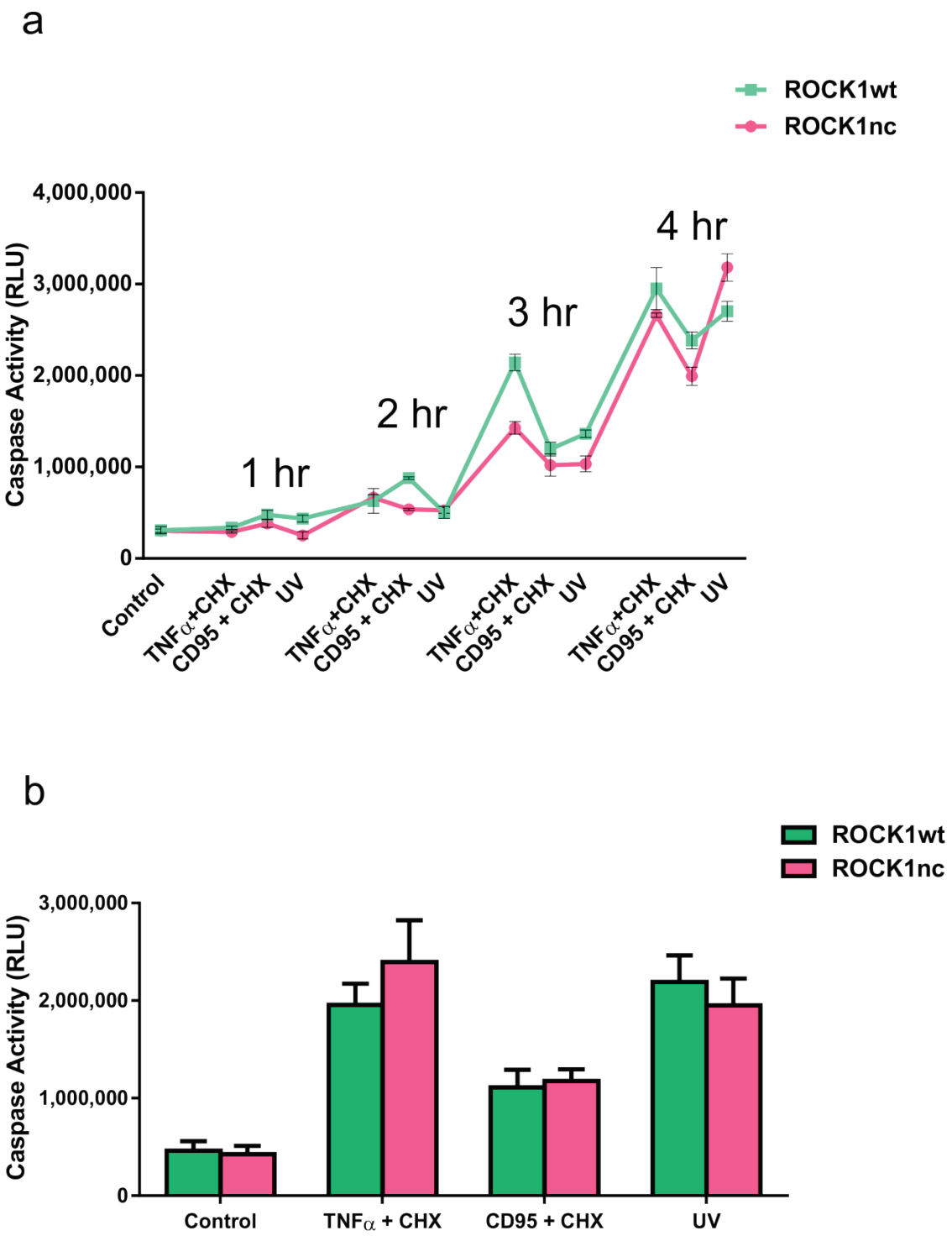

Figure 3-3 ROCK1 cleavage is not required for cell death

a) Line graph (mean ± SEM) shows caspase activity (determined by Caspase Glo assay) of MEFs from ROCK1wt and ROCK1nc mice, treated with different apoptotic inducers for increasing lengths of time. b) Bar graph (mean ± SEM) shows caspase activity in wild-type and ROCK1nc MEFs 4 hours after induction of apoptosis with different inducers. Data analysed by Student's t-test. RLU=Relative Luminescence Units.

3.2.3 ROCK1nc is resistant to caspase cleavage during apoptosis

To confirm that the knock-in mutation in ROCK1 rendered the protein resistant to caspase cleavage during apoptosis in MEFs, western blotting was performed on lysates from wild-type and ROCK1nc fibroblasts that were treated with TNFα and CHX for 4 hours as well as untreated fibroblasts. This work was performed by Dr. Grant Wickman and Dr. Nicola Rath.

ROCK1 expression remained unaltered in untreated MEFs (Figure 3-4). However, upon induction of apoptosis, cleavage of ROCK1 was observed in ROCK1wt MEF lysates with the appearance of two bands. In ROCK1nc MEFs, apoptosis induction using TNFα and CHX did not result in cleavage of ROCK1 protein, which confirmed that the knock-in mutation indeed rendered the protein resistant to caspase cleavage during apoptosis. Induction of apoptosis was confirmed by the presence of cleaved poly (ADP-ribose) polymerase (PARP), which is a classical marker of apoptosis. PARP cleavage was observed in both ROCK1wt and ROCK1nc MEFs that were treated with TNFα and CHX, while the untreated counterparts did not reveal a cleaved PARP product. Caspase cleavage and activation of ROCK1 was confirmed by blotting for phosphorylated MLC (pMLC), a marker of ROCK1 activation. Apoptosis in wild-type fibroblasts resulted in increased phosphorylation of MLC when compared to untreated samples. This however, was not observed in apoptotic ROCK1nc MEFs, confirming that caspase cleavage of ROCK1 during apoptosis results in phosphorylation of MLC, which would then induce actomyosin contractility, thus driving classical apoptotic features including cell contraction and membrane blebbing.

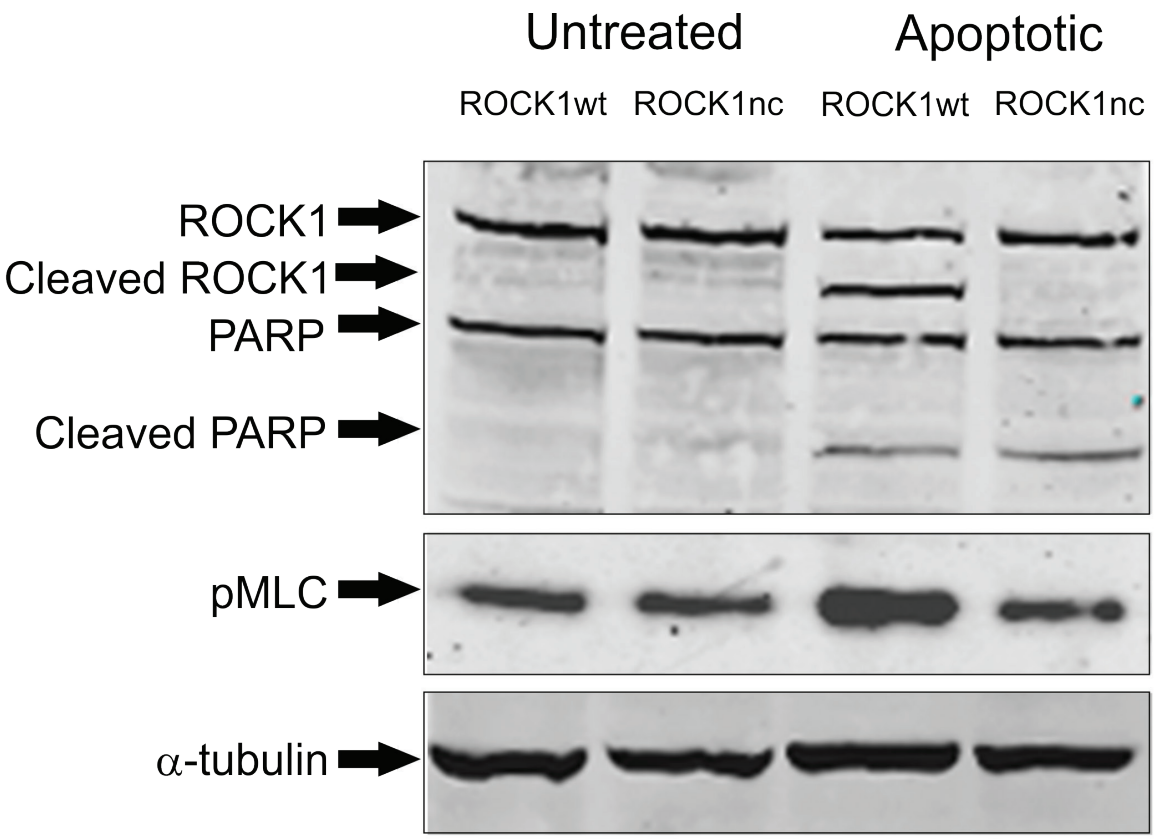

Figure 3-4 ROCK1nc is resistant to caspase cleavage during apoptosis
Representative western blot image of MEF lysates from ROCK1wt and ROCK1nc treated with and without TNFα and CHX for 4 hours as indicated. Membrane was probed for ROCK1, PARP, pMLC and α-tubulin. Cleaved ROCK1 and PARP were detected as lower molecular weight bands as indicated. Figure courtesy of Dr. Nicola Rath.

3.2.4 Inhibition of ROCK1 cleavage does not affect phosphatidylserine externalization

Loss of membrane asymmetry and the concomitant externalization of phosphatidylserine (PS) is a common feature of apoptotic cells. The ability of PS to act as a recognition signal for clearance of apoptotic cells by phagocytes was demonstrated many years ago (Fadok et al., 1992b, Fadok et al., 1992a). The seminal report that revealed the caspase cleavage site of ROCK1 also reported that externalization of PS was independent of ROCK1 activity (Coleman et al., 2001). To verify whether MEFs from ROCK1nc mice also showed similar results, PS externalization was evaluated using flow cytometry by exploiting the property of Annexin V to bind specifically to PS. This work was kindly performed by June Munro. MEFs from wild-type and ROCK1nc mice were either left in starve medium (untreated) or treated with TNFα and CHX. After 4 hours, cells were collected and stained with fluorescently labelled Annexin V and propidium iodide (PI) (Figure 3-5a). This work was done in quadruplicates and repeated four times. Within 4 hours of treatment, almost 40 % of cells from both ROCK1wt and ROCK1nc mice bind Annexin V, and thus externalize PS, when compared to less than 10 % in control untreated cells (Figure 3-5b). Notably, no significant difference in Annexin V binding was observed between MEFs expressing wild-type ROCK1 and non-cleavable ROCK1 (Figure 3-5b). Thus, the defect in caspase cleavage of ROCK1 appears to disturb the morphological features associated with apoptosis and does not affect externalization of PS during apoptosis.

3.2.5 Apoptotic blebs focalize complement C1q

C1q, a component of the classical complement cascade, has been shown to enhance recognition and clearance of apoptotic cells by phagocytes (Ogden et al., 2001). C1q binds through its globular head to the membrane blebs on apoptotic keratinocytes (Korb and Ahearn, 1997) and endothelial cells (Navratil et al., 2001). When C1q protein was added to apoptotic MEFs (TNFα and CHX) from ROCK1wt and ROCK1nc mice, there was high-density localization specifically on the surface blebs on ROCK1wt cells (Figure 3-6). However, C1q binding was minimal on apoptotic ROCK1nc MEFs that lacked prominent surface blebs, suggesting that membrane blebs were essential for C1q binding (Figure 3-6).

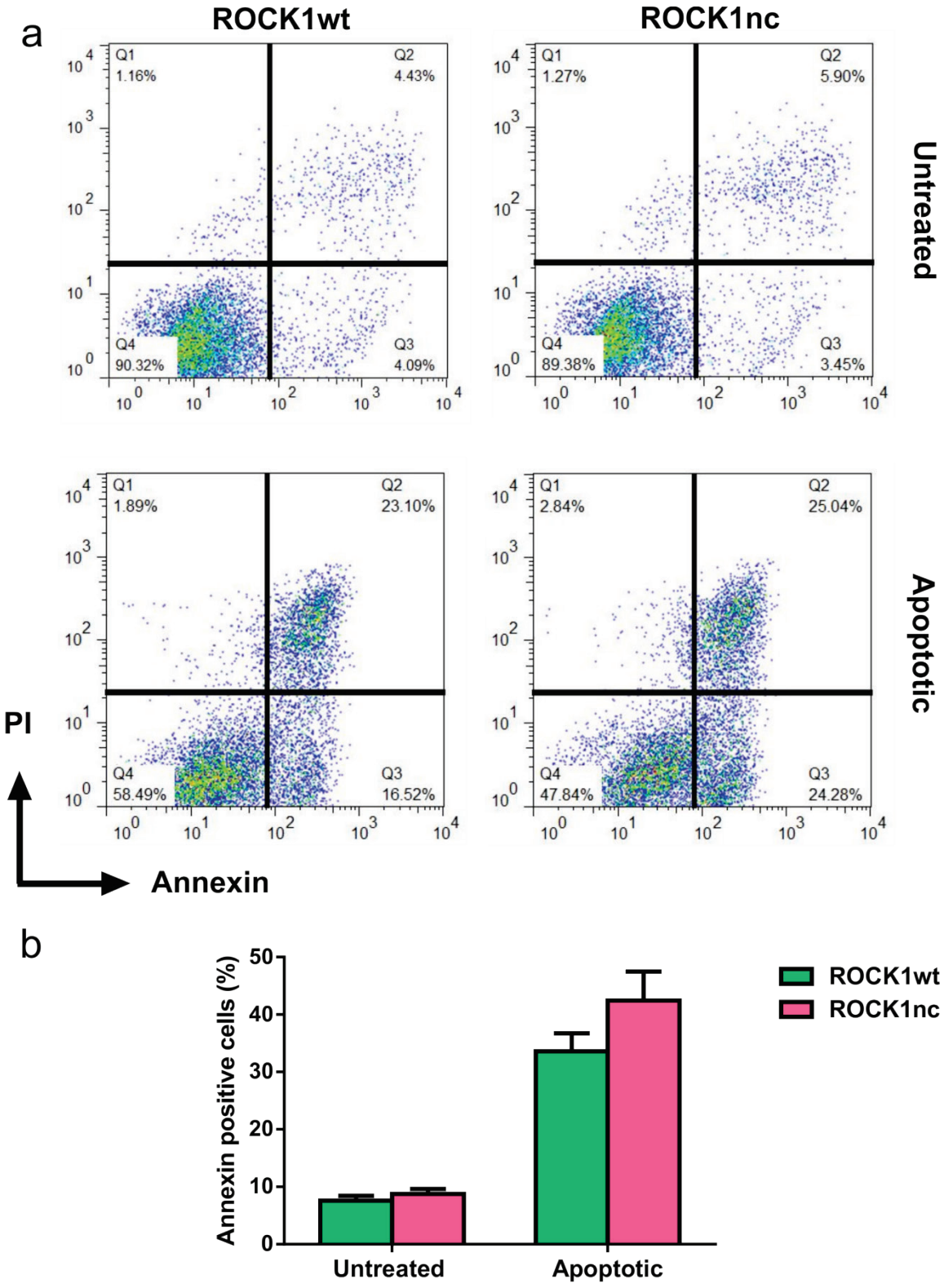

Figure 3-5 Phosphatidylserine externalization is not dependent on ROCK1 cleavage
a) Representative FACS dot plots of ROCK1wt and ROCK1nc MEFs treated with and without TNFα and CHX for 4 hours. Cells were stained with Annexin to detect externalization of phosphatidylserine and with propidium iodide (PI) to determine membrane integrity b) Bar graph (mean ± SEM) shows percentage of Annexin V positive cells (quadrant Q2 + quadrant Q3) in untreated and treated MEFs from ROCK1wt and ROCK1nc mice. Data analysed by Student's t-test.

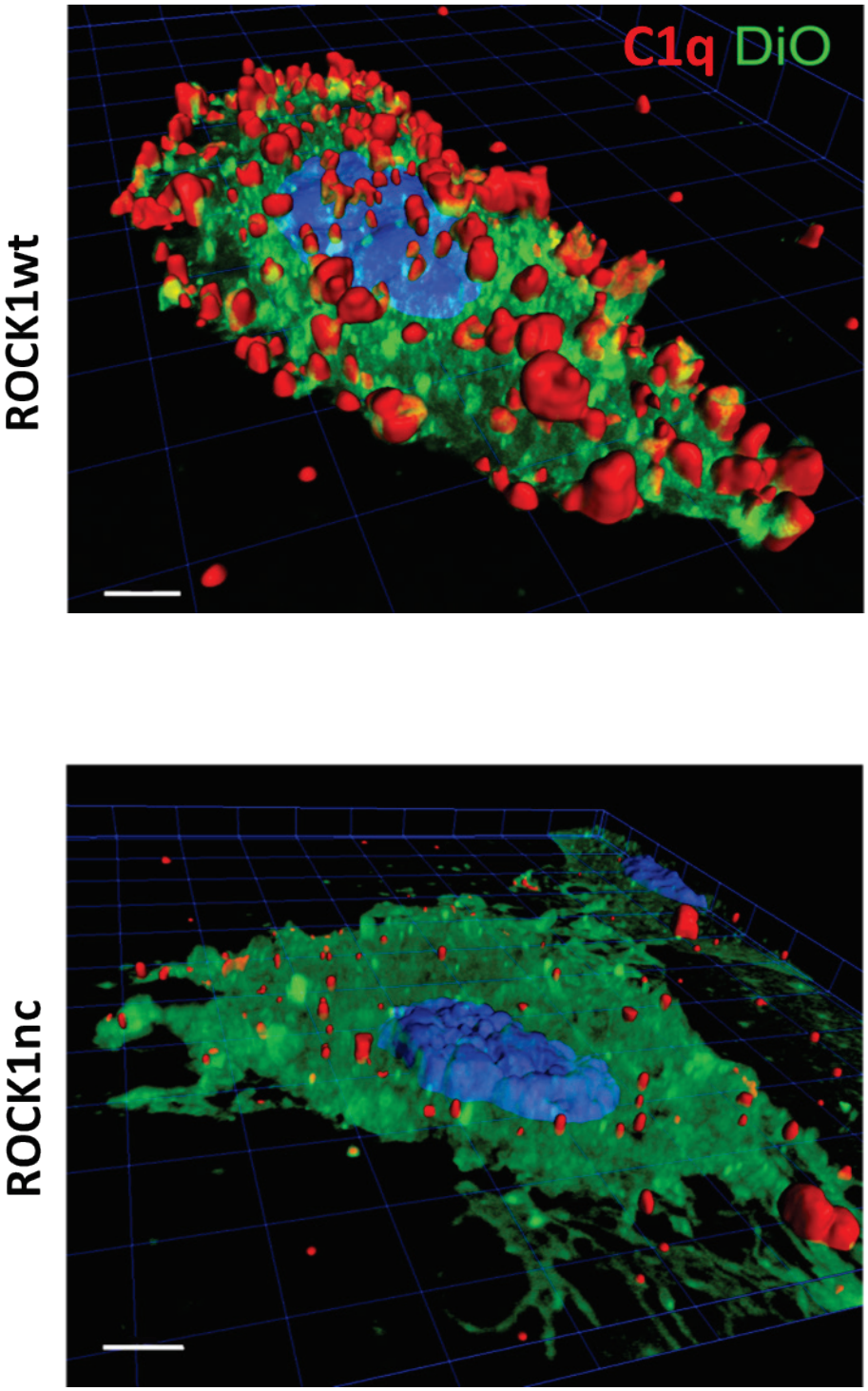

Figure 3-6 Apoptotic blebs focalize complement C1q
Representative images of 3D reconstruction and volumetric rendering of apoptotic MEFs, showing. C1q (red) binding specifically to surface blebs. Cell membrane was stained with lipid dye DiO (green), and nucleus with DAPI (blue). Scale bars represent 7 μm. Work done along with Dr. Grant Wickman (Wickman et al., 2012).

3.2.6 Hepatocytes from ROCK1nc mice display morphological defects during apoptosis

Having confirmed that mesenchymal cells like fibroblasts from ROCK1nc mice exhibited morphological defects during apoptosis, I wondered whether this would hold true for epithelial cells as well. As a filter organ, the liver is constantly exposed to microbes and toxic substances making it vulnerable to cell death. The bulk of the liver is made up of hepatocytes, which are epithelial cells. Primary mouse hepatocytes were isolated from ROCK1wt and ROCK1nc mice by the two-step liver perfusion method, where first the liver is perfused with medium at physiological pH to clear the blood, followed by perfusion with medium containing collagenase for cell dissociation.

Primary hepatocytes isolated from ROCK1wt and ROCK1nc mice were seeded on 6-well glass bottom dishes that were coated with collagen. To induce apoptosis in hepatocytes, I used 1μM of ABT-199, a Bcl2-specific BH3 mimetic. Morphological features of apoptosis were observed using time-lapse microscopy. Images were taken at 3 minute time intervals for a maximum period of 17 hours. Analysis of time-lapse images showed that unlike fibroblasts, membrane blebbing was not prominent in these epithelial cells. However, comparison of wild-type and ROCK1nc hepatocytes demonstrated a defect in apoptotic morphology in ROCK1nc hepatocytes (Figure 3-7). ROCK1wt hepatocytes underwent forceful contraction and formed compact apoptotic bodies, however, ROCK1nc hepatocytes failed to retract properly. Cellular processes remained adhered to the plate surface thus exhibiting a failure to form compact apoptotic cell bodies (Figure 3-7). This confirmed that apoptotic morphological features were altered in epithelial cells like hepatocytes from ROCK1nc mice.

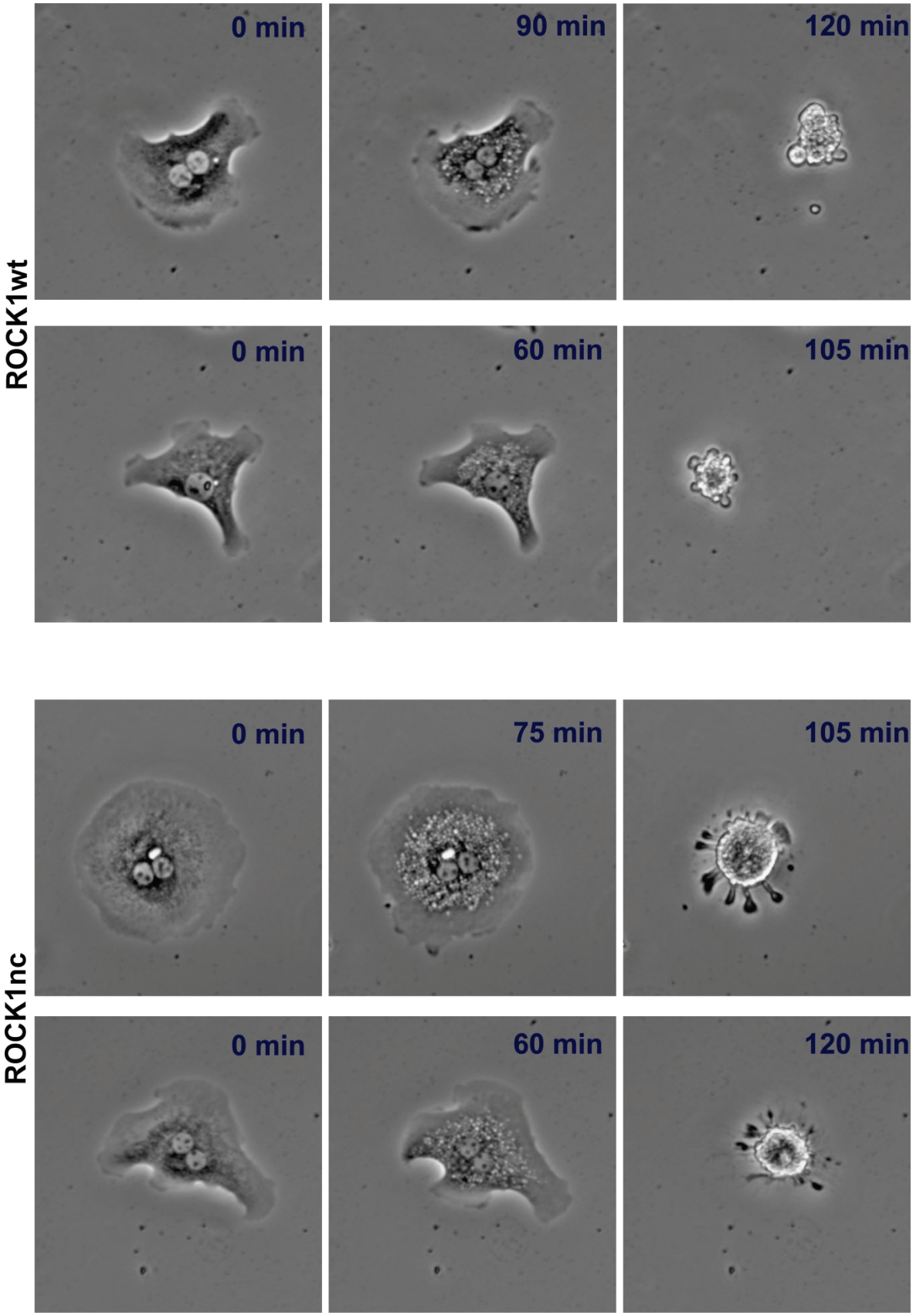

Figure 3-7 Apoptotic ROCK1nc hepatocytes display an inability to retract
Two panels of representative time lapse images at indicated times of ROCK1wt and ROCK1nc hepatocytes induced with apoptosis with ABT-199 which were taken at 3-minute time interval for up to 120 minutes.

3.2.7 ROCK1nc mutation affects apoptotic morphologies in 3D *ex-vivo* tissue

Typically, apoptotic morphological features have been observed mainly under *in vitro* conditions. Given that we now know the effect of defective caspase cleavage of ROCK1nc in apoptotic morphologies under *in vitro* conditions, we questioned whether these morphological defects would be manifested *in vivo*. To achieve this, I crossed ROCK1nc mice with Tyr-Cre:LifeAct-GFP mice, kindly provided by Prof. Laura Machesky, to generate Tyr-Cre:Lifeact-GFP:ROCK1wt and Tyr-Cre:Lifeact-GFP:ROCK1nc. Lifeact is a 17-amino-acid peptide isolated from yeast that binds specifically to F-actin (Riedl et al., 2008). Tyr-Cre:LifeAct-GFP mice obtained by crossing Tyr-Cre mice that expresses Cre recombinase under the control of the Tyrosinase promoter to mice that express Lifeact-GFP on the HPRT locus allowed GFP expression in melanocyte lineage in vivo (Schachtner et al., 2012). E15.5 embryonic trunk skin was isolated and treated with the PI3-kinase inhibitor LY-294002 to induce cell death. Using live time-lapse confocal imaging of embryonic skin explants, I assessed the apoptotic morphologies of GFP-expressing melanoblasts over a maximum period of 17 hours. ROCK1wt melanoblasts showed evidence of blebbing and fragmentation into multiple small apoptotic bodies that went out of focus in a short span of time (Figure 3-8a). However, ROCK1nc melanoblasts also exhibited fragmentation but the apoptotic bodies generated remained attached to each other for long periods, suggesting that these cells lacked the forceful actomyosin contraction to form discrete apoptotic bodies (Figure 3-8a). These *ex vivo* observations correlated well with my *in vitro* observations.

To confirm that ROCK1 activity did not have an effect on melanoblast death induced by the PI3-kinase inhibitor, I checked for caspase 3/7 activity in immortalized melanocyte cells, kindly provided by Ang Li (Prof. Laura Machesky's Lab), in the absence or presence of ROCK inhibitor Y-27632. Caspase activity was determined with Caspase Glo assay at 0, 4, 8 and 24 hours after treatment. The experiment was done in triplicate and repeated three times. There was no significant difference in caspase activity when ROCK was inhibited; suggesting that inhibition of ROCK activity did not affect melanoblast death (Figure 3-8b).

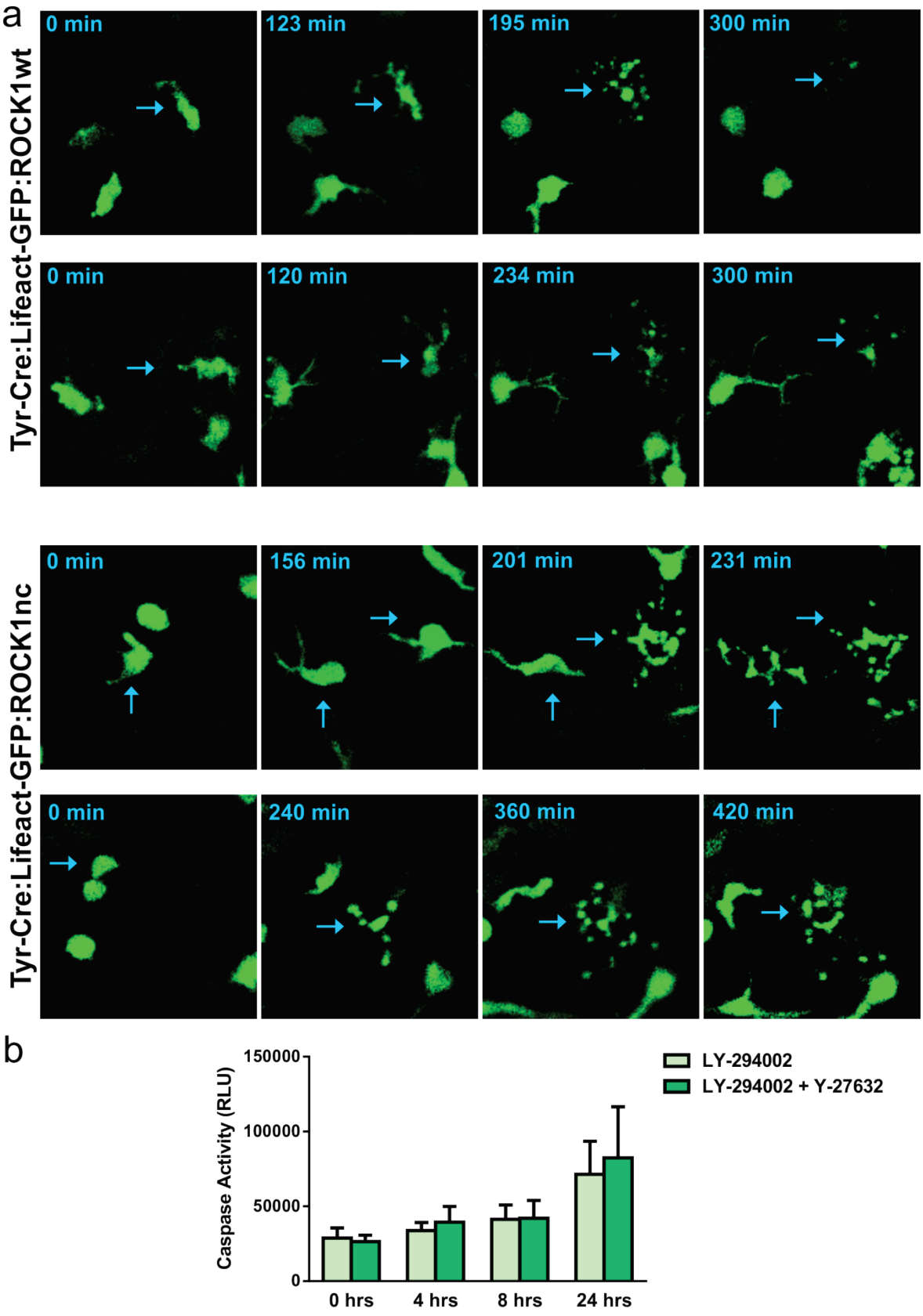

Figure 3-8 ROCK1 cleavage is required for apoptotic features in 3D *ex vivo* tissue
a) Two panels of representative confocal time lapse images of GFP-expressing melanoblasts induced with apoptosis using LY-294002 in E15.5 embryonic skin mounts at indicated time points Arrows indicate the melanoblasts under observation. b) Bar graphs (mean ± SEM) shows no difference in caspase activity in immortalized melanocyte cells treated with LY-294002 in the absence or presence of ROCK inhibitor Y-27632. RLU=Relative Luminescence Units. Data analysed by Student's t-test.

3.2.8 ROCK1nc mice do not display a strong autoimmune phenotype

Given the compelling evidence of defective morphological features during apoptosis in ROCK1nc mice, we wondered whether this would lead to defective clearance of apoptotic cells eventually resulting in autoimmunity. As previously mentioned, ROCK1nc mice did not display any overt phenotype when compared to wild-type controls. I further examined these mice at the histological level for signs of autoimmunity.

Glomerulonephritis is a chronic kidney condition frequently seen in autoimmune disease like Systemic Lupus Erythematosus (SLE) and has been linked with defective clearance of apoptotic cells (Botto et al., 1998). I examined H&E-stained liver sections for signs of glomerular hypercellularity but did not observe any apparent anomalies. Thickening of the glomerular basement membrane due to deposition of antibodies or immune complexes is a common feature in glomerulonephritis. Periodic acid-Schiff (PAS) stain that is used to highlight the basement membrane of glomerular capillaries did not reveal any obvious variations between ROCK1wt and ROCK1nc mice (Figure 3-9a). Transmission electron microscopy (TEM) of kidneys revealed indications of electron dense deposits in the basement membrane as well as loss of podocyte foot processes (podocyte effacement) in ROCK1nc mice (Figure 3-9b), although this was not confirmed in more samples. Symptoms of podocyte effacement include proteinuria or leakage of proteins into urine. However, both ROCK1wt and ROCK1nc mice exhibited only trace amounts of proteins (negative in some cases) in urine as detected by Protein Reagent Strips for Urinalysis.

The spleen is responsible for the destruction of old and damaged erythrocytes. Splenic macrophages phagocytose erythrocytes and the iron from the haemoglobin is converted to hemosiderin for storage in spleen (Bennett and Kay, 1981). Increased hemosiderin indicates high rate of erythrocyte removal, usually observed in autoimmune diseases like haemolytic anaemia (Suttie, 2006).Perls Prussian Blue stain was used to visualize hemosiderin. However, spleen sections from both wild-type and mutant mice showed hemosiderin deposition in the spleen, but with no difference (Figure 3-9c). Moreover, splenomegaly, a typical finding in an autoimmune phenotype was also not observed in ROCK1nc mice

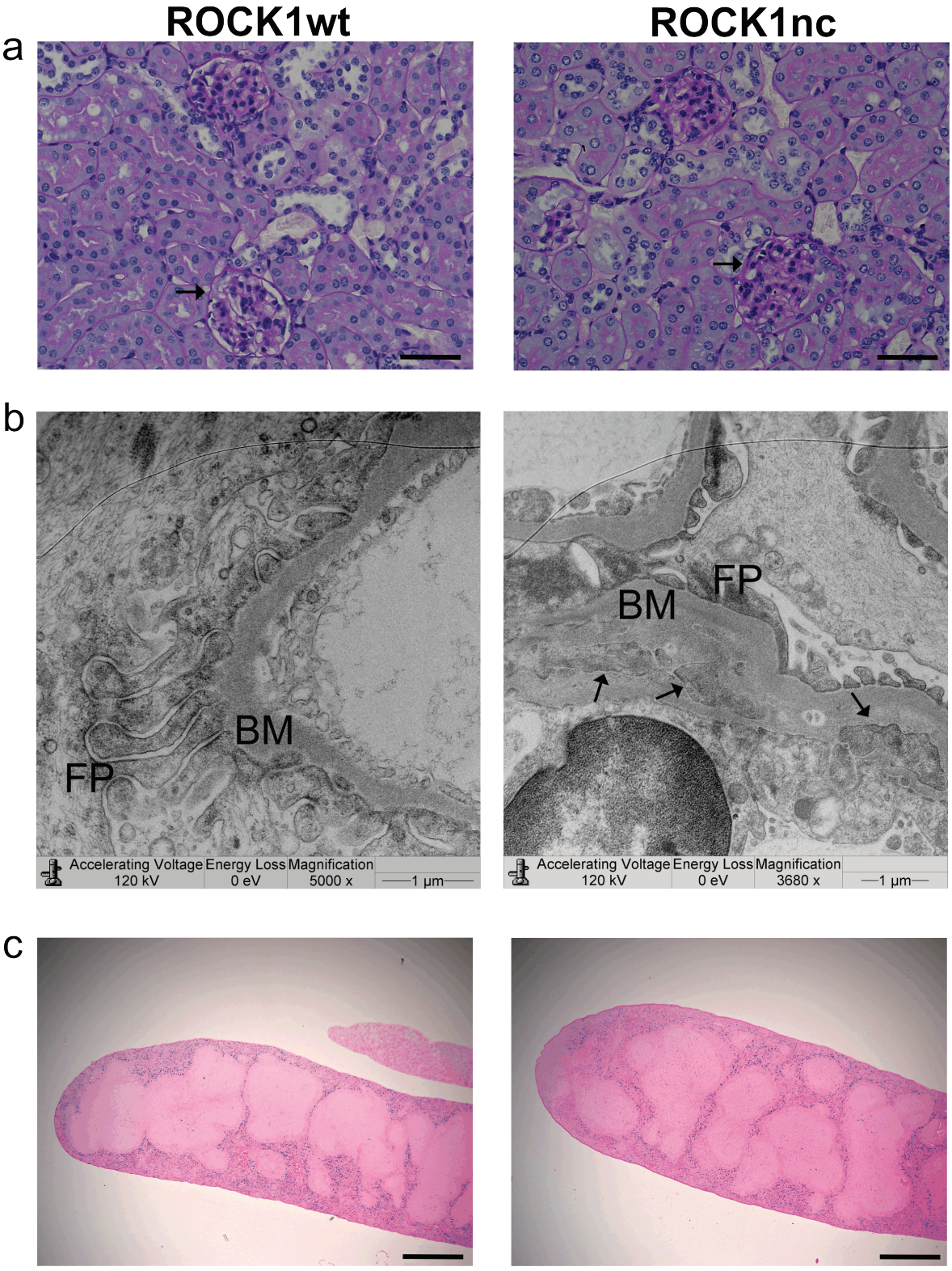

Figure 3-9 ROCK1nc mice do not display a strong autoimmune phenotype
a) Representative PAS-stained kidney sections from ROCK1wt and ROCK1nc mice showing no difference in basement membrane thickening (arrows). Scale bars represent 100 µm. b) Representative transmission electron micrographs of kidneys showing electron dense deposits (arrows) in the basement membrane (BM) as well as abnormal foot processes (FP) in ROCK1nc mice. Scale bars represent 1 µm. c) Representative Perls Prussian Blue-stained spleen sections showing no difference in hemosiderin deposition between the two genotypes. Scale bars represent 500 µm.

3.2.9 Haematological analysis of ROCK1nc mice

Blood collected from 10 week-old mice were sent to the Clinical Pathology lab at Veterinary School for complete haematology analysis (Figure 3-10). On review, ROCK1nc mice displayed significantly lower haematocrit (HCT) and mean corpuscular volume (MCV) when compared to wild-type. HCT is the amount of space occupied in the blood by RBCs, and the reduced size of the RBC (MCV) correlates well with reduced HCT. However, it should be noted that the total haemoglobin level and the number of RBCs remained the same. Analysis of white blood cell (WBCs) revealed no major differences in WBC numbers between the two genotypes except for eosinophil numbers, which was significantly more in ROCK1nc mice. In addition to platelet (PLT) numbers, different platelet indices including mean platelet volume (MPV), plateletcrit (PCT) and platelet distribution width (PDW) were also analysed. Similar to RBC, size of platelets (MPV) and the percentage of whole blood occupied by platelets (PCT) were also significantly reduced in ROCK1nc mice, even though platelet numbers remained similar between the two genotypes.

3.2.10 Decreased cytokine levels in ROCK1nc mice

Cytokines are messengers produced mainly by the cells of the innate and adaptive immune system in response to a number of environmental stimuli including infection and tissue damage. The functions of cytokines are often redundant and vary depending on the immunological milieu as well as the presence or absence of other cytokines. To investigate whether defective cleavage of ROCK1 during apoptosis was affecting the immunological milieu, serum obtained from 10-week old mice were analysed for levels of 15 cytokines and chemokines using mouse Milliplex magnetic bead panel. This included cytokines like INF-γ, IL-1α, IL-1ß, IL-2, IL-4, IL-5, IL-6, IL-10, IL-12p40, IL-12p70, IL-17, TNFα and chemokines MCP-1, MIP-1α and MIG. All analytes measured except for MIG was reduced in ROCK1nc mice with IL-1ß, IL-2, IL-4, IL-6, IL-10, IL-12p40, IL-12p70, IL-17 and TNFα reaching significance (Figure 3-11).

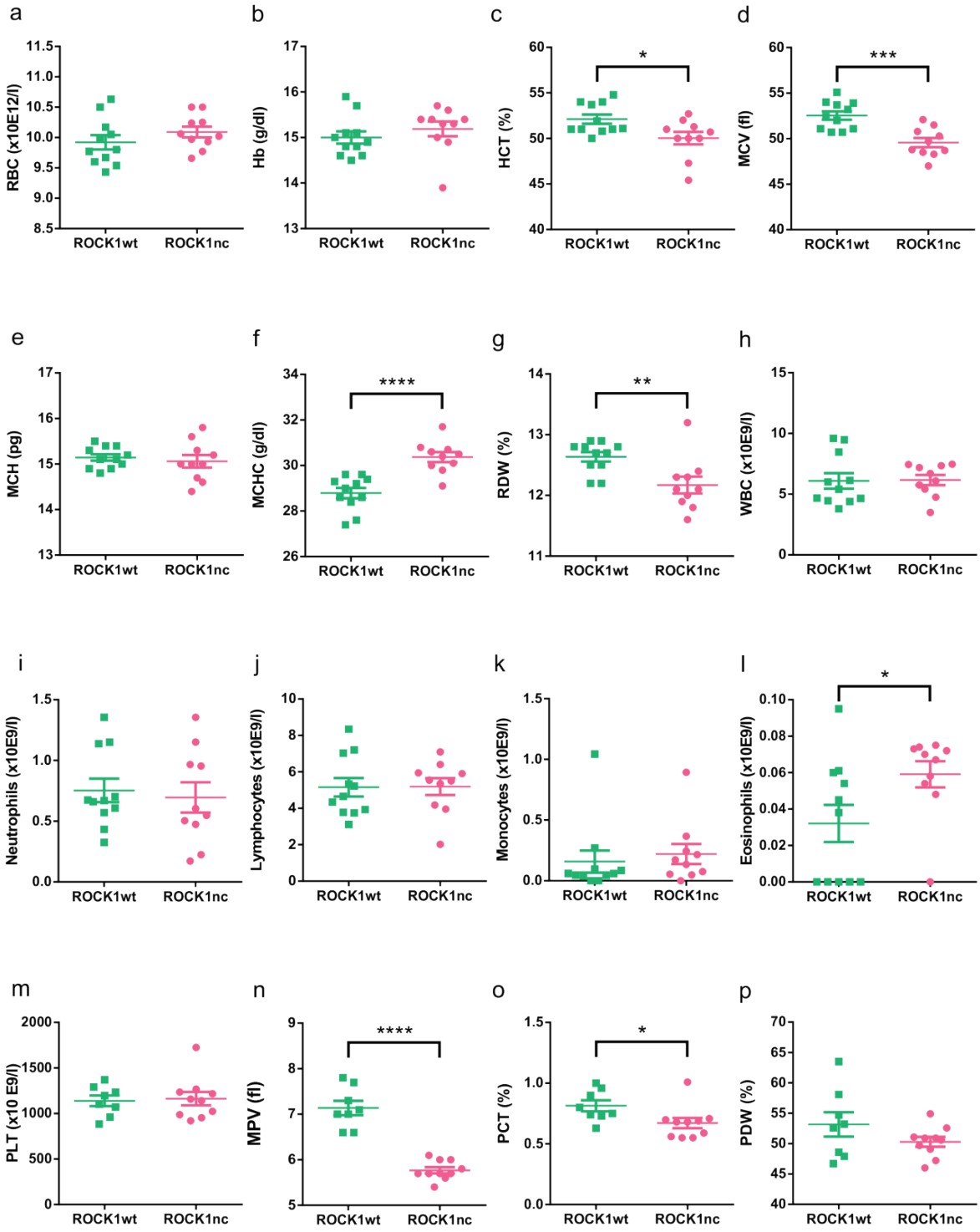

Figure 3-10 Haematological analysis of ROCK1nc mice

Scatter dot-plots (Mean ±SEM) for a) red blood cell count (RBC), b) haemoglobin (Hb), c) haematocrit (HCT), d)mean corpuscular volume (MCV), e) mean corpuscular haemoglobin (MCH), f) mean corpuscular haemoglobin concentration (MCHC), g) RBC distribution width (RDW), h) white blood cell count (WBC), i) neutrophils, j) lymphocytes, k) monocytes, l) eosinophils, m) platelet count (PLT), n) mean platelet volume (MPV), o) plateletcrit (PCT) and p) platelet distribution width (PDW) from ROCK1wt and ROCK1nc mice. Data analysed using Student's t-test. *=p<0.05, **=p<0.01, ***=p<0.001, ****=p<0.0001.

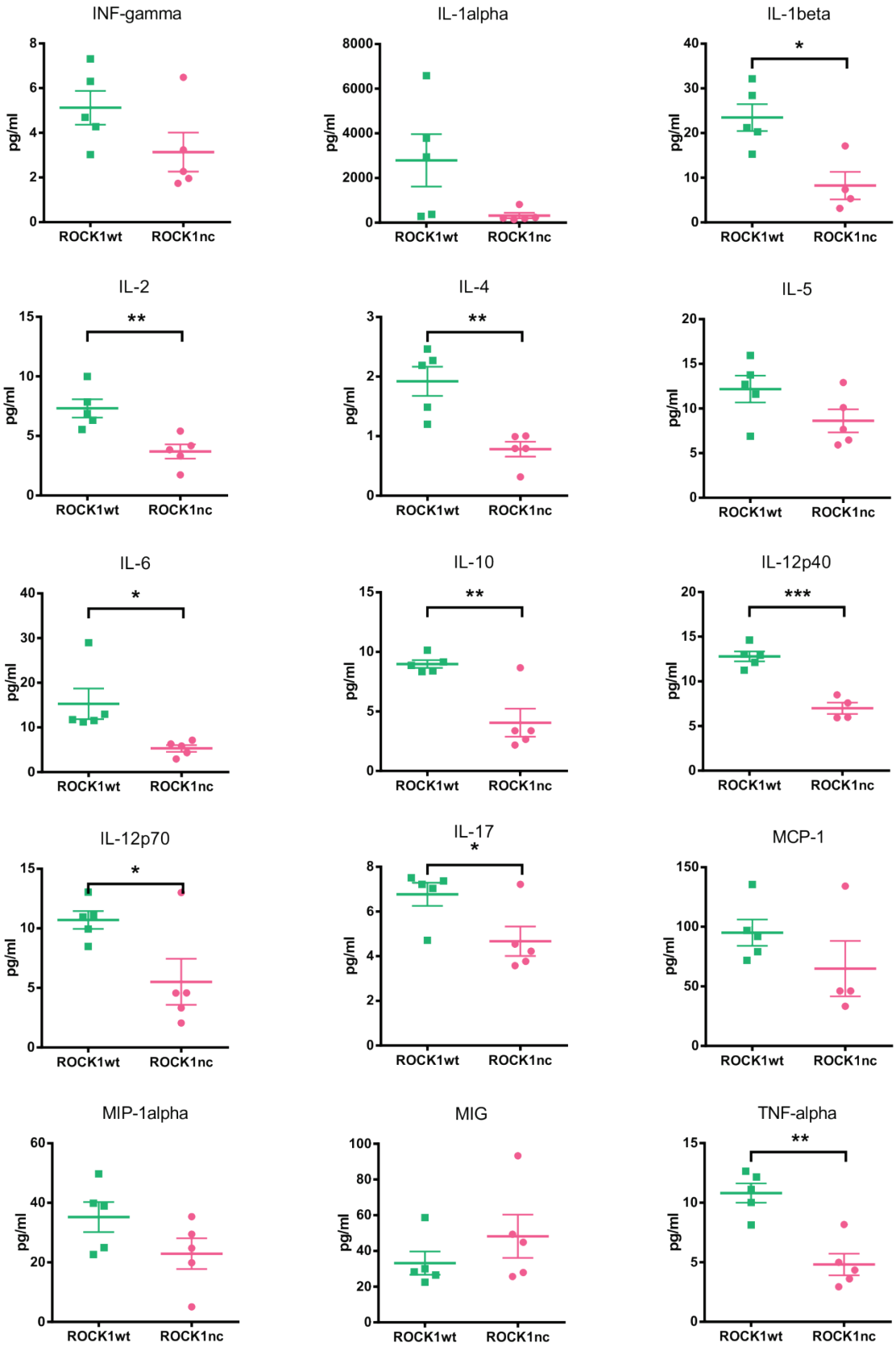

Figure 3-11 Decreased cytokine levels in ROCK1nc mice
Scatter dot-plots (mean ± SEM) showing serum levels of 15 different immune analytes from 10-week old ROCK1wt and ROCK1nc mice. Data analysed using Student's t-test. *=p<0.05, **=p<0.01, ***=p<0.001.

3.3 Discussion

Morphological features of apoptosis were described more than 40 years ago. Yet, the biological significance of these dramatic events still remains unclear. In this chapter, I have introduced a novel mouse model that was generated at the Beatson Institute that would enable us to understand the *in vivo* role of apoptotic membrane blebbing. The ROCK1nc model carries a knock-in mutation at the caspase cleavage site of ROCK1 which makes the protein resistant to activation during apoptosis. To confirm the role of caspase cleavage of ROCK1 in mediating the morphological features of apoptosis, MEFs and hepatocytes were isolated from wild-type and ROCK1nc mice and induced with apoptosis. Apoptotic morphological features as observed by time-lapse microscopy and scanning electron microscopy showed obvious defects in cells from ROCK1nc mice even though cell death as measured by caspase activity was not different between cells from the two genotypes. ROCK1nc cells lacked the forceful contraction due to inactivation of ROCK1 and hence displayed an inability to contract and bleb. In addition, by imaging death of GFP-expressing melanoblasts in ex vivo embryonic skin explants, we confirmed that the knock in mutation in ROCK1 inhibited the typical morphological features seen during apoptosis.

In spite of the strong phenotype exhibited by apoptotic ROCK1nc cells both *in vitro* and *ex vivo*, ROCK1nc mice were viable and fertile. As discussed in Introduction, several GM mouse models have shown that accumulation of apoptotic debris can lead to the development of autoimmune-induced pathologies. There are some minor indications of mild autoimmune pathologies in ROCK1nc mice, including reduced haematocrit, mean RBC volume and RBC distribution width that are consistent with a form of autoimmune anaemia. However, histologically ROCK1nc mice did not show an increased hemosiderin deposition in the spleen, which is a typical finding of haemolytic anaemia. There were slight perturbations in the kidney, suggestive of an autoimmune pathology, for example, the presence of dense electron deposits in the basement membrane as evidenced by TEM. Despite the absence of a strong autoimmune phenotype, an interesting finding was the significantly decreased cytokine levels in ROCK1nc mice. In the upcoming chapters, I will address the role of apoptotic morphological features in tissue homeostasis and tumour development.

Results

Caspase Cleavage of ROCK1 in Tissue Homeostasis

4 Apoptotic blebbing is required for the maintenance of tissue homeostasis during acute damage in the liver

4.1 Introduction

4.1.1 Role of ROCK1 dependant apoptotic blebbing in the liver

Apoptosis is a well-choreographed physiological process of cell death that is essential for the elimination of superfluous and damaged cells. Dying cells undergo several biochemical and morphological alterations during the execution phase of apoptosis that aid in the efficient recognition and prompt clearance of cell debris (Julian and Olson, 2015). This is believed to prevent the release of potentially noxious intracellular contents into the surrounding milieu. Hence, the rapid clearance of apoptotic debris is well suited to a role in the maintenance of tissue homeostasis.

This liver is a crucial organ for detoxification of chemicals and metabolizing drugs, and is constantly exposed to microbes and toxic substances, thus making it susceptible to cell death. N-nitrosodiethylamine, also known as diethylnitrosamine (DEN), is a genotoxic carcinogen that is bioactivated in the liver by cytochrome P450 enzymes leading to the formation of DNA adducts by ethylation (Williams et al., 1996). DEN treatment also results in the depletion of nicotinamide adenine dinucleotide in hepatocytes leading to a blockade in oxidative phosphorylation, thereby driving the cells to a hypoxic state (Rawling et al., 1993).

The role of ROCK1 in the execution phase of apoptosis was previously established using pharmacological inhibitors such as Y-27632 and/or RNAi approaches that alter ROCK1 expression. Although these data implicate ROCK1 activity as being important, they did not prove that ROCK1 activation by caspase cleavage is the critical mechanism. Using our ROCK1nc mouse model, I sought to determine the *in vivo* physiological function of caspase cleavage of ROCK1 during acute damage in the liver by using DEN as a damage-inducing agent. I hypothesized that defects in apoptotic membrane blebbing as a consequence of non-cleavage of

ROCK1 during apoptosis would result in inefficient apoptotic cell clearance thus affecting homeostasis in the liver.

4.1.2 Experimental Aims

The objective of this study was to examine the biological significance of apoptotic blebbing in the maintenance of homeostasis in the liver by using the caspase cleavage resistant ROCK1 (ROCK1nc) mouse model. To achieve this, I investigated the following.

a) Do ROCK1nc mice show a defect in prompt apoptotic cell clearance?

b) Does defective apoptotic blebbing affect the immunological milieu in the liver?

c) Is ROCK1-dependant apoptotic blebbing required to protect the liver and maintain homeostasis in response to acute damage?

4.2 Results

4.2.1 Liver histology and histopathology

Histologically, the liver is composed of a vast network of hepatocytes arranged in single- cell thick plates, separated by sinusoids that are lined by Kupffer cells (resident macrophages) and endothelial cells. There are two sources of blood supply to the liver, with the oxygenated arterial blood coming through the hepatic artery and the nutrient/metabolite rich blood from the gastrointestinal tract emerging through the hepatic portal vein. These two blood vessels, along with the bile duct and lymphatic vessels form the portal tract or portal triad (Figure 4-1a). Blood traverses through the hepatic sinusoids and ultimately drains through the central vein (CV) (Figure 4-1a). For the purpose of histopathological evaluation, the liver acinus is divided into three regions. The area located close to the portal tract is known as periportal region (zone 1) and is the first to be supplied with oxygen and nutrients. The region most distant from the portal triad and close to the central vein is the perivenular or centrilobular region (zone 3). The region between zone 1 and 3 is called intermediate or mid zonal region (zone 2) (Figure 4-1a).

Hepatotoxic drugs produce various histopathological lesions, most of which can be identified from H&E sections. Some of them relevant to this project will be discussed here. An inflammatory reaction, which involves the accumulation of immune cells, is often seen in drug-induced liver damage. If the inflammatory foci are in close proximity to the vessels, they are named after the zone in which they accumulate, for example centrilobular or periportal inflammation (Figure 4-1c). If the inflammatory foci appear in the liver parenchyma, they are commonly referred to as lobular inflammation. Steatosis or accumulation of fat in the hepatocytes is also often seen in drug-induced liver injuries. By convention, any quantity of lipid that occupies more than 5% of the liver mass may be considered ‘pathological’. Macrovesicular steatosis involves the accumulation of large lipid droplets within hepatocytes causing the nucleus to be displaced peripherally (Figure 4-1b). In contrast, microvesicular steatosis involves smaller lipid droplets giving the hepatocyte a foamy appearance (Figure 4-1b). If steatosis is companied by inflammation, necrosis and hepatocyte injury including hepatocyte ballooning, then it is termed steatohepatitis.

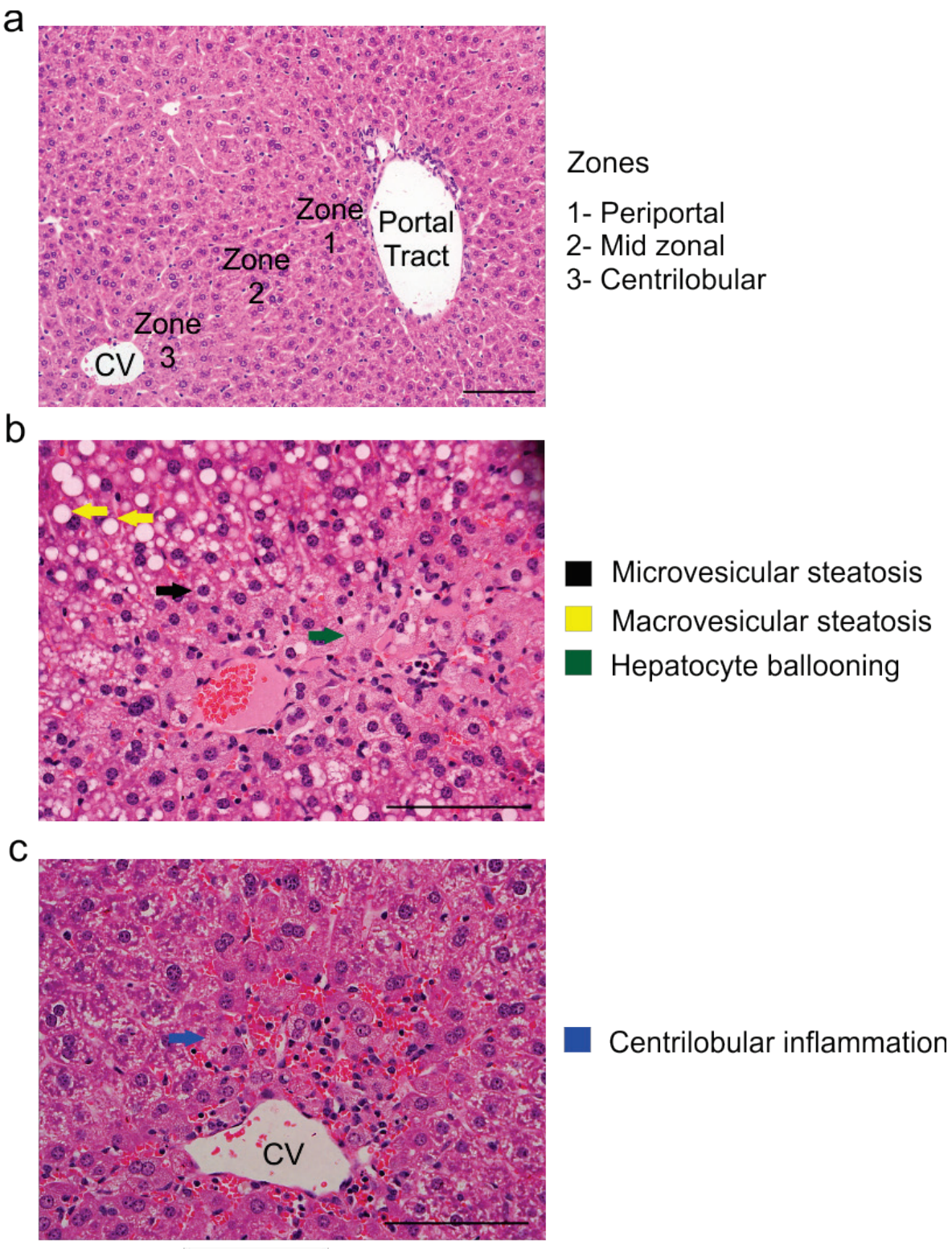

Figure 4-1 Histology and histopathology of liver
Representative H&E stained liver sections showing a) different zones of the liver, b and c) different types of liver lesions. Scale bars represent 100 µm. CV= Central vein.

4.2.2 Optimal dosage of liver damaging agent DEN

Firstly, to determine the optimal concentration of DEN required for studying the effects of defective apoptotic blebbing in liver, I tested two different doses, 50 mg/kg (body weight) and 100mg/kg (body weight) in ROCK1wt and ROCK1nc mice. Single doses of DEN were administered by intraperitoneal injection and mice were monitored for lethargy and weight loss. Animals that were given 50 mg/kg of DEN did not display overt clinical signs even after 6 days. Assessment of H&E stained liver sections from ROCK1wt and ROCK1nc mice did not reveal gross histological anomalies (Figure 4-2a). However, with 100 mg/kg, mice were lethargic and suffered weight loss by 72 hours. Analysis of H&E stained sections revealed that DEN triggered more hepatocellular damage, inflammation and both micro and macrovesicular steatosis in ROCK1nc livers (Figure 4-2b). This provided preliminary evidence that defective apoptotic blebbing in ROCK1nc mice caused more tissue damage and that a higher dose of damage inducing agent was required to delineate the role of apoptotic blebbing in the liver.

Next, to investigate the consequences of defective apoptotic blebbing in apoptotic cell clearance, I decided to perform a time-course experiment to see if ROCK1nc mice were exhibiting a delay in apoptotic cell clearance. With the surety from pilot experiments, 100 mg/kg was finalized as the dose of DEN to be used for the time-course experiment on ROCK1wt and ROCK1nc mice. 10-week old mice were intraperitoneally injected with DEN. Blood (via cardiac puncture) and livers were collected at 24, 48, 72 and 96 hours after DEN treatment.

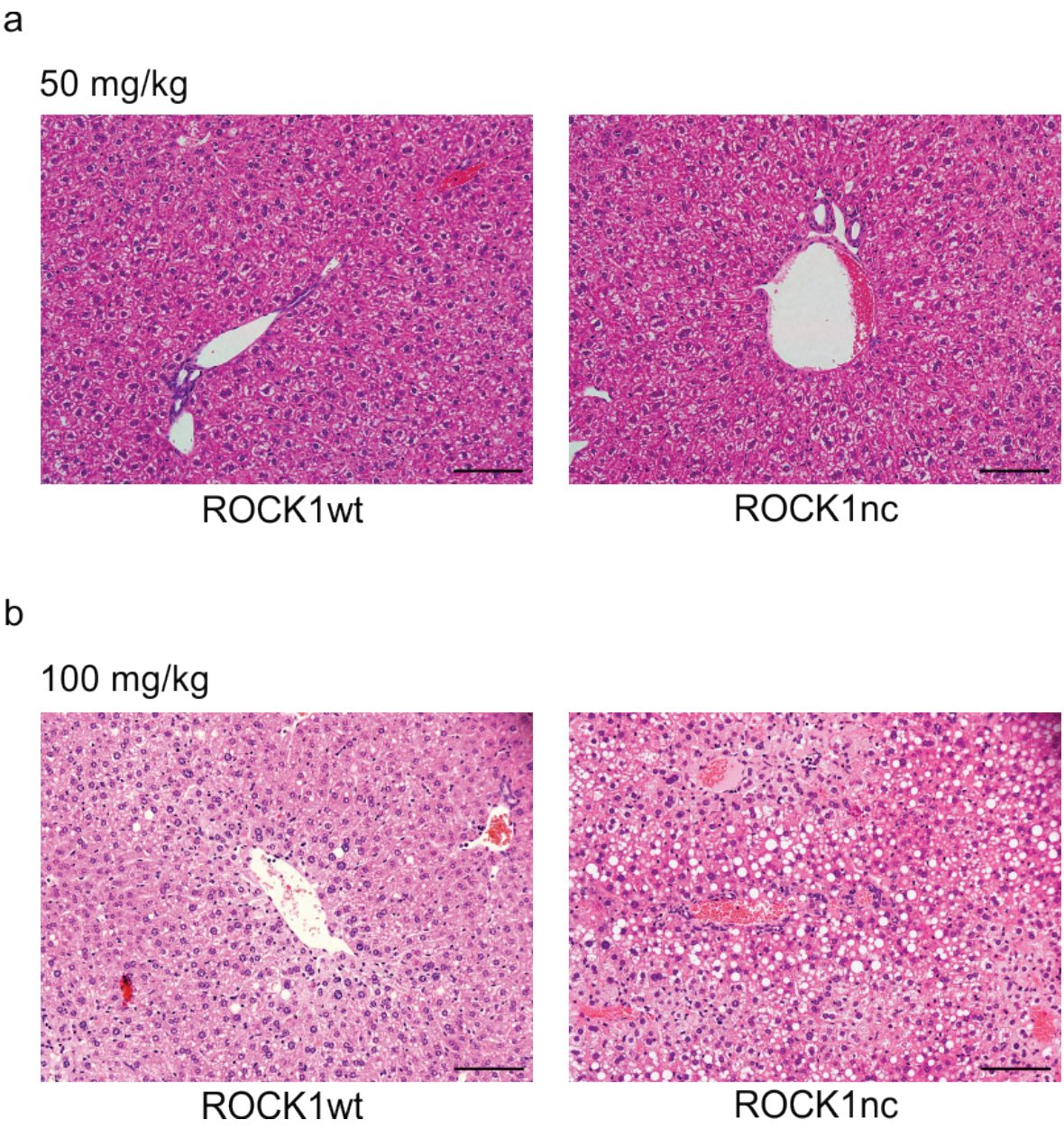

Figure 4-2 Optimal dosage of DEN
Representative H&E stained ROCK1wt and ROCK1nc liver sections with single intraperitoneal injection of a) 50 mg/kg of DEN and collected after 6 days showing no overt histopathological lesions and b) 100 mg/kg of DEN and collected after 3 days showing more inflammation, steatosis and hepatocellular damage in ROCK1nc liver. Scale bars represent 100 μm.

4.2.3 Defective blebbing in ROCK1nc mice results in increased accumulation of apoptotic debris

To investigate accumulation of apoptotic debris in the livers of ROCK1wt and ROCK1nc mice, I utilized the TUNEL assay to detect apoptotic cells. The terminal deoxynucleotidyl transferase-mediated dUTP Nick-End Labelling (TUNEL) assay exploits a biochemical feature of apoptosis, namely DNA fragmentation, and relies on the ability of the enzyme terminal deoxynucleotidyl transferase to incorporate labelled dUTP (deoxyuridine triphosphate) into free 3'-hydroxy termini of fragmented DNA. TUNEL staining was performed on paraffin embedded liver sections and the nuclei were counterstained with DAPI. An apoptotic index was calculated as the percentage of TUNEL-positive cells relative to the total number of DAPI-positive cells.

Analysis of TUNEL staining revealed that in untreated control mice, there were few apoptotic cells (Figure 4-3a, f). By 24 hours after the DEN administration, there was a marked increase in apoptotic debris in both genotypes when compared to untreated mice (Figure 4-3b, f). The amount of cellular debris continued to increase 48 hours after DEN administration in ROCK1wt and ROCK1nc livers (Figure 4-3c, f).

However, by 72 hours, there was a decrease in the apoptotic index in ROCK1wt mice (Figure 4-3f). Yet, in ROCK1nc livers, apoptotic debris continued to accumulate, with a significant increase when compared to ROCK1wt mice at 72 hours (Figure 4-3d, f). This suggested a delay in the clearance of apoptotic remnants in the ROCK1nc mice. At 96 hours, the livers from both genotypes showed a reduction in the apoptotic index suggesting clearance of apoptotic debris by that time (Figure 4-3e, f).

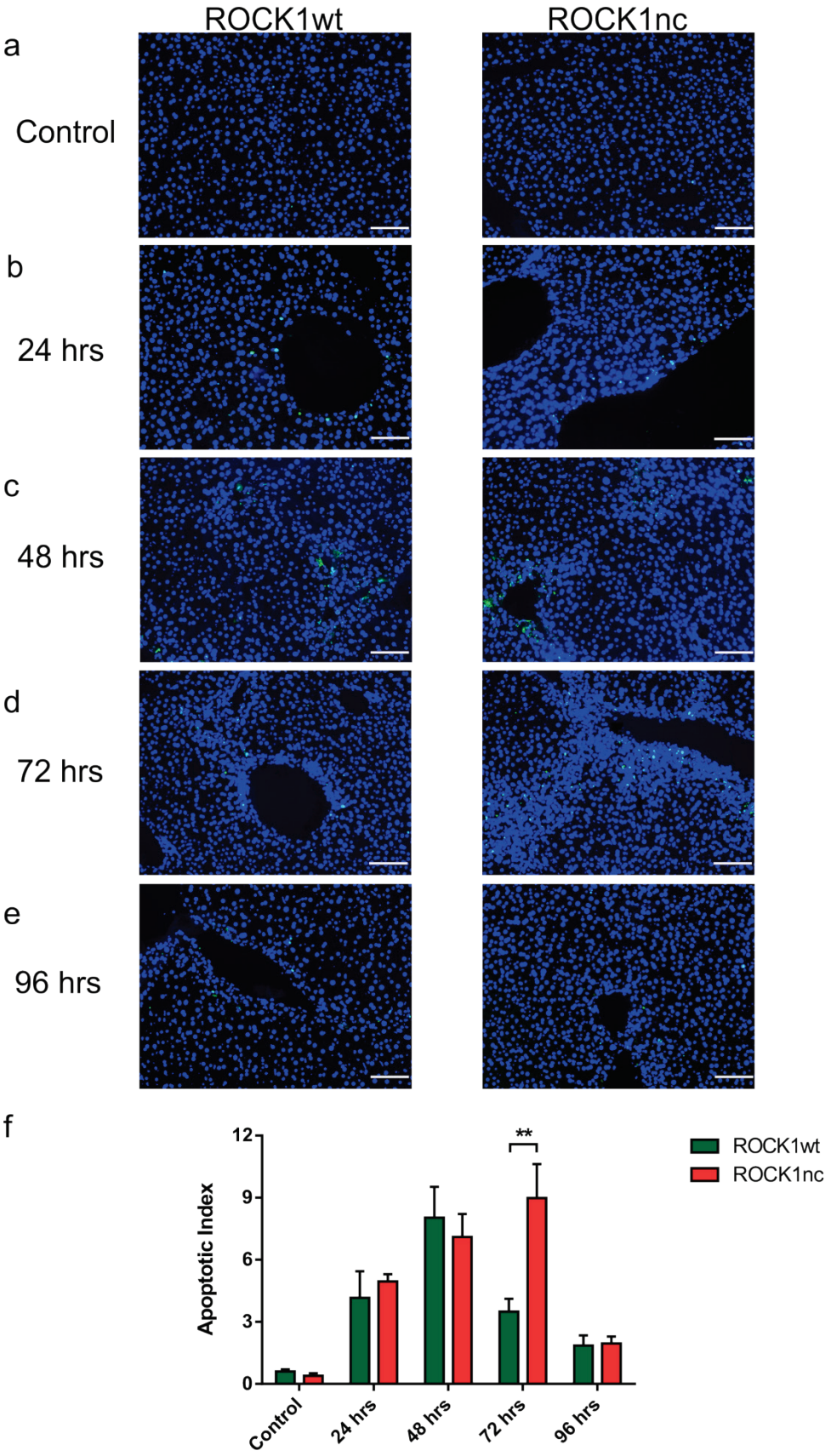

Figure 4-3 Accumulation of apoptotic debris in ROCK1nc livers

a-e) Representative images of immunofluorescence analysis of liver sections showing TUNEL-positive apoptotic debris (green), and counterstained with DAPI (blue). Scale bars represent 100 µm. f) Bar graph represents percentage apoptotic index analysed using TUNEL assay (n=3-11 per group). Data analysed by Student's t-test. Error bars represents SEM. **= $p<0.01$.

4.2.4 Defective blebbing in ROCK1nc mice aggravated hepatocellular damage

Mice were euthanized at different time points after a single dose of DEN and livers were subjected to histopathological analysis using H&E stained slides in order to assess the hepatocellular damage caused by blebbing defects. To quantify the necrotic area, ten random fields from H&E stained liver sections were assessed for each liver.

At 24 hours, both ROCK1wt and ROCK1nc livers exhibit hepatocyte ballooning and mild microvesicular steatosis around the centrilobular region (Figure 4-4a). One ROCK1wt liver also exhibited mild macrovesicular steatosis near the periportal region along with microvesicular steatosis. Occasional apoptotic and necrotic cells were seen in the liver parenchyma of both genotypes, sometimes associated with lobular inflammation.

By 48 hours, there was evidence of necrosis and inflammation in the centrilobular region in both genotypes (Figure 4-4b). The necrotic area and associated inflammatory foci was greater in the ROCK1nc livers when compared to the wild-type (Figure 4-4e). There was also evidence of mild microvesicular steatosis in many of the ROCK1nc liver sections after 48 hours of DEN treatment.

72 hours after DEN treatment, the liver sections showed marked histopathological differences between the two genotypes. ROCK1nc livers exhibited significantly more centrilobular necrotic area associated with inflammation when compared to wild-type livers (Figure 4-4e). The ROCK1nc livers also displayed hepatocellular ballooning, micro and macrovesicular steatosis at the centrilobular zone (Figure 4-4c).

By 96 hours, livers from both genotypes exhibited a lesser extent of damage-associated lesions (Figure 4-4d). There was a drop in the necrotic area associated with inflammatory foci when compared to livers from 72 hours. However, the ROCK1nc livers continued to display significantly more necrotic area when compared to the wild-type livers (Figure 4-4e).

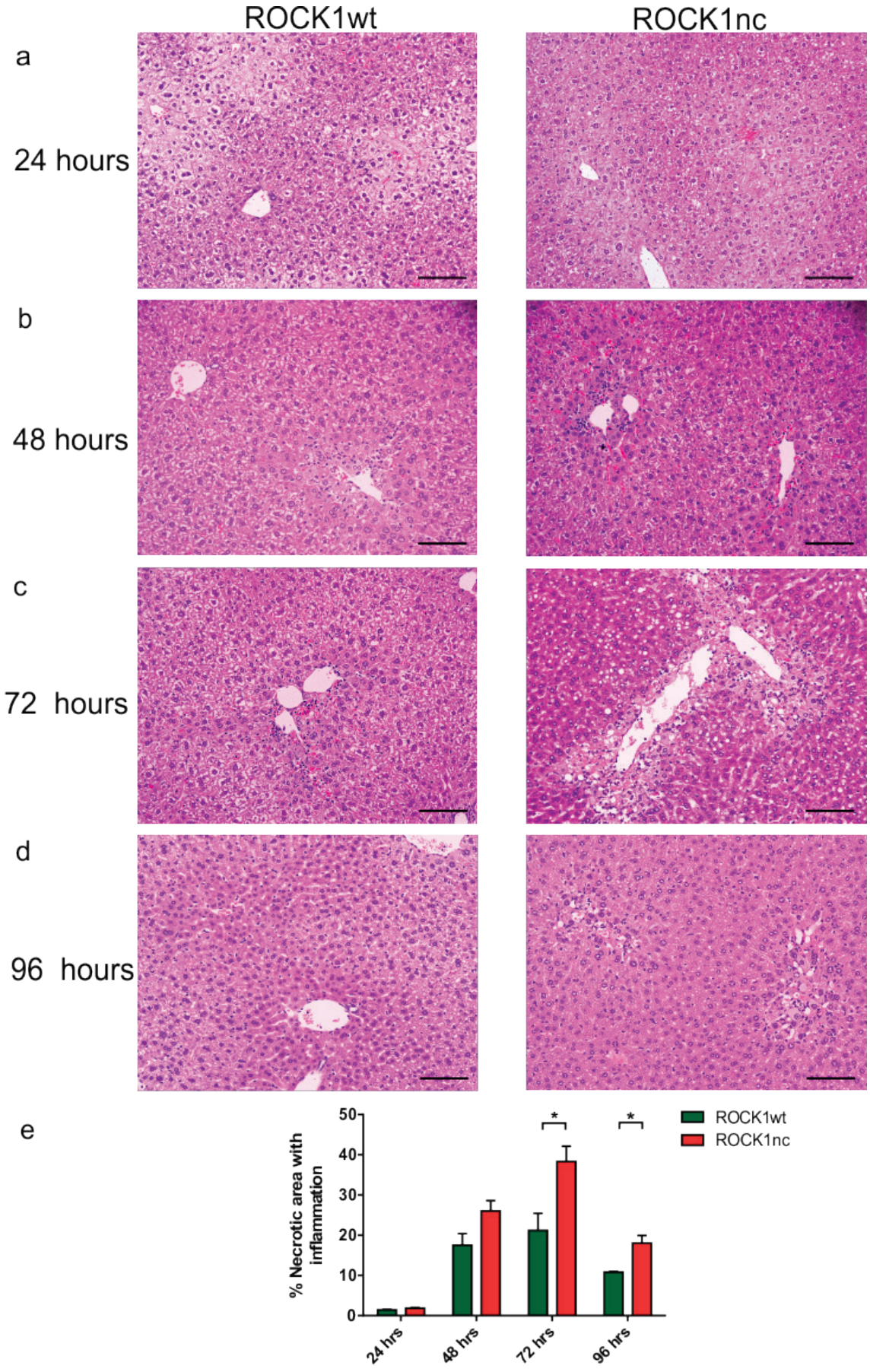

Figure 4-4 Increased hepatocellular damage in ROCK1nc livers
a-d) Representative H&E stained liver sections. Scale bars represent 100 μm. e) Bar graph represents percentage necrotic area with inflammation analysed using H&E staining (n=3-11 per group). Data analysed by Student's t-test. Error bars represent SEM. *=p<0.05.

4.2.5 Accumulation of apoptotic debris is associated with neutrophil recruitment in ROCK1nc livers

Neutrophils are an essential component in the defence against microbes or any other agent that elicits tissue damage. To combat infection, neutrophils can perform phagocytosis, form neutrophil extracellular traps, produce toxic metabolites and release proteolytic enzymes (Kruger et al., 2015). Infiltration of neutrophils in the liver is an acute response to on-going damage accompanied by inflammatory signals. I therefore examined the accumulation of neutrophils in the DEN-treated livers from both wild-type and ROCK1nc livers by immunohistochemistry and quantified the number of neutrophils per mm^2 by analysing five random fields for each liver section.

In untreated age-matched control livers, neutrophils constitute a very small percentage of non-parenchymal cells in both genotypes (Figure 4-5a). The number of neutrophils remained relatively constant 24 hours after DEN treatment (Figure 4-5b). By 48 hours, there was a slight increase in neutrophil numbers in both genotypes, with ROCK1nc livers exhibiting more; albeit not significant numbers when compared to the wild-type livers (Figure 4-5c, f). This observation coincided with the histopathological finding of larger area of inflammatory foci in the ROCK1nc liver (Figure 4-4e).

By 72 hours, as supported by the significant increase in apoptotic debris and significantly larger inflammatory foci in the ROCK1nc mice, there was a drastic increase in the number of neutrophils in their livers (Figure 4-5d, f). 96 hours after DEN treatment, neutrophil numbers in both genotypes had returned to steady state levels, which again coincided with the drop in accumulated debris and the histopathological evidence at this time point (Figure 4-5e, f).

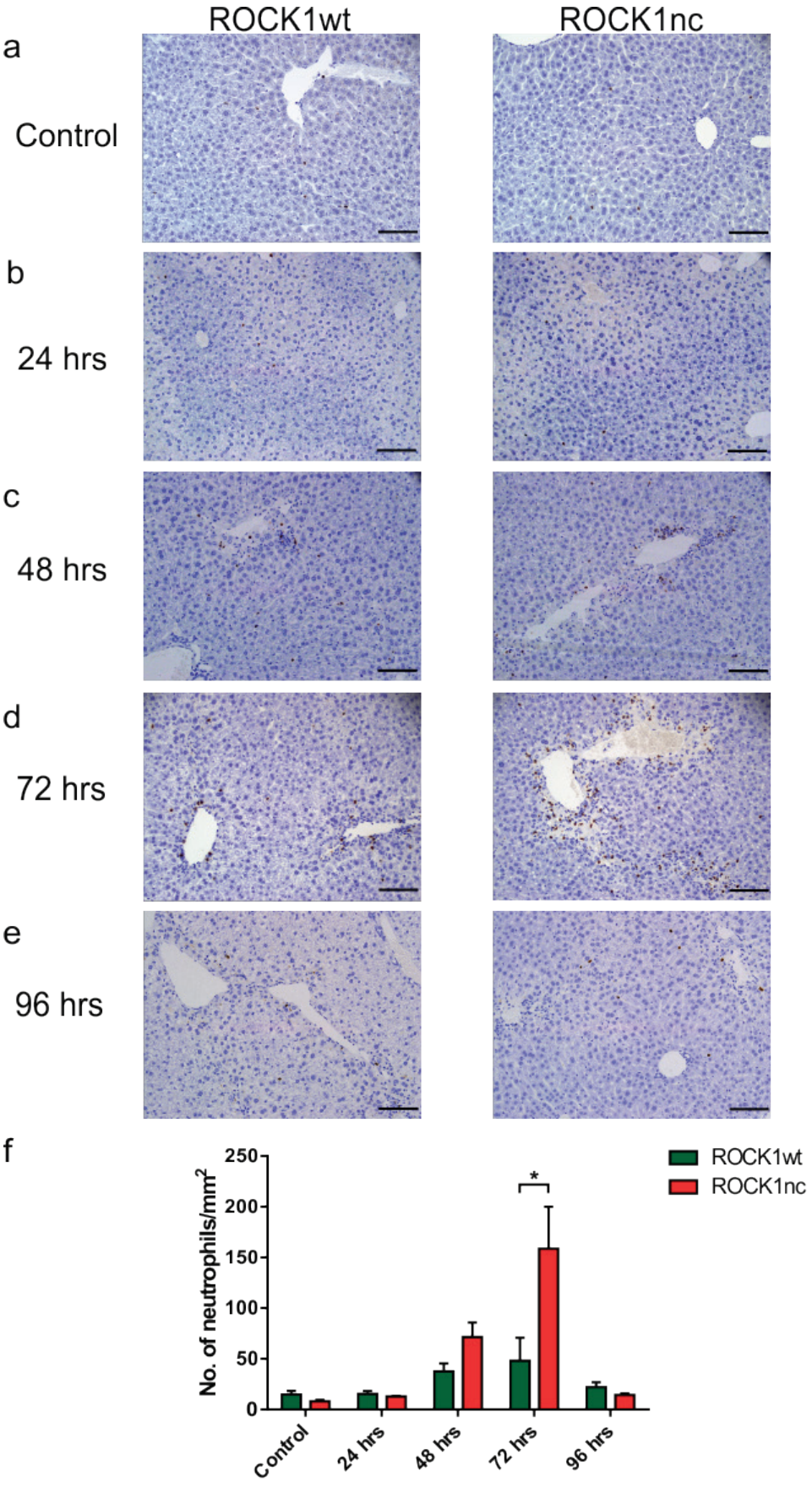

Figure 4-5 Increased recruitment of neutrophils to ROCK1nc livers

a-e) Representative S100A9 stained liver sections showing neutrophils (brown) and counterstained with haematoxylin. Scale bars represent 100 μm. f) Bar graph represents number of neutrophils/mm^2 (n=3-11 per group). Data analysed by Student's t-test. Error bars represent SEM. *=p<0.05.

4.2.6 Accumulation of apoptotic debris increases the number of macrophages in ROCK1nc livers

Owing to its unique function of filtering blood-borne pathogens from the digestive tract and also detoxifying and metabolizing drugs, the liver has its own resident macrophages, known as Kupffer cells. Indeed, the liver harbours the most abundant pool of resident macrophages in the body (Ishibashi et al., 2009). Due to their potent phagocytic activity, macrophages play central roles in the clearance of pathogens and cellular debris. They are also responsible for the maintenance of immunological tolerance in the surrounding milieu, thus balancing the incessant toxic insults. In order to examine whether defective blebbing was altering the number of macrophages in the liver, I quantified the number of F4/80-positive macrophages per mm^2 by analysing five random fields for each liver section.

As expected, liver sections from untreated steady state animals displayed high numbers of macrophages in both genotypes (Figure 4-6a, f). These numbers remained the same even 24 hours after DEN treatment (Figure 4-6b, f). After 48 hours, compared to the 24-hour time point, there was a minor dip in the number of macrophages in both livers, albeit more in ROCK1nc livers (Figure 4-6c, f).

The increased number of macrophages in the ROCK1nc livers became significantly higher by 72 hours after DEN treatment (Figure 4-6d, f). By 96 hours, there was no significant difference in the number of macrophages between the two genotypes (Figure 4-6e, f). However, when compared to the 72 hour time point, the number of macrophages showed a moderate increase and approached steady-state levels in the ROCK1wt livers, but there was an abrupt decline in macrophage numbers in the ROCK1nc livers (Figure 4-6f).

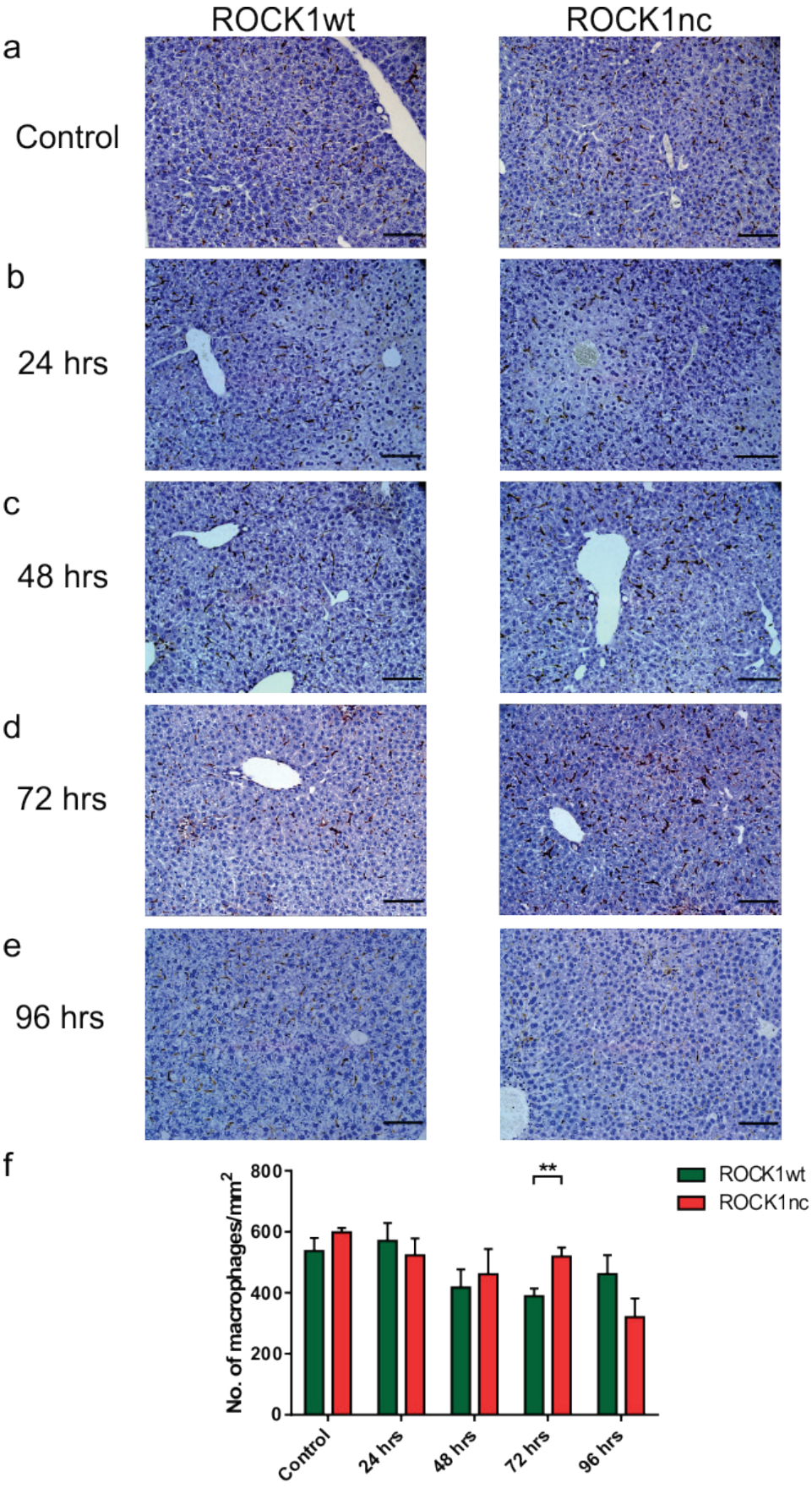

Figure 4-6 Accumulation of macrophages in ROCK1nc livers by 72 hours
a-e) Representative F4/80 stained liver sections showing macrophages (brown) and counterstained with haematoxylin. Scale bars represent 100 μm. f) Graph represents number of macrophages/mm^2 (n=3-11 per group). Data analysed by Student's t-test. Error bars represent SEM. **=p<0.01.

4.2.7 Increased hepatocellular damage in ROCK1nc mice elevates serum levels of alanine aminotransferase and bilirubin

Apart from its obvious role in detoxification and filtering blood borne pathogens, the liver produces enzymes that are required to perform various functions. Alterations in the levels of liver enzymes in the serum are considered as a good indicator of hepatocellular damage. In order to determine whether increased hepatocellular damage, as demonstrated by histopathological studies, was reflected in the serum levels of liver enzymes, I collected serum from untreated and DEN-treated animals. Alanine aminotransferase (ALT) is a standard clinical biomarker of hepatotoxicity (Au et al., 2011) and analysis revealed very low levels in untreated mice (Figure 4-7b). The levels remained low even after 24 hours after DEN treatment. By 48 hours, there was a sharp increase in the levels of ALT in both genotypes, with the ROCK1nc mice exhibiting higher levels when compared to the wild-type (Figure 4-7b). 72 hours after DEN administration, there was a decline in serum ALT levels in the ROCK1wt that coincided with the clearance of apoptotic debris in these mice. ALT levels in ROCK1nc mice remained high after 72 hours, and it was significantly more than their wild-type counterparts (Figure 4-7b). The high serum ALT values were in accordance with the accumulation of apoptotic debris and the increased hepatocellular damage in the ROCK1nc mice (Figure 4-7a). By 96 hours, the level of ALT in serum dropped sharply in ROCK1nc mice and reached similar levels to the wild-type mice (Figure 4-7b). This observation reflected the histopathological analysis at this time point.

The level of bilirubin was also significantly higher in the ROCK1nc mice by 72 hours (Figure 4-7c) (Au et al., 2011), which in conjunction with elevated ALT levels provided a clear indication of hepatotoxicity. Other clinical parameters analysed in the serum include levels of alkaline phosphatase, which surprisingly decreased significantly in the ROCK1nc mice at 72 hours (Figure 4-8a). The liver is also responsible for the production of serum proteins like albumin and globulin. ROCK1nc mice displayed a significant increase in the level of globulin at 72 hours, which can also be a general response to inflammation (Figure 4-8d). Although not significant, there was a decrease in the albumin to globulin ratio, which is also an indicator of hepatocellular injury (Figure 4-8e).

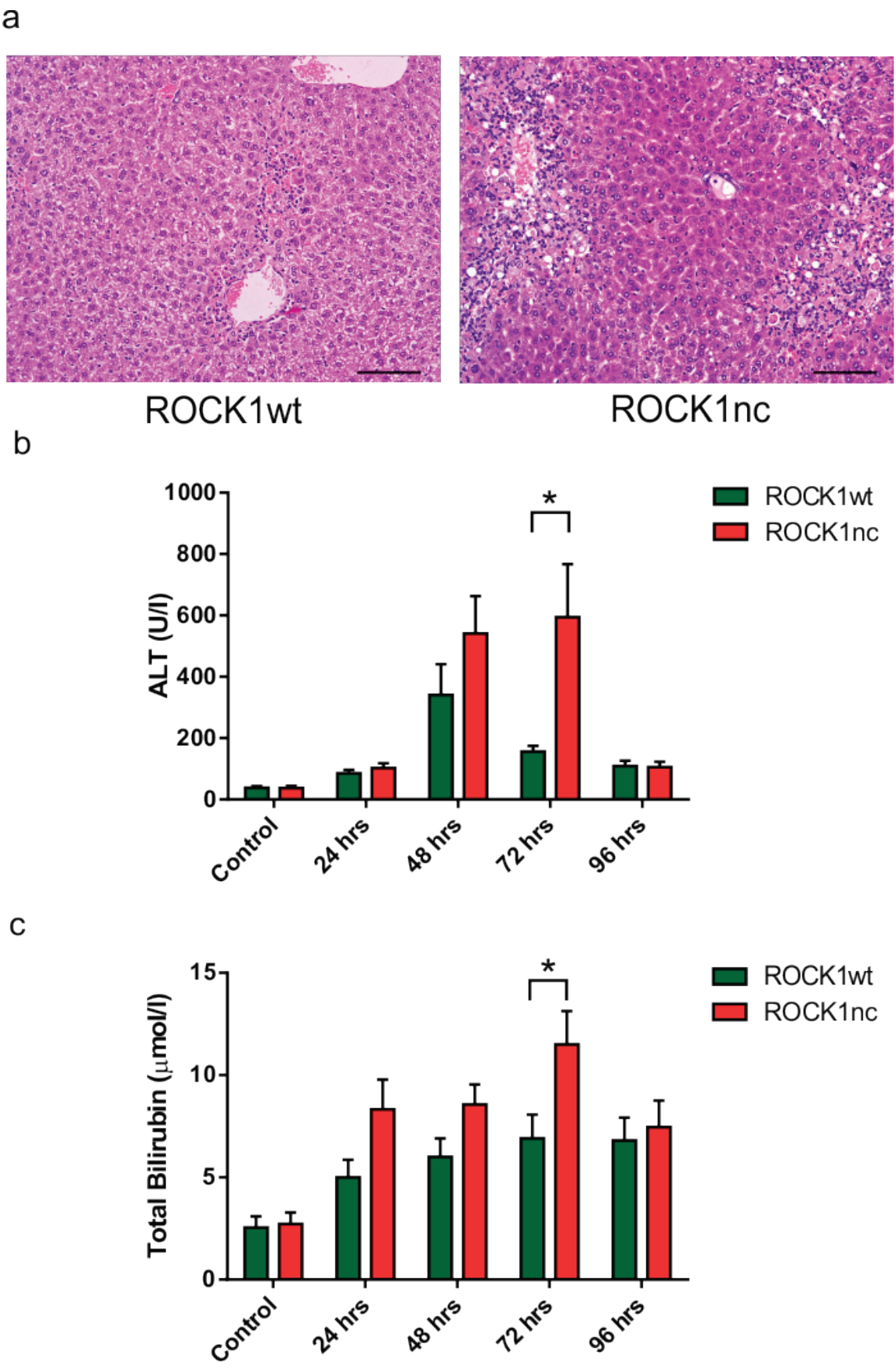

Figure 4-7 Elevated levels of serum ALT and bilirubin in ROCK1nc mice
a) Representative H&E stained liver sections after 72 hours of DEN treatment showing increased centrilobular inflammation and hepatocellular damage in ROCK1nc liver. Scale bars represent 100 µm. b) and c) Serum collected from untreated and DEN treated ROCK1wt and ROCK1nc mice at indicated time points and assayed for ALT and total bilirubin, respectively (n=6-11 per group). Data analysed by Student's t-test. Error bars represent SEM. *=p<0.05.

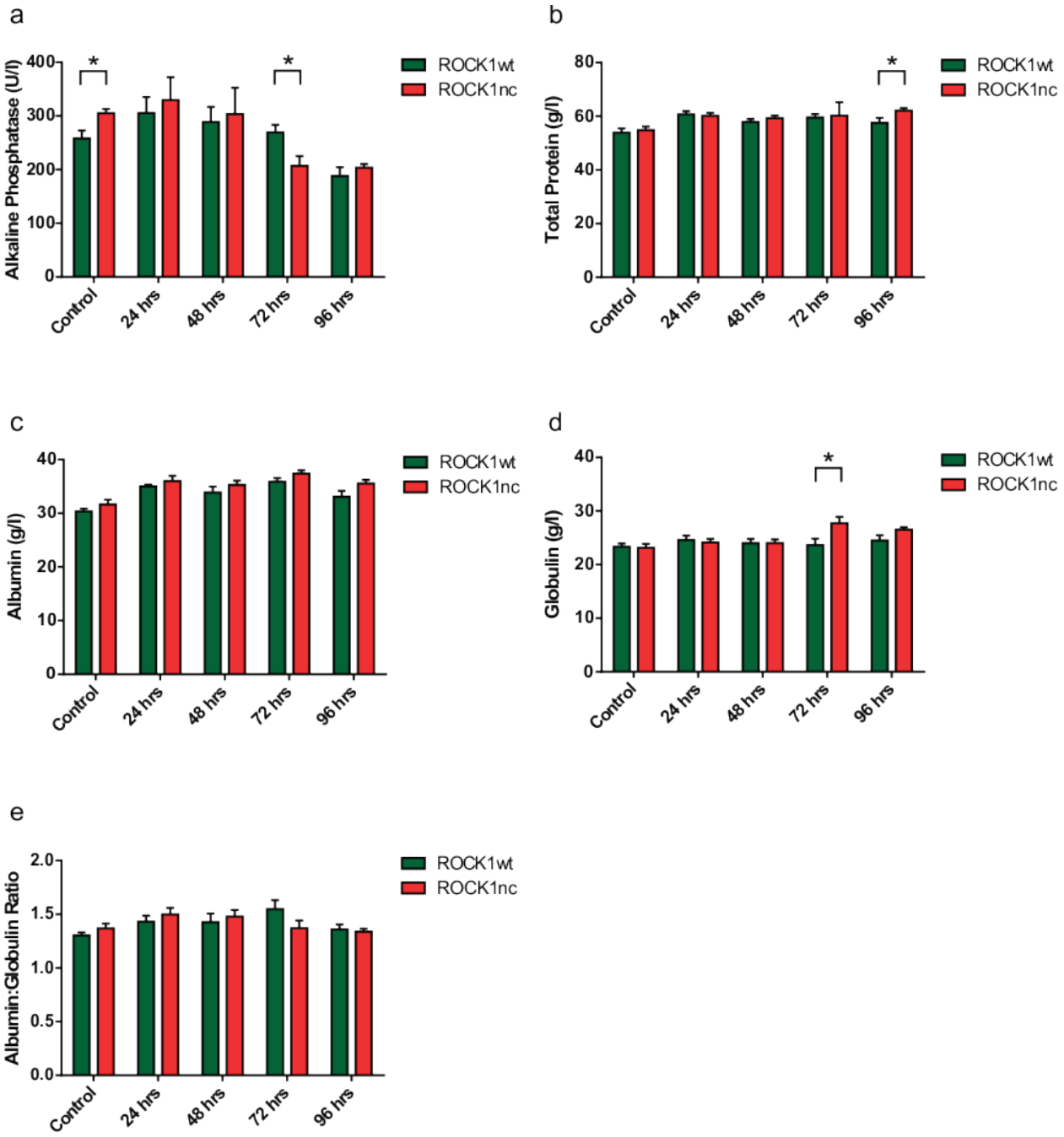

Figure 4-8 Additional parameters of liver function

Serum collected from untreated and DEN treated ROCK1wt and ROCK1nc mice at indicated time points and assayed for a) alkaline phosphatase, b) total protein, c) albumin, d) globulin and e) albumin to globulin ratio (n=6-11 per group). Data analysed by Student's t-test. Error bars represent SEM. *=$p<0.05$.

4.2.8 Defective blebbing increases the levels of serum cytokines in ROCK1nc mice at 72 hours

Cytokines are messengers produced by cells that regulate various inflammatory responses in the body. Levels of serum cytokines have been used as biomarkers for many liver diseases including alcoholic steatohepatitis and cirrhosis (Tilg et al., 1992). A high level of serum cytokines was an indicator of poor prognosis (Felver et al., 1990). Owing to the fact that defective blebbing had a significant impact on the clearance of cellular debris resulting in hepatocellular damage and necrotic inflammation at 72 hours, I wanted to investigate whether this had an influence on the levels of serum cytokines. For this, serum was collected from ROCK1wt and ROCK1nc mice 72 hours after DEN treatment and from the untreated control mice. Concentrations of 15 cytokines in sera were determined using a mouse 15-plex assay (INF-γ, IL-1α, IL-1ß, IL-2, IL-4, IL-5 IL-6, IL-10, IL12p40, IL12p70, IL-17, MCP-1, MIP-1α, MIG and TNFα). The values from the DEN treated samples were normalized to the respective control group.

The levels of all 15 cytokines analysed was increased in DEN- treated ROCK1nc mice after 72 hours when compared to the wild-type. This correlated well with previous findings demonstrating a positive correlation between the level of serum cytokines and hepatic inflammation (Neuman et al., 2002, Neuman et al., 2007). Of these, IL-1α, IL-1ß, IL-2, IL-4, IL-6, IL-10, IL12p40, MCP-1 and TNFα were significantly higher in the treated ROCK1nc mice and increase in IFN-γ levels almost reached significance ($p=0.0506$).

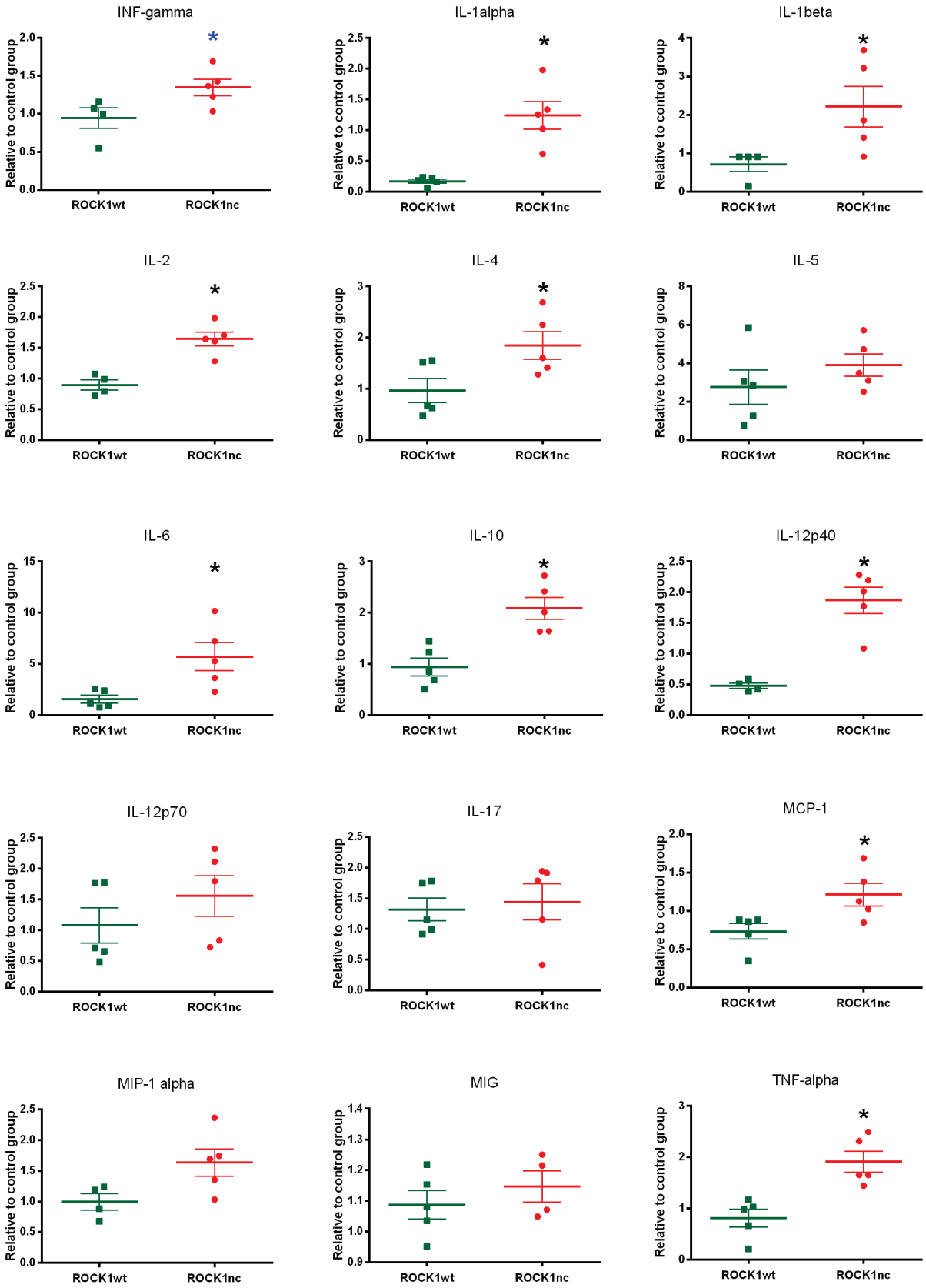

Figure 4-9 Increased levels of serum cytokines by 72 hours

Serum levels of 15 different immune analytes relative to their respective control group collected from wild-type and ROCK1nc mice 72 hours after DEN injection (n=5 per genotype). * = $p<0.05$; * $p = 0.0506$ (Student's t-test).

4.3 Discussion

4.3.1 ROCK1-mediated membrane blebbing is required for swift clearance of apoptotic debris

The liver performs a wide range of fundamental physiological functions and also plays a vital role as a metabolic organ to detoxify drugs and other harmful substances in the blood. Its role in detoxification and drug metabolism owes to the expression of metabolic enzymes and to its unique vascular supply that brings in blood from the gastrointestinal tract. This also makes it quite susceptible to drug-induced hepatocellular damage. Young mice of around 10 weeks old were administered a high dose of DEN and their livers were examined at different time points for the accumulation of apoptotic debris by TUNEL assay. Wild-type mice showed an increase in the accumulation of cellular debris from 24 to 48 hours. By 72 hours, there was a dramatic decrease in debris in wild-type mice, which continued to decrease by 96 hours. However, in ROCK1nc mice, although the increase in debris was similar to the wild-type mice at 24 and 48 hours, debris continued to accumulate even 72 hours after DEN treatment. The debris was cleared only by 96 hours in the ROCK1nc mice, where the debris levels dropped to the same level as the wild-type mice. This clearly suggested a delay in the clearance of apoptotic debris in ROCK1nc mice. Hence, during apoptosis, caspase-cleavage mediated ROCK1 induced membrane blebbing is essential for the prompt removal of apoptotic debris. An alternative or additional factor that could contribute to the pattern of increased apoptotic debris in ROCK1nc mice is that inflammatory response, such as neutrophil recruitment, might feed-forward to further increase the levels of cell death induced by DEN treatment.

4.3.2 Increased number of immune sentinels at the site of debris accumulation

Neutrophils are generally the first cell type to arrive at sites of inflammation. Infiltration of neutrophils is a hallmark of the innate immune response and forms the first line of defence during infection and injury. In response to chemotactic factors released at inflammatory sites, neutrophils migrate from the blood stream to the target site (Butcher, 1991). During steady-state, neutrophils constitute a very small percentage of non-parenchymal cells in the liver. Unlike

during bacterial infection in the liver, when the neutrophil numbers increase by almost 10 to 20-fold within two hours (Gregory et al., 1996), neutrophil numbers remained almost similar to steady state levels even 24 hours after DEN administration. Accumulating apoptotic debris in the wild-type and ROCK1nc mice by 48 hours onwards correlated with an increase in the number of neutrophils infiltrating the livers. In response to the significant increase in apoptotic debris in ROCK1nc mice at 72 hours, there were significantly more neutrophils as well. By 96 hours, neutrophil numbers returned to basal levels in both genotypes, which again correlated well with the decreased cellular debris at this time point.

Owing to its inherent role in encountering pathogens and environmental toxins from the gut, the liver is endowed with its own resident macrophage population, known as Kupffer cells. These cells represent almost 35% of the non-parenchymal liver cells in normal adult mice (Gregory and Wing, 1990). These phagocytes line the liver sinusoids and play an important role in the homeostasis of the liver. Whether circulating monocytes contribute to the Kupffer cell pool or whether the Kupffer cells self-renew during adult life has been a topic of debate over many years (Zimmermann et al., 2012). However, recent studies have highlighted that during liver injury, the resident macrophage population is in fact expanded by circulating monocytes (Holt et al., 2008, Karlmark et al., 2009, Zimmermann et al., 2010).

In steady-state conditions, there were large numbers of resident macrophages in both wild-type and ROCK1nc mice. The number of macrophages remained similar even 24 hours after DEN treatment. However, by 48 hours, there was slight decrease in the macrophage numbers in both genotypes, the reason for which is not known. A previous study had also shown a similar decrease in F4/80- positive macrophages after paracetamol-induced liver injury (Dambach et al., 2002). However, a recent study aimed at characterizing macrophages in paracetamol-induced liver injury identified two populations in the liver, the resident Kupffer cells (CD11b-low, F4/80-high) and infiltrating monocytes (CD11b-high; F4/80-low) (Holt et al., 2008). They identified an increase in circulating monocytes accompanied by a decrease in the resident macrophage population at 24 and 48 hours after paracetamol challenge (Holt et al., 2008). This could be a possible explanation for the decrease in macrophage numbers seen in my experiment

since I had employed immunohistochemical identification of macrophages using the F4/80 monoclonal antibody, which presumably failed to detect the increasing number circulating monocytes at 48 hours. By 72 hours, with accumulating apoptotic debris, there was a significant increase in the number of macrophages in the ROCK1nc livers when compared to the wild-type livers. However, it is highly likely that in this study, the macrophage numbers at 48, 72 and 96-hour time points are under-represented because of the aforementioned limitation in immunohistochemical detection.

4.3.3 Delayed clearance of cellular debris causes increased hepatocellular damage

Combining histological analysis of liver sections and clinical liver function tests is often employed for the assessment of drug-induced liver injury. Depending on the drug used, the liver can exhibit a plethora of histological injury patterns including steatosis, necrosis with or without inflammation, cholestasis, hepatocellular ballooning and vascular abnormalities (Ramachandran and Kakar, 2009). In this experiment, histomorphological features of DEN-induced liver damage included steatosis, hepatocyte ballooning and centrilobular necrosis with inflammation. At 72 hours, parallel to the delayed clearance and significantly higher numbers of inflammatory cells, ROCK1nc livers also revealed increased centrilobular necrosis, steatosis and hepatocyte ballooning. By definition, steatosis when accompanied by inflammation and hepatocellular injury is termed as steatohepatitis.

The higher degree of steatohepatitis seen in ROCK1nc livers at 72 hours was also echoed in the liver function tests. The elevation of alanine aminotransferase (ALT) in the serum is an excellent marker for hepatocellular injury and liver damage (Au et al., 2011). Serum collected from ROCK1nc mice showed significantly high levels of ALT when compared to wild-type at 72 hours. Total bilirubin was also significantly higher in the ROCK1nc serum at the same time point. Elevated levels of bilirubin can indicate cholestasis or impaired bile flow. Yet, upon histological analysis, I did not see any indication of this pathology in any of the liver sections. This was not surprising since increased bilirubin with minimal or no increase in ALT can indicate cholestasis. An elevated bilirubin level along with increased ALT levels is a good marker for liver damage (Au et

al., 2011). At 72 hours, serum from ROCK1nc mice also showed a significant increase in the level of globulin proteins, which can also be a general response to inflammation. Although not significant, albumin to globulin ratio in ROCK1nc serum was decreased, which is an additional indicator of hepatocellular injury.

Hepatocellular damage seen in the centrilobular zone of ROCK1nc liver sections can be attributed to the presence of increased numbers of immune cells in addition to the presence of accumulating apoptotic debris. Despite its role as a defence mechanism against infection and injury, infiltrating neutrophils have a dark side in that they can cause tissue damage in the liver. In fact, neutrophils exacerbating tissue injury has been reported in a number of liver-damage models (Gujral et al., 2003, Liu et al., 2006). After accumulating in the hepatic sinusoids, neutrophils extravasate into the liver parenchyma in response to signals released by dying or distressed hepatocytes (Jaeschke and Hasegawa, 2006). Once in the liver parenchyma, neutrophils make contact with the hepatocytes through integrins and subsequently release reactive oxygen intermediates and serine proteases which contribute to hepatocellular damage (Jaeschke and Hasegawa, 2006).

Similarly, liver-resident macrophages also can have damaging effects in the liver. Despite their well-known role in the maintenance of homeostasis in the liver, several studies have implicated Kupffer cells in the pathogenesis of drug – induced liver damage (Michael et al., 1999, Ito et al., 2003). The strategic position in the liver sinusoidal space enables them to easily traverse this barrier and directly interact with hepatocytes. Activated Kupffer cells release a number of cytokines and other mediators including reactive oxygen species and proteases that aggravate acute injury in the liver (Roberts et al., 2007). Thus it is possible that along with the detrimental effects of uncleared apoptotic debris, the resident and recruited immune cells may contribute to exacerbating the damage in the liver.

4.3.4 Increased hepatocellular damage owing to clearance defects increases the level of serum cytokines

Cytokines are messengers produced mainly by the cells of the innate and adaptive immune system in response to a number of environmental stimuli

including infection and tissue damage. The functions of cytokines are often redundant and vary depending on the immunological milieu as well as the presence or absence of other cytokines. Levels of serum cytokines have been used as biomarkers for the pathogenesis of many chronic liver diseases (Tilg et al., 1992). The levels of serum cytokines correlate with the degree of hepatic inflammation and fibrosis (Neuman et al., 2007).

As expected, serum levels of 15 cytokines were high in the mice treated with DEN after 72 hours when compared to the wild-type. Of these, IL-1α, IL-1ß, IL-2, IL-4, IL-6, IL-10, IL12p40, MCP-1 and TNFα were significantly higher in the treated ROCK1nc mice and the increase in IFN-γ levels almost reached significance. The high level of serum cytokines in ROCK1nc mice is a good biomarker for the on-going hepatocellular damage upon DEN administration. The accumulating immune cells in the ROCK1nc livers are the conceivable source of these cytokines in the serum. Elevated levels of cytokines including TNFα, primarily released by Kupffer cells, have been implicated in aggravating drug-induced liver damage (Roberts et al., 2007). Cytokines including IL-1 and IL-6 produced by Kupffer cells can mediate neutrophil accumulation in the hepatic microvasculature (Ramaiah and Jaeschke, 2007). Monocyte chemoattractant protein 1 (MCP-1), produced by hepatic stellate cells, hepatocytes and macrophages, is responsible for the recruitment of pro-inflammatory monocytes to the liver thus counteracting resolution of inflammation (Baeck et al., 2014). Interestingly, anti-inflammatory cytokines like IL-10 are also elevated in the serum of ROCK1nc mice. IL-10 is produced by Kupffer cells and normally has a protective role by inducing tolerance in drug-induced liver damage (Erhardt et al., 2007). It could be possible that increased numbers of macrophages in the ROCK1nc liver by 72 hours are attempting to restore tolerance by the release of cytokines involved in resolution.

4.4 Summary

Apoptotic membrane blebbing by caspase cleavage of ROCK1 is essential for the maintenance of liver homeostasis. Defective blebbing causes tissue damage possibly by the release of toxic intracellular contents from the uncleared apoptotic debris. The assembly of immune cells at the site of damage can aggravate the damage and ultimately cause a breakdown in tissue homeostasis.

5 Damaging effects of defective blebbing is mediated by HMGB1

5.1 Introduction

5.1.1 Secondary necrotic cells release DAMPs to signal the immune system

The robust nature of apoptotic clearance mechanisms is illustrated in the difficulty to detect apoptotic cells even in tissues with high turnover. If apoptotic cells are not removed efficiently, they proceed to a necrotic stage, which was termed as 'secondary necrosis' (Wyllie et al., 1980). Secondary necrotic cells release their cytotoxic intracellular contents, thus instigating inflammation (Gaipl et al., 2004). Accumulation of apoptotic cell remnants due to inefficient clearance affects tissue homeostasis and contributes to the establishment and progression of a number of pathologies including autoimmunity, respiratory and neurological diseases (Elliott and Ravichandran, 2010). Release of danger signals from necrotic cells is considered as a major distinction from apoptotic cells. These endogenous danger signals, known as damage-associated molecular patterns (DAMPs) are molecules released by stressed or necrotic cells. They have the ability to promote and exacerbate immune responses. An ever growing list of DAMPs have been identified over the years including HMGB1, S100 proteins, heat shock proteins and IL-1α (Kang et al., 2015). Of these, one of the most extensively characterized DAMP is high-mobility group box protein 1 (HMGB1).

5.1.2 High-Mobility Group Box 1 (HMGB1)

HMGB1 is a small protein of 215 amino acid residues. The protein structure is composed of three distinct domains: two consecutive positively charged L-shaped basic domains (called HMG boxes A and B) of approximately 80 amino acids and a negatively charged 30 amino acid-long acidic tail at the C-terminal, connected by short flexible linkers. HMGB1 also has two close relatives, HMGB2 and HMGB3, with 80% amino acid identity amongst the three proteins. HMGB1 is a non-histone DNA binding protein that binds to the minor groove of double-stranded DNA without sequence specificity (Bianchi et al., 1989). It facilitates the assembly of nucleoprotein complexes and also regulates gene transcription,

replication and repair (Bianchi and Agresti, 2005). Its physiological importance was highlighted in studies in which HMGB1 knockout mice died within 24 hours due to hypoglycaemia (Calogero et al., 1999).

Apart from its structural role in the nucleus, HMGB1 can also function as a cytokine. Secretion of HMGB1 to the extracellular milieu occurs either actively by immune cells or passively from damaged or necrotic cells (Lotze and Tracey, 2005). Secretion of HMGB1 requires the shuttling of the protein from the nucleus into the cytoplasm. Post–translational modifications including methylation, acetylation and phosphorylation, results in the translocation of HMGB1 to the cytosol, where it is packaged into specialized secretory lysosomes and finally released into extracellular space via fusion of these lysosomes to the plasma membrane (Sims et al., 2010). HMGB1 is secreted by macrophages, monocytes, dendritic cells and natural killer cells, in response to activation by pro-inflammatory stimuli such as LPS, IL-1β, interferon (IFN)-γ, or TNFα (Lotze and Tracey, 2005). Once secreted, HMGB1 can act as a cytokine by triggering the release of additional cytokines from monocytes and neutrophils. On the other hand, HMGB1 passively released from the nucleus due to loss of membrane integrity is a signal of necrotic cell death. Although early investigators concluded that apoptotic cells do not significantly secrete HMGB1, since apoptotic cells modify the chromatin so that HMGB1 binds irreversibly (Scaffidi et al., 2002), these findings were subsequently re-evaluated (Bell et al., 2006). Further studies showed that cells undergoing apoptosis do release considerable amounts of HMGB1 but induces a tolerogenic response instead of an inflammatory one (Kazama et al., 2008).

The role of HMGB1 as a potent pro-inflammatory cytokine was underpinned by an early study that showed it could mediate endotoxin lethality in mice (Wang et al., 1999). Whether HMGB1 can promote pro-inflammatory activity directly, or indirectly by attracting inflammatory cells, has been a topic of debate. Once secreted, HMGB1 induces inflammatory responses through many binding receptors including receptor for advanced glycation end products (RAGE), and toll-like receptors TLR4 and TLR2. When HMGB1 binds to these receptors, it results in NF-kB activation, which would eventually promote the transcription of pro-inflammatory genes, such as IL-1β, IL-6, and TNFα (Sims et al., 2010).

5.1.3 Glycyrrhizin- an inhibitor of HMGB1

Glycyrrhizin (GLZ) is a glycoconjugated triterpene produced by the liquorice plant, *Glycyrrhiza glabra* and is responsible for its sweet taste. This compound has been associated with different pharmacological effects, including anti-viral, anti-inflammatory, anti-tumour and hepato-protective functions (Asl and Hosseinzadeh, 2008). Moreover, it is extensively used in Japan to treat patients with chronic hepatitis (Arase et al., 1997). GLZ can bind directly to HMGB1 (Kd ~ 150 μM), where it interacts with two shallow concave surfaces formed by the arms of both HMG boxes (Mollica et al., 2007). It was reported that upon binding to the specific pocket, GLZ inhibits the cytokine activities of HMGB1 by inhibiting its chemoattractant and mitogenic activities (Mollica et al., 2007, Sitia et al., 2007). Over the years, GLZ has been used to alleviate HMGB1-associated damage in a number of organs including the liver (Ogiku et al., 2011, Wang et al., 2013), heart (Zhai et al., 2012), pancreas (Xiang et al., 2014) and brain (Zhang et al., 2014).

5.1.4 Experimental Aims

The aim of this study is to examine whether blocking the cytokine activity of HMGB1 released by accumulating apoptotic debris, using Glycyrrhizin, can reduce the damaging effects of defective blebbing in ROCK1nc mice. To achieve this, I examined the following

a) Does Glycyrrhizin treatment affect the accumulation of apoptotic debris caused by DEN?

b) Does Glycyrrhizin treatment affect the immunological milieu in mice with defective blebbing?

c) Would blocking the cytokine activity of HMGB1 reduce the damage caused by defective blebbing in ROCK1nc mice?

5.2 Results

5.2.1 Increased cytoplasmic translocation of HMGB1 in DEN-induced damage in ROCK1nc livers

As discussed above, HMGB1 is a non-histone nuclear protein that plays an important role in the regulation of gene transcription. However, extracellular release of HMGB1 contributes to the pathogenesis of various inflammatory diseases as it has the potential to function as damage associated molecular pattern protein (Bianchi, 2007).

72 hours after DEN treatment, livers from ROCK1nc mice exhibited significantly more centrilobular necrosis, and infiltration of immune cells when compared to ROCK1wt livers. To determine the cellular localization of HMGB1 in livers from DEN- treated ROCK1wt and ROCK1nc mice, immunohistochemical staining was performed on paraffin sections. Following immunostaining with HMGB1, it was evident that the subcellular localization of HMGB1 in hepatocytes was different between the two genotypes (Figure 5-1a). ROCK1wt livers exhibited predominantly nuclear localization of HMGB1, with some cells showing the presence of HMGB1 in the cytoplasm as well (Figure 5-1b). In contrast, HMGB1 was typically found both in the nucleus and cytoplasm in ROCK1nc hepatocytes (Figure 5-1b). In some ROCK1nc hepatocytes, HMGB1 staining was observed in the cytoplasm alone and was barely detectable in the nucleus (Figure 5-1b). Hepatocytes with cytoplasmic localization of HMGB1 with or without nuclear expression were mostly restricted to the inflamed centrilobular regions. Liver sections from both genotypes also exhibited strong HMGB1 staining in some immune cells as well (Figure 5-1 b).

Analysis of the percentage of hepatocytes with cytoplasmic translocation of HMGB1 from three random fields revealed significantly more translocation in ROCK1nc hepatocytes when compared to ROCK1wt (Figure 5-1c). Cytoplasmic translocation of HMGB1 has been reported both in animal models as well as in patients with acute liver failure and it has been suggested that its presence in the cytoplasm is a necessary step for extracellular release (Zhou et al., 2011).

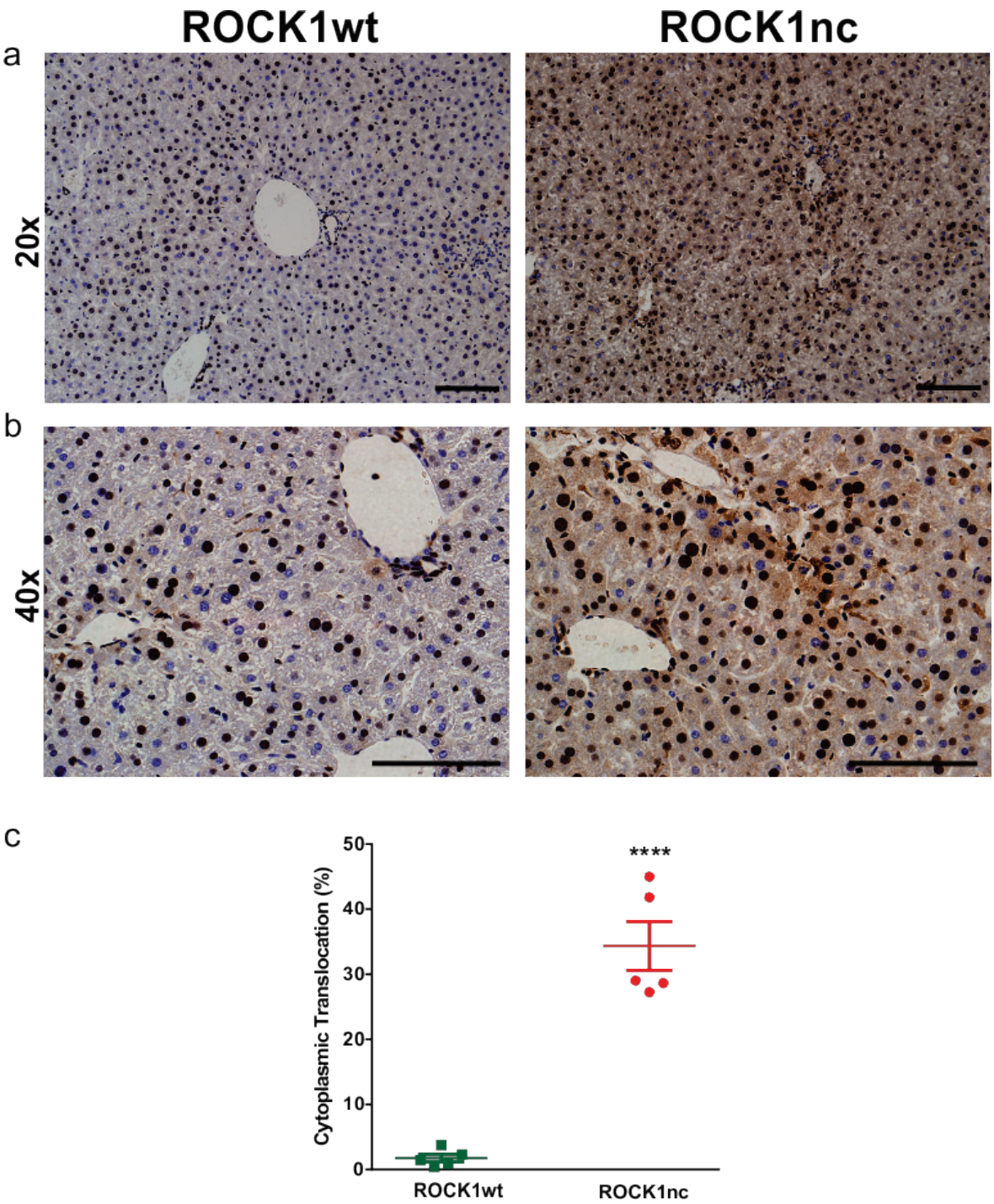

Figure 5-1 Increased cytoplasmic translocation of HMGB1 in ROCK1nc hepatocytes
Representative images from HMGB1- stained liver sections, from ROCK1wt and ROCK1nc mice 72 hours after DEN treatment at, a) 20x and b) 40x magnification, showing predominantly cytoplasmic staining in ROCK1nc hepatocytes. Scale bars represent 100 µm. c) Scatter dot plot (mean ± SEM) represents percentage cytoplasmic translocation of HMGB1 in hepatocytes. Data was analysed using Student's t-test. **** = $p<0.0001$.

5.2.2 Inhibiting the cytokine activity of HMGB1 using Glycyrrhizin

Induction of acute liver damage using DEN resulted in the accumulation of apoptotic debris and recruitment of inflammatory cells in ROCK1nc mice after 72 hours. Interestingly, livers from these mice exhibited cytoplasmic translocation of HMGB1 that is indicative of an immediate extracellular release. Extracellular HMGB1 is a well-known damage associated molecular pattern that has been shown to exacerbate inflammation. To better understand the role of HMGB1 in ROCK1 dependent apoptotic cell clearance, I investigated whether GLZ, an inhibitor of HMGB1, can reduce the accumulation of apoptotic debris and inflammation and in turn alleviate hepatocellular damage in ROCK1nc mice that have been administered with the damage-inducing agent, DEN.

To achieve this, mice were injected intraperitoneally with two doses of GLZ (200mg/kg per injection) prior to DEN (100 mg/kg) or vehicle (PBS) injection. Following administration of DEN/Vehicle, mice were again given GLZ, twice daily for the next two days. Mice were necropsied three days after DEN/Vehicle treatment (Figure 5-2a). Intraperitoneal injection of a total of six doses of GLZ (200 mg/kg per dose) without DEN injection over a period of four days did not have an untoward effect on the mice, as evidenced by their body weight and liver weight measurements (Figure 5-2c) and histopathological analysis (Figure 5-2b). H&E stained liver sections from ROCK1wt and ROCK1nc from both genotypes did not exhibit any overt histopathological lesions but maintained healthy tissue architecture (Figure 5-2b). Administration of six doses of GLZ over a period of four days did not have a significant impact on body weight, with both genotypes losing around 5 % weight (Figure 5-2c). Having confirmed that GLZ on its own had no undesirable effects in the mice, I proceeded to combine GLZ treatment with DEN-induced damage by following the treatment regimen as detailed in Figure 5-2a.

a

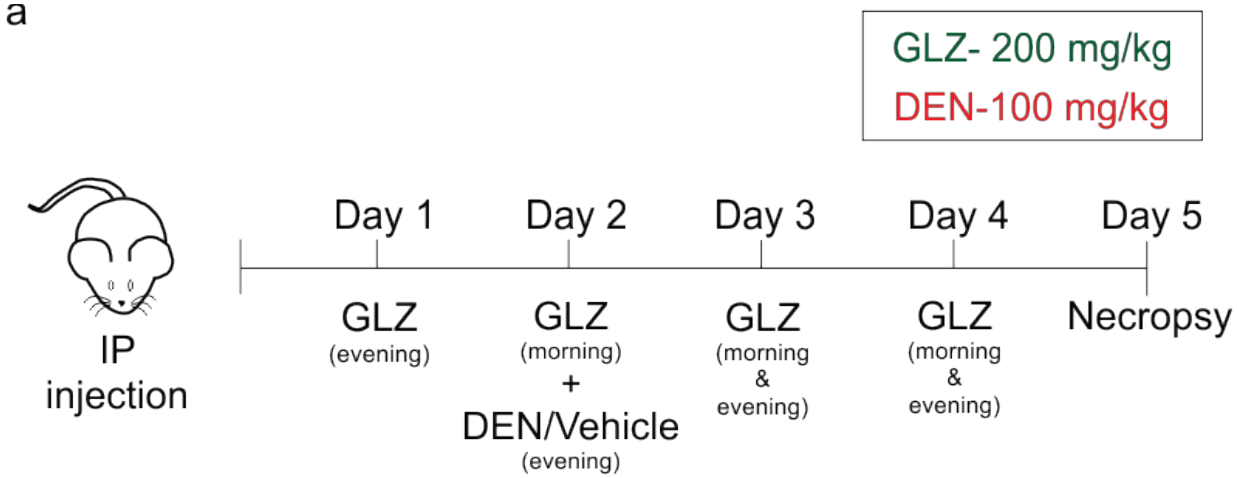

b

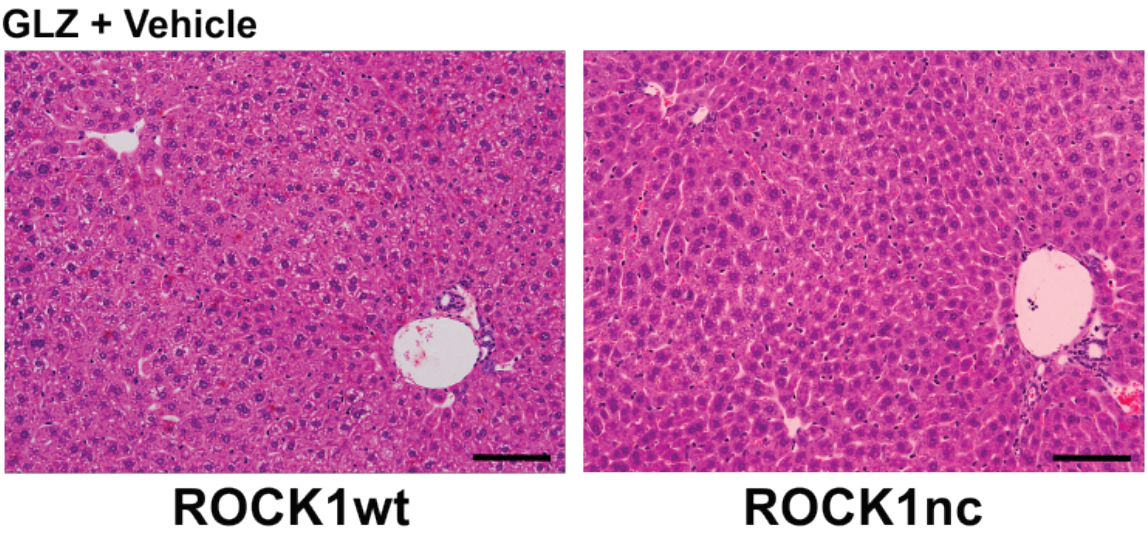

c

GLZ + Vehicle

Genotype	Initial Body Weight (g)	Final Body Weight (g)	Weight Loss (%)	Liver Weight (g)	Relative Liver Weight
ROCK1wt	24.6 ±4.3	23.4±4.6	4.9±4.9	1.3±0.3	5.6±0.8
ROCK1nc	23.8 ±3.5	22.5±3.1	4.9±5.2	1.1±0.2	4.8±0.6

Figure 5-2 Using Glycyrrhizin as an inhibitor for HMGB1

a) Schematic representation of the treatment regimen with Glycyrrhizin (GLZ) and Diethylnitrosamine (DEN) in ROCK1wt and ROCK1nc mice. b) Representative H&E stained liver sections from ROCK1wt and ROCK1nc mice treated with GLZ and Vehicle (PBS) exhibiting no overt histopathological lesions. Scale bars represent 100 µm. c) Table shows the effect of GLZ on body weight and liver weight in mice. Numbers represent mean values ± standard deviation (n= 6-8 per genotype).

5.2.3 Glycyrrhizin treatment reduced accumulation of apoptotic debris in ROCK1nc mice

Accumulation of apoptotic debris was significantly greater in ROCK1nc livers compared to the wild-type within 72 hours of DEN-induced damage (Figure 5-3a). To examine whether treatment with GLZ in mice exposed to the damaging effects of DEN had an impact on the accumulation of apoptotic cells by 72 hours, TUNEL staining was performed on paraffin-embedded liver sections and counterstained with DAPI. Three representative fields from each sample were imaged by fluorescence microscopy and analysed using Image J software. An apoptotic index was calculated as a percentage of TUNEL positive apoptotic debris relative to the number of DAPI positive nuclei. Data was analysed by one-way ANOVA and multiple comparisons with a Bonferroni post-hoc test.

The apoptotic indices in ROCK1wt and ROCK1nc treated with GLZ and vehicle were similar to the respective untreated controls suggesting that GLZ on its own had no effect on apoptotic cell accumulation (Figure 5-3c). However, analysis of TUNEL staining in ROCK1wt and ROCK1nc mice treated with DEN and GLZ showed a decrease in apoptotic index, which reflected a decrease in the accumulation of apoptotic debris upon GLZ treatment (Figure 5-3b, c). This decrease was significant in ROCK1nc (Figure 5-3c). The percentage of apoptotic cell debris accumulating in hepatic tissue following treatment with GLZ and DEN was still slightly higher in ROCK1nc when compared to wild-type although not significant (Figure 5-3c). Hence, blocking the cytokine activity of HMGB1 with GLZ resulted in a significant decrease in accumulation of apoptotic remnants in damaged ROCK1nc livers.

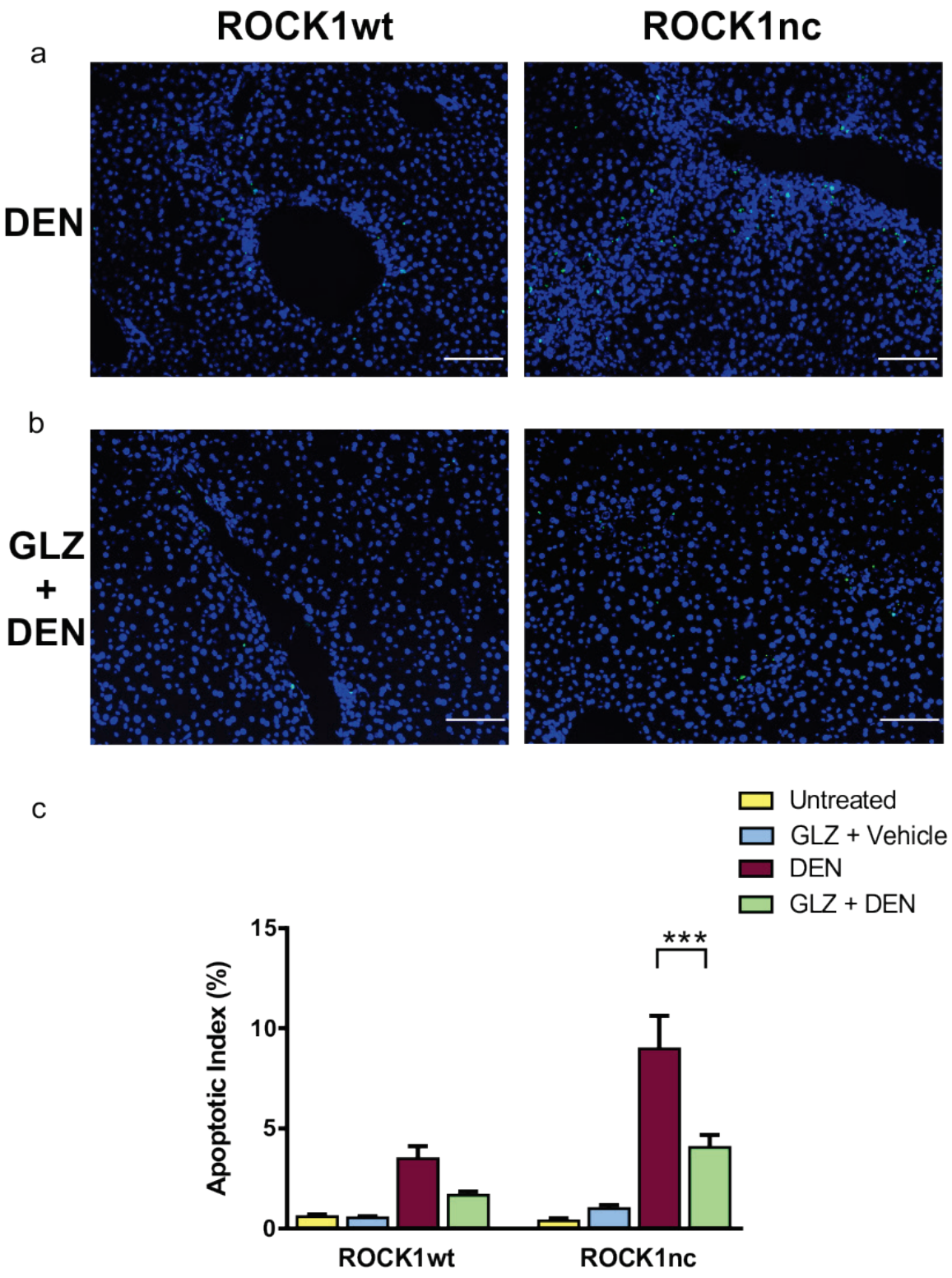

Figure 5-3 Accumulation of apoptotic remnants is reduced upon Glycyrrhizin treatment
Representative merged images of liver sections stained with TUNEL (green) and counterstained with DAPI (blue) from a) ROCK1wt and ROCK1nc mice after 72 hours of DEN treatment showing increased accumulation in ROCK1nc liver (Fig 4-3d), b) GLZ-treated ROCK1wt and ROCK1nc treated mice 72 hours after DEN treatment showed less apoptotic debris in both genotypes. Scale bars represent 100 μm. c) Bar graph represents percentage apoptotic index under different treatment conditions (n=3-10 per group). DEN alone data is from the primary experiment mentioned in the previous chapter. Data was analysed using one-way ANOVA and multiple comparisons with a Bonferroni post-hoc test. Error bars represent SEM. *** = $p<0.001$.

5.2.4 Glycyrrhizin treatment alleviated hepatocellular damage caused by DEN

To determine whether administration of GLZ could alleviate DEN-induced liver damage, I performed histopathological analysis of H&E stained liver sections. As shown in Figure 5-4a, typical pathological lesions found in DEN- induced damage including hepatocellular ballooning, large necrotic areas around the centrilobular regions, as well as the prevalence of steatohepatitis, were effectively lessened upon GLZ administration (Figure 5-4b). ROCK1wt livers from GLZ treated animals exhibited reduced centrilobular damage and associated inflammation when compared to DEN treatment alone. Livers sections looked relatively healthy, with very small areas of damage around the centrilobular region that is evident in Figure 5-4b.

In the same way, GLZ also alleviated hepatic injury in ROCK1nc livers caused by DEN injection. Except for two ROCK1nc livers, none of the other eight sections showed any signs of steatosis. Also evident was the lack of large numbers of inflammatory cells in the damaged areas of livers from both genotypes (Figure 5-4b). Analysis of the percentage of damaged area with associated inflammation in livers from both genotypes treated with GLZ and DEN revealed a decrease when compared to livers from the respective genotype treated with DEN alone (Figure 5-4c). A sharp decrease in the percentage of necrotic area in ROCK1nc mice with GLZ treatment resulted in values similar to that obtained in ROCK1wt mice treated with GLZ. These findings suggest that blocking HMGB1 activity with GLZ treatment can mitigate the increased hepatocellular damage caused by blebbing defects.

Alterations in body weight as well as the relative liver weight (liver weight/body weight) of experimental mice exposed to GLZ and DEN/Vehicle were also recorded during necropsy. DEN treatment in GLZ-treated ROCK1nc mice, however, caused significant weight loss (Figure 5-5a) and significant reduction in relative liver weight (Figure 5-5b), when compared to GLZ-treated ROCK1wt mice.

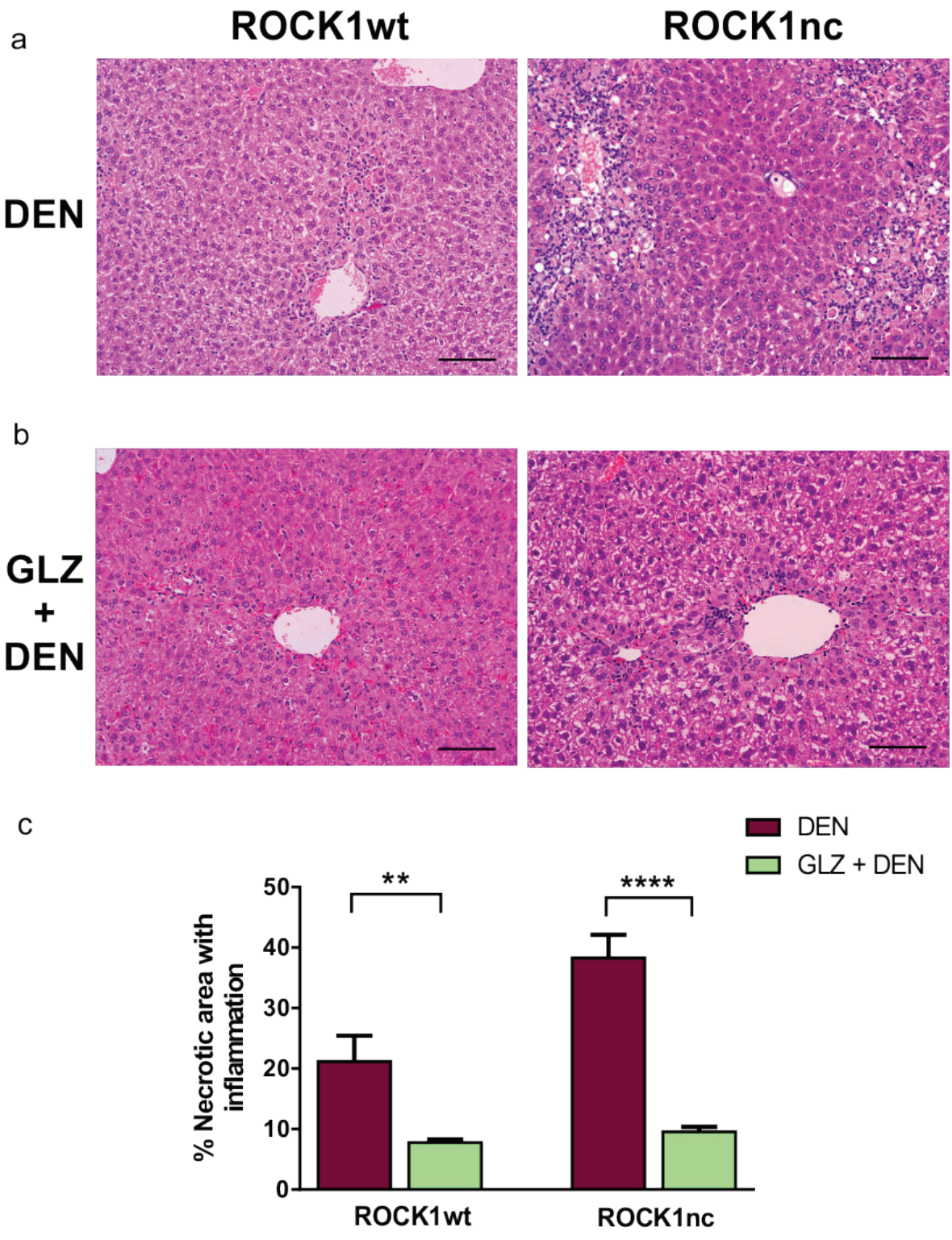

Figure 5-4 Glycyrrhizin treatment alleviates hepatocellular damage

a) Representative H&E stained liver sections after 72 hours of DEN treatment showing increased hepatocellular damage in ROCK1nc mice (Fig 4-7a). b) Representative H&E stained liver sections from GLZ-treated mice after 72 hours of DEN showing decreased hepatocellular damage in both genotypes. Scale bars represent 100 µm. c) Bar graph represents percentage necrotic area with inflammation analysed using H&E stained liver sections (n=5-6 per group). DEN alone data is from the primary experiment mentioned in the previous chapter. Data was analysed using one-way ANOVA and multiple comparisons with Bonferroni post-hoc test. Error bars represent SEM. ** = $p<0.01$, ****= $p<0.0001$.

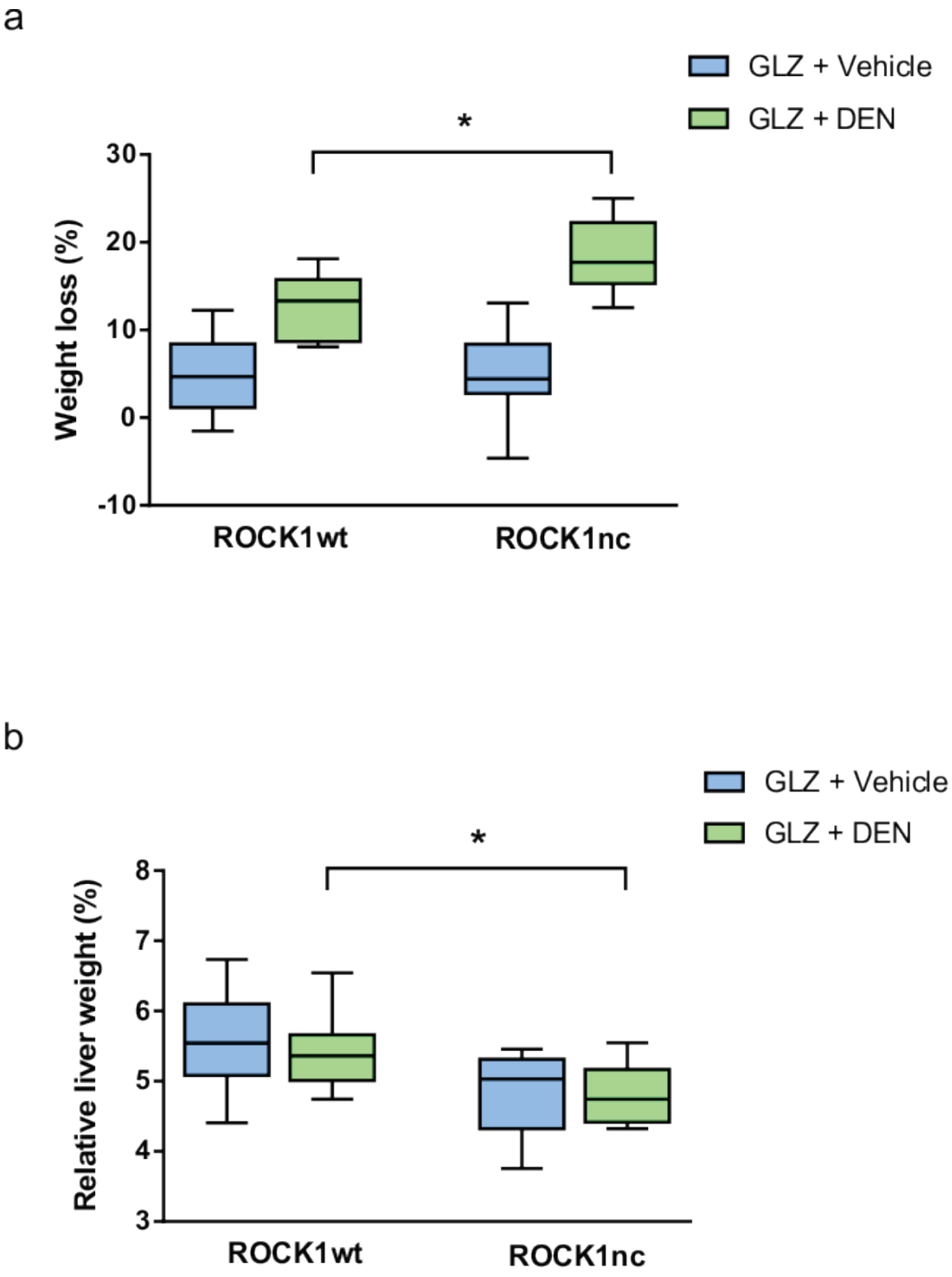

Figure 5-5 Effect of Glycyrrhizin on body weight and liver weight in mice exposed to DEN
Box and whisker plots showing a) percentage body weight loss and b) relative liver weight in ROCK1wt and ROCK1nc mice with GLZ and DEN/Vehicle treatment (n= 6-10 per group). Data was analysed using one-way ANOVA and multiple comparisons with Bonferroni post-hoc test. Whiskers represent 5-95 percentiles. * = $p<0.05$.

5.2.5 Recruitment of neutrophils to ROCK1nc liver decreased upon Glycyrrhizin treatment

Having demonstrated that administration of GLZ reduced DEN-induced hepatocellular damage and accumulation of apoptotic debris, I further investigated whether neutrophil infiltration to the liver was also affected. As stated in the previous chapter, DEN treatment significantly increased neutrophil recruitment in ROCK1nc livers after 72 hours (Figure 5-6a). Since HMGB1 is a potent inducer of inflammation, I speculated that blocking HMGB1 would reduce recruitment of inflammatory cells to the liver. Moreover, since it is possible that infiltrating neutrophils are capable of aggravating DEN-induced hepatocellular damage, it is highly likely that the lesser damage seen in GLZ-treated mice might be a reflection of lower neutrophil infiltration. To test this, I quantified the number of S100A9-positive neutrophils from five random fields in the liver section from each mouse sample. Data was analysed by one-way ANOVA and corrected for multiple comparisons with a Bonferroni test.

Treatment with GLZ alone did not result in a discernible change in neutrophil numbers in the livers when compared to the respective untreated controls (Figure 5-6c). Consistent with the findings from TUNEL assays, inhibiting the cytokine activity of HMGB1 significantly reduced infiltration of neutrophils when compared to DEN treatment alone (Figure 5-6b, c). The reduction in neutrophil numbers in ROCK1nc mice was quite dramatic since it achieved almost similar levels to ROCK1wt mice treated with both DEN and GLZ (Figure 5-6c). This suggested that blocking the cytokine activity of HMGB1 affected the recruitment of neutrophils to the damaged areas in livers.

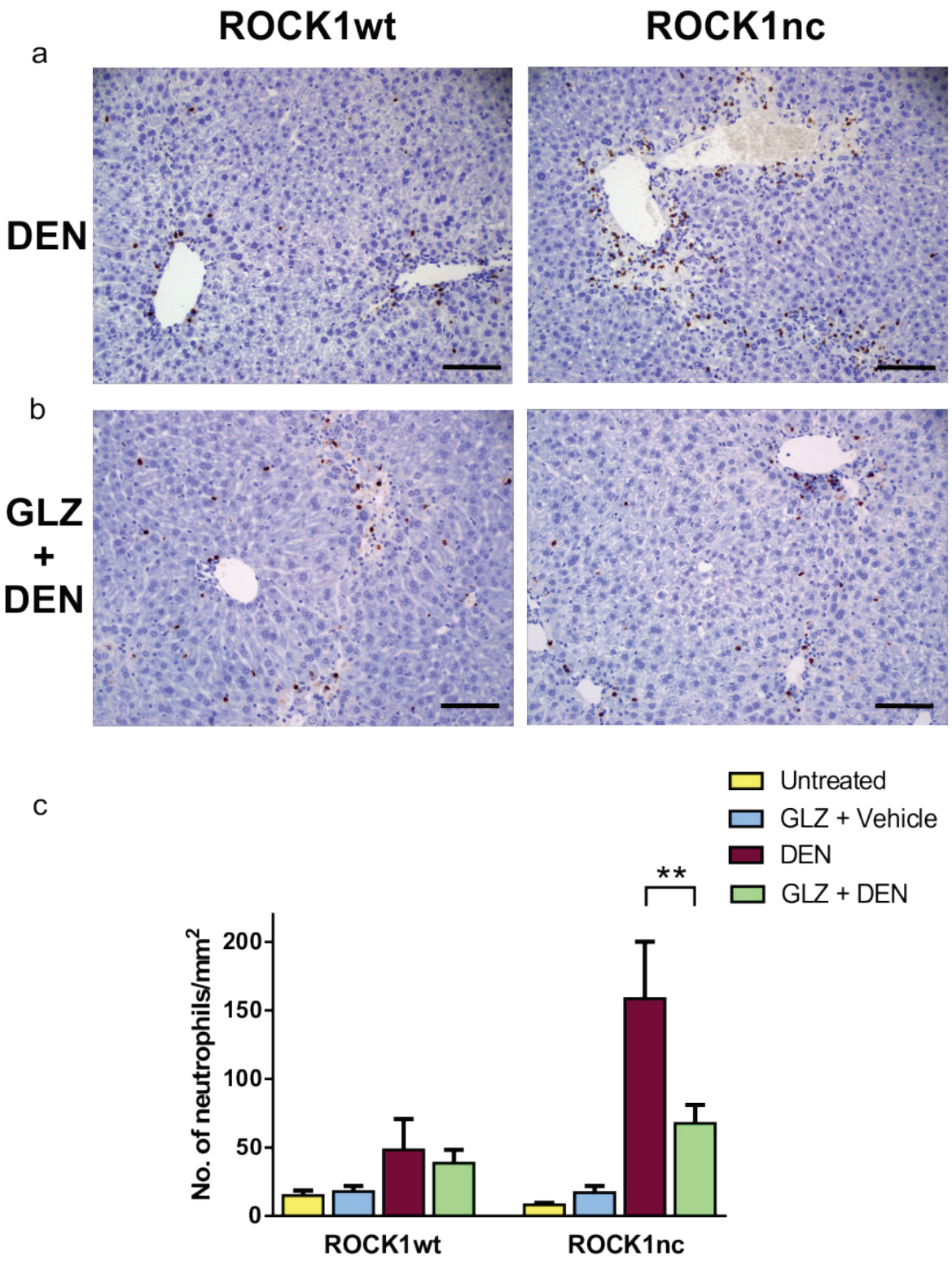

Figure 5-6 Glycyrrhizin reduced neutrophil infiltration to damaged liver

Representative images from S100A9- stained liver sections staining neutrophils (brown) and counterstained with haematoxylin from, a) ROCK1wt and ROCK1nc mice after 72 hours of DEN treatment showing increased infiltration in ROCK1nc liver (Fig 4-5d), b) GLZ- treated ROCK1wt and ROCK1nc treated mice 72 hours after DEN treatment showing reduced infiltration in ROCK1nc liver. Scale bars represent 100 µm. c) Bar graph represents number of neutrophils per mm^2 under different treatment conditions (n=3-10 per group). DEN alone data is from the primary experiment mentioned in the previous chapter. Data was analysed using one-way ANOVA and multiple comparisons with Bonferroni post-hoc test. Error bars represent SEM. ** = $p<0.01$.

5.2.6 Macrophage numbers in ROCK1nc livers exposed to DEN were not affected by Glycyrrhizin treatment

Macrophages in the liver, which play an important role in the maintenance of homeostasis, were significantly more numerous 72 hours after DEN-induced damage in ROCK1nc mice relative to ROCK1wt mice (Figure 5-7a). Whether the increase in macrophage numbers observed in ROCK1nc livers was a consequence of increased number of infiltrating monocytes differentiating into macrophages or proliferation of the resident Kupffer cells, could not be determined from my experiments (discussed in previous section).

However, I wanted to examine if GLZ treatment, with or without DEN treatment, had an impact on macrophage numbers in the liver. For this, number of F4/80-positive macrophages from five random fields in the liver section from each mouse sample was quantified. Data was analysed by one-way ANOVA and corrected for multiple comparisons with a Bonferroni test.

Interestingly, GLZ treatment on its own increased macrophage numbers in ROCK1wt livers when compared to the wild-type untreated control (Figure 5-7c). However, a similar increase was not observed in ROCK1nc livers. In wild-type livers, compared to DEN treatment alone, there was significant increase in macrophage numbers when GLZ was combined with DEN treatment. This however was not observed in ROCK1nc livers. Instead, macrophage numbers remained constant between DEN and DEN+GLZ treatments (Figure 5-7a, b).

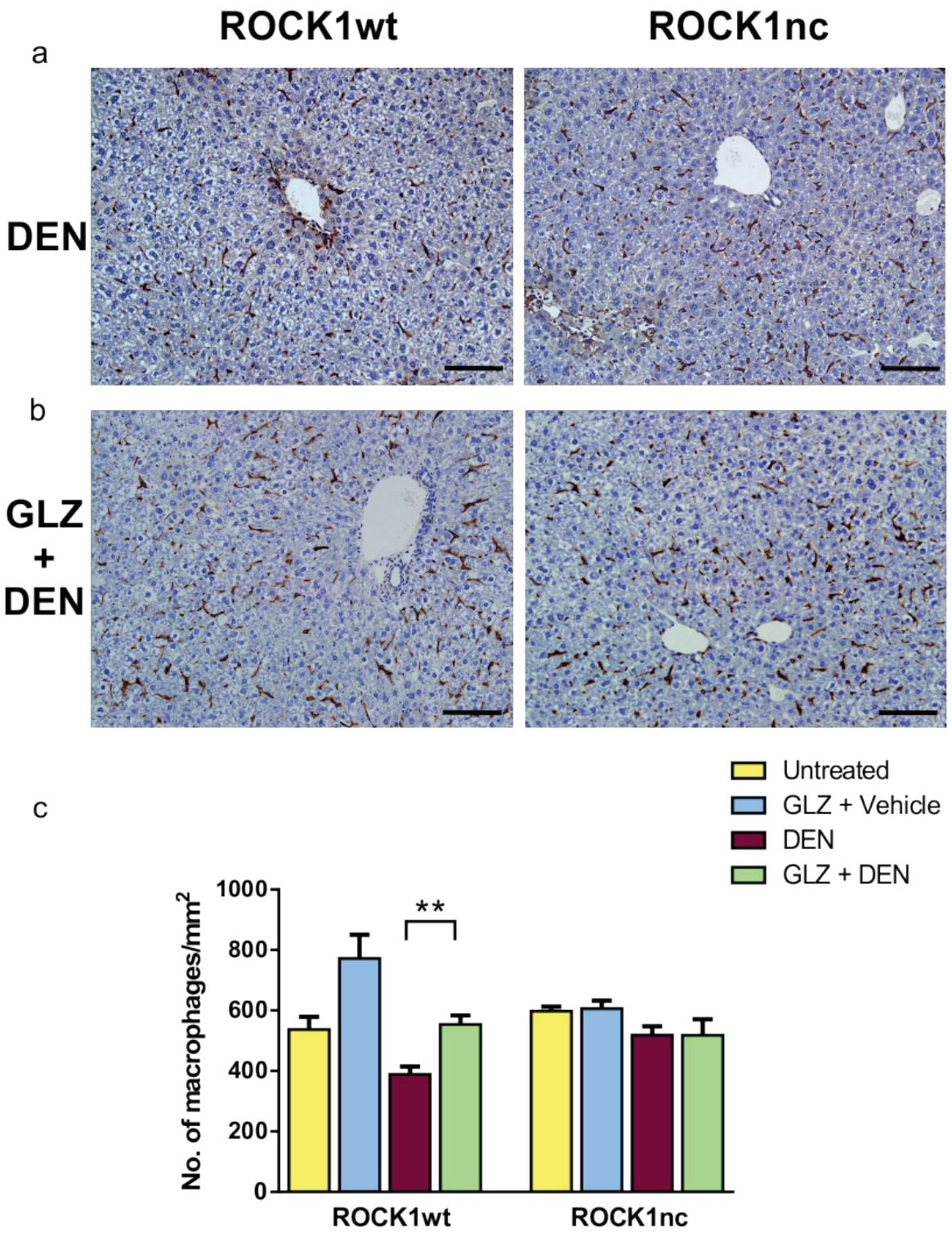

Figure 5-7 Effect of Glycyrrhizin on macrophage numbers in mice exposed to DEN
Representative images from F4/80- stained liver sections staining macrophages (brown) and counterstained with haematoxylin from, a) ROCK1wt and ROCK1nc mice after 72 hours of DEN treatment, b) GLZ- treated ROCK1wt and ROCK1nc treated mice 72 hours after DEN treatment showing an increase in wild-type liver but no difference in ROCK1nc. Scale bars represent 100 μm. c) Bar graph represents number of macrophages per mm^2 under different treatment conditions (n=3-10 per group). DEN alone data is from the primary experiment mentioned in the previous chapter. Data was analysed using one-way ANOVA and corrected for multiple comparisons with Bonferroni test. Error bars represent SEM. ** = $p<0.01$.

5.2.7 Decreased hepatocellular damage with Glycyrrhizin treatment correlated with serum liver profile

As discussed before, levels of liver enzymes and proteins in the serum are good indicators of hepatocellular damage and liver injury. Serum collected from experimental mice were analysed for levels of ALT, total bilirubin, alkaline phosphatase, total protein, albumin and globulin. Data was analysed by one-way ANOVA and corrected for multiple comparisons with Bonferroni test.

Serum levels of liver enzymes such as ALT are routinely analysed to assess hepatic parenchymal damage. 72 hours after DEN treatment, ROCK1nc mice exhibited significantly high levels of ALT, which correlated with greater hepatocellular damage seen in these mice. As expected, GLZ treatment drastically reduced serum ALT levels in DEN-treated ROCK1nc mice, which was consistent with the decrease in hepatocellular damage observed by histopathological analysis (Figure 5-8a). A similar trend was observed with total bilirubin levels in serum (Figure 5-8b). Treatment with GLZ resulted in ALT and bilirubin reaching similar levels in both ROCK1wt and ROCK1nc mice (Figure 5-8a, b). Concomitant decrease in ALT and bilirubin levels was a good indicator of the positive effect of GLZ in reducing liver damage.

Reduction in alkaline phosphatase with higher DEN-induced damage observed in ROCK1nc mice was reversed with GLZ treatment (Figure 5-9a). Alkaline phosphatase levels in ROCK1nc mice were significantly more with DEN injection combined with GLZ treatment compared to DEN treatment alone. However, in ROCK1wt mice, these levels remained similar.

Level of serum proteins also showed alterations with GLZ treatment. Serum levels of albumin significantly dropped to levels similar to that seen in control animals with GLZ treatment in DEN-treated ROCK1wt and ROCK1nc mice (Figure 5-9c). With GLZ treatment, increased globulin levels recorded in DEN-treated ROCK1nc mice also dropped to levels similar to that seen in ROCK1wt mice, although not significant (Figure 5-9d).

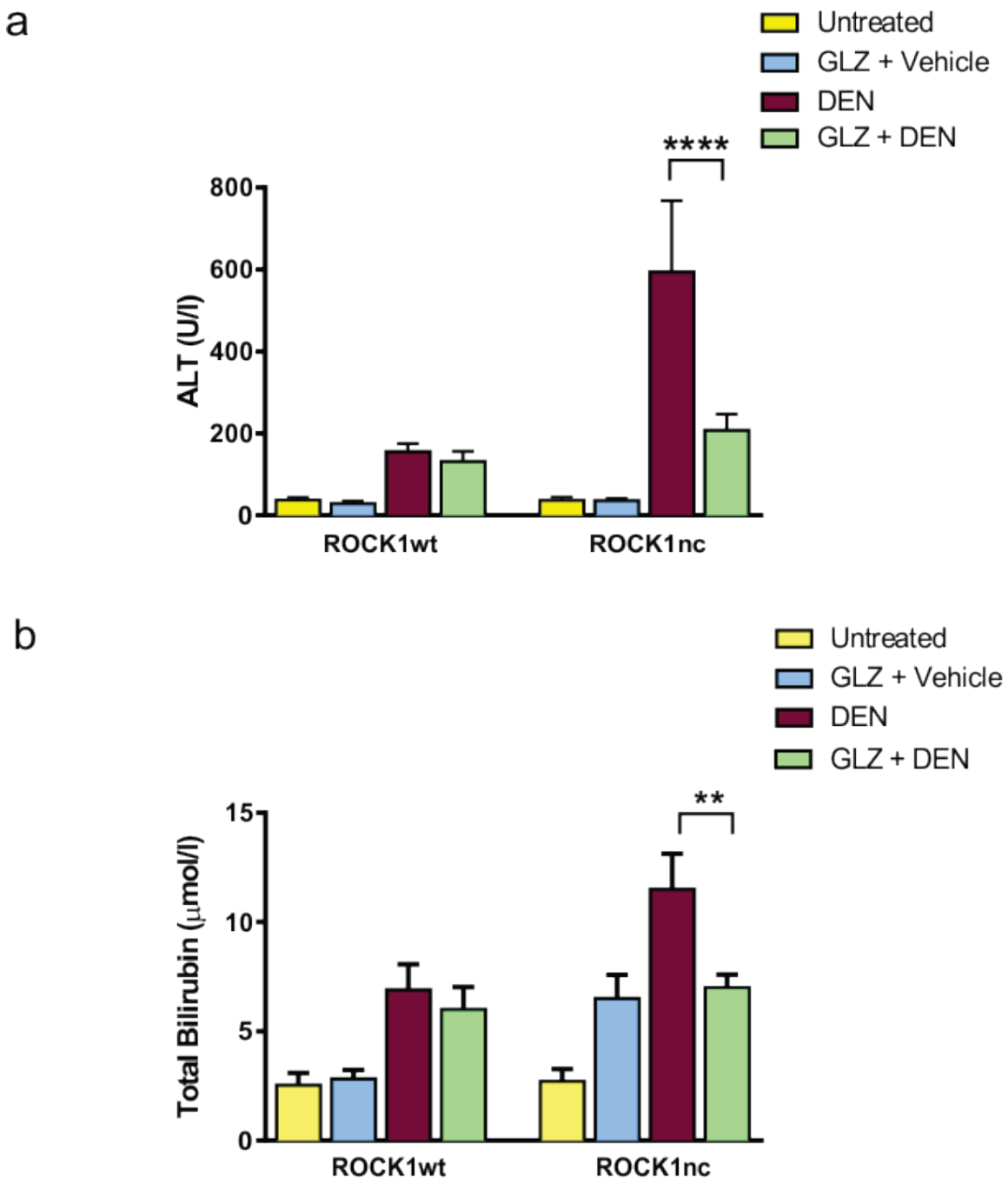

Figure 5-8 Glycyrrhizin reduced serum ALT and bilirubin levels in ROCK1nc mice
Bar graphs represent a) ALT and b) total bilirubin values in serum collected from ROCK1wt and ROCK1nc mice under different treatment conditions (n=3-10 per group). DEN alone data is from the primary experiment mentioned in the previous chapter. Data was analysed using one-way ANOVA and multiple comparisons using Bonferroni post-hoc test. Error bars represent SEM. ** = $p<0.01$; ****$p<0.0001$.

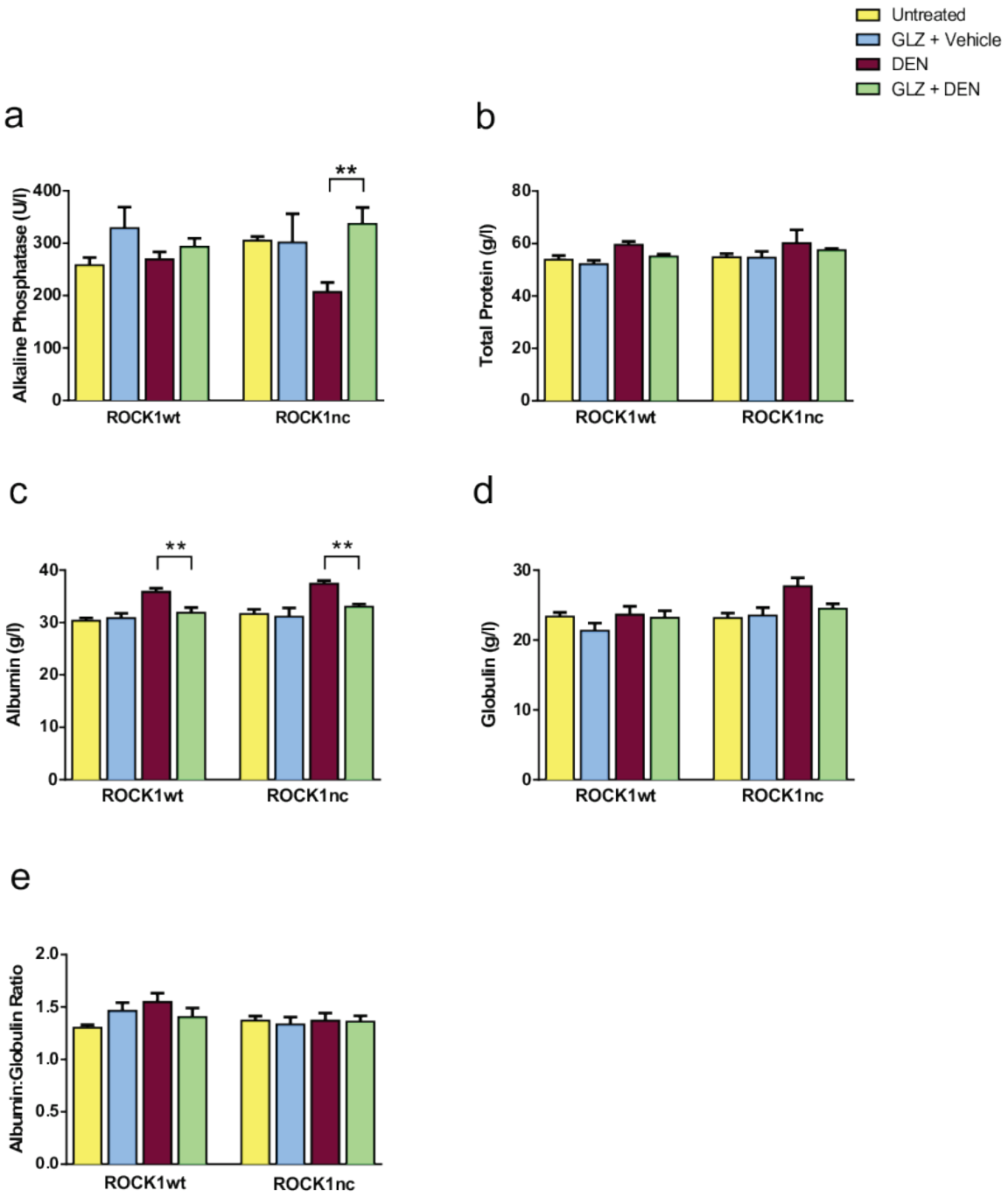

Figure 5-9 Additional parameters of liver function with Glycyrrhizin treatment
Bar graphs represent a) alkaline phosphatase, b) total protein, c) albumin, d) globulin and e) albumin to globulin ratio values in serum collected from ROCK1wt and ROCK1nc mice under different treatment conditions (n=3-10 per group). DEN alone data is from the primary experiment mentioned in the previous chapter. Data was analysed using one-way ANOVA and multiple comparisons using Bonferroni post-hoc test. Error bars represent SEM. ** = $p<0.01$.

5.3 Discussion

Rapid elimination of apoptotic cells is essential for the maintenance of tissue homeostasis. In the previous section, I showed that the defect in caspase-cleavage of ROCK1 resulted in accumulation of apoptotic remnants and infiltration of immune cells in response to DEN-induced damage in the liver after 72 hours. Histopathological analysis revealed extensive liver damage in ROCK1nc mice. Detrimental effects of uncleared apoptotic debris along with the presence of massive numbers of recruited immune cells may contribute to exacerbating liver damage.

If apoptotic cells are not removed promptly by phagocytes, they undergo self-elimination by secondary necrosis. Two possible scenarios may lead to secondary necrosis *in vivo*. The first setting involves excessive apoptosis leading to accumulation of apoptotic cells that may overwhelm the capacity of the phagocytic system. For example, secondary necrosis of hepatocytes was reported in a rat model with extensive hepatocyte apoptosis (Farghali et al., 2003). The second scenario involves defects in efferocytosis mechanisms resulting in the accumulation of apoptotic debris that may eventually undergo transition to secondary necrosis. For example, deficiency in the clearance of apoptotic cells was reported in mouse models which lack phagocytic receptor Mer (Cohen et al., 2002, Thorp et al., 2008).

Secondary necrotic cells that lose their membrane integrity, releases toxic intracellular components known as damage associated molecular patterns (DAMPs) with inflammatory and immunogenic capacities. Of the several DAMPs identified so far, high-mobility group box 1 (HMGB1) is the most extensively studied. It is a non-histone nuclear protein that is actively released by immune cells or passively by damaged or necrotic cells (Scaffidi et al., 2002). Secreted HMGB1 acts as a potent pro-inflammatory cytokine either directly by binding to receptors and promoting transcription of pro-inflammatory genes or indirectly by attracting more inflammatory cells to sites of damage or necrosis.

5.3.1 Blocking cytokine activity of HMGB1 using Glycyrrhizin reduced accumulation of apoptotic debris in DEN-induced ROCK1nc mice

Since ROCK1nc livers exhibited larger necrotic areas 72 hours after DEN treatment, I examined the subcellular localization of HMGB1 in these liver sections. Interestingly, ROCK1nc hepatocytes showed significant cytoplasmic translocation of HMGB1 when compared to ROCK1wt (Figure 5-1). Cytoplasmic translocation of HMGB1 in hepatocytes has been shown to precede an impending extracellular release in both mouse models and patients with acute liver failure (Zhou et al., 2011). This led me to hypothesize a possible link between HMGB1 and increased DEN-induced liver damage with accumulation of apoptotic debris as seen in ROCK1nc mice. To test whether HMGB1 released by the secondary necrotic cells in ROCK1nc was responsible for increased hepatocellular damage, I used Glycyrrhizin (GLZ), which inhibits the cytokine activity of HMGB1. Mice injected with a single intraperitoneal injection of 100 mg/kg of DEN, also received several doses of 200 mg/kg of GLZ until 72 hours after DEN injection (Figure 5-2a).

Analysis of TUNEL staining in ROCK1wt and ROCK1nc mice treated with GLZ revealed a significant reduction in the accumulation of apoptotic debris in ROCK1nc mice 72 hours after DEN treatment (Figure 5-3 a, b). With GLZ treatment, the levels of apoptotic debris in ROCK1wt and ROCK1nc mice were almost identical (Figure 5-3 c). This suggested that HMGB1 was playing a crucial role in the accumulation of apoptotic remnants in ROCK1nc mice with defects in caspase- cleavage of ROCK1. Necrotic hepatocytes may not be the only source of HMGB1. It is possible that the activated immune cells in the liver may also be actively secreting HMGB1 (Figure 5-1 b).

5.3.2 Administration of Glycyrrhizin reduced neutrophil infiltration in DEN-induced ROCK1nc mice

The role of HMGB1 in the regulation of inflammation has been highlighted in a number of instances including LPS-induced shock (Wang et al., 1999), tissue injury (Scaffidi et al., 2002) and UV irradiation (Bald et al., 2014). Inhibiting HMGB1 abrogated UV-dependent neutrophilic infiltration in mice skin (Bald et al., 2014). A recent study demonstrated the role of HMGB1 in neutrophil

recruitment to necrotic liver using two different injury models (Huebener et al., 2015). Consistent with these data, blocking the cytokine activity of HMGB1 using GLZ in the DEN-induced damage model, ROCK1nc mice displayed a profound reduction in neutrophil infiltration to the liver (Figure 5-6 a, b). Moreover, with GLZ treatment there was no significant difference between neutrophil infiltrations to the liver in response to DEN-induced damage between the two genotypes (Figure 5-6 c). From this observation, it is conceivable that HMGB1 released by the accumulating debris in ROCK1nc liver is a potent inducer of neutrophilic infiltration.

In contrast to neutrophils, which are mainly recruited to the liver in the event of an injury, large numbers of resident macrophages, known as Kupffer cells, are present in the liver. Figure 5-7c shows an increase in macrophage numbers in ROCK1wt mice upon administration of GLZ without DEN-induced damage. This was an unexpected result and GLZ treatment has not been reported to increase macrophage numbers in the liver. As described in the earlier section, since I had employed an immunohistochemical method for the detection of macrophages, my experiments failed to identify whether the increase was due to increased monocyte infiltration or due to proliferation of the resident Kupffer population. Moreover, GLZ treatment resulted in a significant increase in macrophage numbers in DEN-induced ROCK1wt livers compared to DEN treatment alone in these mice. However, analysis of macrophage numbers revealed that the increase in macrophage numbers only reached baseline levels seen in untreated wild-type livers. It is possible that GLZ mediated reduction in hepatocellular injury (discussed later on) might be responsible for the repopulation of Kupffer cells in ROCK1wt livers. With respect to ROCK1nc livers, GLZ seems to have no effect on macrophage numbers in the DEN-induced damage model. This is not surprising since HMGB1 does not increase macrophage numbers in the liver following injury (Huebener et al., 2015).

Recent studies had shown that HMGB1 has the ability to inhibit the phagocytic activity of macrophages (Liu et al., 2008a, Friggeri et al., 2010). It is possible that the increased secretion of HMGB1 by damaged hepatocytes in ROCK1nc livers had an inhibitory effect on the Kupffer cells, which was reduced by GLZ treatment, thus resulting in less apoptotic debris in the livers.

5.3.3 Glycyrrhizin treatment alleviated DEN-induced hepatocellular damage in ROCK1nc mice

Histopathological analysis of liver sections combined with clinical liver function tests was employed to assess the effect of GLZ on DEN-induced liver damage. Analysis of H&E-stained liver sections revealed that the higher degree of pathological lesions including centrilobular necrosis, steatohepatitis and hepatocellular ballooning seen in ROCK1nc mice, were effectively alleviated with GLZ treatment (Figure 5-4 a, b). Analysis of the percentage of necrotic area revealed a significant decrease with GLZ treatment when compared to DEN treatment alone. This decrease was highly significant in ROCK1nc livers considering the larger areas of necrosis seen in these mice after 72 hours of DEN injections (Figure 5-4 c). Of importance was the similar percentage of necrotic area between the genotypes, which highlighted the role of HMGB1 in aggravating hepatocellular damage in a defective blebbing setting.

Measurement of serum levels of ALT and total bilirubin correlated well with the histopathological analysis. Administration of GLZ in DEN-treated animals resulted in significant decreases in ALT and bilirubin levels in ROCK1nc mice, thus bringing the values down to levels similar to ROCK1wt mice (Figure 5-8). These findings were in concert with previous reports which showed the protective effects of GLZ in different models of liver injury (Abe et al., 2008, Ogiku et al., 2011).

As discussed in the previous section, neutrophils can exacerbate tissue injury in liver damage models. To test whether neutrophils were responsible for the increased liver injury in ROCK1nc mice, I had used the 1A8 monoclonal antibody to deplete neutrophils. However, this treatment resulted in more neutrophil numbers in the livers as evidenced by S100A9 immunohistochemical staining, the reason for which is not known (data not shown). If the uncleared apoptotic debris and the presence of inflammatory cells are responsible for exacerbating tissue damage, it is conceivable that GLZ mediated reduction in accumulation of apoptotic debris and reduction in neutrophil infiltration work in concert to reduce hepatocellular damage in ROCK1nc mice.

5.4 Summary

Defective blebbing results in the accumulation of apoptotic debris, which may progress to secondary necrosis. HMGB1 released by necrotic hepatocytes aggravates hepatocellular damage by recruiting more neutrophils to the liver. Inhibiting the cytokine activity of HMGB1 with Glycyrrhizin reduced neutrophil infiltration to the liver, which in turn alleviated hepatocellular damage in DEN-induced liver injury model.

Results

Caspase cleavage of ROCK1 in Tumour Development

6 Hepatocellular Carcinoma Model

6.1 Introduction

6.1.1 DEN-induced Hepatocellular Carcinoma

Hepatocellular carcinoma (HCC), a dominant form of primary liver cancer, ranks third on the list of most lethal cancers, and worldwide is the fifth most common cancer in men and seventh among women (Mittal and El-Serag, 2013). Risk factors include chronic hepatitis B or C infection, alcohol consumption, toxic exposure to aflatoxin, vinyl chloride and non-alcoholic fatty liver disease (NAFLD) or non-alcoholic steatohepatitis (NASH) caused by obesity or diabetes. HCC is more common in men than women as hepatitis B or C infection and alcohol consumption are more prevalent in men. Several mouse models have been developed over the years that have contributed immensely in defining the pathogenesis of HCC. This includes chemically induced models, xenograft models and genetically modified models. Of these, chemically induced models are generally favoured owing to their similarity to disease pathogenesis seen in humans.

To date, the most frequently used genotoxic carcinogen is Diethylnitrosamine (DEN), also known as N-nitrosodiethylamine. From a clinical perspective, DEN is found in a number of products to which humans are exposed including tobacco smoke and whisky. DEN is bioactivated to α-hydroxynitrosamine, by a cytochrome P450 enzyme that has its highest activity in centrilobular hepatocytes (Verna et al., 1996). An electrophilic ethyldiazonium ion thus formed causes DNA damage by ethylation of DNA bases. Furthermore, reactive oxygen species (ROS) generated by the P450 enzyme induces oxidative stress by the formation of hydrogen peroxide and superoxide anions that can contribute to HCC formation (Qi et al., 2008).

Several mechanisms are believed to be involved in the complex pathogenesis of HCC including oncogene activation, abrogation of DNA-damage checkpoints, telomere dysfunction, activation of inflammatory pathways, and formation of ROS, which lead to malignant transformation and disease progression (Sanyal et al., 2010). However, the exact role of these pathways still remains unclear. DEN-

induced ethyl DNA adducts can interrupt base pairing, thus resulting in tumours that frequently harbour mutations in the H-ras proto-oncogene (Buchmann et al., 1991, Chen et al., 1993) and p53 (Smith et al., 1991). Although mutations in Ras-oncogenes are rarely seen in human HCC (Schwarz et al., 1995), Ras-activation is enhanced in human HCC when compared with non-neoplastic regions (Calvisi et al., 2006). However, gene expression pattern analysis of several HCC models revealed that the DEN model was a good representation of human HCC with poor prognosis (Lee et al., 2004).

Several dosing strategies have been tested over the years for inducing HCC in mice using DEN. The dose administered, along with age, sex and strain of mice had an effect on the time needed for HCC development (Heindryckx et al., 2009). In some studies, two-stage models of HCC induction were utilized. One model involves DEN being used as the initiating agent and phenobarbital (PB) acting as a promoting agent that enhances carcinogenesis (Heindryckx et al., 2009). Another model, known as the Solt-Farber model, mostly performed in rats, involves HCC induction using hepatocarcinogen like DEN in conjunction with partial hepatectomy, which induces rapid proliferation of the initiated cells (Farber et al., 1977). Over the years, DEN-induced HCC model has been successfully used to study the effect of specific genetic changes in carcinogen-induced tumours.

6.1.2 Experimental Aim

The objective of this study was to elucidate the role of caspase-cleavage of ROCK1 in hepatocellular carcinoma.

6.2 Results

6.2.1 DEN-induced hepatocellular carcinoma in ROCK1nc mice

To address the role of caspase-cleavage of ROCK1 in carcinogenesis, I utilized the well-established model of hepatocellular carcinoma using the same carcinogen that was used for the acute liver studies, specifically DEN. A single intraperitoneal injection of DEN to two-week old mice results in the induction of HCC (Vesselinovitch et al., 1984). Over the years, several laboratories have used different doses, resulting in HCC induction after 40-104 weeks depending on the age, strain and sex of mice (Heindryckx et al., 2009) . Young mice are generally used for DEN-induction since the developing liver is more susceptible to genotoxic carcinogens. For the present study, 14-day old ROCK1wt and ROCK1nc mice were given 400 µg of DEN by intraperitoneal injection (Figure 6-1a). Mice were routinely monitored for lethargy, weight loss, immobility and palpable tumours.

By 41 weeks of age, some mice exhibited palpable tumours and signs of discomfort. Hence, 41 weeks (9 months) was selected as the end point for this experiment and all DEN-induced mice were sacrificed at this time point. Additionally, some mice were sacrificed at 28 weeks of age (6 months) to assess for preneoplastic lesions in wild-type and ROCK1nc mice (Figure 6-1a). By 41 weeks, all male mice showed gross evidence of liver tumours from both ROCK1wt and ROCK1nc mice (Figure 6-1b). However, female mice from both genotypes did not show any evidence of tumours at this time point. Some DEN-induced female mice were aged to 50-70 weeks, but still failed to display any signs of liver tumours (Figure 6-1b). This was not surprising, as genetic disparity has been previously reported in DEN-induced HCC models, with only 10-30% females developing tumours, which was attributed to the inhibitory effect of estrogen on hepatocarcinogenesis (Nakatani et al., 2001). Gender disparity in HCC development has been attributed to higher levels of the cytokine IL-6 in the serum of male mice when compared to females where estrogen hormone inhibits IL-6 secretion (Naugler et al., 2007).

a

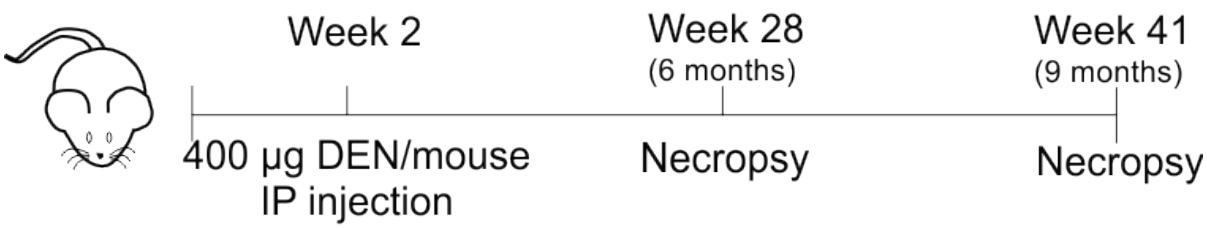

b

Gross evidence of tumour

Genotype	Male (41 weeks)	Female (> 50 weeks)
ROCK1wt	12/12	0/14
ROCK1nc	12/12	0/8

Figure 6-1 DEN-induced hepatocellular carcinoma
a) Schematic representation of the treatment regimen for DEN-induced hepatocellular carcinoma. Mice were injected with 400µg of DEN at two weeks of age and then sacrificed at 6 months or 9 months. b) Table shows incidence of gross evidence of tumours in male mice at 41 weeks of age and female mice after 50 weeks of age, demonstrating gender disparity. Incidence is represented as the number of animals with gross evidence of tumours over the total number of mice in that group.

6.2.2 Fewer hepatic tumours in ROCK1nc mice

DEN-induced mice were sacrificed at 41 weeks of age. All mice were injected intraperitoneally with BrdU two hours prior to sacrifice. After euthanasia, body weights were recorded and blood collected via cardiac puncture. Liver weights were recorded and the number of visible tumours in each liver lobe counted. Each tumour was measured using digitised vernier callipers to calculate the volume. Macroscopic examination of tumour numbers, 9 months after DEN induction revealed that ROCK1nc mice had significantly fewer hepatic tumours when compared to the wild type (Figure 6-2a, e and f). The majority of ROCK1nc livers had fewer than 20 tumour foci, with the exception of one exhibiting 29 tumour foci. However, tumour numbers in wild-type mice ranged from 25 to 70 in most samples. Few livers from wild type mice had less than 20 visible tumour foci. Analysis of tumour volume revealed that there was no significant difference in tumour volume 9 months after a single injection of DEN between the two genotypes (Figure 6-2b). Although most ROCK1nc livers had lower tumour volumes (less than 2500 mm^3) when compared to wild type (mostly ranging between 2000-5000 mm^3), three ROCK1nc samples exhibited high tumour volume, accounting for the loss of significance. Additionally, there was no significant difference in absolute liver weight and relative liver weight between the two genotypes (Figure 6-2c, d). Macroscopic examination of ROCK1wt and ROCK1nc livers revealed that tumours were clearly demarcated from the surrounding tissue and involved different liver lobes. Tumours from both genotypes were often paler than the surrounding hepatic parenchyma. However, some tumours appeared red and highly vascularized (Figure 6-2e). Tumours were typically nodular with most livers from both genotypes presenting multiple nodules with one or two dominant, large ones. In some samples, multiple small nodules coalescing to form a single large nodule were also observed.

Metastases to the lungs have been reported in DEN-induced HCC (Heindryckx et al., 2009). Analysis of H&E-stained lung sections revealed presence of metastatic nodules and thickening of the alveolar septa (Figure 6-3a). Blinded analysis of metastatic score did not reveal any significant difference; however most ROCK1nc mice had a lower metastatic score when compared to the wild type (Figure 6-3b).

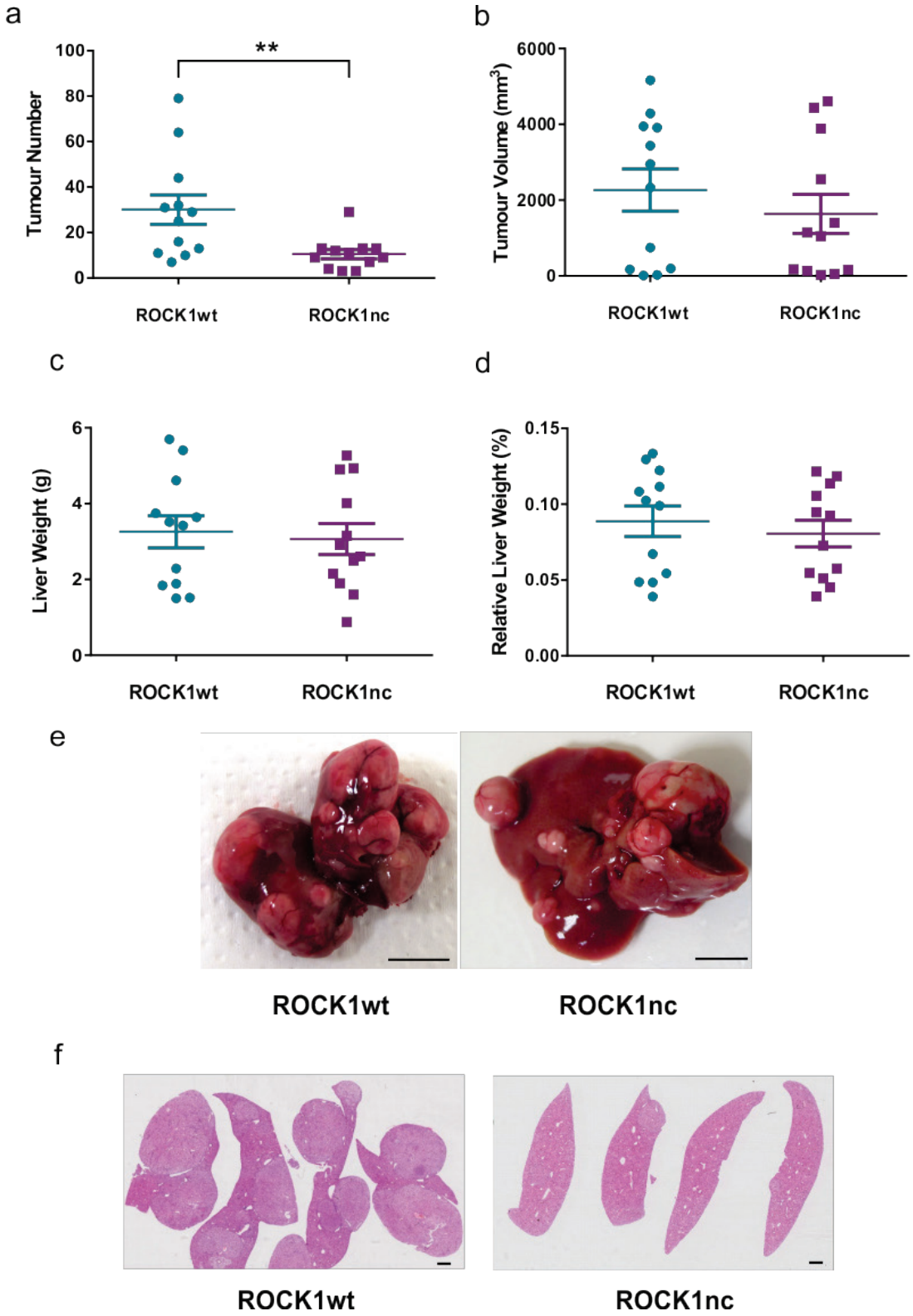

Figure 6-2 Decreased tumour number in ROCK1nc mice

Scatter dot plots (mean ± SEM) showing a) tumour number, b) tumour volume, c) absolute liver weight and d) relative liver weight in male mice injected with DEN and maintained for 9 months (n=12 per genotype). Data was analysed using Student's t-test. ** = p< 0.01. e) Macroscopic view of representative livers from ROCK1wt and ROCK1nc mice 9 months after HCC initiation with DEN. Scale bars represent 1 cm. f) Representative H&E stained liver sections from ROCK1wt and ROCK1nc mice showing more tumours in wild-type liver. Scale bars represent 1 mm.

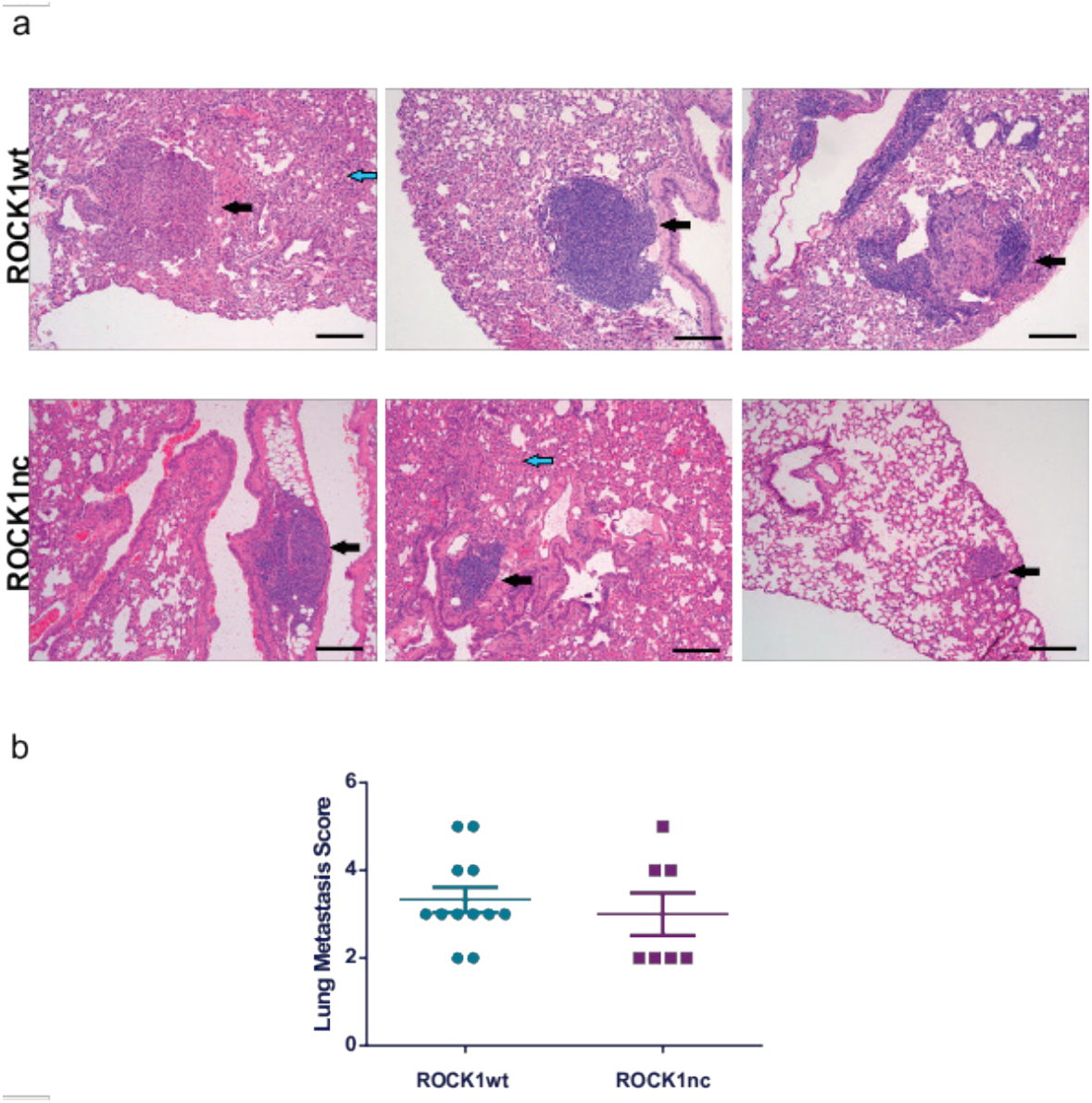

Figure 6-3 Lung metastasis in DEN-induced HCC
a) Representative H&E-stained lung sections from ROCK1wt and ROCK1nc male mice 9 months after DEN-induction (n=7-12 per genotype). Black arrow indicates metastatic nodules and blue arrow indicates thickening of the alveolar septa. Scale bars represent 100 μm b) Scatter dot plot (mean ± SEM) shows lung metastatic score in ROCK1wt and ROCK1nc lungs. Data analysed using Mann-Whitney test.

6.2.3 Histopathological evaluation of HCC tumours

Histopathological evaluation of HCC tumours from wild-type and ROCK1nc mice using H&E stained sections revealed typical features of HCC in both genotypes. Most tumour nodules had a well-defined border with compression of the adjacent hepatic parenchyma (Figure 6-4a). Some tumours from both genotypes displayed a trabecular pattern where the hepatocytes are arranged in plates of various thicknesses and separated by sinusoidal spaces (Figure 6-4b). The trabeculae sometimes increased in thickness to form macrotrabecular structures (Figure 6-4c) or compressed to form a compact mass (Figure 6-4d). Large areas of necrotic foci were seen in the bigger tumours obtained from both wild-type and ROCK1nc tumours (Figure 6-4e). Some ROCK1nc tumours exhibited large inflammatory foci as well (Figure 6-4f).

Using H&E-stained sections, liver tumours in this study were classified into three types: Hepatic nodule 1 (HN1), Hepatic nodule 2 (HN2) and HCC in increasing order of tumour grade as described by Yanagi and co-workers (Yanagi et al., 1984). HN1 type mainly comprised of tumour nodules with slight difference from the normal hepatic architecture but produced obvious compression of the surrounding parenchyma. HN2 category consisted of two to three- cell thick irregular trabecular arrangements with well- maintained sinusoidal spaces. The highest grade type, namely HCC exhibited irregular macrotrabecular arrangement with dilated sinusoidal spaces.

12 ROCK1wt and 12 ROCK1nc end-point tumours were scored based on this classification. For specimens that exhibited mixed morphology, the most advanced classification was taken into consideration. Analysis revealed that 8 out of 12 of both genotypes exhibited full-blown HCC. Rest of them displayed tumours of lower grade, namely HN1 or HN2 (Figure 6-4g).

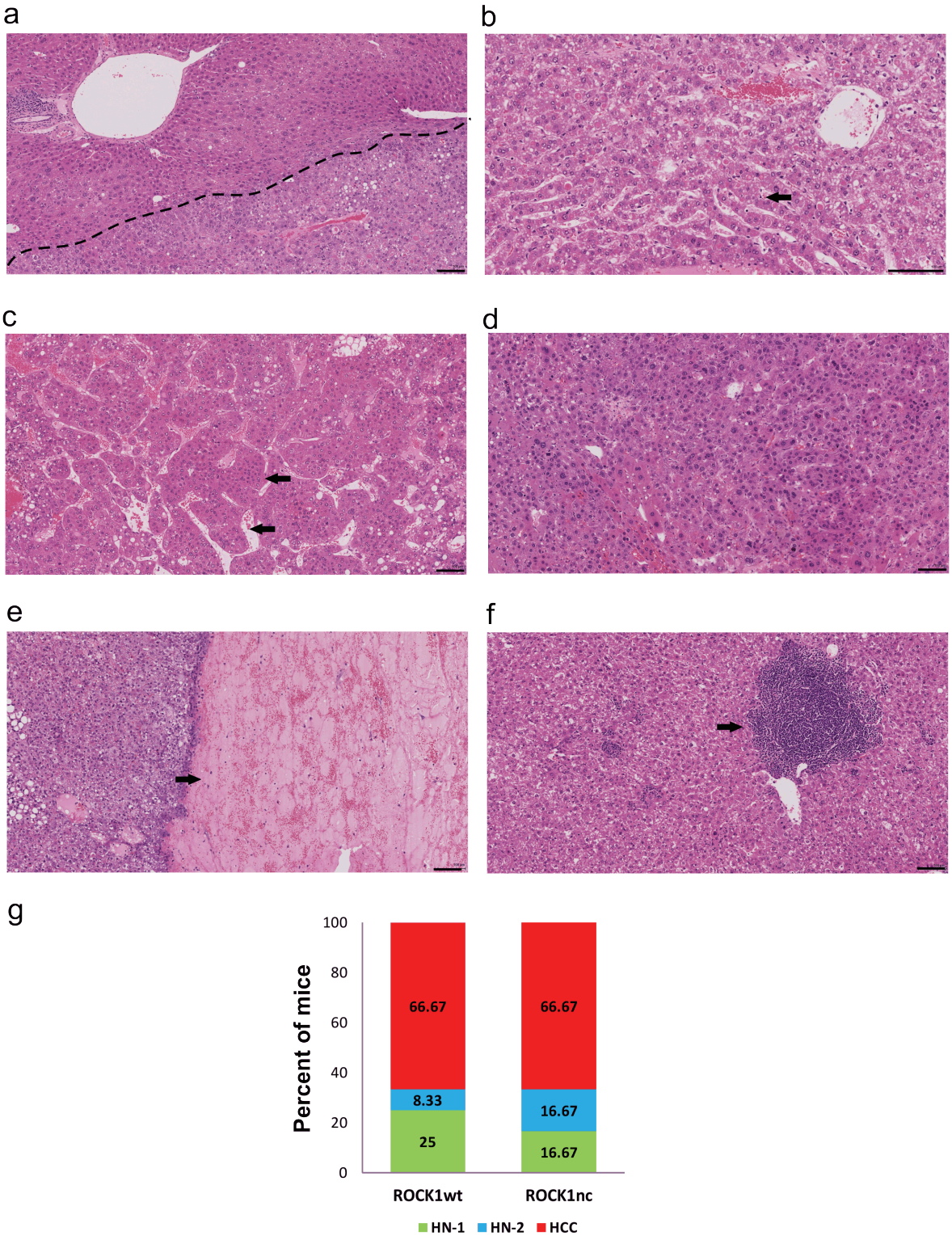

Figure 6-4 Histopathological features of DEN-induced HCC
Representative H&E stained liver sections from male mice with DEN-induced HCC showing a) tumour border (dotted line), b) trabecular pattern (arrow), c) macrotrabecular structures (arrow), d) compact tumour mass, e) necrotic foci (arrow) and f) inflammatory foci (arrow). Scale bars represent 100 µm. g) Stacked bar graph shows the percentage of ROCK1wt and ROCK1nc mice with different grades of tumours.

6.2.4 Higher steatotic grade in ROCK1nc tumours

Tumours from wild-type and ROCK1nc mice also exhibited microvesicular and macrovesicular steatosis which was evident on H&E-stained liver sections (Figure 6-5a). Out of the 12 ROCK1nc liver sections analysed, all samples exhibited steatosis (Figure 6-5b). In the wild-type, 10 out of 12 liver sections showed signs of steatosis (Figure 6-5b). Steatosis was graded on H&E-stained sections based on semi-quantitative estimation of percentage of steatotic hepatocytes, according to the following criteria: grade 0- less than 5%, grade 1- 5 to 25%, grade 2- 26 to 50%, grade 3- 51to 75% and grade 4- more than 75%. 33% of ROCK1nc mice displayed grade 4 steatosis while only 8% of ROCK1wt mice exhibited the highest grade (Figure 6-5c). More than 80% of ROCK1wt livers had a steatotic grade of 2 or less while only around 50% of ROCK1nc liver exhibited these low grades of steatosis (Figure 6-5c).

Presence of fibrosis or excessive accumulation of extracellular matrix proteins including collagen is an indicator of persistent or progressive hepatic injury and was detected by staining liver sections with Sirius red and Fast Green (Figure 6-6a). Sirius Red specifically binds to collagen and Fast Green is used as a counterstain as it binds to non-collagenous proteins. Both wild-type and ROCK1nc tumours presented a small degree of fibrosis which was mostly portal. Perivenular fibrosis (centrilobular zone) as well as pericellular fibrosis (extending along the sinusoids) was also observed in both genotypes. Analysis of Sirius Red stained liver sections using TissueAnalyzer software showed no significant difference in the percentage of fibrotic area between the two genotypes (Figure 6-6b).

a

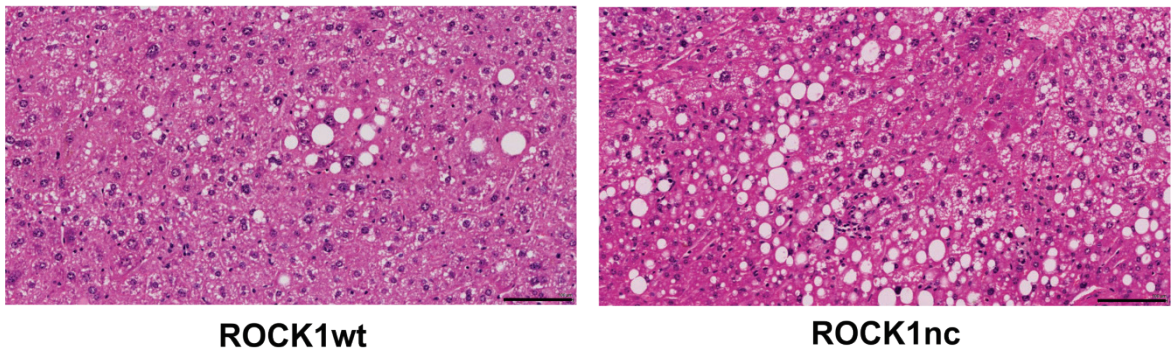

b

Genotype	Incidence of steatosis
ROCK1wt	10/12
ROCK1nc	12/12

c

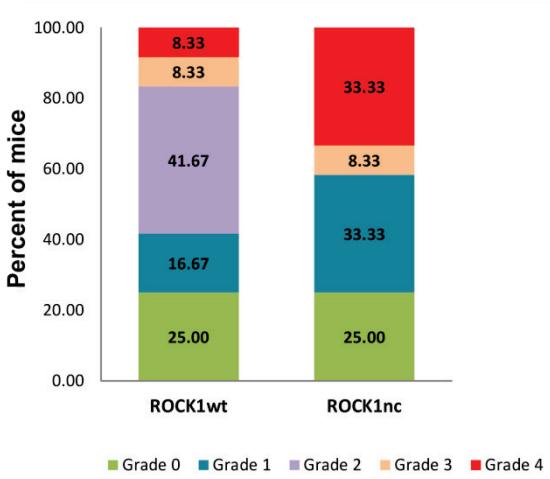

Figure 6-5 Higher steatotic grade in ROCK1nc mice

a) Photomicrographs of liver sections from ROCK1wt and ROCK1nc male mice with HCC 9 months after DEN injection showing steatosis in the tumours. Scale bars represent 100 μm. b) Table shows incidence of steatosis in the two genotypes. Incidence is represented as the number of animals with evidence of steatosis over the total number of mice in that group. c) Stacked bar graph shows the percentage of ROCK1wt and ROCK1nc mice with different grades of steatosis (n=12 per genotype).

a

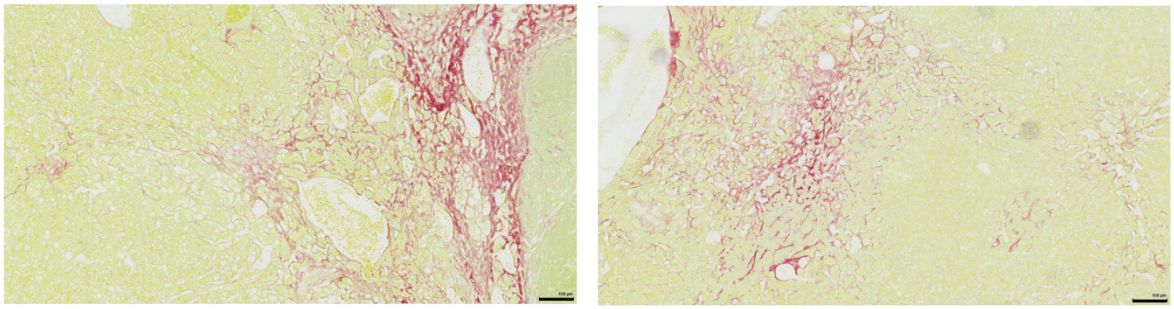

b

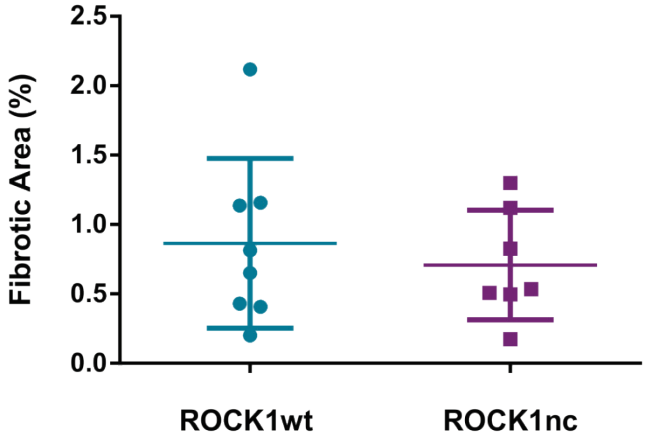

Figure 6-6 Fibrosis in DEN-induced HCC

a) Photomicrographs of liver sections from ROCK1wt and ROCK1nc male mice 9 months after DEN injection stained with Sirius Red and counterstained with Fast Green. Scale bars represent 100 μm. b) Scatter dot plot (mean ± SEM) of percentage fibrotic area measured as Sirius Red positive area relative to the total area analysed, showing no significant difference between the two genotypes (n=7-8 per genotype). Data analysed using Student's t-test.

6.2.5 Higher rates of immune cell proliferation in ROCK1nc mice

Proliferation rates in DEN-induced HCC from ROCK1wt and ROCK1nc mice were determined by either BrdU (5-bromo-2'-deoxyuridine) incorporation or Ki67 staining. Mice were injected with BrdU two hours prior to sacrifice and paraffin-embedded liver sections were stained with BrdU antibody. I quantified the number of BrdU-positive cells per mm^2 by analysing five random fields for each liver section. Analysis of BrdU-stained liver sections revealed no significant difference in the tumours between the two genotypes (Figure 6-7a, b).

Tumours were also stained for Ki-67 and five random fields were analysed for each liver section (Figure 6-7c). Ki-67 score was calculated as a percentage of positively stained tumour cells to the total number of tumour cells. Analysis of Ki-67 stained tumour sections revealed no significant difference in proliferation rates in the hepatocytes (Figure 6-7d). Additionally, I observed large numbers of immune cells with their distinctive small nuclei also stained positive for Ki-67. Analysis of Ki-67 score in immune cells alone showed a significant increase in ROCK1nc tumours when compared to wild-type tumours 9 months after DEN injection suggesting that the immune cells in ROCK1nc livers were more proliferative (Figure 6-7e).

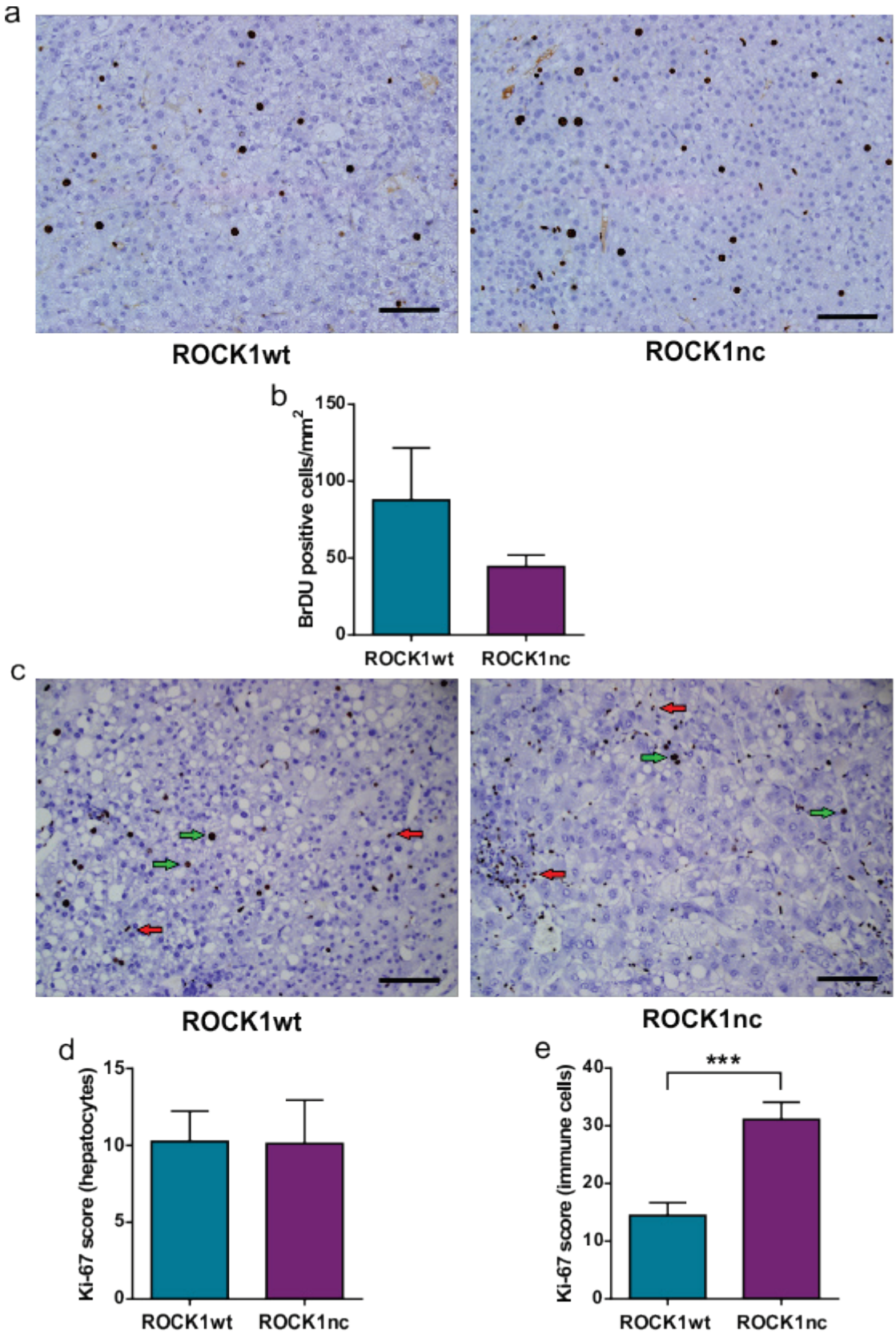

Figure 6-7 Higher rates of immune cell proliferation in ROCK1nc mice

a) & b) Representative BrdU-stained liver sections and corresponding bar graph (mean ± SEM) showing no significant difference between the two genotypes. c) Representative Ki67-stained liver sections and d) & e) corresponding bar graphs (mean ± SEM) showing no significant difference in Ki67 score in hepatocytes and significant difference in immune cells between the two genotypes respectively (n=7-8 per genotype). Scale bars represent 100 µm. Data analysed using Student's t-test. *** =p<0.001

6.2.6 Increased infiltration of immune cells in ROCK1nc tumours

H&E-stained liver sections from tumours exhibited more immune cells in ROCK1nc mice. Tumours were hence further analysed for the presence of neutrophils, macrophages, and T cells by immunohistochemistry.

Infiltration of neutrophils was analysed by staining tumour sections with S100A9 antibody (Figure 6-8a). Analysis revealed significant increase in neutrophil infiltration in ROCK1nc tumours when compared to the wild-type and the neutrophils were mostly localized within the tumour nodules (Figure 6-8b). Analysis of macrophage numbers in tumours sections stained with F4.80 revealed no significant difference between the two genotypes (Figure 6-8 c, d). However, in most ROCK1nc tumours, macrophages appeared in clusters within the tumours and also strongly localized at the tumour borders. Infiltration of T cells was quantified using CD3 antibody, which is a pan T cell marker. Analysis revealed a trend towards more T cell infiltration in ROCK1nc tumours that was not significant (Figure 6-8 e, f).

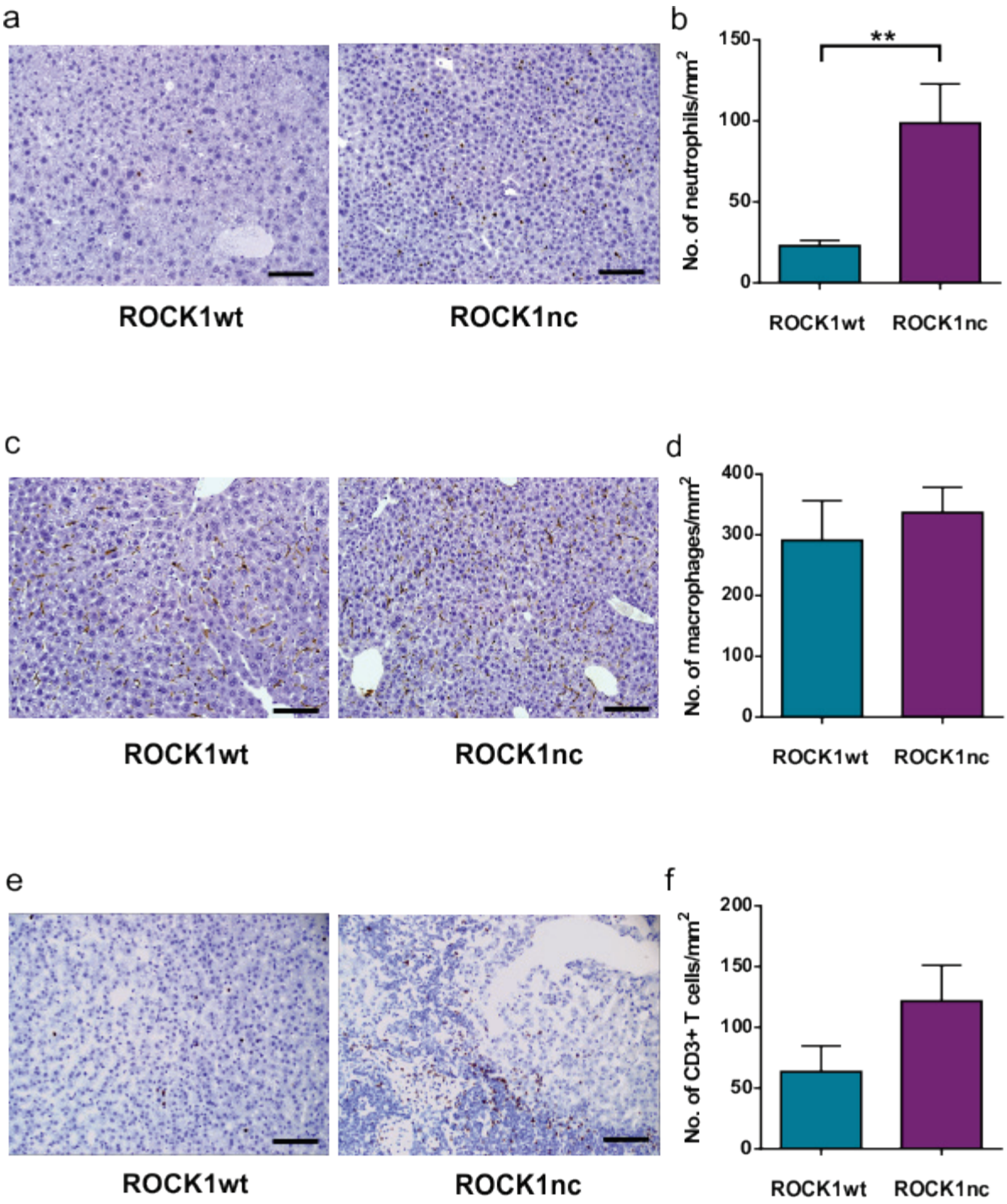

Figure 6-8 Increased infiltration of immune cells in ROCK1nc tumours
a) Representative images of S100A9-stained liver sections showing increased neutrophils (brown) in ROCK1nc tumours and, b) corresponding bar graph. c) Representative F4/80-stained liver sections showing macrophages (brown) and, d) corresponding bar graph. e) Representative CD3-stained liver sections showing increased T cell infiltration (brown) in ROCK1nc tumours and, f) corresponding bar graph. Sections counterstained with haematoxylin (blue) (n=7-10 per genotype). Scale bars represent 100 μm. Bar graphs represent mean ± SEM. Data analysed using Student's t-test. **= $p<0.01$.

6.2.7 Increased infiltration of CD8+ T cells in ROCK1nc tumours

Of the different tumour infiltrating lymphocytes, CD8+ T cells or cytotoxic T lymphocytes (CTLs) play a key role in antitumor immunity (Tanaka et al., 1999). Given the data that there was a trend towards more T cell infiltration in ROCK1nc tumours, I wanted to find out if these were CD8+ T cells. Since CD8 staining does not work on paraffin embedded section, I utilized frozen liver sections obtained from the caudate lobe of the liver. Immunofluorescence staining with CD8 antibody revealed significantly more CD8+ T cells in ROCK1nc tumours (Figure 6-9 a, b).

Natural killer (NK) cells are a subset of cytotoxic lymphoid cells that have the ability to distinguish and kill tumour cells (Vivier et al., 2012). Analysis of frozen tumour sections by immunofluorescence using NK1.1 antibody, which is specific for natural killer cells, revealed that HCC from both genotypes did not harbour many NK cells (Figure 6-10a). In addition to NK cells, natural killer T cells (NKT) have also been shown to have a role in tumour immunosurveillance (Vivier et al., 2012). NKT cells will be double positive for NK1.1 and CD3 staining; however, I did not observe any NKT cells in tumour sections from both genotypes (Figure 6-10 a).

Along with CTLs, NKs and NKTs, another population of T cells that have gained considerable interest over the years are the regulatory T cells (Tregs) that maintain self-tolerance and hence hinder effective tumour immunity (Nishikawa and Sakaguchi, 2010). These cells specifically express the transcription factor Foxp3 (Forkhead box P3) that can be exploited for immunohistochemical detection on paraffin embedded sections. However, analysis of Foxp3-positive cells did not reveal any significant difference between the two genotypes (Figure 6-10 b, c). Interestingly, hepatocytes with tumour regions displayed reduced cytoplasmic staining of Foxp3 in both ROCK1wt and ROCK1nc mice when compared to the strong cytoplasmic expression in the surrounding hepatic parenchyma (Figure 6-10 d). Although increased cytoplasmic localization of Foxp3 when compared to the surrounding normal cells has been reported in many cancer types (Triulzi et al., 2013), its reduced expression in tumour regions compared to normal tissue regions has not been reported yet.

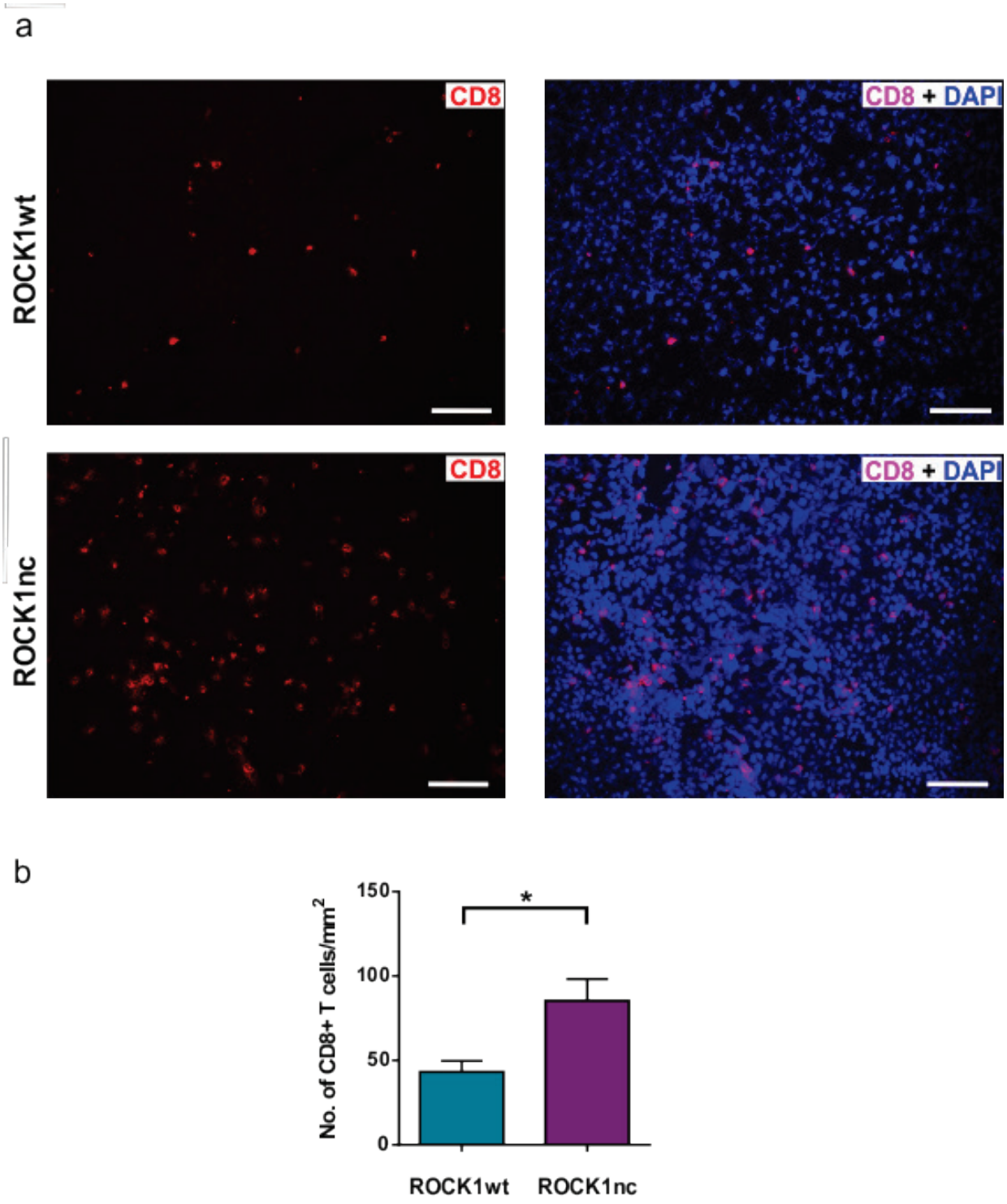

Figure 6-9 Increased infiltration of CD8+ T cells in ROCK1nc tumours
a) Representative images of CD8-stained (red) frozen liver sections and merged images (CD8 + DAPI), showing increased CD8+T cell infiltration in ROCK1nc tumours. Scale bars represent 100 µm. b) Bar graph (mean ± SEM) shows significant increase in the number of CD8+ T cells/ mm^2 in ROCK1nc tumours (n=5 per genotype). Data analysed using Student's t-test. * = $p<0.05$.

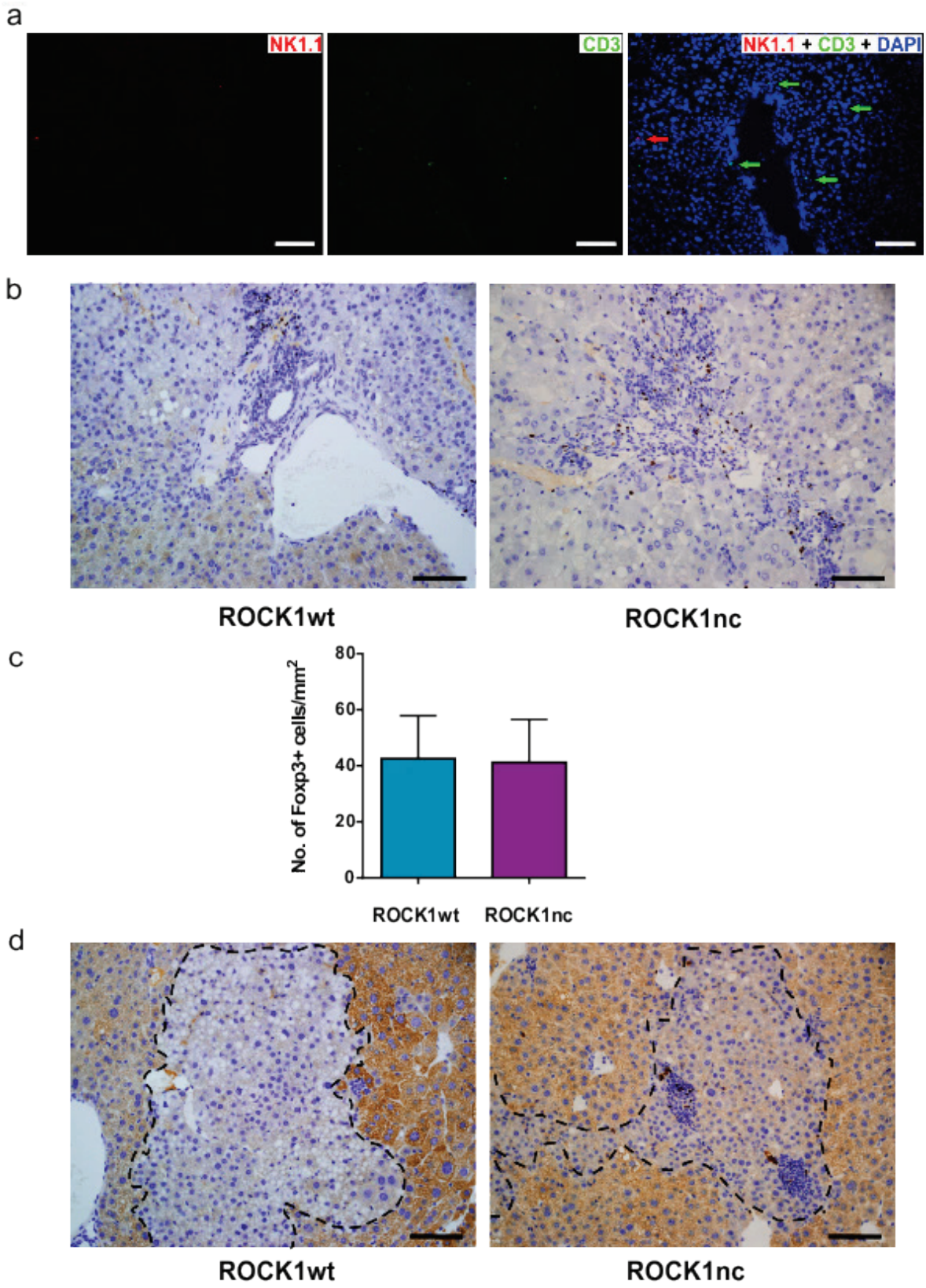

Figure 6-10 Presence of natural killer cells and Foxp3 cells in HCC tumours
a) Representative image of NK1.1-stained (red), CD3-stained (green) frozen liver sections and merged images (NK1.1 + CD3 + DAPI) in tumours. b) & c) Representative Foxp3-stained liver sections and the corresponding bar graph (mean ± SEM) showing no significant difference between the two genotypes. d) Representative Foxp3-stained liver sections showing reduced expression in the tumour regions. Sections counterstained with haematoxylin (blue) (n=6 per genotype). Dotted line represents tumour border. Scale bars represent 100 μm. Data analysed using Student's t-test.

6.2.8 Decreased tumour numbers in preneoplastic ROCK1nc livers

DEN-induced mice were sacrificed at 6 months of age to look at preneoplastic livers. After euthanasia, body weights were recorded and blood collected via cardiac puncture. Weights of the livers were recorded and the number of visible tumours in each liver lobe counted. Each tumour was measured using digitised vernier callipers to calculate the volume.

Analysis of tumour number 6 months after DEN induction revealed that ROCK1nc mice had significantly lower number of hepatic tumours when compared to the wild type (Figure 6-11 a). Two out of five ROCK1nc livers did not exhibit any tumour foci while all preneoplastic livers obtained from wild-type mice showed evidence of tumour nodules. Analysis of tumour volume revealed that there was no significant difference in tumour volume 6 months after a single injection of DEN between the two genotypes (Figure 6-11 b). ROCK1nc livers had lower tumour volumes (less than 10 mm^3) when compared to wild type which ranged between 2-50 mm^3. Additionally, there was no significant difference in absolute liver weight and relative liver weight between the two genotypes (Figure 6-11 c, d).

Metastases to the lungs were also scored in preneoplastic mice. Analysis of H&E-stained lung sections revealed a drastic difference between lungs obtained from the two genotypes (Figure 6-12 a). All ROCK1wt mice exhibited presence of metastatic nodules and thickening of the alveolar septa in the lungs. On the other hand, two out of five ROCK1nc lungs did not show any evidence of metastasis and the other three mice had small metastatic nodules. In accordance with this observation, blinded analysis of metastatic score revealed a significantly lower score in ROCK1nc preneoplastic mice when compared to wild-type mice (Figure 6-12 b).

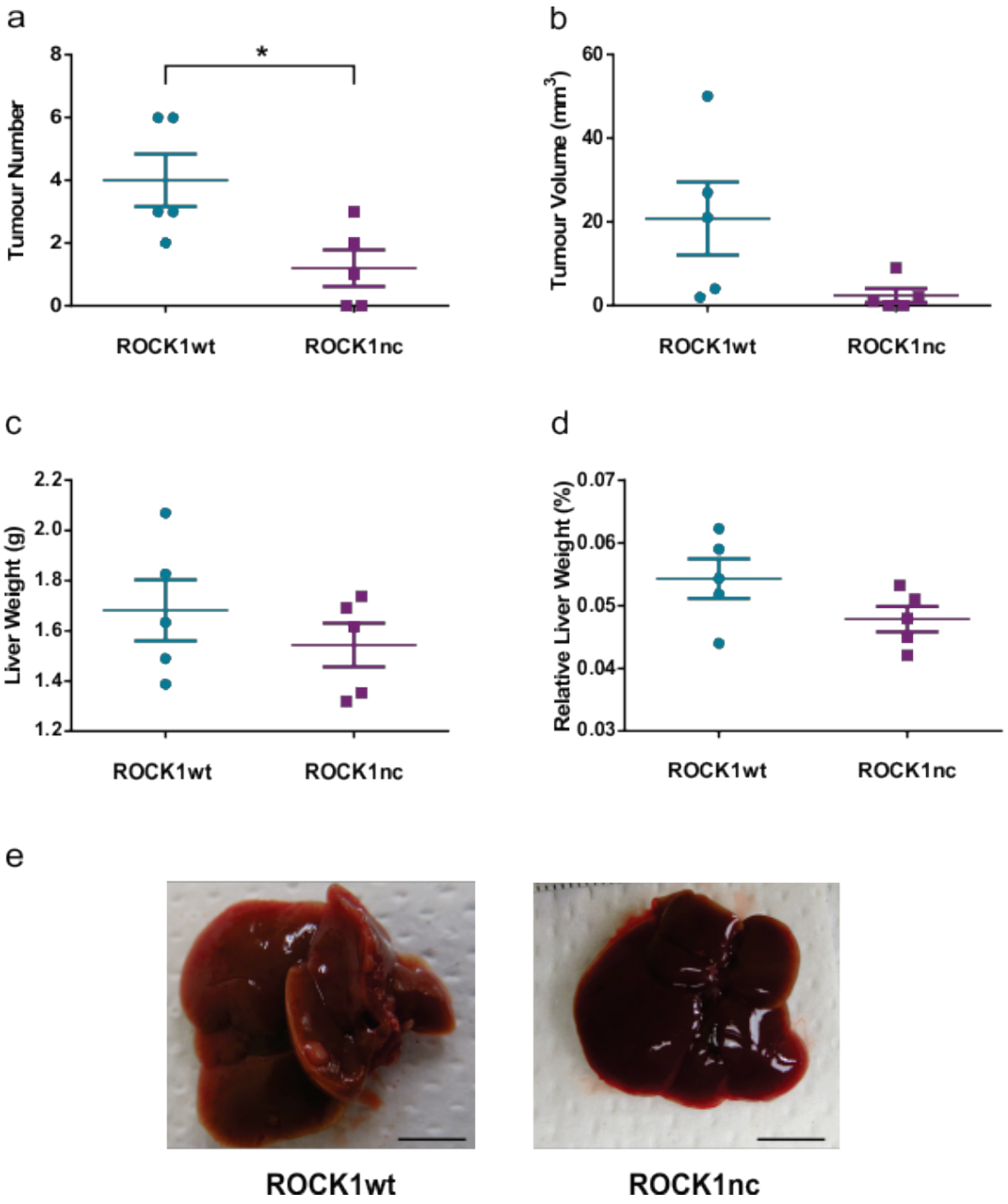

Figure 6-11 Decreased tumour numbers in preneoplastic ROCK1nc livers
Scatter dot plots (mean ± SEM) showing a) tumour number, b) tumour volume, c) absolute liver weight and d) relative liver weight in male mice injected with DEN and maintained for 6 months (n=5 per genotype). Data was analysed using Student's t-test. * = $p < 0.05$. e) Macroscopic view of representative preneoplastic livers from ROCK1wt and ROCK1nc mice 6 months after HCC initiation with DEN. Scale bars represent 1 cm.

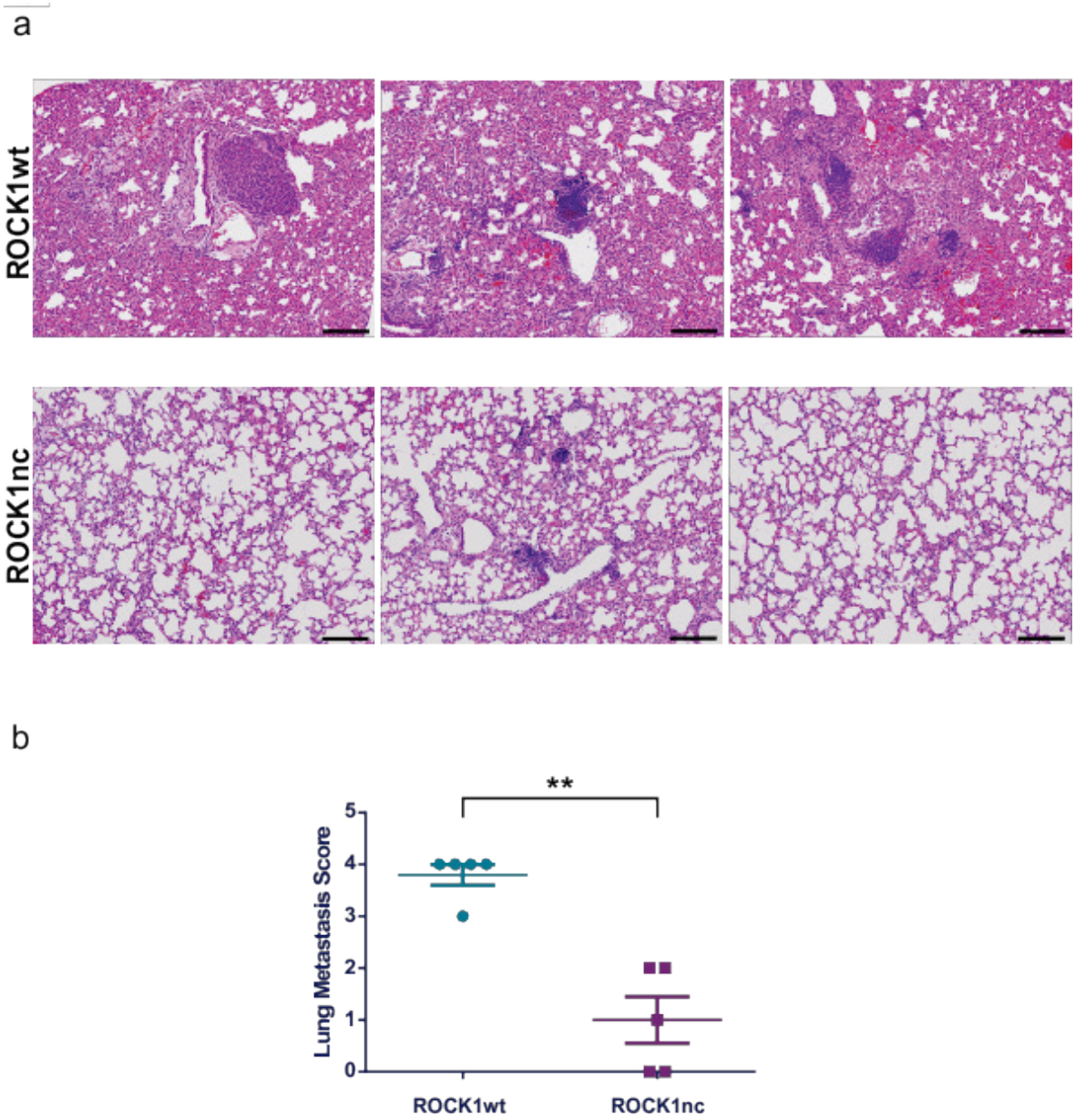

Figure 6-12 Decreased lung metastasis in preneoplastic ROCK1nc mice
a) Representative H&E-stained lung sections from ROCK1wt and ROCK1nc male mice 6 months after DEN-induction (n=5 per genotype). Scale bars represent 100 µm b) Scatter dot plot (mean ± SEM) shows decreased metastatic score in ROCK1nc lungs. Data analysed using Mann-Whitney test. ** =p<0.01.

6.2.9 Increased macrophage numbers in preneoplastic ROCK1nc livers

Preneoplastic tumours were analysed for the presence of neutrophils, macrophages, and T cells by immunohistochemistry. Infiltration of neutrophils was analysed by staining tumour sections with S100A9 antibody. Analysis revealed no difference in neutrophil infiltration in preneoplastic tumours from both genotypes (Figure 6-13 a, b). However, analysis of F4/80-stained liver sections from preneoplastic tumours at 6 months after DEN-induction revealed significantly more macrophages in ROCK1nc tumours when compared to wild-type tumours (Figure 6-13 c, d). Infiltration of T cells was quantified by immunohistochemistry using CD3 antibody, which is a pan T cell marker. Analysis revealed a trend towards more T cell infiltration in ROCK1nc tumours which was not significant (Figure 6-13 e, f).

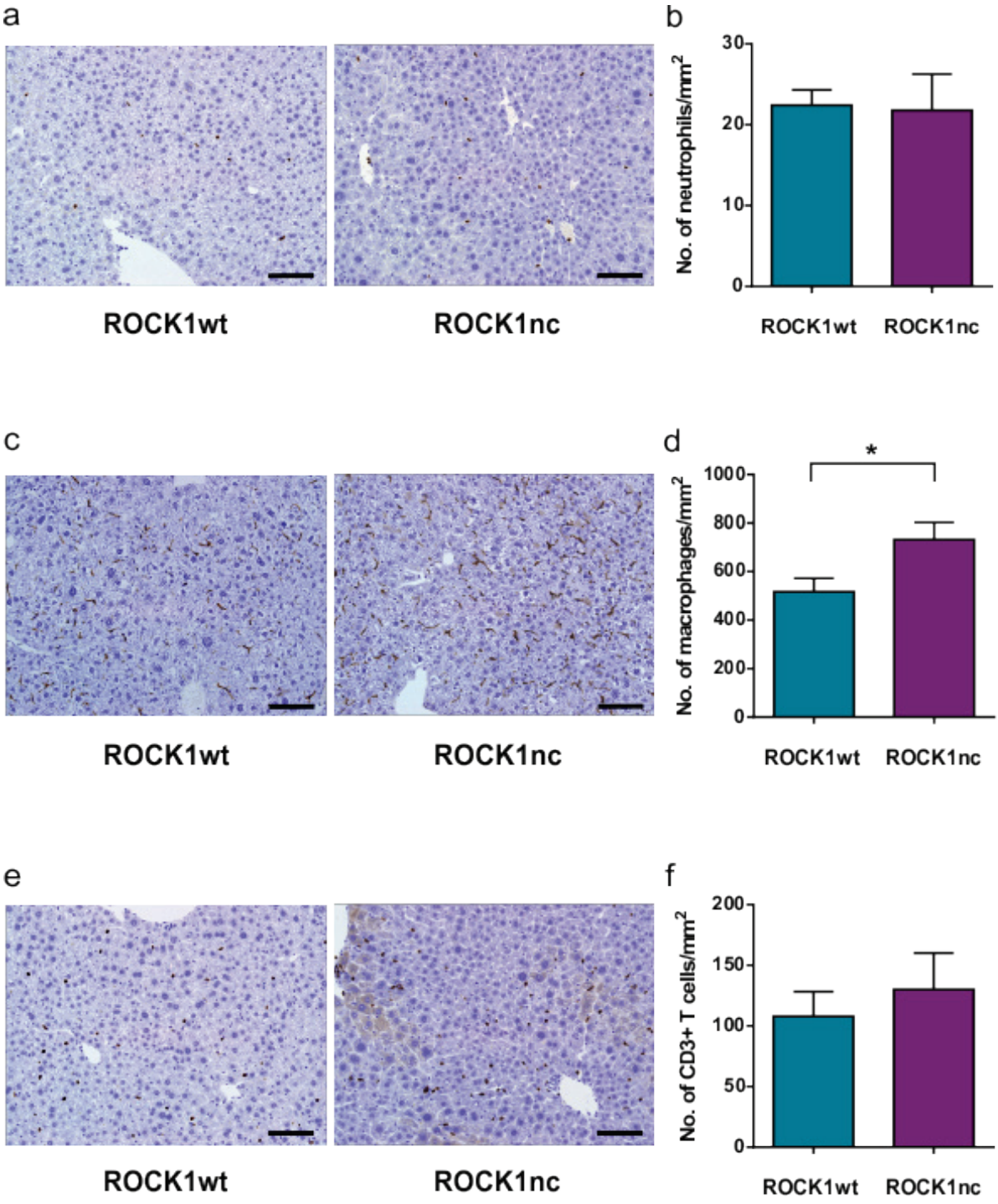

Figure 6-13 Increased macrophage numbers in preneoplastic ROCK1nc livers
a) Representative images of S100A9-stained liver sections showing neutrophils (brown) in preneoplastic livers and, b) corresponding bar graph. c) Representative images of F4/80-stained liver sections showing increased number of macrophages (brown) in ROCK1nc preneoplastic liver and, d) corresponding bar graph. e) Representative images of CD3-stained liver sections showing T cell infiltration (brown) in preneoplastic livers and, f) corresponding bar graph. Sections counterstained with haematoxylin (blue) (n=5 per genotype). Scale bars represent 100 μm. Bar graphs represent mean ± SEM. Data analysed using Student's t-test. * = $p<0.05$.

6.2.10 Liver function test for DEN-induced HCC

Serum collected from ROCK1wt and ROCK1nc mice during necropsy at 6 months and 9 months were assayed for different liver parameters. Serum ALT and AST levels were not different between the two groups at 6 months and 9 months (Figure 6-14). However, both values were higher after 9 months of DEN induction when compared to the control group, possibly reflecting liver injury induced by DEN. Alkaline phosphatase on the other hand decreased in both ROCK1wt and ROCK1nc mice with DEN induction. Total protein concentration, albumin, globulin and albumin: globulin ratio was significantly different in preneoplastic mice between the two genotypes (Figure 6-14 e, f, g, h). However, this difference was lost by 9 months of DEN-induction. Significant low levels of albumin and low albumin: globulin ratio values were seen in ROCK1wt mice when compared to ROCK1nc mice is associated with liver disease and correlates well with more tumour numbers observed in the wild-type preneoplastic mice (Figure 6-14f, h). These differences seen in serum protein levels are also lost 9 months after DEN induction.

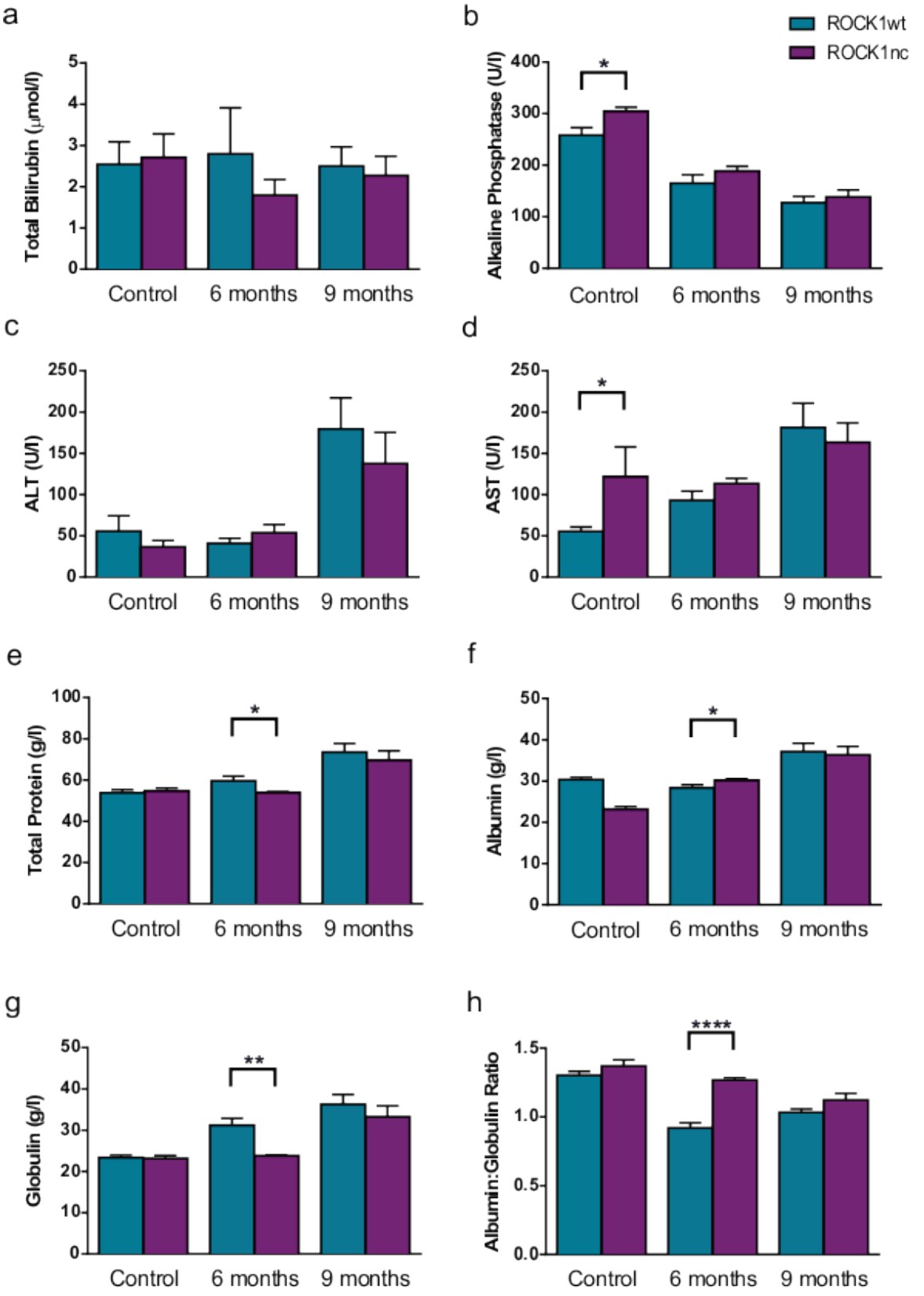

Figure 6-14 Parameters of liver function test in DEN-induced HCC

Serum collected from ROCK1wt and ROCK1nc mice during necropsy from control mice, DEN-induced HCC preneoplastic mice (6 months) and end-point DEN-induced HCC (9 months) and assayed for a) total bilirubin, b) alkaline phosphatase, c) ALT, d) AST, e) total protein, f) albumin, g) globulin and e) albumin to globulin ratio (n=5-12 per group). Data analysed by Student's t-test. * =p<0.05, ** =p<0.01, **** =p<0.0001.

6.3 Discussion

6.3.1 Defective caspase cleavage of ROCK1 reduced tumour numbers in DEN-induced HCC

In the previous chapters, ROCK1-dependant apoptotic blebbing was shown to be important for the maintenance of homeostasis in the liver. In this chapter, the role of caspase cleavage of ROCK1 in tumourigenesis was studied by utilizing the DEN-induced HCC model. DEN has been extensively used as a carcinogen and several strategies of HCC induction have been developed over the years. While some strategies involved using DEN on its own as a tumour initiator, others employed a promoting agent like phenobarbital along with DEN to induce hepatic tumours. Since the efficacy of phenobarbital as a tumour promoter has come under scrutiny especially in C57BL/6 strain (Lee et al., 1989, Bursch et al., 2005), I decided to utilize DEN on its own for my experiments. ROCK1wt and ROCK1nc mice were injected with DEN at two weeks of age and monitored for tumour formation.

Gender disparity in HCC formation was observed in both genotypes with the female mice not showing macroscopic evidence of tumours, possibly due to difference in IL-6 production in response to liver injury as previously reported (Naugler et al., 2007). Remarkably, ROCK1nc male mice presented with significantly lesser tumour numbers both in preneoplastic stage (6 months) as well as at end point (9 months) suggesting that defective caspase cleavage of ROCK1 during apoptosis had reduced tumour initiation in these mice. Although tumour volumes after 9 months of DEN injection were generally lower in ROCK1nc mice, three of them had large tumours that were comparable to ROCK1wt tumours, which accounted for the loss of significance in tumour volume. Lung metastasis was observed in both end-point as well as preneoplastic stage. ROCK1nc mice exhibited significantly lower metastatic score at preneoplastic stage. However, after 9 months even though most ROCK1nc mice had a lower metastatic score, this was not significantly different when compared to wild type, possibly because of the lower number of ROCK1nc lungs analysed. Liver damage, evaluated by the measurement of various liver enzymes and proteins did not reveal any differences between the two genotypes 9 months after DEN-induction. However, in preneoplastic mice significant low

levels of albumin and low albumin: globulin ratio were seen in ROCK1wt mice when compared to ROCK1nc mice and this may be associated with greater hepatocellular damage due to greater tumour numbers seen in wild-type preneoplastic mice.

Histopathological evaluation of ROCK1wt and ROCK1nc tumours at end point did not reveal any obvious differences between the two genotypes. Classification of hepatic tumours using the H&E-stained sections revealed that more than 60% mice from both genotypes exhibited full-blown HCC and the rest exhibited hepatic nodules of lower grade. Although HCC development in humans often features fibrotic liver damage, commonly used rodent models including DEN-induced HCC model are seldom accompanied by fibrosis (Uehara et al., 2014).This study reaffirmed previous findings demonstrating very low percentage of fibrotic areas with an average of less than 1% of the total tumour area in both genotypes. Microvesicular and macrovesicular steatosis was observed in end point tumours of both genotypes and analysis revealed that 4 out of 12 ROCK1nc mice had a higher steatotic grade compared to just 1 out of 12 ROCK1wt mice. Detailed analysis revealed that ROCK1nc mice with higher steatotic grade had large tumours as well, with the exception of one. Although hepatic steatosis has been linked with HCC development (Ohata et al., 2003, Park et al., 2010), it is not clear why ROCK1wt mice with large tumours failed to display higher steatotic grade.

Nonetheless, hepatic steatosis has been conceptualised as a precursor for inflammation (Peverill et al., 2014) and this correlated well with the large inflammatory infiltrates seen in ROCK1nc tumours. Detailed analysis of these immune cells by immunohistochemistry revealed that these infiltrates were mainly composed of neutrophils, macrophages and T cells. There was increased infiltration of neutrophils in ROCK1nc tumours and a trend towards increased T-cell infiltration as well. Similar to the acute liver damage model where defective ROCK1 cleavage exacerbated infiltration of inflammatory cells like neutrophils, as detailed in the previous chapter, it is possible that a similar scenario unfolded in a tumour microenvironment as well.

6.3.2 Defective caspase cleavage of ROCK1 results in increased infiltration of CD8+ T cells

Human HCC is an inflammation-induced cancer, with risk factors like viral hepatitis and alcohol abuse causing chronic inflammation. Role of infiltrating immune cells in the development and progression of liver cancer was neatly demonstrated in a recent study where reduced immune cell trafficking to the liver resulted in dramatic reduction in tumour development (Barashi et al., 2013). In this study, ROCK1nc mice presented with significantly more macrophages at preneoplastic stage and significantly more neutrophils at the timed end-point of 9 months after DEN injection. Also increased in ROCK1nc tumours at end-point were the number of infiltrating T cells which however were not in significant numbers when compared to wild type tumours.

Infiltration of neutrophils is associated with poor prognosis in a variety of human cancers including HCC (Dumitru et al, 2013). As discussed in the previous chapter, damage to the hepatic parenchyma triggers neutrophil infiltration and their persistence in the liver subsequently can promote more damage through the production of ROS and proteases in an acute damage scenario. Recent study by Wilson et al showed that in DEN-induced HCC model, neutrophils promote HCC by causing telomere damage in hepatocytes (Wilson et al., 2015). Hence their increased presence in ROCK1nc tumours was puzzling. The role of macrophages in tumour progression has been extensively studied and as discussed earlier, inhibiting macrophage recruitment in a spontaneous model of HCC resulted in a reduction in liver tumours (Barashi et al., 2013). Another set of immune cells that has received considerable attention are tumour infiltrating T cells. Different subsets of T cells including CD4+, CD8+ and regulatory T cells (Tregs) have been identified in solid tumours mostly by immunohistochemical techniques, and the presence of CD8 as well as high CD8/Foxp3 ratios had a positive effect on survival (Gooden et al., 2011). Remarkably, analysis of infiltrating CD8+ T cells revealed a significant increase in ROCK1nc tumours when compared to wild type tumours. Analysis of Foxp3 positive Treg cells did not show a significant difference between the two genotypes. It is possible that the infiltrating CD8+ T cells keep tumour numbers in check in ROCK1nc mice, but the high numbers of infiltrating neutrophils promote tumourigenesis in the

already formed tumours hence accounting for the lack of difference in tumour volume between the two genotypes.

6.4 Summary

DEN-induced HCC was repressed in ROCK1nc mice but exhibited higher grade of steatosis. Defective caspase-cleavage of ROCK1 resulted in increased infiltration of CD8+ cytotoxic T cells in ROCK1nc livers which may be responsible for the decreased tumour numbers seen in ROCK1nc mice. As shown in the previous chapter, in the liver, apoptotic blebbing suppresses inflammation which may be beneficial for maintenance of homeostasis in an acute scenario. However; in a tumour setting, suppression of inflammation may prove detrimental since this can curb immunosurveillance and subsequent elimination of tumours.

7 Eμ-myc lymphoma model

7.1 Introduction

7.1.1 Eμ-myc lymphoma

The Eμ-myc transgenic mice model resembles human Burkitt lymphoma that bears the MYC/Ig gene translocation t(8;14)(q24;q32). Myc is a nuclear transcription factor that regulates several target genes involved in proliferation, differentiation, apoptosis, metabolism and DNA repair (Dang, 2012). The myc family of oncogenes (c-myc, N-myc and L-myc) is activated in most rapidly dividing malignancies and elevated myc levels lead to hyperproliferative DNA damage responses as well as apoptosis (Soucek and Evan, 2010). Of these, the c-myc oncogene has been extensively studied using one of the earliest models, the Eμ-myc model, described by Adams and colleagues in 1985 (Adams et al., 1985). In this transgenic model, expression of c-myc is deregulated as it is under the control of immunoglobulin heavy chain enhancer (Eμ). Hence, Eμ-myc transgenic mice overexpress c-myc in the B cell lineage and hence succumb to B cell lymphomas with a mean survival of 4-6 months (Adams et al., 1985, Harris et al., 1988).

c-myc expression not only confers a proliferative advantage but also induces apoptosis. Therefore, Myc-induced lymphoma is preceded by a prolonged precancerous phase in which the increased proliferative rates of B cells is offset by a high apoptotic index (Jacobsen et al., 1994). This latency period reflects an ability of c-myc to induce a p53-dependant apoptotic program. However, additional mutations in the p53 tumour suppressor pathway result in the emergence of a clonal B-cell lymphoma (Eischen et al., 1999, Jacobs et al., 1999). Since its creation more than three decades ago, this model is frequently crossed with other genetically altered mice to investigate the effect of different genes in how they alter lymphoma onset time or modulate response to chemotherapy.

7.1.2 Experimental Aim

To determine whether defective caspase cleavage of ROCK1 affects tumourigenesis in Eμ-myc-lymphoma model.

7.2 Results

7.2.1 Defective caspase cleavage of ROCK1 increases lymphoma-free survival

Eμ-myc transgenic mice which express the c-myc oncogene under the control of the immunoglobulin heavy chain enhancer (Eμ) die from tumours of the B lymphocyte lineage (Adams et al., 1985). To determine whether defective caspase cleavage of ROCK1 influences the development of Eμ-myc-induced lymphoma, Eμ-myc transgenic male on a C57Bl/6 background, kindly provided by Dr. Karen Blyth, were crossed with ROCK1nc mice (Figure 7-1). Eμ-myc/ROCK1het males were then crossed with ROCK1wt or ROCK1nc females to generate Eμ-myc/ROCK1wt and Eμ-myc/ROCK1nc mice, respectively (Figure 7-1). Female mice carrying the Eμ-myc gene were not used for breeding because of their high risk of developing lymphomas before their pups reached weaning age.

Mice bearing the Eμ-myc transgene were examined three times a week for signs of morbidity and lymphoma emergence. This included presence of enlarged lymph nodes, hunched posture, slow movement, ruffled fur, swollen abdomen and/or tachypnoea/dyspnoea. Mice were sacrificed once they displayed any of these symptoms and the date of necropsy was utilized for survival analysis. As expected, Eμ-myc/ROCK1wt mice succumbed to lymphoma at a median age of 106 days (15 weeks). However, Eμ-myc/ROCK1nc mice displayed a significantly delayed onset of lymphoma with a median age of 152 (21 weeks) (Figure 7-2 a). All Eμ-myc/ROCK1wt mice died before 184 days while 26% of Eμ-myc/ROCK1nc mice survived beyond 200 days (Figure 7-2 a). Kaplan Meier survival analysis was only done for 3rd (F3) and 4th generation (F4) animals as I noticed a difference in survival in both genotypes between generations and this was significant in Eμ-myc/ROCK1wt mice (Figure 7-2 b and c). Since the numbers of 2nd generation Eμ-myc/ROCK1wt mice were not enough for comparison (n=3), this generation was omitted from the final analysis (Figure 7-2 a).

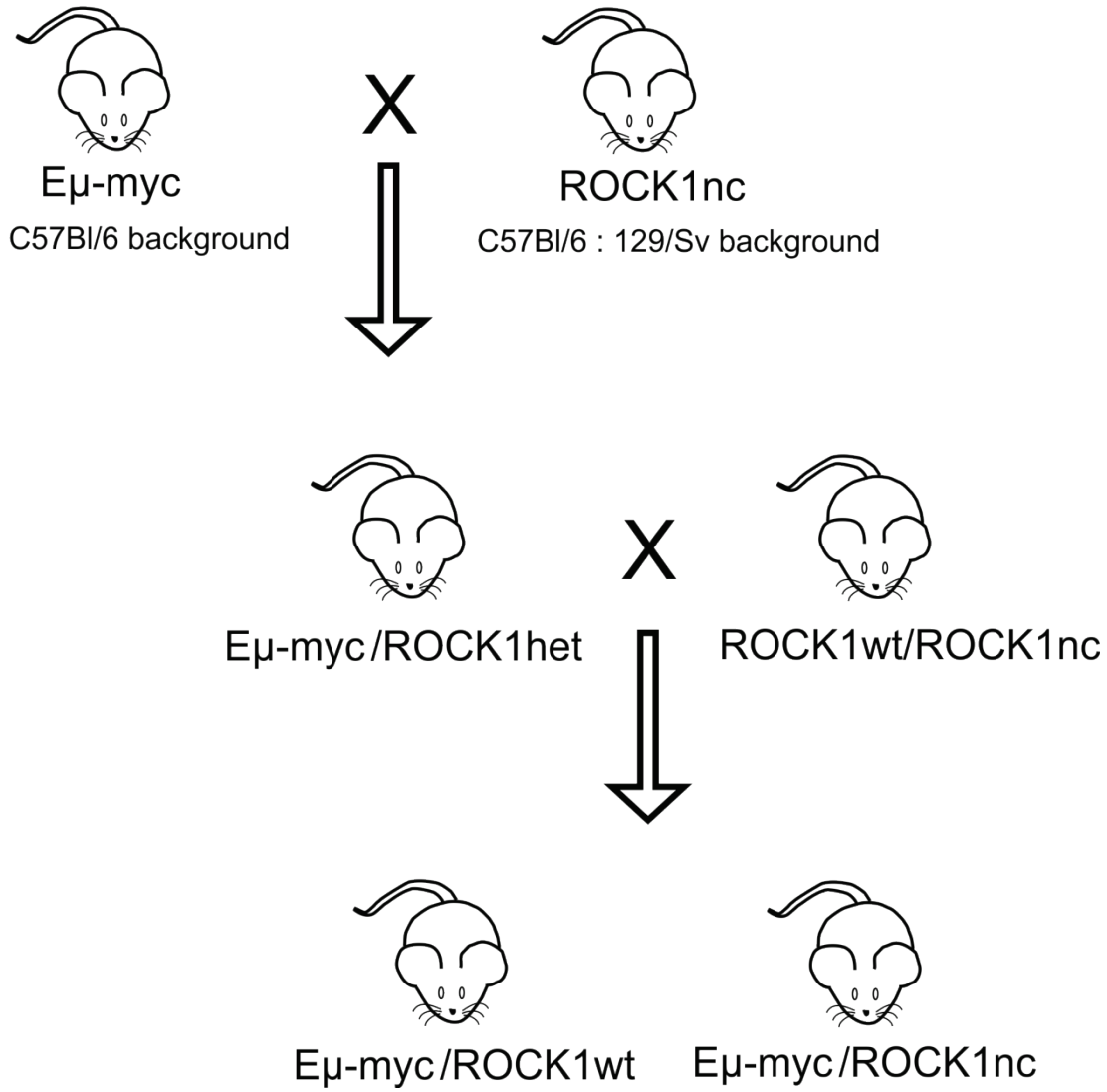

Figure 7-1 Generation of Eμ-myc/ROCK1wt and Eμ-myc/ROCK1nc mice

Schematic representation of breeding strategy shows generation of Eμ-myc/ROCK1wt and Eμ-myc/ROCK1nc mice. Matings are indicated with an X and the resultant desired offspring with an arrow.

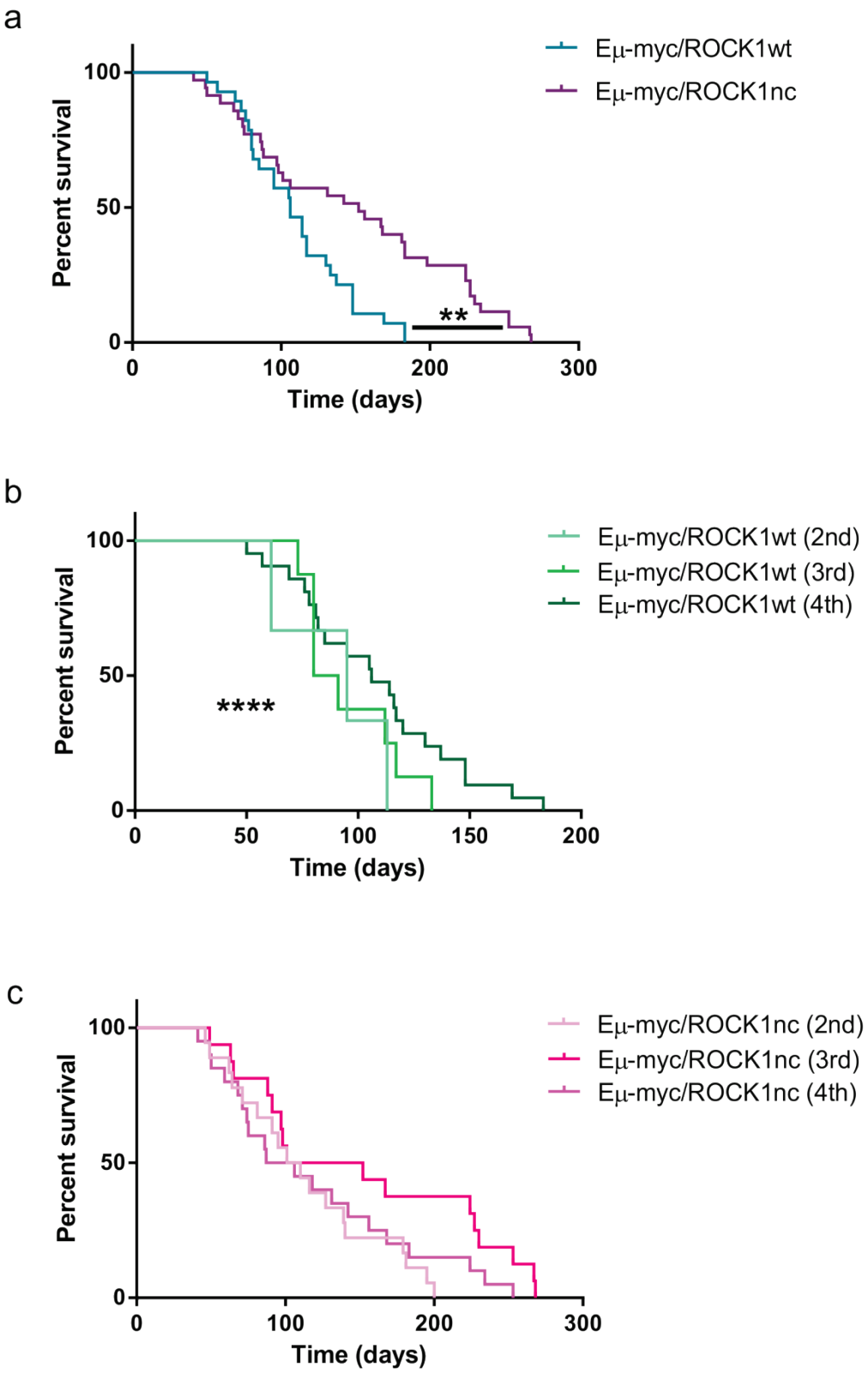

Figure 7-2 Increased survival of Eμ-myc/ROCK1nc mice

a) Kaplan-Meier survival curve for Eμ-myc/ROCK1wt (n = 29) and Eμ-myc/ROCK1nc (n = 36) showing delayed lymphoma development in mice carrying ROCK1nc mutation. b) & c) Kaplan-Meier curves showing differences in survival between different generations in Eμ-myc/ROCK1wt [2^{nd} (n = 3), 3^{rd} (n = 8), 4^{th} (n = 21)] and Eμ-myc/ROCK1nc [2^{nd} (n = 18), 3^{rd} (n = 16), 4^{th} (n = 20)] mice, respectively Data analysed by Mantel-Cox test. ** = $p<0.01$; **** = $p<0.0001$.

7.2.2 Analysis of Eμ-myc/ROCK1wt and Eμ-myc/ROCK1nc tumours

Mice exhibiting morbidity and lymphoma emergence were euthanized by carbon dioxide inhalation. Blood was collected for haematological analysis via cardiac puncture and body weights were recorded prior to necropsy. During necropsy, all lymphoid organs including the thymus, spleen and lymph nodes were harvested and their weights recorded.

Haematological analysis revealed high number of WBCs, namely lymphocytes and neutrophils in Eμ-myc mice as expected, but otherwise did not show any significant differences across the blood parameters analysed (data not shown). Analysis of body weight at necropsy did not reveal any significant differences between the two genotypes (Figure 7-3 c). Necropsy of tumour bearing Eμ-myc/ROCK1wt and Eμ-myc/ROCK1nc mice revealed disseminated disease mostly involving the thymus spleen and lymph nodes, particularly the axillary, brachial, inguinal and mesenteric lymph nodes. Based on the major lesions identified, tumours were classified as follows; a)thymic lymphoma, if the mice succumbed to an enlarged thymic tumour that was the predominant lesion, b) lymphoma, if the mice exhibited spleen and lymph node enlargement without thymic involvement and c) multicentric lymphoma, if all the lymphoid organs were enlarged. Analysis revealed that 47% of Eμ-myc/ROCK1nc mice exhibited thymic lymphoma when compared to 10.5% in Eμ-myc/ROCK1wt mice (Figure 7-3 a, b). High incidence of thymic lymphoma was reported in the initial characterisation of Eμ-myc transgenic mice and they were shown to be B-lineage tumours (Harris et al, 1988). Nonetheless, analysis of weights of thymus did not reveal any significant differences between the two genotypes, albeit some Eμ-myc/ROCK1nc mice displayed very high thymic weights (Figure 7-3 d). Analysis of spleen and lymph node weights also did not unveil any significant difference (Figure 7-3 e, f). Immunophenotyping of tumours by FACS analysis with B220 and sIg (IgM and IgD) revealed that most of lymphomas analysed from Eμ-myc/ROCK1nc mice were mature B lymphomas (37.5%) or mixed pre-B/B-lymphomas (43.75%) (Figure 7-4 a, b). Additionally, only 18.75% of Eμ-myc/ROCK1nc tumours were pre-B lymphoma when compared to 35% in Eμ-myc/ROCK1wt mice (Figure 7-4 a, b).

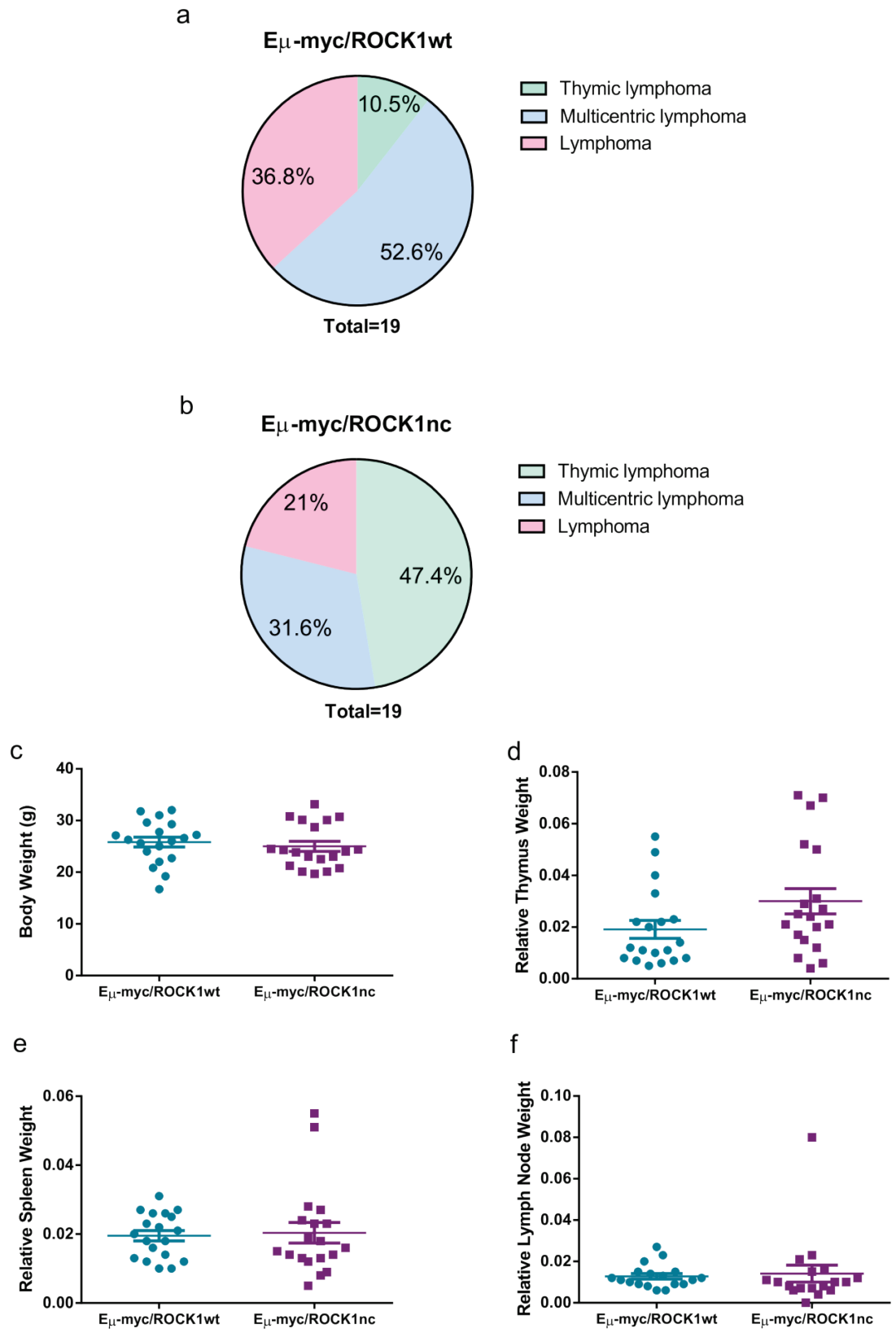

Figure 7-3 Analysis of Eμ-myc/ROCK1wt and Eμ-myc/ROCK1nc tumours
Pie chart shows percentages of each tumour type in a) Eμ-myc/ROCK1wt and b) Eμ-myc /ROCK1nc mice. Scatter dot plots (Mean ± SEM) shows no significant differences between c) body weight recorded at necropsy, d) relative thymus weight, e) relative spleen weight and f) relative lymph node weight (n=19 per genotype). Data analysed by Student's t-test.

a

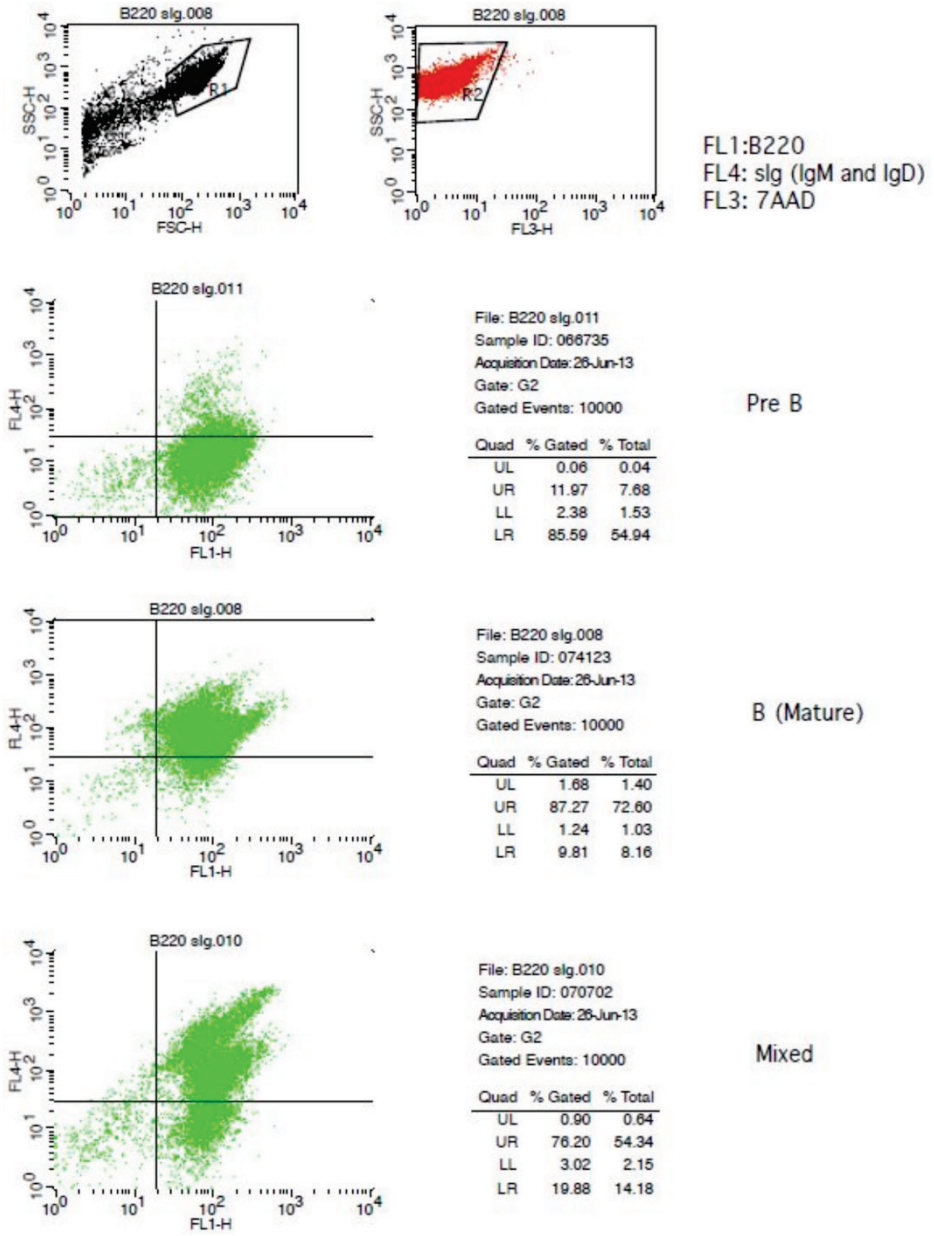

b

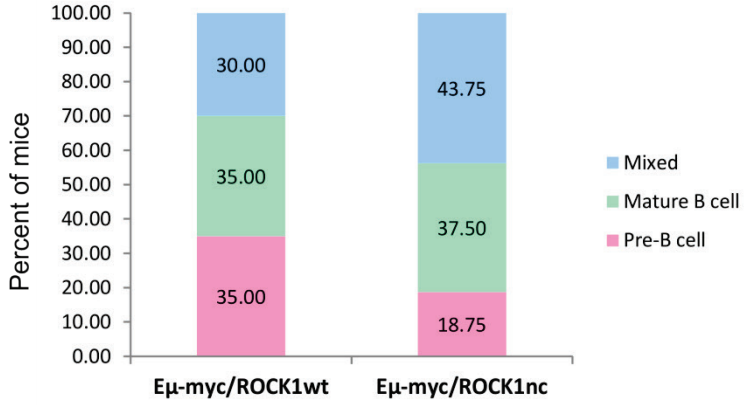

Figure 7-4 Immunophenotyping of lymphoma tumours

a) Representative FACS plots (FL1- B220; FL-4- sIg) show gating strategy for pre-B cell, mature B cell and mixed B cell lymphoma. b) Stacked bar graph shows the percentage of Eμ-myc/ROCK1wt and Eμ-myc/ROCK1nc mice with different tumour phenotypes.

7.3 Discussion

The Myc family (c-myc, N-myc and L-myc) of transcription factors regulates several genes involved in regulating proliferation and apoptosis, and in several human tumours, myc is aberrantly activated. Of these, the c-myc proto-oncogene has been shown to be overexpressed in over 50% of human tumour and hence has been extensively studied (Morton and Sansom, 2013). Eμ-myc transgenic mice carry a c-myc oncogene under the control of immunoglobulin heavy chain enhancer (Eμ) and hence c-myc is overexpressed in B lymphocytes (Adams et al., 1985). This results in tumours of B-cell lineage and mice succumb to lymphoma within 4-6 months (Adams et al., 1985). These tumours arise after a pre-cancerous phase in which increased proliferation of B cells is counterbalanced by a high apoptotic index (Jacobsen et al., 1994). Eventually, the cell cycle and apoptotic checkpoints fail due to additional mutations and the mice develop full-blown lymphomas.

To address the role of apoptotic blebbing in tumourigenesis, I made use of this apoptosis-prone transgenic mouse model of lymphomagenesis (Eμ-myc) to investigate whether defective apoptotic blebbing can influence lymphomagenesis. To achieve this, ROCK1nc mice were crossed with Eμ-myc transgenic mice to generate Eμ-myc/ROCK1wt and Eμ-myc/ROCK1nc mice. In this study, I have shown that defective caspase cleavage of ROCK1 significantly extended the survival of Eμ-myc expressing mice. Eμ-myc on a C57Bl/6 background was crossed with ROCK1nc which was on a mixed background (C57Bl/6 : 129/Sv). Hence, each generation of Eμ-myc/ROCK1wt and Eμ-myc/ROCK1nc mice had different genetic backgrounds. The effect of genetic background on lymphoma onset was evident in Eμ-myc/ROCK1wt upon survival analysis with later generations surviving longer. To avoid the effect of genetic background on lymphoma development, I analysed tumours from the same generation henceforth.

Based on the major lesions observed during necropsy, most Eμ-myc/ROCK1nc displayed enlarged thymus. Despite the delay in lymphomagenesis and the prevalence of thymic lymphoma in Eμ-myc/ROCK1nc mice, assessment of tumour load in the thymus and in other lymphoid organs did not reveal a significant difference between the two genotypes. However, immunophenotyping of

tumours from Eμ-myc/ROCK1wt and Eμ-myc/ROCK1nc revealed a difference in their stage of maturation. The majority of the Eμ-myc/ROCK1nc tumours were mature B lymphomas or mixed pre-B/B lymphomas. Eμ-myc mice mostly developed pre-B lymphoma because c-myc expression throughout B-cell development provokes an expansion of pre-B cells and reduces differentiation to a mature B-cell stage (Langdon et al., 1986).It is possible that defective caspase cleavage of ROCK1 favours the rapid clearance of premalignant B cells, thus contributing to the prolonged survival of these animals. Analysis of immune infiltration in pre-neoplastic mice will shed more light.

7.4 Summary

Defective caspase cleavage of ROCK1 significantly delays lymphomagenesis in the Eμ-myc model, probably by clearance of pre malignant B cells by the immune cells.

8 p53-deficient mouse model

8.1 Introduction

8.1.1 *Trp53*-deficient mouse model

The high propensity for mutation in the *p53* gene (TP53) in a wide range of human cancers, as well as deregulation of the p53 pathway in tumours that retain the wild-type allele implies a role as a critical tumour suppressor (Kenzelmann Broz and Attardi, 2010). p53 limits proliferation of tumour cells by inducing apoptosis, cell-cycle arrest or senescence in response to a variety of stresses, including genotoxic damage, oncogene activation and hypoxic conditions (Vousden and Prives, 2009). In addition to the frequent occurrence of acquired p53 mutations in spontaneously arising tumours, humans carrying germ line p53 mutations are associated with Li-Fraumeni syndrome, a familial cancer disorder characterised by predisposition to a broad spectrum of malignancies including breast carcinomas, bone and soft tissue sarcomas, brain tumours and haematological neoplasms (Varley, 2003). To complement studies on the role of p53 in a cell culture environment, a number of mouse models were created by manipulating the mouse *Trp53* gene, with knockouts as well as knock-in mutations commonly found in humans being created. These genetically modified mouse models proved to be integral in providing invaluable insights into the function of p53 in complex tissue environments.

Genetic knockout of the *Trp53* gene in the mouse originally described in 1992 by Donehower *et al* and then in 1994 by Jacks *et al*, demonstrated that p53 is largely dispensable for normal development, but all genetically-modified mice eventually developed some form of malignant growth and succumbed to cancer (Donehower et al., 1992, Jacks et al., 1994). Most animals developed thymic lymphomas and a range of sarcomas. Predisposition to tumours was evident in *Trp53* heterozygous mice as well, however the tumour spectra and latency was different from that seen in the *Trp53* null animals with heterozygotes mostly developing mesenchymal cancers including fibrosarcomas, osteosarcomas and hemangiosarcomas at later time points. Carcinomas or epithelial cancers occur less frequently in *Trp53* null and *Trp53* heterozygous mice but humans with *Trp53* mutation or loss are mostly diagnosed with carcinomas (Malkin et al.,

1990). Also striking was the effect of genetic background on tumour spectra. For example, *Trp53* heterozygous mice on a Balb/C background develop significant number of breast carcinomas (Kuperwasser et al., 2000) and Trp53 null mice on a 129/Sv background exhibited higher incidence of testicular tumours (Harvey et al., 1993) whereas the pioneering work on *Trp53* models by Donehower *et al* and Jacks *et al* were performed on a mixed C57BL/6 and 129/Sv background (Donehower et al., 1992, Jacks et al., 1994). This strongly suggested an effect of genetic modifiers in influencing the cancer spectra. Crossing tumour-prone mouse strains to a *Trp53* null background accelerated tumourigenesis, which not only revealed genetic interactions between *p53* and other genes involved in tumour development but also further supported the importance of *p53* in preventing cancer (Attardi and Jacks, 1999).

8.1.2 Experimental Aim

To determine whether defective caspase cleavage of ROCK1 will alter the tumour incidence and/or tumour spectra associated with *p53*-deficiency.

8.2 Results

8.2.1 Generation of *p53*-deficient ROCK1wt and ROCK1nc mice

The broad spectrum of tumours observed in *p53*-deficient mice can be utilized to study the effect of candidate mutations in alterations on tumour spectra and tumour latency. To determine whether defective caspase cleavage of ROCK1 can change the tumour spectra of *p53*-deficient mice, heterozygous 129-Trp53^{tm1Tyj}/J mice were crossed with ROCK1nc mice that were already backcrossed to 129/Sv background for eight generations. Subsequent crosses yielded p53$^{-/-}$/ROCK1wt, p53$^{-/-}$/ROCK1nc, p53$^{+/-}$/ROCK1wt and p53$^{+/-}$/ROCK1nc mice (Figure 8-1 a).

Survival of p53-deficient mice had led to the conclusion that p53 was dispensable for normal development (Donehower et al., 1992, Jacks et al., 1994). Crosses between heterozygous (p53$^{+/-}$) mice yielded 23 % of p53$^{-/-}$ at weaning, which approached the expected Mendelian ratio of 25% (Figure 8-1 b). Crosses between p53$^{-/-}$ male and p53$^{+/-}$ female yielded 50 % of p53$^{-/-}$ mice at the time of weaning which was equal to the expected Mendelian ratio (Figure 8-1 b). This suggested that p53 function was not necessary for mouse development. Nonetheless, it should be noted that 10 mice from heterozygous crosses were found dead prior to weaning and the cause of death is unknown.

However, detailed analysis of the number of p53$^{-/-}$ males and females weaned from these crosses revealed that homozygous loss of p53 in both ROCK1wt and ROCK1nc mice resulted in fewer female homozygotes at the time of weaning. In both p53$^{-/-}$/ROCK1wt and p53$^{-/-}$/ROCK1nc, only 36% of mice weaned were females, which was significantly low (Figure 8-1 c). Reduced recovery of female homozygotes has been previously reported in other studies where subsequent analysis of embryos revealed defects in neural tube closure that were strongly, but not exclusively associated with the female gender (Armstrong et al., 1995, Sah et al., 1995). Defects in neural tube closure causes exencephaly in embryos that result from overgrowth of neural tissue in the mid-brain, and female preponderance has been associated with sex-dependent differences in neurulation during development. (Copp et al., 1990).

a

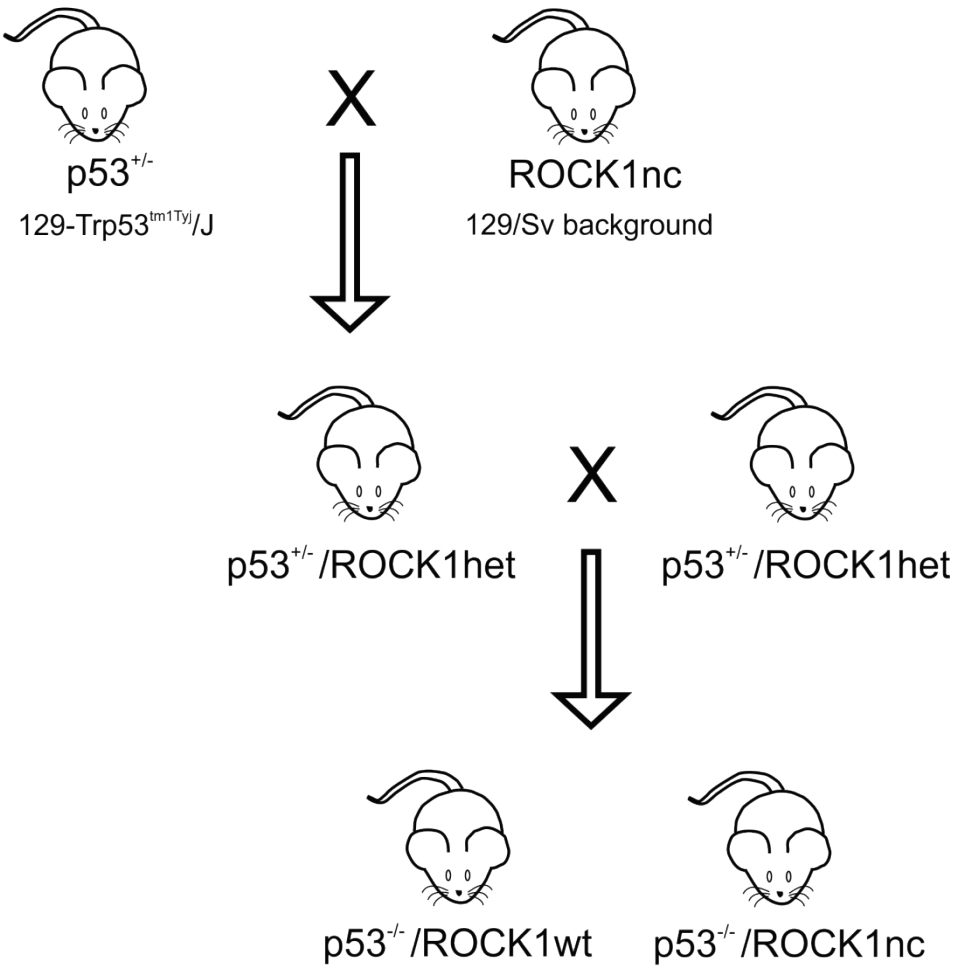

b

Heterozygous ♂ x Heterozygous ♀

Genotype	Expected	Observed
$p53^{-/-}$	25%	23.02 % (32)
$p53^{+/-}$	50%	51.08 % (71)
$p53^{+/+}$	25%	25.90 % (36)

Homozygous ♂ x Heterozygous ♀

Genotype	Expected	Observed
$p53^{-/-}$	50%	50 % (14)
$p53^{+/-}$	50%	50 % (14)

c

Genotype	Males	Females
$p53^{-/-}$/ROCK1wt	9 (64 %)	5 (36 %) **
$p53^{-/-}$/ROCK1nc	9 (64 %)	5 (36 %) **

Figure 8-1 Generation of p53-deficient ROCK1wt and ROCK1nc mice
a) Breeding strategy showing generation of $p53^{-/-}$/ROCK1wt and $p53^{-/-}$/ROCK1nc mice. Matings are indicated with an X, and the resulted desired offspring with an arrow. b) Tables show expected (Mendelian) and observed percentage of mice from crosses with the indicated genotypes. c) Table shows number of males and females born and the percentage for each genotype in brackets. Data analysed by Chi-squared test. ** = $p < 0.01$.

8.2.2 Defective caspase cleavage of ROCK1 does not alter survival rate of mice deficient in p53

In this chapter, I will describe the survival and tumour spectrum of p53-nullizygous mice as the heterozygous p53-deficient mice cohort is still ongoing due to an expected delay in tumour formation. $p53^{-/-}$/ROCK1wt and $p53^{-/-}$/ROCK1nc mice were checked thrice weekly for the presence of tumours and sacrificed when the animal displayed signs of discomfort and/ or presence of tumours either visually or by palpation. As expected, p53 wild-type control mice did not exhibit any tumours during monitoring. Weights of mice were recorded during necropsy and tumours were harvested. In addition, heart, lungs, thymus, spleen, pancreas, liver, kidneys, reproductive organs and brain were also collected routinely for histological evaluation.

Analysis of tumour-free survival of $p53^{-/-}$/ROCK1wt (n = 10) and $p53^{-/-}$/ROCK1nc (n = 11) showed that the median time for tumour onset did not differ significantly between the two genotypes, with most mice succumbing to tumours before 5 months. Few mice developed tumours within 3 months of age. $p53^{-/-}$/ROCK1wt had a median survival of 131 days and $p53^{-/-}$/ROCK1nc had 140 days (Figure 8-2 a). Separate analysis of males and females showed that among males, $p53^{-/-}$/ROCK1nc mice had a shorter median age of survival of 107 days compared to 131 days for $p53^{-/-}$/ROCK1wt mice. Among females, $p53^{-/-}$/ROCK1nc mice exhibited slightly better tumour-free survival with 178 days, although not significant (Figure 8-2 b, c). However, it should be noted that the number of females analysed is only three per genotype and hence not conclusive. Analysis of body weight during necropsy did not reveal any difference between the two genotypes (Figure 8-2 d).

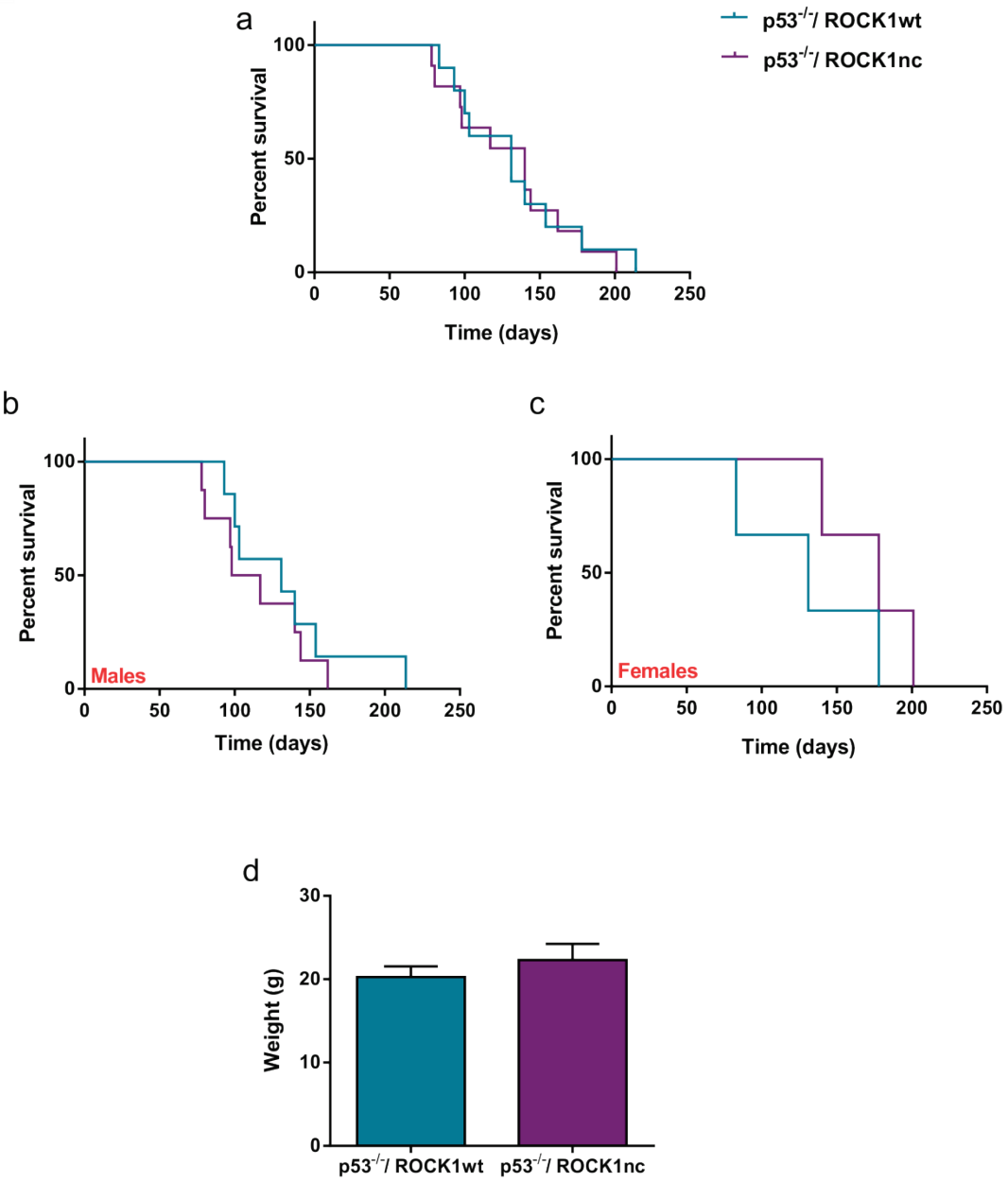

Figure 8-2 ROCK1nc mutation does not affect tumour free survival
a) Kaplan Meier survival curve for $p53^{-/-}$/ROCK1wt (n=10) and $p53^{-/-}$/ROCK1nc (n=11). b) Survival curve for males $p53^{-/-}$/ROCK1wt (n=7) and $p53^{-/-}$/ROCK1nc (n=8). c) Survival curve for females $p53^{-/-}$/ROCK1wt (n=3) and $p53^{-/-}$/ROCK1nc (n=3). Comparison of survival curves by Mantel-Cox test. d) Bar graph represents weight (in grams) of mice recorded at necropsy showing no significant difference between the two genotypes. Error bars represent SEM. Data analysed by Student's T test.

8.2.3 Analysis of tumour spectra

The co-operative effect of defective caspase cleavage of ROCK1 and p53-deficiency on tumour spectra was analysed macroscopically and by histopathological evaluation. A total of 21 animals were analysed for this study. Two animals were found dead, however necropsy did not reveal any detectable lesions.

The tumour type most frequently observed was lymphoma, with 15 mice (8 $p53^{-/-}$/ROCK1wt and 7 $p53^{-/-}$/ROCK1nc) displaying thymic lymphoma (Figure 8-3 a). These mice presented respiratory distress by 4 to 5 months due to lung compression caused by the enlarged thymus. Histologically, metastasis of lymphoid cells was frequently detected in the lungs and less frequently in the liver and kidney. Two of these mice, one from each genotype, also displayed testicular tumour of one testis.

Two $p53^{-/-}$/ROCK1nc mice displayed testicular tumour of both testes. These tumours arose in less than 3 months. The tumours were large in size and one of them weighing up to 4.7g in weight. Upon histological evaluation, these tumours displayed features akin to teratomas, with recognisable endodermal, mesodermal and ectodermal regions (Figure 8-4c, d). These mice also presented splenic lymphoma (Figure 8-4 b). Hence, while three $p53^{-/-}$/ROCK1nc mice presented testicular tumours, only one $p53^{-/-}$/ROCK1wt displayed the same.

One $p53^{-/-}$/ROCK1wt mice presented a large necrotic mass of around 1.47 g located near the testis. Unfortunately, the tissue of origin could not be determined. The mice also presented ascites and splenic lymphoma. One $p53^{-/-}$/ROCK1wt and one $p53^{-/-}$/ROCK1nc mice exhibited stomach tumours and splenic lymphoma. The livers from these mice exhibited small nodular pale lesions which were macroscopically visible. One $p53^{-/-}$/ROCK1nc mice presented subcutaneous sarcoma (Figure 8-4 e, f).

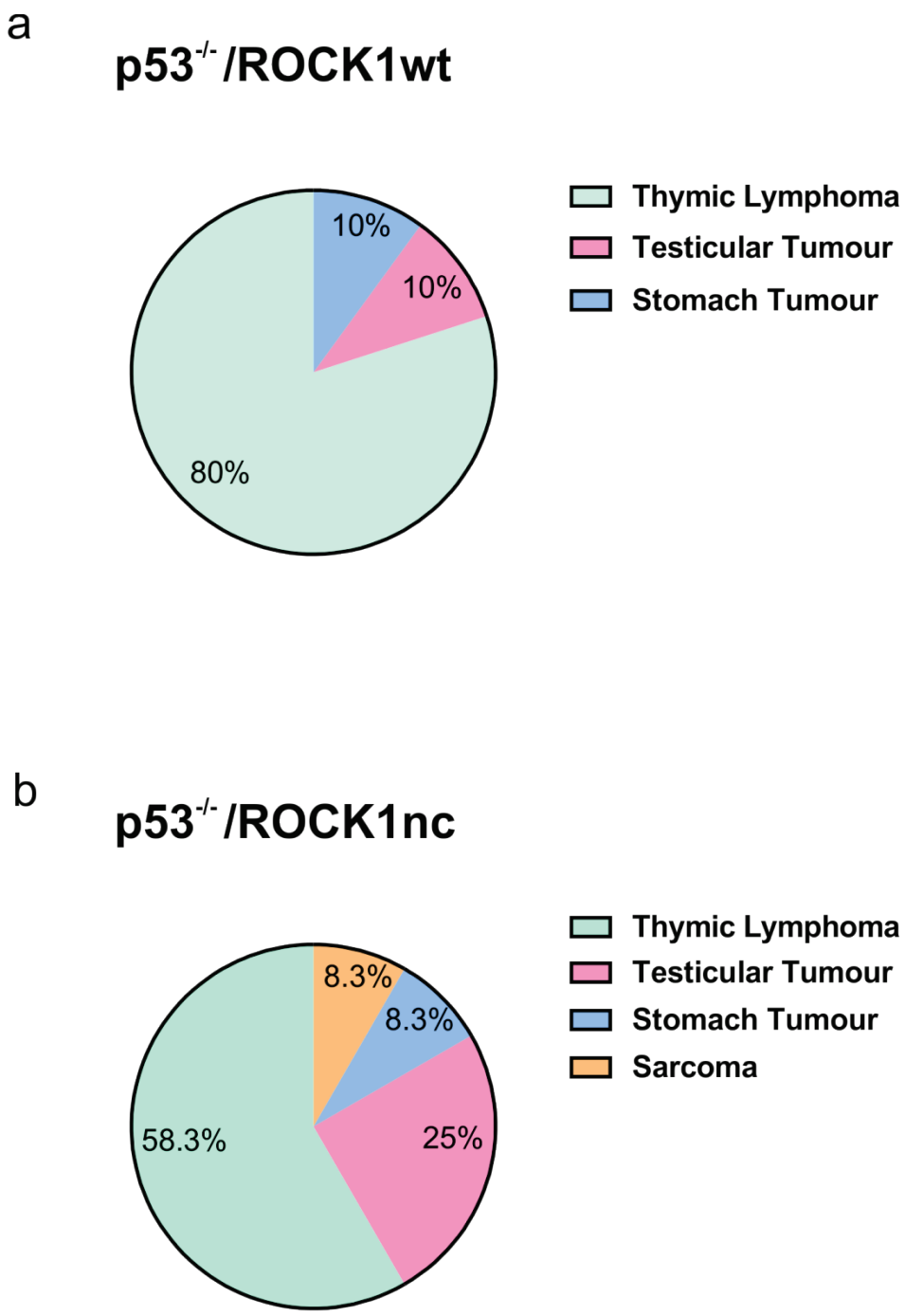

Figure 8-3 Comparison of tumour spectrum

Pie chart shows percentages of each tumour type in a) $p53^{-/-}$/ROCK1wt (n=8) and b) $p53^{-/-}$/ROCK1nc mice (n=7).

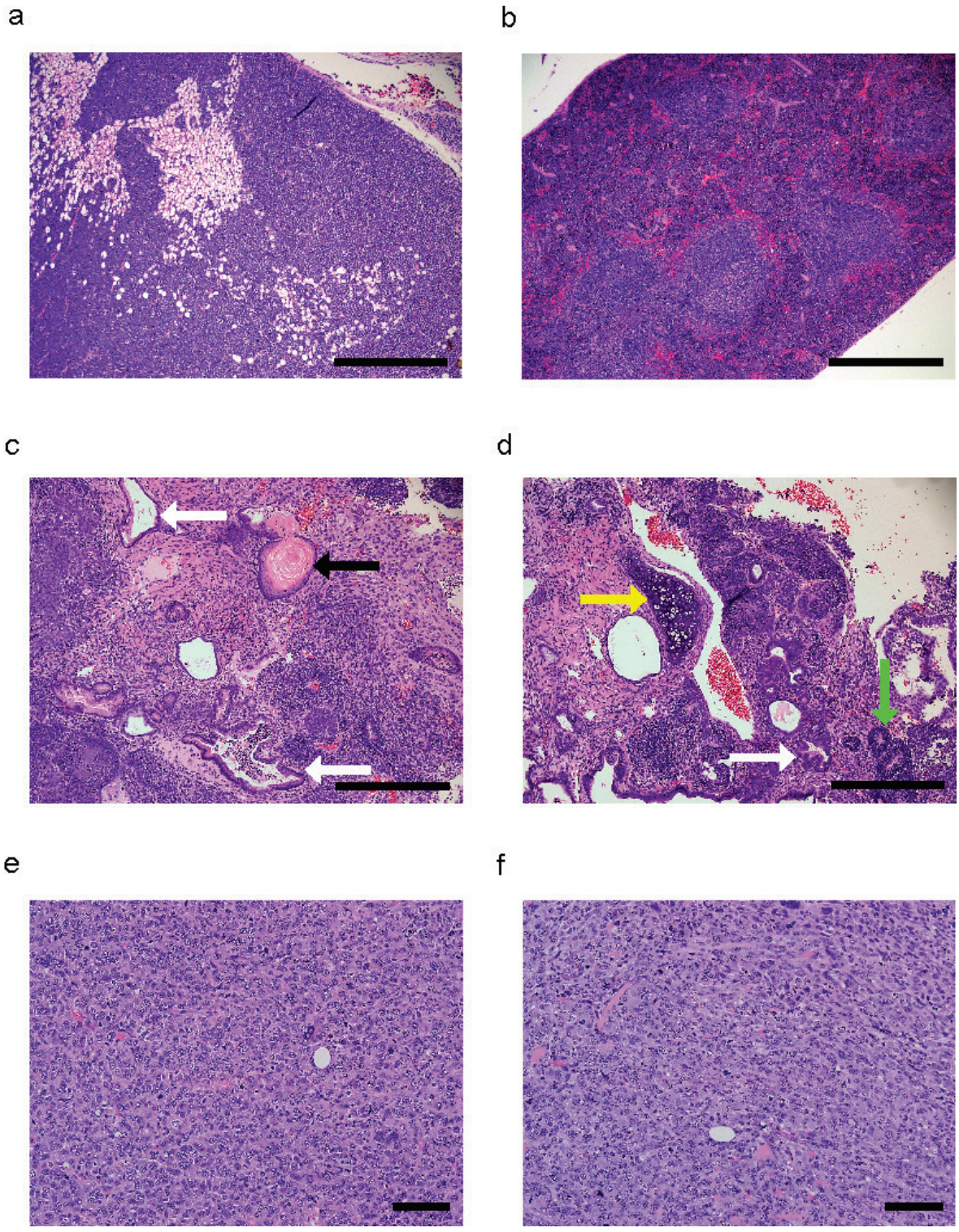

Figure 8-4 Histopathological evaluation of tumours
Representative H&E-stained sections from a) thymic lymphoma, b) splenic lymphoma, c) and d) testicular teratoma showing tissue from the three germ layers: keratin pearl (black arrow; ectoderm), cartilage (yellow arrow; mesoderm), glandular epithelium (white arrows; endoderm) and remnant testicular tissue (green arrow), e) and f) sarcoma. Scale bars represent 100 µm.

8.3 Discussion

Mutations in the p53 tumour suppressor gene are found at high frequency in most human cancers. Germline p53 mutations have been associated with an inherited predisposition to early onset cancer called Li-Fraumeni syndrome. Generation of p53-deficient mice proved to be crucial in establishing the tumour suppressive function of the gene. Both nullizygous and heterozygous mice succumb to tumours, albeit with delayed tumour latency in heterozygous mice (Donehower et al., 1992, Jacks et al., 1994). The types of tumours observed in mice are predominantly lymphomas and sarcomas, but the tumour spectrum has a strong dependence on the genetic background of mice (Attardi and Jacks, 1999). Several studies have systematically defined the tumour spectra of p53-deficient mice with different genetic backgrounds (Kenzelmann Broz and Attardi, 2010). In addition, a number of studies have successfully looked at the effect of p53-deficiency in combination with other tumour-promoting mutations or mutations in tumour-suppressive genes (Attardi and Jacks, 1999).

In this study, I used the p53-deficient mouse model to investigate whether defective caspase-cleavage of ROCK1, and in-effect, whether defective apoptotic blebbing would alter tumour latency and tumour spectra. This study was also aimed at identifying tumours where apoptotic blebbing would play a crucial role. Heterozygous p53-deficient mice, on a 129 background, purchased from Charles River UK were crossed with ROCK1nc that were already backcrossed to 129/Sv background for eight generations. Generation of ROCK1wt and ROCK1nc mice with homozygous or heterozygous p53-deficiency with expected Mendelian ratios reaffirmed previous findings that p53 had no effect on normal development. Female-specific lethality that was observed in homozygous p53-deficient mice also correlated with previous reports (Armstrong et al., 1995, Sah et al., 1995); however ROCK1nc mutation had no influence on this gender-related lethality.

While studying the effect of genetic background on tumour incidence and spectra, it was found that the onset of tumours was earlier on a 129/Sv background when compared to mixed background (C57BL/6 and 129/Sv) (Harvey et al., 1993). Analysis of tumour-free survival of p53-/-/ROCK1wt and p53-/-/ROCK1nc showed that the median time to tumour onset did not differ

significantly between the two genotypes, with most mice succumbing to tumours before 5 months. Analysis of tumour spectra revealed that as expected, lymphomas were the most frequently observed tumour in both genotypes. Lymphomas are quite common in both 129/Sv as well as mixed background, but the percentage is slightly lower in the 129/Sv background (Harvey et al., 1993). The second most frequently observed tumours in this study were testicular tumours. Three p53-/-/ROCK1nc compared to one p53-/-/ROCK1wt mice displayed testicular tumour either as a primary tumour or in combination with thymic lymphoma, thus hinting at the possibility of a role of ROCK1-dependant apoptotic blebbing in tumour formation in the testis. However, the small number of animals used in this study hampers the possibility of conclusive evidence. Testicular tumours were early-onset tumours in both genotypes and displayed features of teratoma. Sarcomas are also common in this background and one p53-/-/ROCK1nc mice presented subcutaneous sarcoma. The high frequency of lymphomas and small number of animals analysed for this study is a major caveat in determining the effect of apoptotic blebbing in this model. Also, heterozygous p53-deficient mice with a broader range of tumour types would be a more suitable model for this investigation.

8.4 Summary

Defective caspase-cleavage of ROCK1 does not change tumour-free survival in homozygous *p53*-deficient mice but hints at a possible role in testicular tumour formation.

Results

Actomyosin-dependant protein release from apoptotic blebs

9 Actomyosin dependant protein release from early apoptotic cells alert the immune system

9.1 Introduction

9.1.1 Apoptotic cells advertise their presence

The prompt removal of apoptotic cells by phagocytes is important for maintaining homeostasis in multicellular organisms. To facilitate their removal, apoptotic cells advertise their presence to the immune system. This is achieved by the display of 'eat me' signals like phosphatidylserine on the surface of apoptotic membrane. Over the years, a number of 'find me' signals released by apoptotic cells including nucleotides (ATP/UTP), lysophosphatidylcholine (LPC) and sphingosine-1 phosphate have been identified which act as chemoattractants for phagocytes (Poon et al., 2014). Prompt clearance sequesters the dying cell and prevents the release of potentially noxious intracellular contents into the surrounding environment. This is a key distinction from necrotic cell death where membrane integrity is lost resulting in the unregulated release of intracellular contents like DAMPs that can provoke a strong inflammatory response. In addition to display of 'eat me' signals, apoptotic cells can be distinguished from their viable counterparts based on their morphological features including cell contraction, nuclear condensation and fragmentation, membrane blebbing and apoptotic body formation. We now know that the driving force behind actomyosin contractility during apoptosis is caspase-mediated cleavage and consequent activation of ROCK1 (Coleman et al., 2001, Sebbagh et al., 2001). Despite the widely held notion that apoptotic cells preserve membrane integrity, work from our lab provided evidence that blebs and apoptotic bodies can lose membrane integrity (Wickman et al., 2013) thus hinting at the possibility that membrane blebs and apoptotic bodies can release proteins prior to secondary necrosis.

9.1.2 Experimental Aims

To investigate whether membrane blebs and apoptotic bodies release proteins in an actomyosin dependant manner prior to secondary necrosis and to identify the proteins released using a SILAC-based mass spectrometry approach.

9.2 Results

[The results outlined in this chapter was published in Cell Death and Differentiation (Wickman et al., 2013).]

9.2.1 Actomyosin-dependant blebs and apoptotic bodies release proteins

Given the importance of actomyosin contractility in mediating membrane blebbing and apoptotic body formation, we wanted to investigate whether the contractile force generated by the actin-myosin cytoskeleton can influence the release of proteins that can act as potential 'find me' signals. For this, I induced apoptosis in NIH3T3 fibroblasts using TNFα and CHX in the presence of Blebbistatin or ROCK1 inhibitor Y-27632. Blebbistatin is a myosin ATPase inhibitor that impairs blebbing by inhibiting actomyosin contractility (Cheung et al., 2002). 4 hours after apoptosis induction, the conditioned medium was collected. Proteins in the conditioned medium were then concentrated using StrataClean Resin by following a protocol kindly provided by Dr. Juan Hernandez, and then separated on polyacrylamide gels (Figure 9-1 a).

Staining the polyacrylamide gel with Coomassie Blue revealed that there was a clear increase in bulk protein release 4 hours after treatment with the apoptotic inducer (lane 2 and lane 5) when compared to untreated cells (lane 1 and lane 4) (Figure 9-1 b). However, the amount of proteins released from apoptotic cells was visibly reduced if cells were treated with ROCK1 inhibitor Y-27632 (lane 3) or Blebbistatin (lane 6) (Figure 9-1 b). This suggested that contrary to popular belief, substantial amount of proteins are released from apoptotic cells and this occurs in an actomyosin-dependant manner.

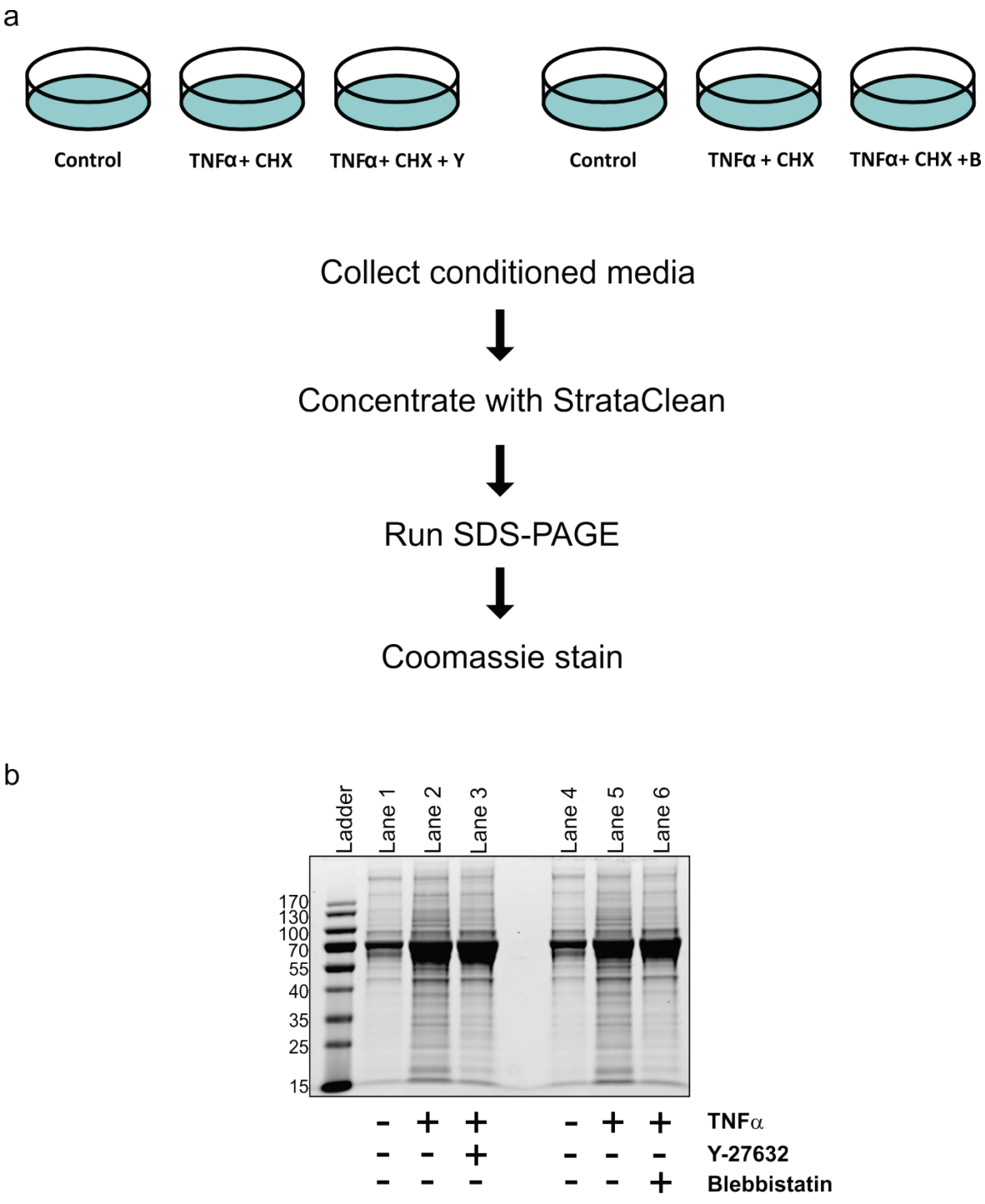

Figure 9-1 Actomyosin-dependant protein release from apoptotic cells
a) Experimental workflow for studying protein release from apoptotic cells. b) Coomassie-stained polyacrylamide gel of concentrated proteins in conditioned media from equal cell numbers for indicated treatments (Wickman et al., 2013).

9.2.2 Proteomic analysis of proteins released from apoptotic cells

Quantitative proteomic analysis using an adapted approach combining stable isotope labelling with amino acids in cell culture (SILAC) and mass spectrometry was performed to identify proteins released by apoptotic cells. The SILAC technique relies upon labelling proteins with amino acids lysine (Lys) and arginine (Arg) that contains stable heavier isotopes, followed by mass spectrometry analysis for identification, characterization and quantitation of proteins. Cells are cultured in media supplemented with labelled amino acids instead of the natural amino acids for at least five doublings, thus allowing incorporation into ~97% of proteins. Proteins from unlabelled and labelled samples are pooled and individual proteins, due to their mass difference, can then be easily distinguished from different samples using liquid chromatography and mass spectrometry (LC-MS).

To determine whether proteins released during apoptosis were dependant on membrane blebbing, profiles of proteins in the conditioned media after apoptosis induction with TNFα and CHX, in the absence or presence of Y-27632 or Blebbistatin were compared. For this study, I performed the Triple SILAC labelling of NIH3T3 cells. Briefly, individual NIH3T3 fibroblast populations were grown in defined SILAC medium containing light (Lys0, Arg0), medium (Lys4, Arg6) or heavy (Lys8, Arg10) amino acids. Each labelled population was then assigned an experimental treatment: reference (control); apoptosis (TNFα and CHX); apoptosis with reduced apoptotic body formation (TNFα and CHX with Y-27632 or Blebbistatin). Six replicate experiments were performed with each set of conditions cycled through the SILAC labels, i.e. 3 of which included Y-27632 treatment and 3 of which included Blebbistatin treatment. After 4 hours, conditioned medium was collected and pooled from each of the different sets. The proteins in the conditioned media were concentrated using StrataClean Resin. This was followed by electrophoresis, tryptic digestion and analysis of protein tryptic fragments by mass spectrometry (Figure 9-2).

A list was compiled of proteins that were significantly different between treatment groups, which were enriched for release from apoptotic cells relative to untreated cells (control), and which were reduced by both Y-27632 and Blebbistatin treatment. Using these criteria, we identified 231 proteins that were released from apoptotic bodies in an actomyosin-dependent manner. Of these, the top 20 most enriched proteins released in an actomyosin-dependant manner are listed here (Table 9-1). Nucleosomal histones (H1.2, H2A, H2B, H3 and H4) were the most highly enriched proteins in the apoptotic supernatant that were released in an actomyosin–dependant manner. Histones are characterized as potent DAMPs that activate cells of the innate immune system by binding to Toll-Like receptors (Huang et al., 2011, Allam et al., 2012). Gene ontology analysis revealed that most proteins were either structural/adapter proteins (61%) or enzymes (27%) (Figure 9-3 a). Upon comparison of fold enrichment in protein release with protein mass, it was apparent that the majority of the proteins were less than 100 kDa in size and of these, the smaller proteins were the most abundantly released (Figure 9-3 b). In addition to this, release of five extracellular matrix proteins were actually reduced in apoptotic cells (Fibronectin1, Sparc, Timp2, Thrombospondin2 and Decorin), which was at least partially restored by Y-27632 and Blebbistatin (Figure 9-3 c).

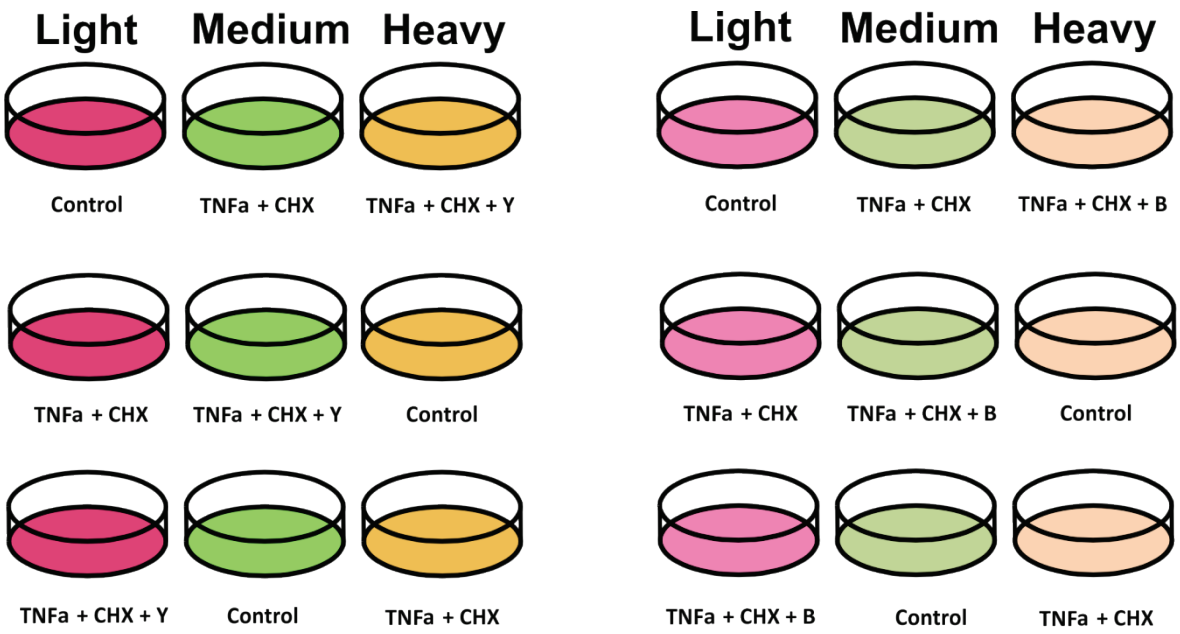

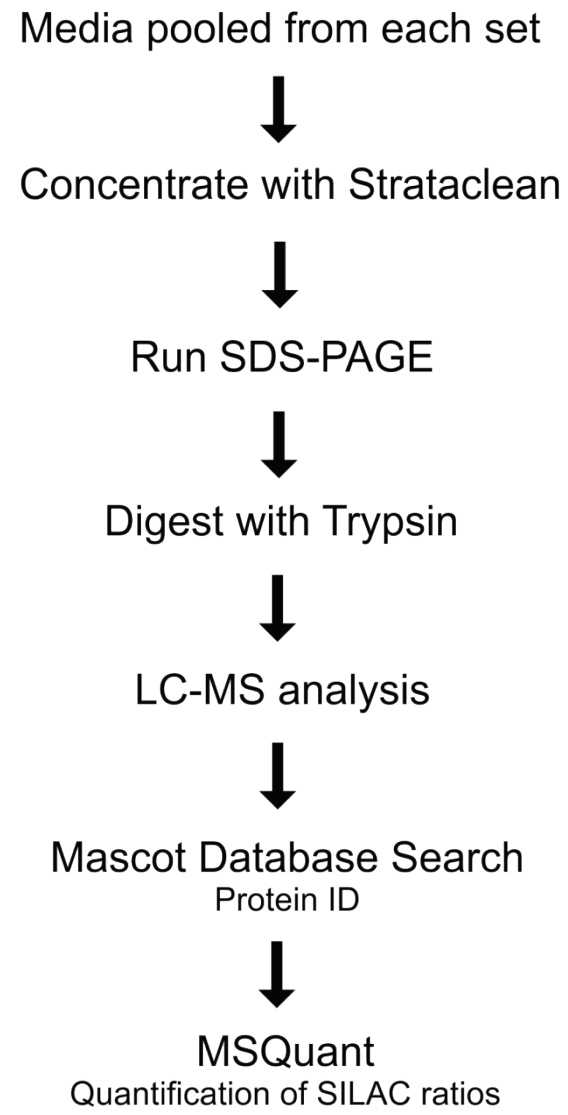

Figure 9-2 Experimental flow chart for quantitative SILAC mass spectrometry

Protein Identified	Gene Name	Permutation Test (p value)	Fold enrichment (± SEM) (apoptotic/ reference)	Reduction by Y-27632 (%)	Reduction by Blebbistatin (%)
Histone H4	Hist1h4a	-3.50E-11	11.57 ± 2.58	13.0	38.6
Histone H2B	Hist1h2bb	-2.10E-11	11.27 ± 2.43	2.4	43.2
Histone H3	H3f3a	-9.40E-06	11.17 ± 1.52	10.7	39.7
Histone H2A	Hist1h2af	-2.30E-07	10.67 ± 1.82	15.9	32.5
Histone H1.2	Hist1h1c	-2.30E-04	9.34 ± 3.01	31.1	37.9
Lamin-B1	Lmnb1	-6.50E-07	7.65 ± 0.93	22.4	35.5
Heterogeneous nuclear ribonucleoprotein K	Hnrnpk	-4.90E-04	6.57 ± 1.35	7.1	46.2
Lamin-A	Lmna	-5.00E-15	6.29 ± 0.93	22.6	32.7
Polypyrimidine tract-binding protein 1	Ptbp1	-1.30E-02	5.78 ± 1.11	13.5	52.4
Nuclear mitotic apparatus protein 1	Numa1	-1.80E-05	5.20 ± 1.25	37.8	22.4
Heterogeneous nuclear ribonucleoproteins C1/C2	Hnrnpc	-4.90E-02	4.08 ± 0.93	4.4	17.5
Nuclear ubiquitous casein and cyclin-dependent kinases substrate	Nucks1	-2.00E-02	3.98 ± 0.93	20.9	40.5
Heterogeneous nuclear ribonucleoprotein U	Hnrnpu	-3.80E-04	3.78 ± 0.62	1.0	22.5
Adenylate kinase 2	Ak2	-2.20E-05	3.68 ± 0.55	21.3	37.6
Coatomer subunit alpha	Copa	-1.70E-02	3.64 ± 0.82	10.3	16.2
Caldesomon	Cald1	-7.80E-07	3.58 ± 0.71	14.4	27.4
Gelsolin Isoform 2	Gsn	-4.20E-08	3.42 ± 0.59	26.8	17.1
Heat shock 70kDa protein 5	Hspa5	-2.40E-05	3.38 ± 0.75	22.2	3.4
Eukaryotic initiation factor 4A-III	Eif4a3	-2.30E-02	3.35 ± 0.39	1.5	27.4
S-methyl-5'-thioadenosine phosphorylase	Mtap	-1.00E-03	3.33 ± 0.35	8.0	25.0
Heat shock protein 90kDa beta member 1	Hsp90b1	-5.10E-04	3.31 ± 0.71	33.6	20.6

Table 9-1 Top 20 most enriched proteins released by apoptotic cells in an actomyosin-dependant manner

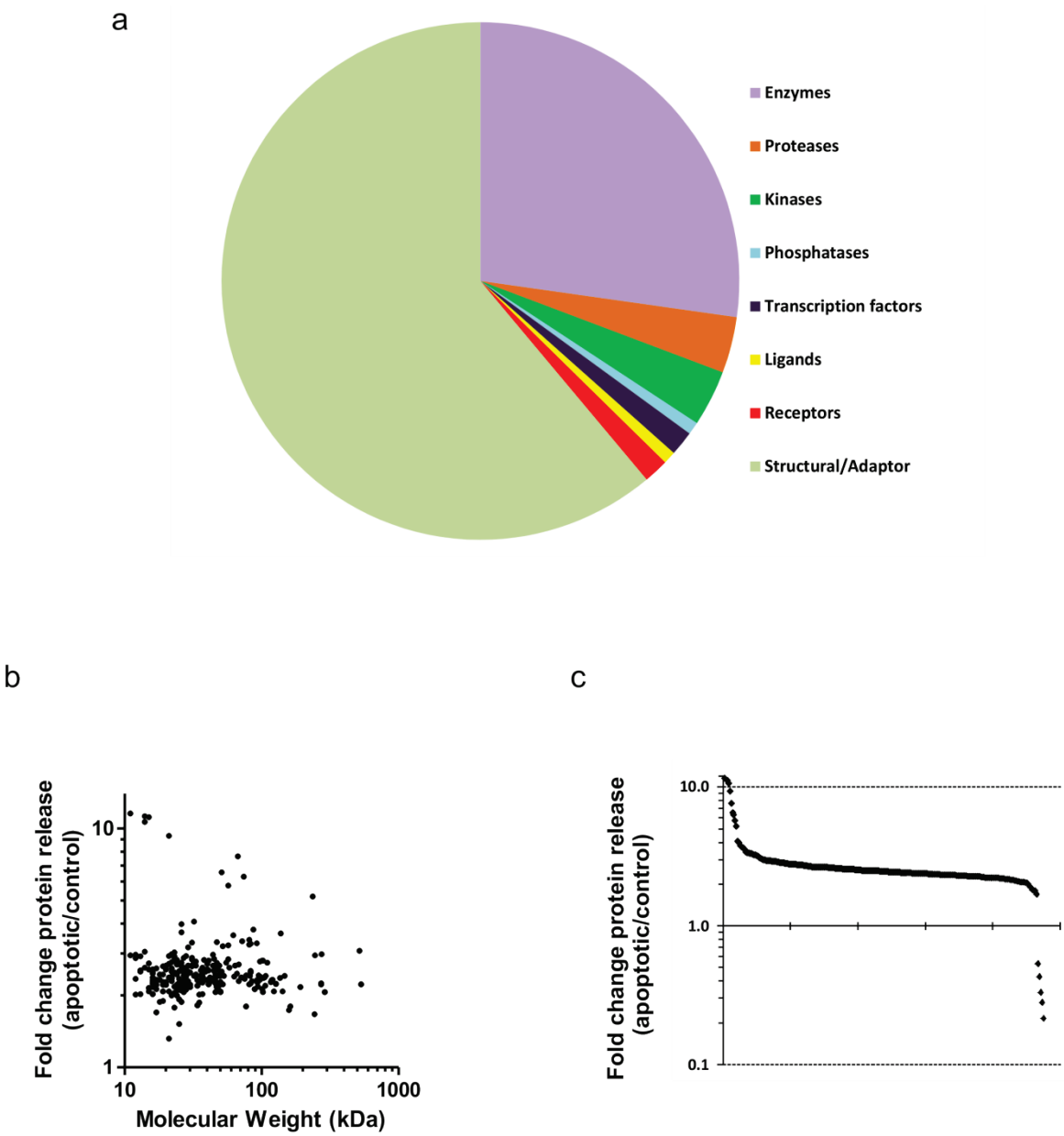

Figure 9-3 Analysis of proteins released from apoptotic cells
a) Classification of proteins released from apoptotic cells based on their function as determined by GeneGo gene ontology analysis. b) Log-plot of fold change in individual protein release (apoptotic/control) in conditioned media compared with the log-plot of molecular weights of proteins. c) Log-plot of fold change in individual protein release (apoptotic/control) in conditioned media. (Wickman et al., 2013).

9.2.3 Macrophage phagocytosis of proteins released from apoptotic cells

Mononuclear phagocytes and macrophages are integral components of the immune system as they have the capacity to ingest a variety of proteins that may influence the inflammatory response and contribute to antigen presentation (Underhill and Goodridge, 2012). We hypothesized that macrophages can take up proteins released by apoptotic cells. To identify potential protein targets that can be phagocytosed by macrophages, I collected conditioned medium from heavy (Lys8, Arg10) labelled NIH 3T3 fibroblasts that has been induced with apoptosis using UV (0.1 J/cm^2) for 4 hours. The conditioned media was then added to culture plates containing RAW 264.7 cells, which is a commonly used macrophage cell line, and incubated for 2 hours. Prior to incubation with apoptotic conditioned media, the macrophages were pre-treated with Bafilomycin A1 to block endosome acidification and subsequent proteolysis of ingested proteins. Macrophage cell lysates were prepared after washing the cells and for each protein a minimum of two SILAC-labelled tryptic peptides were unambiguously identified on the basis of their mass difference from endogenous peptides (Figure 9-4).

Heavy labelled proteins released from fibroblasts during apoptosis and phagocytosed by the macrophages were identified by mass spectrometry. Interestingly, four out of five nucleosomal histones (H2A, H2B, H3 and H4), which were the most highly enriched proteins in the apoptotic supernatant and released in an actomyosin-dependant manner, were identified as being phagocytosed by RAW 264.7 macrophage cells from conditioned medium (Table 9-2). In addition, Vimentin was also identified as being phagocytosed by RAW 264.7 cells (Table 9-2).

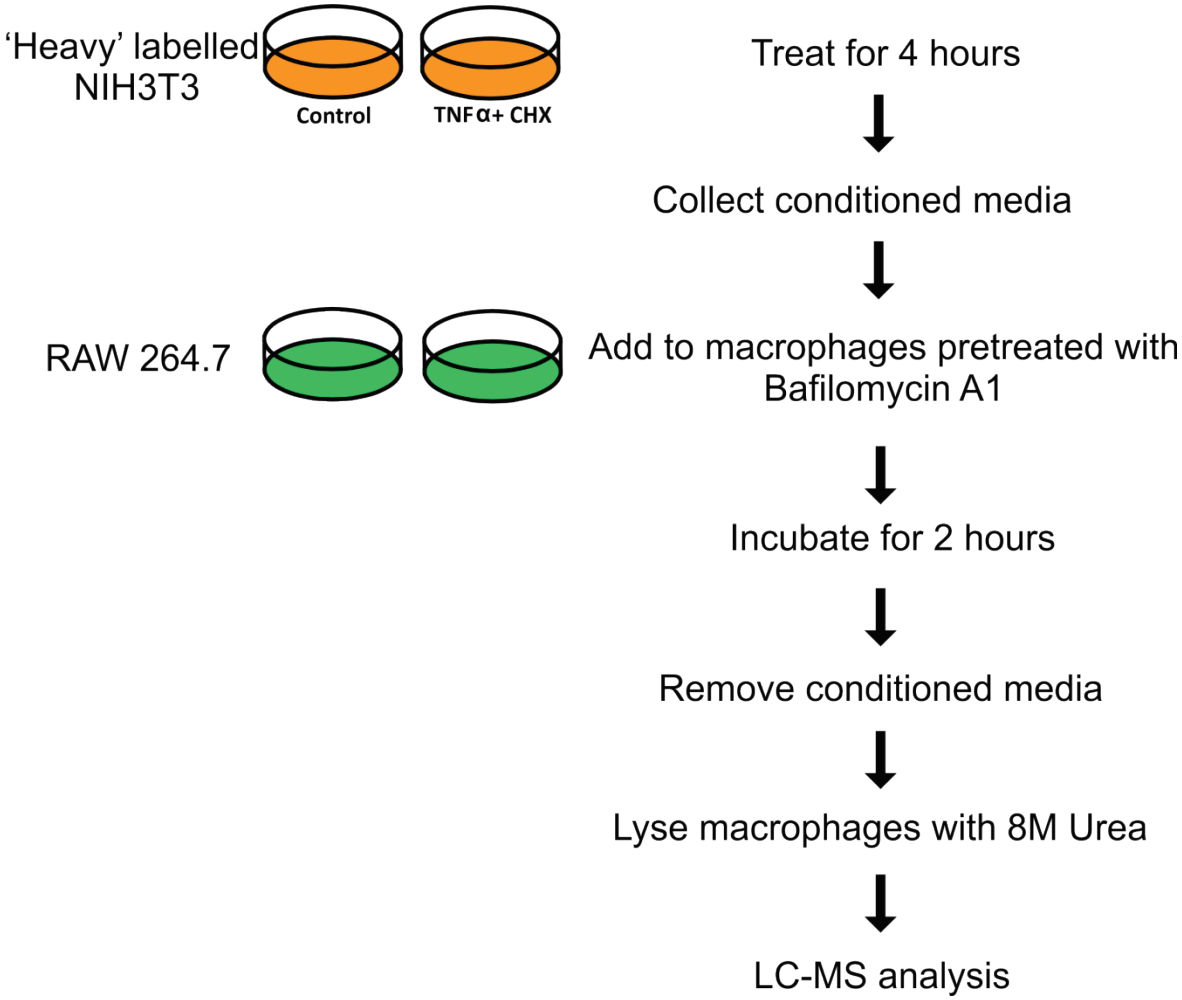

Figure 9-4 Experimental flowchart to study macrophage phagocytosis of proteins released by apoptotic cells using SILAC

Protein Identified	Gene Name	Molecular Weight (kDa)
Histone H2A	Hist1h2af	14
Histone H2B	Hist1h2bb	14
Histone H3	H3f3a	15
Histone H4	Hist1h4a	11
Vimentin	Vim	54

Table 9-2 'Heavy' labelled proteins from apoptotic cells that were phagocytosed by macrophages

9.2.4 Histones released by apoptotic blebs activate macrophages

Apart from playing an imperative role in phagocytosis, activated macrophages also produce a variety of cytokines, such as TNFα, IL-1, IL-6, IL-8, etc. which can contribute to the cytokine cascade. We hypothesized that histones released by apoptotic cells in an actomyosin-dependant manner and ingested by macrophages can cause macrophage activation. This was confirmed by measuring TNFα released by macrophages upon treatment with histones using an ELISA kit. Treatment of RAW 264.7 cells with varying amounts of purified recombinant histone proteins resulted in significant release of TNFα induced by H2A, H2B and H3, but not H4 (Figure 9-5 a). I also checked for release of IL-1ß and IL-6 from macrophages upon treatment with histones. 1L-ß levels released from macrophages were below the detection limit for all histones and IL-6 levels showed a slight increase (38 pg/ml) with histone H2B treatment alone (data not shown).

Toll-like receptors (TLRs) play a central role in macrophage activation and they signal through the NF-κB pathway (Kawai and Akira, 2007). In addition, as discussed earlier, histones activate immune cells by binding to TLRs. Consistent with this, treatment with 10 µg/ml of histone H2A dramatically increased NFKBIA (IkBa) phosphorylation (Figure 9-5 b), which was statistically significant (Figure 9-5 c). Together, these results show that proteins released from actomyosin-dependent blebs and apoptotic bodies engage with macrophages, revealing a mechanism of communication between early apoptotic cells and components of the innate immune system.

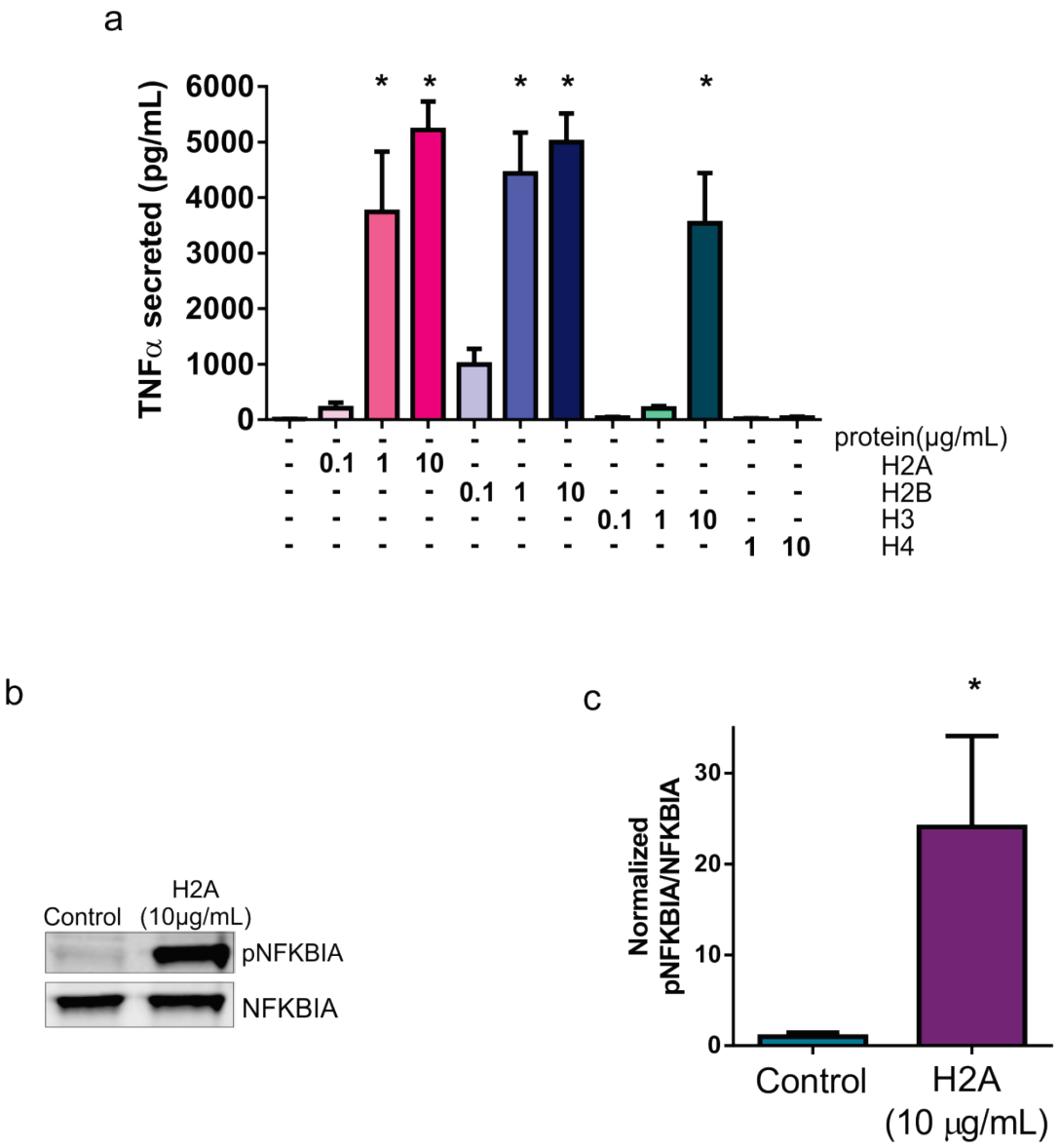

Figure 9-5 Histones released by apoptotic cells activate macrophages
a) Bar graph (Mean ± SEM) shows TNFα release from macrophages (RAW 264.7 cell line) with indicated histone treatments. Data analysed by ANOVA followed by Dunnett's multiple comparison test. b) Representative western blotting of phosphorylated and total NFKBIA from control and H2A treated macrophages. c) Bar graph (Mean ± SEM) showing relative phosphorylated NFKBIA (pNFKBIA) to total NFKBIA ratio, normalized to an average control value = 1. Data analysed by Student's t-test. (Wickman et al., 2013).

9.3 Discussion

Traditionally, apoptosis has been regarded as the 'silent' form of cell death because it does not trigger an inflammatory response. This defining feature of apoptotic cells is mainly attributed to its preservation of membrane integrity, which prevents the release of intracellular contents into the local environment. However, based on data from our lab, apoptotic body permeabilization can occur during early apoptosis, which would provide a route for the release of intracellular contents (Wickman et al., 2013). Indeed, induction of apoptosis using TNFα and CHX in fibroblasts resulted in acute protein release within 4 hours of induction. However, inhibition of membrane blebbing and apoptotic body formation using ROCK1 inhibitor Y-27632 or myosin ATPase inhibitor Blebbistatin resulted in a reduction in bulk protein release from apoptotic cells, suggesting that protein release is dependent on actomyosin contractility.

Systematic quantitative SILAC survey of conditioned media identified numerous proteins released during early apoptosis that were sensitive to inhibition of actomyosin contraction. The most highly enriched proteins were nucleosomal histones, which have been validated as potent DAMPs. Other DAMPs including S100 proteins and heat shock proteins released in an actomyosin dependant manner were also identified in the screen. Additionally, using SILAC approach, we observed that nucleosomal histones along with vimentin released by apoptotic cells are taken up by phagocytes like macrophages. Histones act on macrophages through TLRs to produce cytokines like TNFα which can contribute to a cytokine cascade that will alert the innate immune system. Together, these observations give strong indications regarding an active role for blebs and apoptotic bodies in allowing limited release of intracellular proteins that can engage with the immune system. Therefore, apart from breaking down apoptotic cells into bite-sized pieces for efficient phagocyte uptake, actomyosin contractility dependent blebbing and apoptotic body formation may have additional roles in promoting faster clearance by alerting the immune system of an impending danger prior to transition to secondary necrotic state.

10 Final Discussion and Future Directions

The field of cell death has witnessed an explosive development in the past few decades with the advent of genetic manipulation methods, electron microscopy as well as improved histochemical techniques. Although observations of cell death were recorded as early as the mid-nineteenth century, it was only in 1972 that John Kerr, Andrew Wyllie and Alastair. R. Currie highlighted the significance of cell death in the maintenance of tissue homeostasis in multicellular organisms. Together, they coined the term 'apoptosis' to define a controlled, programmed cell death mechanism and distinguish it from the uncontrolled cell death, necrosis (Kerr et al., 1972). In their seminal report, they described the distinct morphological features displayed by apoptotic cells including nuclear and cytoplasmic condensation and protrusions of plasma membrane to form blebs which eventually separated from the cell to form what they called 'apoptotic bodies'. The underlying signalling pathways that governed this mode of cellular demise transpired from numerous investigations of programmed cell death in nematode *Caenorhabditis elegans* (Horvitz, 1999).

Much effort has gone into elucidating different inducers of apoptosis and their downstream targets, in particular the caspases that were identified as central components of the apoptotic program. Beyond the cell intrinsic mechanisms associated with apoptosis, another integral part of the program is the efficient removal of apoptotic cells, termed as efferocytosis. For many years, the significance of efferocytosis and its biological purpose was underestimated However, the efficient cell clearance capacity seen in tissues with high cellular turnover, as well as evidence linking failed apoptotic cell clearance to pathological consequences, spurred a great deal of research that improved our understanding of this complex and evolutionarily conserved process. To date, a plethora of apoptotic cell derived ligands, phagocytic receptors and ligand-receptor bridging molecules involved in apoptotic corpse removal have been identified, which hints at an apparent redundancy in clearance mechanisms. Yet, the importance of apoptotic morphological features and how they might assist efferocytosis to expedite the removal of cellular corpses has only been deliberated, predominantly by means of *in vitro* studies. Hence, an *in vivo* genetic model system was long overdue.

10.1 ROCK1nc Mouse Model

Our lab had previously showed that during apoptosis, caspase cleavage and consequent activation of ROCK1 drives the actomyosin contractile force generation that is responsible for the observed morphological features (Coleman et al., 2001) and for nuclear disintegration (Croft et al., 2005). Identification of the caspase cleavage site of ROCK1 enabled the generation of a mouse model that expressed a non-cleavable form of ROCK1 (ROCK1nc) by mutating the cleavage site (D1113A). This is the first genetic model system that would help to define the biological significance of the dramatic morphological changes that occur during apoptosis *in vivo*. Given the importance of cell death and efficient removal of cellular debris in multicellular organisms, I sought to understand whether ROCK1-dependant apoptotic morphological features played a role in tissue homeostasis and tumour development.

Apoptotic cells from ROCK1nc mice showed distinct morphological defects which validated our genetic model and confirmed the role of caspase cleavage of ROCK1 in mediating membrane blebbing and cell contraction. Membrane blebbing and apoptotic body formation has mainly been studied in cell culture environment, leading many to speculate whether these features are an *in vitro* artefact. Our studies using GFP-expressing melanoblasts on *ex vivo* embryonic skin explants have established that membrane blebbing is a *bona fide* biological phenomenon in living tissue. In addition, we confirmed that knock in mutation in ROCK1 inhibited the typical morphological features seen during apoptosis. Defects in apoptotic cell clearance mechanisms have been linked to the development of several pathologies including autoimmunity. How these apoptotic morphological responses cooperate with the different steps of efferocytosis has never been delved into. Using SILAC-based approach on NIH 3T3 cells, we showed that apoptotic cells release damage associated molecular patterns like histones, and this was influenced by actomyosin contractility that drives membrane blebbing and apoptotic body formation. These ‘suicide notes’ dispatched by apoptotic cells prior to secondary necrosis are taken up by macrophages, which may influence their response to dying cells. We also showed that actomyosin contractility contributed to the translocation of histones into blebs and apoptotic bodies (Wickman et al., 2013). Hence, limited membrane permeability during early apoptosis may help in alerting the immune system

before secondary necrosis can occur. For these studies, we utilized the ROCK inhibitor Y-27632 and the myosin ATPase inhibitor Blebbistatin to inhibit the classical apoptotic morphological features. Considering the off-target effects of inhibitors, cells from ROCK1nc mice would be an impressive option in addressing the role of these dramatic morphological responses in the release of potential 'suicide notes' for alerting the neighbouring cells as well as the immune system. Since complete incorporation of labelled amino acids for SILAC experiments is usually achieved only by 5 or 6 passages, this might prove to be challenging for primary cells like MEFs which start senescing in 3 to 4 passages. A way forward would be to SILAC-label immortalized MEFs from these mice or use a label-free proteomics approach for primary MEFs.

Given the evidence of obvious morphological defects during apoptosis in ROCK1nc model, we also questioned whether this might lead to an autoimmune phenotype. Surprisingly, mice were born in expected Mendelian ratios, were viable and fertile, and did not display any overt autoimmune phenotype, suggesting that these morphological defects did not have significant implications at basal level, even in tissues with high cellular turnover. Histologically, ROCK1nc mice did not reveal an autoimmune phenotype even though the kidney showed minor indications of the same. A number of 'eat me' signals have been found to adorn the surface of apoptotic cells that not only set them apart from health viable cells in the vicinity but also aids in establishing a physical contact between the phagocyte and the apoptotic cell. A role for apoptotic blebs to serve as focal points for the aggregation of 'eat me' signals was anticipated. Nonetheless, we did not observe a difference in externalization of phosphatidylserine, a key 'eat me' signal, in ROCK1nc MEFs. This might partly explain the apparent lack of a pathological phenotype in ROCK1nc mice.

On the other hand, focal concentration of C1q, a complement protein that binds to apoptotic cells and expedites phagocytic engulfment by engaging with their C1q receptors (Korb and Ahearn, 1997, Navratil et al., 2001), was compromised in ROCK1nc MEFs due to the obvious lack of discernible membrane blebs. Although C1q-deficient mice developed glomerulonephritis and displayed increased mortality due to impaired clearance of apoptotic cells (Botto et al., 1998), we did not observe the same in our model. This could be because, in an *in vivo* setting, the lack of membrane blebs may not be a limiting factor for C1q

to bind to apoptotic cells. Moreover, the phenotype associated with C1q deficiency was not observed on a different genetic background (Botto et al., 1998), thus suggesting a role for genetic modifiers in the development of autoimmunity.

Genetic predisposition is an important contributor to susceptibility to autoimmune diseases. Several strains of mice spontaneously develop an autoimmune phenotype including NZB/WF1, MRL/Mp-*lpr*/*lpr* and BXSB.Yaa^{B6} (Theofilopoulos and Dixon, 1985). The ROCK1nc mouse model can be backcrossed to any of these strains to check for the contribution of apoptotic morphological defects in the development of autoimmunity. Hybrid strains between 129 and C57Bl/6 are commonly used in the generation of gene-targeted mice. Studies showed that F2 generation of 129 and C57Bl/6 cross demonstrates the expression of a powerful autoimmune phenotype (Bygrave et al., 2004). To test whether ROCK1nc mutation would exacerbate the autoimmune phenotype in this strain which is spontaneously predisposed, we backcrossed the mice to a 129 background for eight generations and then crossed with C57Bl/6 mice. The F2 generation is currently underway and will be analysed for the development of autoimmunity.

10.2 Apoptotic Morphological Responses Maintain Homeostasis in Liver

An intricate balance between two competing processes; cell proliferation versus cell death, regulates tissue homeostasis in multicellular organisms. Maintenance of homeostasis relies heavily on the rapid clearance of apoptotic debris before they cause havoc by undergoing secondary necrosis. While apoptotic morphological responses do not appear to be critical at basal level, this may not be the case when challenged with a strong apoptotic stimulus. Tissues are often exposed to several stresses which can result in cell death. In such cases, the number of cells dying at a given time increases and hence the need for highly efficient clearance mechanisms becomes of paramount importance. Whether these morphological features contribute to efferocytosis in physiologically relevant *in vivo* contexts was definitely intriguing, and the ROCK1nc model was ideal to address this question.

Owing to its central role in detoxifying drugs and other harmful substances in the blood, the liver is quite vulnerable to cell death, thus making it an excellent system to study responses to defective apoptotic morphological features. To induce damage, I used the liver-selective genotoxic carcinogen, diethylnitrosamine (DEN) that forms DNA adducts by ethylation (Williams et al., 1996). Liver function tests combined with histological analysis provided clear indications of higher degrees of hepatocellular damage in ROCK1nc mice. Evidence of increased accumulation of apoptotic debris in ROCK1nc livers suggested the possibility of these corpses releasing toxic intracellular contents thereby causing tissue damage. Furthermore, the increased assembly of immune cells including neutrophils in ROCK1nc livers, possibly in response to the accumulating debris, may also have contributed in aggravating hepatocellular damage by releasing reactive oxygen intermediates and serine proteases (Jaeschke and Hasegawa, 2006).

Increased recruitment of immune cells like neutrophils to sites of damage may be influenced by DAMPs like HMGB1 released by accumulating apoptotic debris in ROCK1nc livers. Increased cytoplasmic translocation of HMGB1 in ROCK1nc hepatocytes gave strong indication of an impending extracellular release (Zhou et al., 2011). This however has to be confirmed in the sera of mice treated with DEN and we are currently collaborating with Professor Marco Bianchi, a leading scientist in the HMGB1 field at San Raffaele University, Italy, to achieve this. A recent study showed that hepatocyte-specific deletion of HMGB1 reduced neutrophil recruitment to the liver in response to acetaminophen overdose or ischemia/reperfusion injury (Huebener et al., 2015). Consistent with this finding, inhibiting the cytokine activity of HMGB1 with Glycyrrhizin reduced neutrophil infiltration to the liver as well as DEN-induced hepatocellular damage in ROCK1nc mice. Together, these results showed that defective apoptotic morphological responses may result in the inadvertent release of HMGB1 which may have contributed to the pathological response via neutrophil mediated amplification of liver injury. Certainly, the link between neutrophil infiltration and amplification of hepatocellular damage is purely hypothetical at this juncture and needs experimental validation. By introducing the ROCK1nc mutation into *Elane*$^{-/-}$ mice deficient for neutrophil elastase that is essential for

neutrophil effector functions (Belaaouaj et al., 1998), it would be possible to confirm the contribution of neutrophils to liver damage.

Glycyrrhizin, the HMGB1 inhibitor used for my studies, is a natural triterpene found in the roots and rhizomes of licorice (*Glycyrrhiza glabra*) that can bind directly to HMGB1 and inhibit its chemoattractant and mitogenic activities (Mollica et al., 2007). The effects of HMGB1 in ROCK1nc model can be further confirmed by using another functional inhibitor BoxA, which is a truncated form of the protein that acts as a competitive antagonist by inhibiting HMGB1 binding to its receptor RAGE (Kokkola et al., 2003) and also by using anti-HMGB1 antibodies. Once secreted, HMGB1 induces inflammatory responses by binding to TLRs and RAGE receptors on immune cells. By combining DEN treatment with TLR4 inhibitor (CLI-095) and/or neutralizing RAGE antibody, it would be possible to delineate the exact mechanism of action of HMGB1 in mediating liver injury during defective apoptotic blebbing.

The effect of defective apoptotic morphological responses in increasing liver damage can be extended to other models of liver injury, especially those which are physiologically relevant such as acetaminophen-induced injury and ischemia/reperfusion injury. Moreover, the consequence of defective ROCK1 cleavage on liver regeneration and fibrosis was not addressed in this study mostly due to the toxic dose of DEN used that made it difficult to maintain the mice for longer periods to study liver regeneration. Moreover, treatment with DEN is not commonly associated with fibrosis (Verna et al., 1996, Zhang et al., 2010). A suitable model would be carbon tetrachloride-induced liver damage that is associated with a very strong fibrotic response (Liedtke et al., 2013). The successful portrayal of the role of apoptotic morphological features in liver homeostasis provides enough confidence in further extending these studies to determine whether the observed phenotype echoes in models of acute apoptosis in other tissues as well. It is highly likely that the consequence of defective apoptotic morphological features may be different in other tissues, probably depending on the presence or absence of tissue-resident professional phagocytes.

10.3 Effect of Apoptotic Morphological Responses on Tumour Development

Having established that ROCK1 cleavage dependent morphological features during apoptosis maintained tissue homeostasis by influencing the immunological microenvironment, I then went on to explore the role of these features in tumour development. Decades of research on the immune system has revealed that the link between inflammation and cancer is complex. While there is considerable evidence pointing towards a causal link between inflammation and cancer, a protective effect of inflammation against tumour development is also appreciated. Considering the fact that defective apoptotic morphologic features modulated the inflammatory microenvironment in tissues, it was intriguing to figure out whether the balance would be tipped to favour tumour development or curb it.

To address this, the ROCK1nc mutation was introduced into two different cancer models, namely hepatocellular carcinoma (HCC) and Eμ-myc lymphoma. In DEN-induced HCC model, ROCK1nc mutation reduced tumour numbers. Similarly, in Eμ-myc lymphoma model, mice with the ROCK1nc mutation survived longer. These data clearly suggested that impairment of ROCK1-mediated apoptotic morphologies had a protective effect against tumour development. It was hypothesized that the reduced tumour growth seen in ROCK1nc mice was associated with immune responses to defective apoptotic morphologies and consequent debris accumulation. Indeed, ROCK1nc liver tumours harboured significantly more tumour suppressive CD8+ T cells. It is possible that defective apoptotic morphological responses in ROCK1nc mice stimulated cancer immunosurveillance wherein immune cells destroyed cancer cells and thus limited tumour formation. This was supported by reduced tumour numbers in preneoplastic ROCK1nc livers. The immune sentinels triggered by defective apoptotic features were successful in curbing tumour development even 9 months after DEN treatment. However, some tumour cells were successful in surviving the ‘elimination’ and ‘equilibrium’ phases and entered the ‘escape’ phase, where their growth was no longer blocked by the immune system. This was evidenced by the presence of large tumours in ROCK1nc mice that was comparable to DEN-induced tumours in wild-type mice, despite the significant reduction in tumour numbers in ROCK1nc mice.

This raises many questions as to what exactly triggered increased infiltration of these cytotoxic T lymphocytes into ROCK1nc liver tumours. Although immunohistochemical analysis did not reveal a difference in HMGB1 staining in ROCK1nc liver tumours when compared to wild-type, this is not conclusive and has to be confirmed in sera of preneoplastic mice. Provided there is substantial evidence supporting the role of HMGB1 in suppressing tumour growth in liver, it would be interesting to study whether introducing ROCK1nc mutation in mice with hepatocyte specific deletion of HMGB1(Huebener et al., 2014, Huebener et al., 2015) will impede the tumour suppressive property of defective apoptotic morphologies. Apart from HMGB1, there are several other DAMPs that could be involved in recruiting tumour-suppressive immune cells, which needs to be investigated as well.

Since the early 1900s, prospective ways to harness the inherent protective features of the immune system to curb tumour growth have been extensively researched. Currently, several immunotherapy strategies have made their way into phase III clinical trials. This includes the administration of synthetic cytokines that can boost immune response in patients, monoclonal antibodies that can specifically target and kill tumour cells, and vaccines that are made from cancer cells (Elert, 2013). Given the finding that defective ROCK1 activation due to non-cleavage by caspases during apoptosis had a tumour suppressive effect and increased infiltration of CD8+ T cells, future strategy would be to use ROCK inhibitors in DEN-induced HCC, and see if they induce a similar tumour suppressive effect by modulating the immune response. If successful, this might prove to be an attractive treatment option that can be used in combination with standard chemotherapy.

10.4 Conclusion

Despite impressive advances to date in the field of cell death and efferocytosis, much remains to be learned about the apoptotic morphological features and their biological significance. Here, I presented data on a novel genetic mouse model that would go a long way in defining the role of membrane blebbing, cell contraction and apoptotic body formation when cells die. Using this model I showed that apoptotic morphologies are crucial for the maintenance of tissue homeostasis during acute damage but enables tumourigenesis in the long run.

References

ABDELWAHID, E., PELLINIEMI, L. J. & JOKINEN, E. 2002. Cell death and differentiation in the development of the endocardial cushion of the embryonic heart. *Microsc Res Tech,* 58**,** 395-403.

ABE, K., IKEDA, T., WAKE, K., SATO, T. & INOUE, H. 2008. Glycyrrhizin prevents of lipopolysaccharide/D-galactosamine-induced liver injury through down-regulation of matrix metalloproteinase-9 in mice. *J Pharm Pharmacol,* 60**,** 91-7.

ADAMS, J. M., HARRIS, A. W., PINKERT, C. A., CORCORAN, L. M., ALEXANDER, W. S., CORY, S., PALMITER, R. D. & BRINSTER, R. L. 1985. The c-myc oncogene driven by immunoglobulin enhancers induces lymphoid malignancy in transgenic mice. *Nature,* 318**,** 533-8.

ADAMS, P. D., SELLERS, W. R., SHARMA, S. K., WU, A. D., NALIN, C. M. & KAELIN, W. G., JR. 1996. Identification of a cyclin-cdk2 recognition motif present in substrates and p21-like cyclin-dependent kinase inhibitors. *Mol Cell Biol,* 16**,** 6623-33.

ALLAM, R., SCHERBAUM, C. R., DARISIPUDI, M. N., MULAY, S. R., HAGELE, H., LICHTNEKERT, J., HAGEMANN, J. H., RUPANAGUDI, K. V., RYU, M., SCHWARZENBERGER, C., HOHENSTEIN, B., HUGO, C., UHL, B., REICHEL, C. A., KROMBACH, F., MONESTIER, M., LIAPIS, H., MORETH, K., SCHAEFER, L. & ANDERS, H. J. 2012. Histones from dying renal cells aggravate kidney injury via TLR2 and TLR4. *J Am Soc Nephrol,* 23**,** 1375-88.

ALNEMRI, E. S., LIVINGSTON, D. J., NICHOLSON, D. W., SALVESEN, G., THORNBERRY, N. A., WONG, W. W. & YUAN, J. 1996. Human ICE/CED-3 protease nomenclature. *Cell,* 87**,** 171.

AMANO, M., CHIHARA, K., KIMURA, K., FUKATA, Y., NAKAMURA, N., MATSUURA, Y. & KAIBUCHI, K. 1997. Formation of actin stress fibers and focal adhesions enhanced by Rho- kinase. *Science,* 275**,** 1308-11.

AMANO, M., CHIHARA, K., NAKAMURA, N., KANEKO, T., MATSUURA, Y. & KAIBUCHI, K. 1999. The COOH terminus of Rho-kinase negatively regulates rho-kinase activity. *J Biol Chem,* 274**,** 32418-24.

AMANO, M., ITO, M., KIMURA, K., FUKATA, Y., CHIHARA, K., NAKANO, T., MATSUURA, Y. & KAIBUCHI, K. 1996. Phosphorylation and activation of myosin by Rho-associated kinase (Rho- kinase). *J Biol Chem,* 271**,** 20246-9.

ANDERSON, H. A., MAYLOCK, C. A., WILLIAMS, J. A., PAWELETZ, C. P., SHU, H. & SHACTER, E. 2003. Serum-derived protein S binds to phosphatidylserine and stimulates the phagocytosis of apoptotic cells. *Nat Immunol,* 4**,** 87-91.

ANDO, K., FUKUHARA, S., MORIYA, T., OBARA, Y., NAKAHATA, N. & MOCHIZUKI, N. 2013. Rap1 potentiates endothelial cell junctions by spatially controlling myosin II activity and actin organization. *J Cell Biol,* 202**,** 901-16.

ARAI, M., SASAKI, Y. & NOZAWA, R. 1993. Inhibition by the protein kinase inhibitor HA1077 of the activation of NADPH oxidase in human neutrophils. *Biochem Pharmacol,* 46**,** 1487-1490.

ARASE, Y., IKEDA, K., MURASHIMA, N., CHAYAMA, K., TSUBOTA, A., KOIDA, I., SUZUKI, Y., SAITOH, S., KOBAYASHI, M. & KUMADA, H. 1997. The long term efficacy of glycyrrhizin in chronic hepatitis C patients. *Cancer,* 79**,** 1494-500.

ARBER, S., BARBAYANNIS, F. A., HANSER, H., SCHNEIDER, C., STANYON, C. A., BERNARD, O. & CARONI, P. 1998. Regulation of actin dynamics through phosphorylation of cofilin by LIM- kinase. *Nature,* 393**,** 805-9.

ARMSTRONG, J. F., KAUFMAN, M. H., HARRISON, D. J. & CLARKE, A. R. 1995. High-frequency developmental abnormalities in p53-deficient mice. *Curr Biol,* 5**,** 931-6.

ARUR, S., UCHE, U. E., REZAUL, K., FONG, M., SCRANTON, V., COWAN, A. E., MOHLER, W. & HAN, D. K. 2003. Annexin I is an endogenous ligand that mediates apoptotic cell engulfment. *Dev Cell,* 4**,** 587-98.

ASANO, T., IKEGAKI, I., SATOH, S., SUZUKI, Y., SHIBUYA, M., TAKAYASU, M. & HIDAKA, H. 1987. Mechanism of action of a novel antivasospasm drug, HA1077. *J Pharmacol Exp Ther,* 241**,** 1033-1040.

ASL, M. N. & HOSSEINZADEH, H. 2008. Review of pharmacological effects of Glycyrrhiza sp. and its bioactive compounds. *Phytother Res,* 22**,** 709-24.

ATTARDI, L. D. & JACKS, T. 1999. The role of p53 in tumour suppression: lessons from mouse models. *Cell Mol Life Sci,* 55**,** 48-63.

AU, J. S., NAVARRO, V. J. & ROSSI, S. 2011. Review article: Drug-induced liver injury--its pathophysiology and evolving diagnostic tools. *Aliment Pharmacol Ther,* 34**,** 11-20.

BAECK, C., WEI, X., BARTNECK, M., FECH, V., HEYMANN, F., GASSLER, N., HITTATIYA, K., EULBERG, D., LUEDDE, T., TRAUTWEIN, C. & TACKE, F. 2014. Pharmacological inhibition of the chemokine C-C motif chemokine ligand 2 (monocyte chemoattractant protein 1) accelerates liver fibrosis regression by suppressing Ly-6C(+) macrophage infiltration in mice. *Hepatology,* 59**,** 1060-72.

BAIN, J., PLATER, L., ELLIOTT, M., SHPIRO, N., HASTIE, C. J., MCLAUCHLAN, H., KLEVERNIC, I., ARTHUR, J. S., ALESSI, D. R. & COHEN, P. 2007. The selectivity of protein kinase inhibitors: a further update. *Biochem J,* 408**,** 297-315.

BALD, T., QUAST, T., LANDSBERG, J., ROGAVA, M., GLODDE, N., LOPEZ-RAMOS, D., KOHLMEYER, J., RIESENBERG, S., VAN DEN BOORN-KONIJNENBERG, D., HOMIG-HOLZEL, C., REUTEN, R., SCHADOW, B., WEIGHARDT, H., WENZEL, D., HELFRICH, I., SCHADENDORF, D., BLOCH, W., BIANCHI, M. E., LUGASSY, C., BARNHILL, R. L., KOCH, M., FLEISCHMANN, B. K., FORSTER, I., KASTENMULLER, W., KOLANUS, W., HOLZEL, M., GAFFAL, E. & TUTING, T. 2014. Ultraviolet-radiation-induced inflammation promotes angiotropism and metastasis in melanoma. *Nature,* 507**,** 109-13.

BALKWILL, F. & MANTOVANI, A. 2001. Inflammation and cancer: back to Virchow? *Lancet,* 357**,** 539-45.

BARASHI, N., WEISS, I. D., WALD, O., WALD, H., BEIDER, K., ABRAHAM, M., KLEIN, S., GOLDENBERG, D., AXELROD, J., PIKARSKY, E., ABRAMOVITCH, R., ZEIRA, E., GALUN, E. & PELED, A. 2013. Inflammation-induced hepatocellular carcinoma is dependent on CCR5 in mice. *Hepatology,* 58**,** 1021-30.

BAUMANN, I., KOLOWOS, W., VOLL, R. E., MANGER, B., GAIPL, U., NEUHUBER, W. L., KIRCHNER, T., KALDEN, J. R. & HERRMANN, M. 2002. Impaired uptake of apoptotic cells into tingible body macrophages in germinal centers of patients with systemic lupus erythematosus. *Arthritis Rheum,* 46**,** 191-201.

BELAAOUAJ, A., MCCARTHY, R., BAUMANN, M., GAO, Z., LEY, T. J., ABRAHAM, S. N. & SHAPIRO, S. D. 1998. Mice lacking neutrophil elastase reveal impaired host defense against gram negative bacterial sepsis. *Nat Med,* 4**,** 615-8.

BELL, C. W., JIANG, W., REICH, C. F. & PISETSKY, D. S. 2006. The extracellular release of HMGB1 during apoptotic cell death. *American journal of physiology. Cell physiology,* 291**,** C1318-25.

BENNETT, G. D. & KAY, M. M. 1981. Homeostatic removal of senescent murine erythrocytes by splenic macrophages. *Experimental hematology,* 9**,** 297-307.

BEVERS, E. M. & WILLIAMSON, P. L. 2010. Phospholipid scramblase: an update. *FEBS Lett,* 584**,** 2724-30.

BIANCHI, M. E. 2007. DAMPs, PAMPs and alarmins: all we need to know about danger. *J Leukoc Biol,* 81**,** 1-5.

BIANCHI, M. E. & AGRESTI, A. 2005. HMG proteins: dynamic players in gene regulation and differentiation. *Curr Opin Genet Dev,* 15**,** 496-506.

BIANCHI, M. E., BELTRAME, M. & PAONESSA, G. 1989. Specific recognition of cruciform DNA by nuclear protein HMG1. *Science,* 243**,** 1056-9.

BLUME, K. E., SOEROES, S., WAIBEL, M., KEPPELER, H., WESSELBORG, S., HERRMANN, M., SCHULZE-OSTHOFF, K. & LAUBER, K. 2009. Cell surface externalization of annexin A1 as a failsafe mechanism preventing inflammatory responses during secondary necrosis. *Journal of immunology (Baltimore, Md. : 1950),* 183**,** 8138-47.

BLUMENSTEIN, L. & AHMADIAN, M. R. 2004. Models of the cooperative mechanism for Rho effector recognition: implications for RhoA-mediated effector activation. *J Biol Chem,* 279**,** 53419-26.

BODDAERT, J., KINUGAWA, K., LAMBERT, J. C., BOUKHTOUCHE, F., ZOLL, J., MERVAL, R., BLANC-BRUDE, O., MANN, D., BERR, C., VILAR, J., GARABEDIAN, B., JOURNIAC, N., CHARUE, D., SILVESTRE, J. S., DUYCKAERTS, C., AMOUYEL, P., MARIANI, J., TEDGUI, A. & MALLAT, Z. 2007. Evidence of a role for lactadherin in Alzheimer's disease. *Am J Pathol,* 170**,** 921-9.

BOERMA, M., FU, Q., WANG, J., LOOSE, D. S., BARTOLOZZI, A., ELLIS, J. L., MCGONIGLE, S., PARADISE, E., SWEETNAM, P., FINK, L. M., VOZENIN-BROTONS, M. C. & HAUER-JENSEN, M. 2008. Comparative gene expression profiling in three primary human cell lines after treatment with a novel inhibitor of Rho kinase or atorvastatin. *Blood Coagul Fibrinolysis,* 19**,** 709-18.

BOISVERT, W. A., ROSE, D. M., BOULLIER, A., QUEHENBERGER, O., SYDLASKE, A., JOHNSON, K. A., CURTISS, L. K. & TERKELTAUB, R. 2006. Leukocyte transglutaminase 2 expression limits atherosclerotic lesion size. *Arterioscler Thromb Vasc Biol,* 26**,** 563-9.

BONDANZA, A., ZIMMERMANN, V. S., ROVERE-QUERINI, P., TURNAY, J., DUMITRIU, I. E., STACH, C. M., VOLL, R. E., GAIPL, U. S., BERTLING, W., POSCHL, E., KALDEN, J. R., MANFREDI, A. A. & HERRMANN, M. 2004. Inhibition of phosphatidylserine recognition heightens the immunogenicity of irradiated lymphoma cells in vivo. *J Exp Med,* 200**,** 1157-65.

BOON, T. & VAN DER BRUGGEN, P. 1996. Human tumor antigens recognized by T lymphocytes. *J Exp Med,* 183**,** 725-9.

BORISENKO, G. G., MATSURA, T., LIU, S. X., TYURIN, V. A., JIANFEI, J., SERINKAN, F. B. & KAGAN, V. E. 2003. Macrophage recognition of externalized phosphatidylserine and phagocytosis of apoptotic Jurkat cells--existence of a threshold. *Arch Biochem Biophys,* 413**,** 41-52.

BOTTO, M., DELL'AGNOLA, C., BYGRAVE, A. E., THOMPSON, E. M., COOK, H. T., PETRY, F., LOOS, M., PANDOLFI, P. P., WALPORT, M. J., DELL' AGNOLA, C., MARINA BOTTO ANNE E. BYGRAVE, E. M. T. H. T. C. F. P. M. L. P. P. P., MARK J. WALPORT, C. D. A. & MARINA BOTTO ANNE E. BYGRAVE, E. M.

T. H. T. C. F. P. M. L. P. P. P. M. J. W. C. D. A. 1998. Homozygous C1q deficiency causes glomerulonephritis associated with multiple apoptotic bodies. *Nature Genetics,* 19**,** 56-59.

BOURNAZOU, I., MACKENZIE, K. J., DUFFIN, R., ROSSI, A. G. & GREGORY, C. D. 2010. Inhibition of eosinophil migration by lactoferrin. *Immunol Cell Biol,* 88**,** 220-3.

BOURNAZOU, I., POUND, J. D., DUFFIN, R., BOURNAZOS, S., MELVILLE, L. A., BROWN, S. B., ROSSI, A. G. & GREGORY, C. D. 2009. Apoptotic human cells inhibit migration of granulocytes via release of lactoferrin. *J Clin Invest,* 119**,** 20-32.

BRANCOLINI, C., LAZAREVIC, D., RODRIGUEZ, J. & SCHNEIDER, C. 1997. Dismantling cell-cell contacts during apoptosis is coupled to a caspase-dependent proteolytic cleavage of beta-catenin. *J Cell Biol,* 139**,** 759-71.

BUCHMANN, A., BAUER-HOFMANN, R., MAHR, J., DRINKWATER, N. R., LUZ, A. & SCHWARZ, M. 1991. Mutational activation of the c-Ha-ras gene in liver tumors of different rodent strains: correlation with susceptibility to hepatocarcinogenesis. *Proc Natl Acad Sci U S A,* 88**,** 911-5.

BURNET, M. 1957. Cancer; a biological approach. I. The processes of control. *Br Med J,* 1**,** 779-86.

BURSCH, W., CHABICOVSKY, M., WASTL, U., GRASL-KRAUPP, B., BUKOWSKA, K., TAPER, H. & SCHULTE-HERMANN, R. 2005. Apoptosis in stages of mouse hepatocarcinogenesis: failure to counterbalance cell proliferation and to account for strain differences in tumor susceptibility. *Toxicol Sci,* 85**,** 515-29.

BUTCHER, E. C. 1991. Leukocyte-endothelial cell recognition: three (or more) steps to specificity and diversity. *Cell,* 67**,** 1033-6.

BYGRAVE, A. E., ROSE, K. L., CORTES-HERNANDEZ, J., WARREN, J., RIGBY, R. J., COOK, H. T., WALPORT, M. J., VYSE, T. J. & BOTTO, M. 2004. Spontaneous autoimmunity in 129 and C57BL/6 mice-implications for autoimmunity described in gene-targeted mice. *PLoS Biol,* 2**,** E243.

CALOGERO, S., GRASSI, F., AGUZZI, A., VOIGTLANDER, T., FERRIER, P., FERRARI, S. & BIANCHI, M. E. 1999. The lack of chromosomal protein Hmg1 does not disrupt cell growth but causes lethal hypoglycaemia in newborn mice. *Nat Genet,* 22**,** 276-80.

CALVISI, D. F., LADU, S., GORDEN, A., FARINA, M., CONNER, E. A., LEE, J. S., FACTOR, V. M. & THORGEIRSSON, S. S. 2006. Ubiquitous activation of Ras and Jak/Stat pathways in human HCC. *Gastroenterology,* 130**,** 1117-28.

CARDONA, A. E., PIORO, E. P., SASSE, M. E., KOSTENKO, V., CARDONA, S. M., DIJKSTRA, I. M., HUANG, D., KIDD, G., DOMBROWSKI, S., DUTTA, R., LEE, J. C., COOK, D. N., JUNG, S., LIRA, S. A., LITTMAN, D. R. & RANSOHOFF, R. M. 2006. Control of microglial neurotoxicity by the fractalkine receptor. *Nat Neurosci,* 9**,** 917-24.

CERRETTI, D. P., KOZLOSKY, C. J., MOSLEY, B., NELSON, N., VAN NESS, K., GREENSTREET, T. A., MARCH, C. J., KRONHEIM, S. R., DRUCK, T., CANNIZZARO, L. A. & ET AL. 1992. Molecular cloning of the interleukin-1 beta converting enzyme. *Science,* 256**,** 97-100.

CHANG, J., XIE, M., SHAH, V. R., SCHNEIDER, M. D., ENTMAN, M. L., WEI, L. & SCHWARTZ, R. J. 2006. Activation of Rho-associated coiled-coil protein kinase 1 (ROCK-1) by caspase-3 cleavage plays an essential role in cardiac myocyte apoptosis. *Proc Natl Acad Sci U S A,* 103**,** 14495-14500.

CHEKENI, F. B., ELLIOTT, M. R., SANDILOS, J. K., WALK, S. F., KINCHEN, J. M., LAZAROWSKI, E. R., ARMSTRONG, A. J., PENUELA, S., LAIRD, D. W., SALVESEN, G. S., ISAKSON, B. E., BAYLISS, D. A. & RAVICHANDRAN, K. S.

2010. Pannexin 1 channels mediate 'find-me' signal release and membrane permeability during apoptosis. *Nature,* 467**,** 863-867.

CHEN, B., LIU, L., CASTONGUAY, A., MARONPOT, R. R., ANDERSON, M. W. & YOU, M. 1993. Dose-dependent ras mutation spectra in N-nitrosodiethylamine induced mouse liver tumors and 4-(methylnitrosamino)-1-(3-pyridyl)-1-butanone induced mouse lung tumors. *Carcinogenesis,* 14**,** 1603-8.

CHEN, G. Y. & NUNEZ, G. 2010. Sterile inflammation: sensing and reacting to damage. *Nat Rev Immunol,* 10**,** 826-37.

CHEN, J., GUERRIERO, E., LATHROP, K. & SUNDARRAJ, N. 2008. Rho/ROCK signaling in regulation of corneal epithelial cell cycle progression. *Invest Ophthalmol Vis Sci,* 49**,** 175-83.

CHEUNG, A., DANTZIG, J. A., HOLLINGWORTH, S., BAYLOR, S. M., GOLDMAN, Y. E., MITCHISON, T. J. & STRAIGHT, A. F. 2002. A small-molecule inhibitor of skeletal muscle myosin II. *Nat Cell Biol,* 4**,** 83-8.

CHEVRIER, V., PIEL, M., COLLOMB, N., SAOUDI, Y., FRANK, R., PAINTRAND, M., NARUMIYA, S., BORNENS, M. & JOB, D. 2002. The Rho-associated protein kinase p160ROCK is required for centrosome positioning. *J Cell Biol,* 157**,** 807-17.

CHUANG, H. H., LIANG, S. W., CHANG, Z. F. & LEE, H. H. 2013. Ser1333 phosphorylation indicates ROCKI activation. *J Biomed Sci,* 20**,** 83.

CHUNG, E. Y., KIM, S. J. & MA, X. J. 2006. Regulation of cytokine production during phagocytosis of apoptotic cells. *Cell Res,* 16**,** 154-61.

COHEN, G. M. 1997. Caspases: the executioners of apoptosis. *Biochem J,* 326 (Pt 1)**,** 1-16.

COHEN, P. L., CARICCHIO, R., ABRAHAM, V., CAMENISCH, T. D., JENNETTE, J. C., ROUBEY, R. A. S., EARP, H. S., MATSUSHIMA, G. & REAP, E. A. 2002. Delayed apoptotic cell clearance and lupus-like autoimmunity in mice lacking the c-mer membrane tyrosine kinase. *The Journal of experimental medicine,* 196**,** 135-40.

COLEMAN, M. L., SAHAI, E. A., YEO, M., BOSCH, M., DEWAR, A. & OLSON, M. F. 2001. Membrane blebbing during apoptosis results from caspase-mediated activation of ROCK I. *Nature cell biology,* 3**,** 339-45.

CONTRERAS, F. X., SANCHEZ-MAGRANER, L., ALONSO, A. & GONI, F. M. 2010. Transbilayer (flip-flop) lipid motion and lipid scrambling in membranes. *FEBS Lett,* 584**,** 1779-86.

COPP, A. J., BROOK, F. A., ESTIBEIRO, J. P., SHUM, A. S. & COCKROFT, D. L. 1990. The embryonic development of mammalian neural tube defects. *Prog Neurobiol,* 35**,** 363-403.

COTTER, T. G., LENNON, S. V., GLYNN, J. M. & GREEN, D. R. 1992. Microfilament-disrupting agents prevent the formation of apoptotic bodies in tumor cells undergoing apoptosis. *Cancer Res,* 52**,** 997-1005.

COUCOUVANIS, E. & MARTIN, G. R. 1995. Signals for death and survival: a two-step mechanism for cavitation in the vertebrate embryo. *Cell,* 83**,** 279-87.

COUCOUVANIS, E. C., MARTIN, G. R. & NADEAU, J. H. 1995. Genetic approaches for studying programmed cell death during development of the laboratory mouse. *Methods Cell Biol,* 46**,** 387-440.

COUSSENS, L. M. & WERB, Z. 2002. Inflammation and cancer. *Nature,* 420**,** 860-7.

CROFT, D. R., COLEMAN, M. L., LI, S., ROBERTSON, D., SULLIVAN, T., STEWART, C. L. & OLSON, M. F. 2005. Actin-myosin-based contraction is responsible for apoptotic nuclear disintegration. *J Cell Biol,* 168**,** 245-255.

CROFT, D. R. & OLSON, M. F. 2006. Conditional Regulation of a ROCK-Estrogen Receptor Fusion Protein. *Methods Enzymol,* 406**,** 541-53.

CROUCH, S. P., SLATER, K. J. & FLETCHER, J. 1992. Regulation of cytokine release from mononuclear cells by the iron-binding protein lactoferrin. *Blood,* 80**,** 235-40.

DAMBACH, D. M., WATSON, L. M., GRAY, K. R., DURHAM, S. K. & LASKIN, D. L. 2002. Role of CCR2 in macrophage migration into the liver during acetaminophen-induced hepatotoxicity in the mouse. *Hepatology,* 35**,** 1093-103.

DANG, C. V. 2012. MYC on the path to cancer. *Cell,* 149**,** 22-35.

DEVITT, A., PARKER, K. G., OGDEN, C. A., OLDREIVE, C., CLAY, M. F., MELVILLE, L. A., BELLAMY, C. O., LACY-HULBERT, A., GANGLOFF, S. C., GOYERT, S. M. & GREGORY, C. D. 2004. Persistence of apoptotic cells without autoimmune disease or inflammation in CD14-/- mice. *J Cell Biol,* 167**,** 1161-70.

DONEHOWER, L. A., HARVEY, M., SLAGLE, B. L., MCARTHUR, M. J., MONTGOMERY, C. A., JR., BUTEL, J. S. & BRADLEY, A. 1992. Mice deficient for p53 are developmentally normal but susceptible to spontaneous tumours. *Nature,* 356**,** 215-21.

DUNN, G. P., BRUCE, A. T., IKEDA, H., OLD, L. J. & SCHREIBER, R. D. 2002. Cancer immunoediting: from immunosurveillance to tumor escape. *Nat Immunol,* 3**,** 991-8.

DUNN, G. P., OLD, L. J. & SCHREIBER, R. D. 2004. The three Es of cancer immunoediting. *Annu Rev Immunol,* 22**,** 329-60.

DVORSKY, R., BLUMENSTEIN, L., VETTER, I. R. & AHMADIAN, M. R. 2004. Structural insights into the interaction of ROCKI with the switch regions of RhoA. *J Biol Chem,* 279**,** 7098-104.

EISCHEN, C. M., WEBER, J. D., ROUSSEL, M. F., SHERR, C. J. & CLEVELAND, J. L. 1999. Disruption of the ARF-Mdm2-p53 tumor suppressor pathway in Myc-induced lymphomagenesis. *Genes Dev,* 13**,** 2658-69.

ELERT, E. 2013. Calling cells to arms. *Nature,* 504**,** S2-3.

ELKINS, J. M., AMOS, A., NIESEN, F. H., PIKE, A. C., FEDOROV, O. & KNAPP, S. 2009. Structure of dystrophia myotonica protein kinase. *Protein Sci,* 18**,** 782-91.

ELLIOTT, M. R., CHEKENI, F. B., TRAMPONT, P. C., LAZAROWSKI, E. R., KADL, A., WALK, S. F., PARK, D., WOODSON, R. I., OSTANKOVICH, M., SHARMA, P., LYSIAK, J. J., HARDEN, T. K., LEITINGER, N. & RAVICHANDRAN, K. S. 2009. Nucleotides released by apoptotic cells act as a find-me signal to promote phagocytic clearance. *Nature,* 461**,** 282-6.

ELLIOTT, M. R. & RAVICHANDRAN, K. S. 2010. Clearance of apoptotic cells: implications in health and disease. *J Cell Biol,* 189**,** 1059-70.

ERHARDT, A., BIBURGER, M., PAPADOPOULOS, T. & TIEGS, G. 2007. IL-10, regulatory T cells, and Kupffer cells mediate tolerance in concanavalin A-induced liver injury in mice. *Hepatology,* 45**,** 475-85.

FADEEL, B. 2004. Plasma membrane alterations during apoptosis: role in corpse clearance. *Antioxidants & redox signaling,* 6**,** 269-75.

FADOK, V. A., BRATTON, D. L., KONOWAL, A., FREED, P. W., WESTCOTT, J. Y. & HENSON, P. M. 1998. Macrophages that have ingested apoptotic cells in vitro inhibit proinflammatory cytokine production through autocrine/paracrine mechanisms involving TGF-beta, PGE2, and PAF. *J Clin Invest,* 101**,** 890-8.

FADOK, V. A., SAVILL, J. S., HASLETT, C., BRATTON, D. L., DOHERTY, D. E., CAMPBELL, P. A. & HENSON, P. M. 1992a. Different populations of

macrophages use either the vitronectin receptor or the phosphatidylserine receptor to recognize and remove apoptotic cells. *J Immunol,* 149**,** 4029-35.

FADOK, V. A., VOELKER, D. R., CAMPBELL, P. A., COHEN, J. J., BRATTON, D. L. & HENSON, P. M. 1992b. Exposure of phosphatidylserine on the surface of apoptotic lymphocytes triggers specific recognition and removal by macrophages. *J Immunol,* 148**,** 2207-16.

FARBER, E., SOLT, D., CAMERON, R., LAISHES, B., OGAWA, K. & MEDLINE, A. 1977. Newer insights into the pathogenesis of liver cancer. *Am J Pathol,* 89**,** 477-82.

FARGHALI, H., CANOVA, N., KUCERA, T., MARTINEK, J. & MASEK, K. 2003. Nitric oxide synthase inhibitors modulate lipopolysaccharide-induced hepatocyte injury: dissociation between in vivo and in vitro effects. *Int Immunopharmacol,* 3**,** 1627-38.

FELVER, M. E., MEZEY, E., MCGUIRE, M., MITCHELL, M. C., HERLONG, H. F., VEECH, G. A. & VEECH, R. L. 1990. Plasma tumor necrosis factor alpha predicts decreased long-term survival in severe alcoholic hepatitis. *Alcohol Clin Exp Res,* 14**,** 255-9.

FENG, J., ITO, M., KUREISHI, Y., ICHIKAWA, K., AMANO, M., ISAKA, N., OKAWA, K., IWAMATSU, A., KAIBUCHI, K., HARTSHORNE, D. J. & NAKANO, T. 1999. Rho-associated kinase of chicken gizzard smooth muscle. *J Biol Chem,* 274**,** 3744-3752.

FISHKIND, D. J., CAO, L. G. & WANG, Y. L. 1991. Microinjection of the catalytic fragment of myosin light chain kinase into dividing cells: effects on mitosis and cytokinesis. *J Cell Biol,* 114**,** 967-75.

FRANZ, S., GAIPL, U. S., MUNOZ, L. E., SHERIFF, A., BEER, A., KALDEN, J. R. & HERRMANN, M. 2006. Apoptosis and autoimmunity: when apoptotic cells break their silence. *Curr Rheumatol Rep,* 8**,** 245-7.

FRIEDL, P. & WOLF, K. 2003. Tumour-cell invasion and migration: diversity and escape mechanisms. *Nat Rev Cancer,* 3**,** 362-74.

FRIGGERI, A., YANG, Y., BANERJEE, S., PARK, Y. J., LIU, G. & ABRAHAM, E. 2010. HMGB1 inhibits macrophage activity in efferocytosis through binding to the alphavbeta3-integrin. *Am J Physiol Cell Physiol,* 299**,** C1267-76.

GAIPL, U. S., FRANZ, S., VOLL, R. E., SHERIFF, A., KALDEN, J. R. & HERRMANN, M. 2004. Defects in the disposal of dying cells lead to autoimmunity. *Curr Rheumatol Rep,* 6**,** 401-7.

GARDAI, S. J., MCPHILLIPS, K. A., FRASCH, S. C., JANSSEN, W. J., STAREFELDT, A., MURPHY-ULLRICH, J. E., BRATTON, D. L., OLDENBORG, P. A., MICHALAK, M. & HENSON, P. M. 2005. Cell-surface calreticulin initiates clearance of viable or apoptotic cells through trans-activation of LRP on the phagocyte. *Cell,* 123**,** 321-34.

GARG, R., RIENTO, K., KEEP, N., MORRIS, J. D. H. & RIDLEY, A. J. 2008. N-terminus-mediated dimerization of ROCK-I is required for RhoE binding and actin reorganization. *The Biochemical journal,* 411**,** 407-14.

GATTI, R. A. & GOOD, R. A. 1971. Occurrence of malignancy in immunodeficiency diseases. A literature review. *Cancer,* 28**,** 89-98.

GHIRINGHELLI, F., APETOH, L., TESNIERE, A., AYMERIC, L., MA, Y., ORTIZ, C., VERMAELEN, K., PANARETAKIS, T., MIGNOT, G., ULLRICH, E., PERFETTINI, J. L., SCHLEMMER, F., TASDEMIR, E., UHL, M., GENIN, P., CIVAS, A., RYFFEL, B., KANELLOPOULOS, J., TSCHOPP, J., ANDRE, F., LIDEREAU, R., MCLAUGHLIN, N. M., HAYNES, N. M., SMYTH, M. J., KROEMER, G. & ZITVOGEL, L. 2009. Activation of the NLRP3 inflammasome in dendritic

cells induces IL-1beta-dependent adaptive immunity against tumors. *Nat Med,* 15**,** 1170-8.

GLYN, M. C., LAWRENSON, J. G. & WARD, B. J. 2003. A Rho-associated kinase mitigates reperfusion-induced change in the shape of cardiac capillary endothelial cells in situ. *Cardiovasc Res,* 57**,** 195-206.

GOLPON, H. A., FADOK, V. A., TARASEVICIENE-STEWART, L., SCERBAVICIUS, R., SAUER, C., WELTE, T., HENSON, P. M. & VOELKEL, N. F. 2004. Life after corpse engulfment: phagocytosis of apoptotic cells leads to VEGF secretion and cell growth. *FASEB J,* 18**,** 1716-8.

GOODEN, M. J., DE BOCK, G. H., LEFFERS, N., DAEMEN, T. & NIJMAN, H. W. 2011. The prognostic influence of tumour-infiltrating lymphocytes in cancer: a systematic review with meta-analysis. *Br J Cancer,* 105**,** 93-103.

GREGORY, C. D. & POUND, J. D. 2010. Microenvironmental influences of apoptosis in vivo and in vitro. *Apoptosis,* 15**,** 1029-1049.

GREGORY, S. H., SAGNIMENI, A. J. & WING, E. J. 1996. Bacteria in the bloodstream are trapped in the liver and killed by immigrating neutrophils. *J Immunol,* 157**,** 2514-20.

GREGORY, S. H. & WING, E. J. 1990. Accessory function of Kupffer cells in the antigen-specific blastogenic response of an L3T4+ T-lymphocyte clone to Listeria monocytogenes. *Infect Immun,* 58**,** 2313-9.

GRIVENNIKOV, S. I., GRETEN, F. R. & KARIN, M. 2010. Immunity, inflammation, and cancer. *Cell,* 140**,** 883-99.

GUASCH, R. M., SCAMBLER, P., JONES, G. E. & RIDLEY, A. J. 1998. RhoE regulates actin cytoskeleton organization and cell migration. *Mol Cell Biol,* 18**,** 4761-71.

GUDE, D. R., ALVAREZ, S. E., PAUGH, S. W., MITRA, P., YU, J., GRIFFITHS, R., BARBOUR, S. E., MILSTIEN, S. & SPIEGEL, S. 2008. Apoptosis induces expression of sphingosine kinase 1 to release sphingosine-1-phosphate as a "come-and-get-me" signal. *The FASEB journal : official publication of the Federation of American Societies for Experimental Biology,* 22**,** 2629-38.

GUJRAL, J. S., FARHOOD, A., BAJT, M. L. & JAESCHKE, H. 2003. Neutrophils aggravate acute liver injury during obstructive cholestasis in bile duct-ligated mice. *Hepatology,* 38**,** 355-63.

GUMIENNY, T. L., BRUGNERA, E., TOSELLO-TRAMPONT, A. C., KINCHEN, J. M., HANEY, L. B., NISHIWAKI, K., WALK, S. F., NEMERGUT, M. E., MACARA, I. G., FRANCIS, R., SCHEDL, T., QIN, Y., VAN AELST, L., HENGARTNER, M. O. & RAVICHANDRAN, K. S. 2001. CED-12/ELMO, a novel member of the CrkII/Dock180/Rac pathway, is required for phagocytosis and cell migration. *Cell,* 107**,** 27-41.

HANAYAMA, R., TANAKA, M., MIWA, K., SHINOHARA, A., IWAMATSU, A. & NAGATA, S. 2002. Identification of a factor that links apoptotic cells to phagocytes. *Nature,* 417**,** 182-7.

HANAYAMA, R., TANAKA, M., MIYASAKA, K., AOZASA, K., KOIKE, M., UCHIYAMA, Y. & NAGATA, S. 2004. Autoimmune disease and impaired uptake of apoptotic cells in MFG-E8-deficient mice. *Science (New York, N.Y.),* 304**,** 1147-50.

HARRIS, A. W., PINKERT, C. A., CRAWFORD, M., LANGDON, W. Y., BRINSTER, R. L. & ADAMS, J. M. 1988. The E mu-myc transgenic mouse. A model for high-incidence spontaneous lymphoma and leukemia of early B cells. *J Exp Med,* 167**,** 353-71.

HARVEY, M., MCARTHUR, M. J., MONTGOMERY, C. A., JR., BRADLEY, A. & DONEHOWER, L. A. 1993. Genetic background alters the spectrum of tumors that develop in p53-deficient mice. *FASEB J,* 7**,** 938-43.

HE, J., YIN, Y., LUSTER, T. A., WATKINS, L. & THORPE, P. E. 2009. Antiphosphatidylserine antibody combined with irradiation damages tumor blood vessels and induces tumor immunity in a rat model of glioblastoma. *Clin Cancer Res,* 15**,** 6871-80.

HEIKKILA, T., WHEATLEY, E., CRIGHTON, D., SCHRODER, E., BOAKES, A., KAYE, S. J., MEZNA, M., PANG, L., RUSHBROOKE, M., TURNBULL, A. & OLSON, M. F. 2011. Co-crystal structures of inhibitors with MRCKbeta, a key regulator of tumor cell invasion. *PLoS One,* 6**,** e24825.

HEINDRYCKX, F., COLLE, I. & VAN VLIERBERGHE, H. 2009. Experimental mouse models for hepatocellular carcinoma research. *Int J Exp Pathol,* 90**,** 367-86.

HERRMANN, M., VOLL, R. E., ZOLLER, O. M., HAGENHOFER, M., PONNER, B. B. & KALDEN, J. R. 1998. Impaired phagocytosis of apoptotic cell material by monocyte-derived macrophages from patients with systemic lupus erythematosus. *Arthritis Rheum,* 41**,** 1241-50.

HODGE, S., HODGE, G., AHERN, J., JERSMANN, H., HOLMES, M. & REYNOLDS, P. N. 2007. Smoking alters alveolar macrophage recognition and phagocytic ability: implications in chronic obstructive pulmonary disease. *Am J Respir Cell Mol Biol,* 37**,** 748-55.

HOEPPNER, D. J., HENGARTNER, M. O. & SCHNABEL, R. 2001. Engulfment genes cooperate with ced-3 to promote cell death in Caenorhabditis elegans. *Nature,* 412**,** 202-6.

HOHENBERGER, P., EING, C., STRAESSNER, R., DURST, S., FREY, W. & NICK, P. 2011. Plant actin controls membrane permeability. *Biochimica et Biophysica Acta - Biomembranes,* 1808**,** 2304-2312.

HOLT, M. P., CHENG, L. & JU, C. 2008. Identification and characterization of infiltrating macrophages in acetaminophen-induced liver injury. *J Leukoc Biol,* 84**,** 1410-21.

HORVITZ, H. R. 1999. Genetic control of programmed cell death in the nematode Caenorhabditis elegans. *Cancer Res,* 59**,** 1701s-1706s.

HRISTOV, M., ERL, W., LINDER, S. & WEBER, P. C. 2004. Apoptotic bodies from endothelial cells enhance the number and initiate the differentiation of human endothelial progenitor cells in vitro. *Blood,* 104**,** 2761-6.

HUANG, H., EVANKOVICH, J., YAN, W., NACE, G., ZHANG, L., ROSS, M., LIAO, X., BILLIAR, T., XU, J., ESMON, C. T. & TSUNG, A. 2011. Endogenous histones function as alarmins in sterile inflammatory liver injury through Toll-like receptor 9 in mice. *Hepatology,* 54**,** 999-1008.

HUEBENER, P., GWAK, G. Y., PRADERE, J. P., QUINZII, C. M., FRIEDMAN, R., LIN, C. S., TRENT, C. M., MEDERACKE, I., ZHAO, E., DAPITO, D. H., LIN, Y., GOLDBERG, I. J., CZAJA, M. J. & SCHWABE, R. F. 2014. High-mobility group box 1 is dispensable for autophagy, mitochondrial quality control, and organ function in vivo. *Cell Metab,* 19**,** 539-47.

HUEBENER, P., PRADERE, J. P., HERNANDEZ, C., GWAK, G. Y., CAVIGLIA, J. M., MU, X., LOIKE, J. D., JENKINS, R. E., ANTOINE, D. J. & SCHWABE, R. F. 2015. The HMGB1/RAGE axis triggers neutrophil-mediated injury amplification following necrosis. *J Clin Invest,* 125**,** 539-50.

IIZUKA, K., YOSHII, A., SAMIZO, K., TSUKAGOSHI, H., ISHIZUKA, T., DOBASHI, K., NAKAZAWA, T. & MORI, M. 1999. A major role for the rho-associated coiled coil forming protein kinase in G-protein-mediated Ca2+ sensitization through inhibition of myosin phosphatase in rabbit trachea. *Br J Pharmacol,* 128**,** 925-33.

IKENOYA, M., HIDAKA, H., HOSOYA, T., SUZUKI, M., YAMAMOTO, N. & SASAKI, Y. 2002. Inhibition of rho-kinase-induced myristoylated alanine-rich C kinase

substrate (MARCKS) phosphorylation in human neuronal cells by H-1152, a novel and specific Rho-kinase inhibitor. *J Neurochem,* 81**,** 9-16.

INADA, H., TOGASHI, H., NAKAMURA, Y., KAIBUCHI, K., NAGATA, K.-I. & INAGAKI, M. 1999. Balance between Activities of Rho Kinase and Type 1 Protein Phosphatase Modulates Turnover of Phosphorylation and Dynamics of Desmin/Vimentin Filaments. *J. Biol. Chem.,* 274**,** 34932-34939.

ISHIBASHI, H., NAKAMURA, M., KOMORI, A., MIGITA, K. & SHIMODA, S. 2009. Liver architecture, cell function, and disease. *Semin Immunopathol,* 31**,** 399-409.

ISHIKURA, K., YAMADA, N., ITO, M., OTA, S., NAKAMURA, M., ISAKA, N. & NAKANO, T. 2006. Beneficial acute effects of rho-kinase inhibitor in patients with pulmonary arterial hypertension. *Circ J,* 70**,** 174-8.

ISHIMOTO, Y., OHASHI, K., MIZUNO, K. & NAKANO, T. 2000. Promotion of the uptake of PS liposomes and apoptotic cells by a product of growth arrest-specific gene, gas6. *J Biochem,* 127**,** 411-7.

ISHIUCHI, T. & TAKEICHI, M. 2011. Willin and Par3 cooperatively regulate epithelial apical constriction through aPKC-mediated ROCK phosphorylation. *Nat Cell Biol,* 13**,** 860-6.

ISHIZAKI, T., MAEKAWA, M., FUJISAWA, K., OKAWA, K., IWAMATSU, A., FUJITA, A., WATANABE, N., SAITO, Y., KAKIZUKA, A., MORII, N. & NARUMIYA, S. 1996. The small GTP-binding protein Rho binds to and activates a 160 kDa Ser/Thr protein kinase homologous to myotonic dystrophy kinase. *Embo J,* 15**,** 1885-93.

ISHIZAKI, T., NAITO, M., FUJISAWA, K., MAEKAWA, M., WATANABE, N., SAITO, Y. & NARUMIYA, S. 1997. p160ROCK, a Rho-associated coiled-coil forming protein kinase, works downstream of Rho and induces focal adhesions. *FEBS Lett,* 404**,** 118-24.

ITO, Y., BETHEA, N. W., ABRIL, E. R. & MCCUSKEY, R. S. 2003. Early hepatic microvascular injury in response to acetaminophen toxicity. *Microcirculation,* 10**,** 391-400.

JACKS, T., REMINGTON, L., WILLIAMS, B. O., SCHMITT, E. M., HALACHMI, S., BRONSON, R. T. & WEINBERG, R. A. 1994. Tumor spectrum analysis in p53-mutant mice. *Curr Biol,* 4**,** 1-7.

JACOBS, J. J., SCHEIJEN, B., VONCKEN, J. W., KIEBOOM, K., BERNS, A. & VAN LOHUIZEN, M. 1999. Bmi-1 collaborates with c-Myc in tumorigenesis by inhibiting c-Myc-induced apoptosis via INK4a/ARF. *Genes Dev,* 13**,** 2678-90.

JACOBS, M., HAYAKAWA, K., SWENSON, L., BELLON, S., FLEMING, M., TASLIMI, P. & DORAN, J. 2006. The Structure of Dimeric ROCK I Reveals the Mechanism for Ligand Selectivity. *J. Biol. Chem.,* 281**,** 260-268.

JACOBSEN, K. A., PRASAD, V. S., SIDMAN, C. L. & OSMOND, D. G. 1994. Apoptosis and macrophage-mediated deletion of precursor B cells in the bone marrow of E mu-myc transgenic mice. *Blood,* 84**,** 2784-94.

JACOBSON, M. D., WEIL, M. & RAFF, M. C. 1997. Programmed cell death in animal development. *Cell,* 88**,** 347-54.

JAESCHKE, H. & HASEGAWA, T. 2006. Role of neutrophils in acute inflammatory liver injury. *Liver Int,* 26**,** 912-9.

JINUSHI, M., NAKAZAKI, Y., CARRASCO, D. R., DRAGANOV, D., SOUDERS, N., JOHNSON, M., MIHM, M. C. & DRANOFF, G. 2008. Milk fat globule EGF-8 promotes melanoma progression through coordinated Akt and twist signaling in the tumor microenvironment. *Cancer Res,* 68**,** 8889-98.

JINUSHI, M., SATO, M., KANAMOTO, A., ITOH, A., NAGAI, S., KOYASU, S., DRANOFF, G. & TAHARA, H. 2009. Milk fat globule epidermal growth

factor-8 blockade triggers tumor destruction through coordinated cell-autonomous and immune-mediated mechanisms. *J Exp Med,* 206**,** 1317-26.

JULIAN, L. & OLSON, M. F. 2014. Rho-associated coiled-coil containing kinases (ROCK): structure, regulation, and functions. *Small GTPases,* 5**,** e29846.

JULIAN, L. & OLSON, M. F. 2015. Apoptotic membrane dynamics in health and disease. *Cell Health and Cytoskeleton,* 7**,** 133-142.

KANG, J. H., JIANG, Y., TOITA, R., OISHI, J., KAWAMURA, K., HAN, A., MORI, T., NIIDOME, T., ISHIDA, M., TATEMATSU, K., TANIZAWA, K. & KATAYAMA, Y. 2007. Phosphorylation of Rho-associated kinase (Rho-kinase/ROCK/ROK) substrates by protein kinases A and C. *Biochimie,* 89**,** 39-47.

KANG, J. W., KIM, S. J., CHO, H. I. & LEE, S. M. 2015. DAMPs activating innate immune responses in sepsis. *Ageing Res Rev*.

KARLMARK, K. R., WEISKIRCHEN, R., ZIMMERMANN, H. W., GASSLER, N., GINHOUX, F., WEBER, C., MERAD, M., LUEDDE, T., TRAUTWEIN, C. & TACKE, F. 2009. Hepatic recruitment of the inflammatory Gr1+ monocyte subset upon liver injury promotes hepatic fibrosis. *Hepatology,* 50**,** 261-74.

KATOH, K., KANO, Y., AMANO, M., ONISHI, H., KAIBUCHI, K. & FUJIWARA, K. 2001. Rho-kinase--mediated contraction of isolated stress fibers. *J Cell Biol,* 153**,** 569-84.

KAWABATA, S., USUKURA, J., MORONE, N., ITO, M., IWAMATSU, A., KAIBUCHI, K. & AMANO, M. 2004. Interaction of Rho-kinase with myosin II at stress fibres. *Genes Cells,* 9**,** 653-60.

KAWAI, T. & AKIRA, S. 2007. Signaling to NF-kappaB by Toll-like receptors. *Trends Mol Med,* 13**,** 460-9.

KAZAMA, H., RICCI, J. E., HERNDON, J. M., HOPPE, G., GREEN, D. R. & FERGUSON, T. A. 2008. Induction of immunological tolerance by apoptotic cells requires caspase-dependent oxidation of high-mobility group box-1 protein. *Immunity,* 29**,** 21-32.

KENZELMANN BROZ, D. & ATTARDI, L. D. 2010. In vivo analysis of p53 tumor suppressor function using genetically engineered mouse models. *Carcinogenesis,* 31**,** 1311-8.

KERR, J. F., WYLLIE, A. H. & CURRIE, A. R. 1972. Apoptosis: a basic biological phenomenon with wide-ranging implications in tissue kinetics. *Br J Cancer,* 26**,** 239-57.

KHONG, H. T. & RESTIFO, N. P. 2002. Natural selection of tumor variants in the generation of "tumor escape" phenotypes. *Nat Immunol,* 3**,** 999-1005.

KINCHEN, J. M. & RAVICHANDRAN, K. S. 2010. Identification of two evolutionarily conserved genes regulating processing of engulfed apoptotic cells. *Nature,* 464**,** 778-82.

KIRKHAM, P. A., SPOONER, G., RAHMAN, I. & ROSSI, A. G. 2004. Macrophage phagocytosis of apoptotic neutrophils is compromised by matrix proteins modified by cigarette smoke and lipid peroxidation products. *Biochem Biophys Res Commun,* 318**,** 32-7.

KLEIN, G. 1966. Tumor antigens. *Annu Rev Microbiol,* 20**,** 223-52.

KNIES, U. E., BEHRENSDORF, H. A., MITCHELL, C. A., DEUTSCH, U., RISAU, W., DREXLER, H. C. & CLAUSS, M. 1998. Regulation of endothelial monocyte-activating polypeptide II release by apoptosis. *Proc Natl Acad Sci U S A,* 95**,** 12322-7.

KOBAYASHI, N., KARISOLA, P., PENA-CRUZ, V., DORFMAN, D. M., JINUSHI, M., UMETSU, S. E., BUTTE, M. J., NAGUMO, H., CHERNOVA, I., ZHU, B., SHARPE, A. H., ITO, S., DRANOFF, G., KAPLAN, G. G., CASASNOVAS, J. M., UMETSU, D. T., DEKRUYFF, R. H. & FREEMAN, G. J. 2007. TIM-1 and TIM-4

glycoproteins bind phosphatidylserine and mediate uptake of apoptotic cells. *Immunity,* 27**,** 927-40.

KOEBEL, C. M., VERMI, W., SWANN, J. B., ZERAFA, N., RODIG, S. J., OLD, L. J., SMYTH, M. J. & SCHREIBER, R. D. 2007. Adaptive immunity maintains occult cancer in an equilibrium state. *Nature,* 450**,** 903-7.

KOKKOLA, R., LI, J., SUNDBERG, E., AVEBERGER, A. C., PALMBLAD, K., YANG, H., TRACEY, K. J., ANDERSSON, U. & HARRIS, H. E. 2003. Successful treatment of collagen-induced arthritis in mice and rats by targeting extracellular high mobility group box chromosomal protein 1 activity. *Arthritis Rheum,* 48**,** 2052-8.

KOOK, S., KIM, D. H., SHIM, S. R., KIM, W., CHUN, J. S. & SONG, W. K. 2003. Caspase-dependent cleavage of tensin induces disruption of actin cytoskeleton during apoptosis. *Biochem Biophys Res Commun,* 303**,** 37-45.

KORB, L. C. & AHEARN, J. M. 1997. C1q binds directly and specifically to surface blebs of apoptotic human keratinocytes: complement deficiency and systemic lupus erythematosus revisited. *J Immunol,* 158**,** 4525-8.

KOSAKO, H., GOTO, H., YANAGIDA, M., MATSUZAWA, K., FUJITA, M., TOMONO, Y., OKIGAKI, T., ODAI, H., KAIBUCHI, K. & INAGAKI, M. 1999. Specific accumulation of Rho-associated kinase at the cleavage furrow during cytokinesis: cleavage furrow-specific phosphorylation of intermediate filaments. *Oncogene,* 18**,** 2783-8.

KOSAKO, H., YOSHIDA, T., MATSUMURA, F., ISHIZAKI, T., NARUMIYA, S. & INAGAKI, M. 2000. Rho-kinase/ROCK is involved in cytokinesis through the phosphorylation of myosin light chain and not ezrin/radixin/moesin proteins at the cleavage furrow. *Oncogene,* 19**,** 6059-64.

KRUGER, P., SAFFARZADEH, M., WEBER, A. N., RIEBER, N., RADSAK, M., VON BERNUTH, H., BENARAFA, C., ROOS, D., SKOKOWA, J. & HARTL, D. 2015. Neutrophils: Between host defence, immune modulation, and tissue injury. *PLoS Pathog,* 11**,** e1004651.

KUPERWASSER, C., HURLBUT, G. D., KITTRELL, F. S., DICKINSON, E. S., LAUCIRICA, R., MEDINA, D., NABER, S. P. & JERRY, D. J. 2000. Development of spontaneous mammary tumors in BALB/c p53 heterozygous mice. A model for Li-Fraumeni syndrome. *Am J Pathol,* 157**,** 2151-9.

KUROSAKA, K., TAKAHASHI, M. & KOBAYASHI, Y. 2003. Activation of extracellular signal-regulated kinase 1/2 is involved in production of CXC-chemokine by macrophages during phagocytosis of late apoptotic cells. *Biochem Biophys Res Commun,* 306**,** 1070-4.

LACY-HULBERT, A., SMITH, A. M., TISSIRE, H., BARRY, M., CROWLEY, D., BRONSON, R. T., ROES, J. T., SAVILL, J. S. & HYNES, R. O. 2007. Ulcerative colitis and autoimmunity induced by loss of myeloid alphav integrins. *Proc Natl Acad Sci U S A,* 104**,** 15823-8.

LANE, J. D., ALLAN, V. J. & WOODMAN, P. G. 2005. Active relocation of chromatin and endoplasmic reticulum into blebs in late apoptotic cells. *Journal of cell science,* 118**,** 4059-71.

LANGDON, W. Y., HARRIS, A. W., CORY, S. & ADAMS, J. M. 1986. The c-myc oncogene perturbs B lymphocyte development in E-mu-myc transgenic mice. *Cell,* 47**,** 11-8.

LAUBER, K., BOHN, E., KROBER, S. M., XIAO, Y. J., BLUMENTHAL, S. G., LINDEMANN, R. K., MARINI, P., WIEDIG, C., ZOBYWALSKI, A., BAKSH, S., XU, Y., AUTENRIETH, I. B., SCHULZE-OSTHOFF, K., BELKA, C., STUHLER, G. & WESSELBORG, S. 2003. Apoptotic cells induce migration of

phagocytes via caspase-3-mediated release of a lipid attraction signal. *Cell,* 113**,** 717-30.

LEE, G. H., NOMURA, K. & KITAGAWA, T. 1989. Comparative study of diethylnitrosamine-initiated two-stage hepatocarcinogenesis in C3H, C57BL and BALB mice promoted by various hepatopromoters. *Carcinogenesis,* 10**,** 2227-30.

LEE, H. H. & CHANG, Z. F. 2008. Regulation of RhoA-dependent ROCKII activation by Shp2. *J Cell Biol,* 181**,** 999-1012.

LEE, J. S., CHU, I. S., MIKAELYAN, A., CALVISI, D. F., HEO, J., REDDY, J. K. & THORGEIRSSON, S. S. 2004. Application of comparative functional genomics to identify best-fit mouse models to study human cancer. *Nat Genet,* 36**,** 1306-11.

LENTZ, B. R. 2003. Exposure of platelet membrane phosphatidylserine regulates blood coagulation. *Prog Lipid Res,* 42**,** 423-38.

LEUNG, T., CHEN, X. Q., MANSER, E. & LIM, L. 1996. The p160 RhoA-binding kinase ROK alpha is a member of a kinase family and is involved in the reorganization of the cytoskeleton. *Mol Cell Biol,* 16**,** 5313-27.

LEUNG, T., MANSER, E., TAN, L. & LIM, L. 1995. A novel serine/threonine kinase binding the Ras-related RhoA GTPase which translocates the kinase to peripheral membranes. *J Biol Chem,* 270**,** 29051-4.

LEVENTIS, P. A. & GRINSTEIN, S. 2010. The distribution and function of phosphatidylserine in cellular membranes. *Annu Rev Biophys,* 39**,** 407-27.

LIEDTKE, C., LUEDDE, T., SAUERBRUCH, T., SCHOLTEN, D., STREETZ, K., TACKE, F., TOLBA, R., TRAUTWEIN, C., TREBICKA, J. & WEISKIRCHEN, R. 2013. Experimental liver fibrosis research: update on animal models, legal issues and translational aspects. *Fibrogenesis Tissue Repair,* 6**,** 19.

LINDSTEN, T., ROSS, A. J., KING, A., ZONG, W. X., RATHMELL, J. C., SHIELS, H. A., ULRICH, E., WAYMIRE, K. G., MAHAR, P., FRAUWIRTH, K., CHEN, Y., WEI, M., ENG, V. M., ADELMAN, D. M., SIMON, M. C., MA, A., GOLDEN, J. A., EVAN, G., KORSMEYER, S. J., MACGREGOR, G. R. & THOMPSON, C. B. 2000. The combined functions of proapoptotic Bcl-2 family members bak and bax are essential for normal development of multiple tissues. *Mol Cell,* 6**,** 1389-99.

LIU, G., WANG, J., PARK, Y. J., TSURUTA, Y., LORNE, E. F., ZHAO, X. & ABRAHAM, E. 2008a. High mobility group protein-1 inhibits phagocytosis of apoptotic neutrophils through binding to phosphatidylserine. *J Immunol,* 181**,** 4240-6.

LIU, X., YU, X., ZACK, D. J., ZHU, H. & QIAN, J. 2008b. TiGER: a database for tissue-specific gene expression and regulation. *BMC Bioinformatics,* 9**,** 271.

LIU, Z. X., HAN, D., GUNAWAN, B. & KAPLOWITZ, N. 2006. Neutrophil depletion protects against murine acetaminophen hepatotoxicity. *Hepatology,* 43**,** 1220-30.

LOHN, M., PLETTENBURG, O., IVASHCHENKO, Y., KANNT, A., HOFMEISTER, A., KADEREIT, D., SCHAEFER, M., LINZ, W., KOHLMANN, M., HERBERT, J. M., JANIAK, P., O'CONNOR, S. E. & RUETTEN, H. 2009. Pharmacological characterization of SAR407899, a novel rho-kinase inhibitor. *Hypertension,* 54**,** 676-83.

LORD-FONTAINE, S., YANG, F., DIEP, Q., DERGHAM, P., MUNZER, S., TREMBLAY, P. & MCKERRACHER, L. 2008. Local inhibition of Rho signaling by cell-permeable recombinant protein BA-210 prevents secondary damage and promotes functional recovery following acute spinal cord injury. *J Neurotrauma,* 25**,** 1309-22.

LOTZE, M. T. & TRACEY, K. J. 2005. High-mobility group box 1 protein (HMGB1): nuclear weapon in the immune arsenal. *Nat Rev Immunol,* 5**,** 331-42.

LOWERY, D. M., CLAUSER, K. R., HJERRILD, M., LIM, D., ALEXANDER, J., KISHI, K., ONG, S. E., GAMMELTOFT, S., CARR, S. A. & YAFFE, M. B. 2007. Proteomic screen defines the Polo-box domain interactome and identifies Rock2 as a Plk1 substrate. *Embo J,* 26**,** 2262-73.

LUCAS, M., STUART, L. M., SAVILL, J. & LACY-HULBERT, A. 2003. Apoptotic cells and innate immune stimuli combine to regulate macrophage cytokine secretion. *J Immunol,* 171**,** 2610-5.

LUND, L. R., ROMER, J., THOMASSET, N., SOLBERG, H., PYKE, C., BISSELL, M. J., DANO, K. & WERB, Z. 1996. Two distinct phases of apoptosis in mammary gland involution: proteinase-independent and -dependent pathways. *Development,* 122**,** 181-93.

LUTGENS, E., TJWA, M., GARCIA DE FRUTOS, P., WIJNANDS, E., BECKERS, L., DAHLBACK, B., DAEMEN, M. J., CARMELIET, P. & MOONS, L. 2008. Genetic loss of Gas6 induces plaque stability in experimental atherosclerosis. *J Pathol,* 216**,** 55-63.

MA, Z., KANAI, M., KAWAMURA, K., KAIBUCHI, K., YE, K. & FUKASAWA, K. 2006. Interaction between ROCK II and nucleophosmin/B23 in the regulation of centrosome duplication. *Mol Cell Biol,* 26**,** 9016-34.

MALKIN, D., LI, F. P., STRONG, L. C., FRAUMENI, J. F., JR., NELSON, C. E., KIM, D. H., KASSEL, J., GRYKA, M. A., BISCHOFF, F. Z., TAINSKY, M. A. & ET AL. 1990. Germ line p53 mutations in a familial syndrome of breast cancer, sarcomas, and other neoplasms. *Science,* 250**,** 1233-8.

MARINCOLA, F. M., JAFFEE, E. M., HICKLIN, D. J. & FERRONE, S. 2000. Escape of human solid tumors from T-cell recognition: molecular mechanisms and functional significance. *Adv Immunol,* 74**,** 181-273.

MATSUI, T., AMANO, M., YAMAMOTO, T., CHIHARA, K., NAKAFUKU, M., ITO, M., NAKANO, T., OKAWA, K., IWAMATSU, A. & KAIBUCHI, K. 1996. Rho-associated kinase, a novel serine/threonine kinase, as a putative target for small GTP binding protein Rho. *Embo J,* 15**,** 2208-16.

MCDONALD, P. P., FADOK, V. A., BRATTON, D. & HENSON, P. M. 1999. Transcriptional and translational regulation of inflammatory mediator production by endogenous TGF-beta in macrophages that have ingested apoptotic cells. *J Immunol,* 163**,** 6164-72.

MCMULLAN, R., LAX, S., ROBERTSON, V. H., RADFORD, D. J., BROAD, S., WATT, F. M., ROWLES, A., CROFT, D. R., OLSON, M. F. & HOTCHIN, N. A. 2003. Keratinocyte Differentiation Is Regulated by the Rho and ROCK Signaling Pathway. *Curr Biol,* 13**,** 2185-9.

MICHAEL, S. L., PUMFORD, N. R., MAYEUX, P. R., NIESMAN, M. R. & HINSON, J. A. 1999. Pretreatment of mice with macrophage inactivators decreases acetaminophen hepatotoxicity and the formation of reactive oxygen and nitrogen species. *Hepatology,* 30**,** 186-95.

MILLIGAN, C. E., PREVETTE, D., YAGINUMA, H., HOMMA, S., CARDWELL, C., FRITZ, L. C., TOMASELLI, K. J., OPPENHEIM, R. W. & SCHWARTZ, L. M. 1995. Peptide inhibitors of the ICE protease family arrest programmed cell death of motoneurons in vivo and in vitro. *Neuron,* 15**,** 385-93.

MILLS, J. C., STONE, N. L., ERHARDT, J. & PITTMAN, R. N. 1998. Apoptotic membrane blebbing is regulated by myosin light chain phosphorylation. *J Cell Biol,* 140**,** 627-36.

MITTAL, D., GUBIN, M. M., SCHREIBER, R. D. & SMYTH, M. J. 2014. New insights into cancer immunoediting and its three component phases--elimination, equilibrium and escape. *Curr Opin Immunol,* 27**,** 16-25.

MITTAL, S. & EL-SERAG, H. B. 2013. Epidemiology of hepatocellular carcinoma: consider the population. *J Clin Gastroenterol,* 47 Suppl, S2-6.

MIYANISHI, M., TADA, K., KOIKE, M., UCHIYAMA, Y., KITAMURA, T. & NAGATA, S. 2007. Identification of Tim4 as a phosphatidylserine receptor. *Nature,* 450, 435-9.

MOCHIZUKI, H., GOTO, K., MORI, H. & MIZUNO, Y. 1996. Histochemical detection of apoptosis in Parkinson's disease. *J Neurol Sci,* 137, 120-3.

MOLLICA, L., DE MARCHIS, F., SPITALERI, A., DALLACOSTA, C., PENNACCHINI, D., ZAMAI, M., AGRESTI, A., TRISCIUOGLIO, L., MUSCO, G. & BIANCHI, M. E. 2007. Glycyrrhizin binds to high-mobility group box 1 protein and inhibits its cytokine activities. *Chem Biol,* 14, 431-41.

MONIER, B., GETTINGS, M., GAY, G., MANGEAT, T., SCHOTT, S., GUARNER, A. & SUZANNE, M. 2015. Apico-basal forces exerted by apoptotic cells drive epithelium folding. *Nature,* 518, 245-8.

MONKS, J., SMITH-STEINHART, C., KRUK, E. R., FADOK, V. A. & HENSON, P. M. 2008. Epithelial cells remove apoptotic epithelial cells during post-lactation involution of the mouse mammary gland. *Biology of reproduction,* 78, 586-94.

MONTEFUSCO, M. C., MERLO, K., BRYAN, C. D., SURKS, H. K., REIS, S. E., MENDELSOHN, M. E. & HUGGINS, G. S. 2010. Little ROCK is a ROCK1 pseudogene expressed in human smooth muscle cells. *BMC Genet,* 11, 22.

MORIMOTO, K., AMANO, H., SONODA, F., BABA, M., SENBA, M., YOSHIMINE, H., YAMAMOTO, H., II, T., OISHI, K. & NAGATAKE, T. 2001. Alveolar macrophages that phagocytose apoptotic neutrophils produce hepatocyte growth factor during bacterial pneumonia in mice. *Am J Respir Cell Mol Biol,* 24, 608-15.

MORTON, J. P. & SANSOM, O. J. 2013. MYC-y mice: from tumour initiation to therapeutic targeting of endogenous MYC. *Mol Oncol,* 7, 248-58.

MURAKAMI, T. & ISHIKAWA, H. 1991. Stress fibers in situ in proximal tubules of the rat kidney. *Cell Struct Funct,* 16, 231-40.

NAGATA, S., HANAYAMA, R. & KAWANE, K. 2010. Autoimmunity and the clearance of dead cells. *Cell,* 140, 619-30.

NAKAGAWA, O., FUJISAWA, K., ISHIZAKI, T., SAITO, Y., NAKAO, K. & NARUMIYA, S. 1996. ROCK-I and ROCK-II, two isoforms of Rho-associated coiled-coil forming protein serine/threonine kinase in mice. *FEBS Lett,* 392, 189-93.

NAKATANI, T., ROY, G., FUJIMOTO, N., ASAHARA, T. & ITO, A. 2001. Sex hormone dependency of diethylnitrosamine-induced liver tumors in mice and chemoprevention by leuprorelin. *Jpn J Cancer Res,* 92, 249-56.

NANDROT, E. F., KIM, Y., BRODIE, S. E., HUANG, X., SHEPPARD, D. & FINNEMANN, S. C. 2004. Loss of synchronized retinal phagocytosis and age-related blindness in mice lacking alphavbeta5 integrin. *J Exp Med,* 200, 1539-45.

NAUGLER, W. E., SAKURAI, T., KIM, S., MAEDA, S., KIM, K., ELSHARKAWY, A. M. & KARIN, M. 2007. Gender disparity in liver cancer due to sex differences in MyD88-dependent IL-6 production. *Science,* 317, 121-4.

NAVRATIL, J. S., WATKINS, S. C., WISNIESKI, J. J. & AHEARN, J. M. 2001. The globular heads of C1q specifically recognize surface blebs of apoptotic vascular endothelial cells. *Journal of immunology (Baltimore, Md. : 1950),* 166, 3231-9.

NEUMAN, M., ANGULO, P., MALKIEWICZ, I., JORGENSEN, R., SHEAR, N., DICKSON, E. R., HABER, J., KATZ, G. & LINDOR, K. 2002. Tumor necrosis factor-alpha and transforming growth factor-beta reflect severity of liver damage in primary biliary cirrhosis. *J Gastroenterol Hepatol,* 17, 196-202.

NEUMAN, M. G., BENHAMOU, J. P., MARCELLIN, P., VALLA, D., MALKIEWICZ, I. M., KATZ, G. G., TREPO, C., BOURLIERE, M., CAMERON, R. G., COHEN, L., MORGAN, M., SCHMILOVITZ-WEISS, H. & BEN-ARI, Z. 2007. Cytokine--chemokine and apoptotic signatures in patients with hepatitis C. *Transl Res,* 149**,** 126-36.

NICHOLSON, D. W., ALI, A., THORNBERRY, N. A., VAILLANCOURT, J. P., DING, C. K., GALLANT, M., GAREAU, Y., GRIFFIN, P. R., LABELLE, M., LAZEBNIK, Y. A. & ET AL. 1995. Identification and inhibition of the ICE/CED-3 protease necessary for mammalian apoptosis. *Nature,* 376**,** 37-43.

NIJHAWAN, D., HONARPOUR, N. & WANG, X. 2000. Apoptosis in neural development and disease. *Annu Rev Neurosci,* 23**,** 73-87.

NISHIKAWA, H. & SAKAGUCHI, S. 2010. Regulatory T cells in tumor immunity. *Int J Cancer,* 127**,** 759-67.

NOBES, C. D., LAURITZEN, I., MATTEI, M. G., PARIS, S., HALL, A. & CHARDIN, P. 1998. A new member of the Rho family, Rnd1, promotes disassembly of actin filament structures and loss of cell adhesion. *J Cell Biol,* 141**,** 187-97.

NOHRIA, A., GRUNERT, M. E., RIKITAKE, Y., NOMA, K., PRSIC, A., GANZ, P., LIAO, J. K. & CREAGER, M. A. 2006. Rho kinase inhibition improves endothelial function in human subjects with coronary artery disease. *Circ Res,* 99**,** 1426-1432.

NOMA, K., GOTO, C., NISHIOKA, K., JITSUIKI, D., UMEMURA, T., UEDA, K., KIMURA, M., NAKAGAWA, K., OSHIMA, T., CHAYAMA, K., YOSHIZUMI, M., LIAO, J. K. & HIGASHI, Y. 2007. Roles of rho-associated kinase and oxidative stress in the pathogenesis of aortic stiffness. *J Am Coll Cardiol,* 49**,** 698-705.

OGDEN, C. A., DECATHELINEAU, A., HOFFMANN, P. R., BRATTON, D., GHEBREHIWET, B., FADOK, V. A. & HENSON, P. M. 2001. C1q and mannose binding lectin engagement of cell surface calreticulin and CD91 initiates macropinocytosis and uptake of apoptotic cells. *J Exp Med,* 194**,** 781-95.

OGIKU, M., KONO, H., HARA, M., TSUCHIYA, M. & FUJII, H. 2011. Glycyrrhizin prevents liver injury by inhibition of high-mobility group box 1 production by Kupffer cells after ischemia-reperfusion in rats. *J Pharmacol Exp Ther,* 339**,** 93-8.

OHASHI, K., HOSOYA, T., TAKAHASHI, K., HING, H. & MIZUNO, K. 2000. A Drosophila Homolog of LIM-Kinase Phosphorylates Cofilin and Induces Actin Cytoskeletal Reorganization. *Biochemical and Biophysical Research Communications,* 276**,** 1178-1185.

OHATA, K., HAMASAKI, K., TORIYAMA, K., MATSUMOTO, K., SAEKI, A., YANAGI, K., ABIRU, S., NAKAGAWA, Y., SHIGENO, M., MIYAZOE, S., ICHIKAWA, T., ISHIKAWA, H., NAKAO, K. & EGUCHI, K. 2003. Hepatic steatosis is a risk factor for hepatocellular carcinoma in patients with chronic hepatitis C virus infection. *Cancer,* 97**,** 3036-3043.

OLD, L. J. & BOYSE, E. A. 1966. Specific antigens of tumors and leukemias of experimental animals. *Med Clin North Am,* 50**,** 901-12.

OLD, L. J. & CHEN, Y. T. 1998. New paths in human cancer serology. *J Exp Med,* 187**,** 1163-7.

OLSON, M. F. 2008. Applications for ROCK kinase inhibition. *Current Opinion in Cell Biology,* 20**,** 242-248.

OPFERMAN, J. T. & KORSMEYER, S. J. 2003. Apoptosis in the development and maintenance of the immune system. *Nat Immunol,* 4**,** 410-5.

OPFERMAN, J. T., LETAI, A., BEARD, C., SORCINELLI, M. D., ONG, C. C. & KORSMEYER, S. J. 2003. Development and maintenance of B and T lymphocytes requires antiapoptotic MCL-1. *Nature,* 426**,** 671-6.

ORLANDO, K. A., STONE, N. L. & PITTMAN, R. N. 2006. Rho kinase regulates fragmentation and phagocytosis of apoptotic cells. *Experimental Cell Research,* 312**,** 5-15.

PARENT, N., SANÃ©, A.-T., DROIN, N. & BERTRAND, R. 2005. Procaspase-2S inhibits procaspase-3 processing and activation, preventing ROCK-1-mediated apoptotic blebbing and body formation in human B lymphoma Namalwa cells. *Apoptosis : an international journal on programmed cell death,* 10**,** 313-22.

PARK, D., TOSELLO-TRAMPONT, A. C., ELLIOTT, M. R., LU, M., HANEY, L. B., MA, Z., KLIBANOV, A. L., MANDELL, J. W. & RAVICHANDRAN, K. S. 2007. BAI1 is an engulfment receptor for apoptotic cells upstream of the ELMO/Dock180/Rac module. *Nature,* 450**,** 430-4.

PARK, E. J., LEE, J. H., YU, G. Y., HE, G. B., ALI, S. R., HOLZER, R. G., OSTERREICHER, C. H., TAKAHASHI, H. & KARIN, M. 2010. Dietary and Genetic Obesity Promote Liver Inflammation and Tumorigenesis by Enhancing IL-6 and TNF Expression. *Cell,* 140**,** 197-208.

PARK, S. Y., JUNG, M. Y., KIM, H. J., LEE, S. J., KIM, S. Y., LEE, B. H., KWON, T. H., PARK, R. W. & KIM, I. S. 2008a. Rapid cell corpse clearance by stabilin-2, a membrane phosphatidylserine receptor. *Cell Death Differ,* 15**,** 192-201.

PARK, S. Y., KANG, K. B., THAPA, N., KIM, S. Y., LEE, S. J. & KIM, I. S. 2008b. Requirement of adaptor protein GULP during stabilin-2-mediated cell corpse engulfment. *J Biol Chem,* 283**,** 10593-600.

PARKIN, D. M. 2006. The global health burden of infection-associated cancers in the year 2002. *Int J Cancer,* 118**,** 3030-44.

PELOSI, M., MARAMPON, F., ZANI, B. M., PRUDENTE, S., PERLAS, E., CAPUTO, V., CIANETTI, L., BERNO, V., NARUMIYA, S., KANG, S. W., MUSARO, A. & ROSENTHAL, N. 2007. ROCK2 and its alternatively spliced isoform ROCK2m positively control the maturation of the myogenic program. *Mol Cell Biol,* 27**,** 6163-76.

PENN, I. & STARZL, T. E. 1970. Malignant lymphomas in transplantation patients: a review of the world experience. *Int Z Klin Pharmakol Ther Toxikol,* 3**,** 49-54.

PERNIOK, A., WEDEKIND, F., HERRMANN, M., SPECKER, C. & SCHNEIDER, M. 1998. High levels of circulating early apoptic peripheral blood mononuclear cells in systemic lupus erythematosus. *Lupus,* 7**,** 113-118.

PETER, C., WAIBEL, M., RADU, C. G., YANG, L. V., WITTE, O. N., SCHULZE-OSTHOFF, K., WESSELBORG, S. & LAUBER, K. 2008. Migration to apoptotic "find-me" signals is mediated via the phagocyte receptor G2A. *The Journal of biological chemistry,* 283**,** 5296-305.

PEVERILL, W., POWELL, L. W. & SKOIEN, R. 2014. Evolving concepts in the pathogenesis of NASH: beyond steatosis and inflammation. *Int J Mol Sci,* 15**,** 8591-638.

PINNER, S. & SAHAI, E. 2008. PDK1 regulates cancer cell motility by antagonising inhibition of ROCK1 by RhoE. *Nat Cell Biol,* 10**,** 127-37.

PLATT, N., SUZUKI, H., KODAMA, T. & GORDON, S. 2000. Apoptotic thymocyte clearance in scavenger receptor class A-deficient mice is apparently normal. *J Immunol,* 164**,** 4861-7.

POON, I. K., LUCAS, C. D., ROSSI, A. G. & RAVICHANDRAN, K. S. 2014. Apoptotic cell clearance: basic biology and therapeutic potential. *Nat Rev Immunol,* 14**,** 166-80.

QI, Y., CHEN, X., CHAN, C. Y., LI, D., YUAN, C., YU, F., LIN, M. C., YEW, D. T., KUNG, H. F. & LAI, L. 2008. Two-dimensional differential gel electrophoresis/analysis of diethylnitrosamine induced rat hepatocellular carcinoma. *Int J Cancer,* 122**,** 2682-8.

RAMACHANDRAN, R. & KAKAR, S. 2009. Histological patterns in drug-induced liver disease. *J Clin Pathol,* 62**,** 481-92.

RAMAIAH, S. K. & JAESCHKE, H. 2007. Role of neutrophils in the pathogenesis of acute inflammatory liver injury. *Toxicol Pathol,* 35**,** 757-66.

RAN, S., HE, J., HUANG, X., SOARES, M., SCOTHORN, D. & THORPE, P. E. 2005. Antitumor effects of a monoclonal antibody that binds anionic phospholipids on the surface of tumor blood vessels in mice. *Clin Cancer Res,* 11**,** 1551-62.

RANA, M. K. & WORTHYLAKE, R. A. 2012. Novel mechanism for negatively regulating Rho-kinase (ROCK) signaling through Coronin1B protein in neuregulin 1 (NRG-1)-induced tumor cell motility. *J Biol Chem,* 287**,** 21836-45.

RAUTOU, P. E., VION, A. C., AMABILE, N., CHIRONI, G., SIMON, A., TEDGUI, A. & BOULANGER, C. M. 2011. Microparticles, vascular function, and atherothrombosis. *Circulation Research,* 109**,** 593-606.

RAWLING, J. M., DRISCOLL, E. R., POIRIER, G. G. & KIRKLAND, J. B. 1993. Diethylnitrosamine administration in vivo increases hepatic poly(ADP-ribose) levels in rats: results of a modified technique for poly(ADP-ribose) measurement. *Carcinogenesis,* 14**,** 2513-6.

REDDIEN, P. W., CAMERON, S. & HORVITZ, H. R. 2001. Phagocytosis promotes programmed cell death in C. elegans. *Nature,* 412**,** 198-202.

REDDIEN, P. W. & HORVITZ, H. R. 2000. CED-2/CrkII and CED-10/Rac control phagocytosis and cell migration in Caenorhabditis elegans. *Nat Cell Biol,* 2**,** 131-6.

RIEDL, J., CREVENNA, A. H., KESSENBROCK, K., YU, J. H., NEUKIRCHEN, D., BISTA, M., BRADKE, F., JENNE, D., HOLAK, T. A., WERB, Z., SIXT, M. & WEDLICH-SOLDNER, R. 2008. Lifeact: a versatile marker to visualize F-actin. *Nat Methods,* 5**,** 605-607.

RIENTO, K., GUASCH, R. M., GARG, R., JIN, B. & RIDLEY, A. J. 2003. RhoE binds to ROCK I and inhibits downstream signaling. *Mol Cell Biol,* 23**,** 4219-29.

RIENTO, K. & RIDLEY, A. J. 2003. Rocks: multifunctional kinases in cell behaviour. *Nat Rev Mol Cell Biol,* 4**,** 446-56.

RIENTO, K., TOTTY, N., VILLALONGA, P., GARG, R., GUASCH, R. & RIDLEY, A. J. 2005. RhoE function is regulated by ROCK I-mediated phosphorylation. *Embo J,* 24**,** 1170-80.

ROBERTS, R. A., GANEY, P. E., JU, C., KAMENDULIS, L. M., RUSYN, I. & KLAUNIG, J. E. 2007. Role of the Kupffer cell in mediating hepatic toxicity and carcinogenesis. *Toxicol Sci,* 96**,** 2-15.

RODRIGUEZ-MANZANET, R., SANJUAN, M. A., WU, H. Y., QUINTANA, F. J., XIAO, S., ANDERSON, A. C., WEINER, H. L., GREEN, D. R. & KUCHROO, V. K. 2010. T and B cell hyperactivity and autoimmunity associated with niche-specific defects in apoptotic body clearance in TIM-4-deficient mice. *Proc Natl Acad Sci U S A,* 107**,** 8706-11.

ROSEN, H. & GOETZL, E. J. 2005. Sphingosine 1-phosphate and its receptors: an autocrine and paracrine network. *Nat Rev Immunol,* 5**,** 560-70.

ROSENBERG, S. A. 1999. A new era for cancer immunotherapy based on the genes that encode cancer antigens. *Immunity,* 10**,** 281-7.

RUMORE, P. M. & STEINMAN, C. R. 1990. Endogenous circulating DNA in systemic lupus erythematosus. Occurrence as multimeric complexes bound to histone. *J Clin Invest,* 86**,** 69-74.

SAH, V. P., ATTARDI, L. D., MULLIGAN, G. J., WILLIAMS, B. O., BRONSON, R. T. & JACKS, T. 1995. A subset of p53-deficient embryos exhibit exencephaly. *Nat Genet,* 10**,** 175-80.

SAHAI, E. & MARSHALL, C. J. 2003. Differing modes of tumour cell invasion have distinct requirements for Rho/ROCK signalling and extracellular proteolysis. *Nat Cell Biol,* 5**,** 711-9.

SAITO, K., OZAWA, Y., HIBINO, K. & OHTA, Y. 2012. FilGAP, a Rho/Rho-associated protein kinase-regulated GTPase-activating protein for Rac, controls tumor cell migration. *Mol Biol Cell,* 23**,** 4739-50.

SAKAGUCHI, S. 2002. Immunologic tolerance maintained by regulatory T cells: implications for autoimmunity, tumor immunity and transplantation tolerance. *Vox Sang,* 83 Suppl 1**,** 151-3.

SAMUEL, M. S. & OLSON, M. F. 2010. Dying alone: A tale of Rho. *Cell Stem Cell,* 7**,** 135-136.

SANYAL, A. J., YOON, S. K. & LENCIONI, R. 2010. The etiology of hepatocellular carcinoma and consequences for treatment. *Oncologist,* 15 Suppl 4**,** 14-22.

SANZ-MORENO, V., GADEA, G., AHN, J., PATERSON, H., MARRA, P., PINNER, S., SAHAI, E. & MARSHALL, C. J. 2008. Rac activation and inactivation control plasticity of tumor cell movement. *Cell,* 135**,** 510-523.

SAPET, C. D., SIMONCINI, S. P., LORIOD, B. A., PUTHIER, D., SAMPOL, J., NGUYEN, C., DIGNAT-GEORGE, F. O. & ANFOSSO, F. 2006. Thrombin-induced endothelial microparticle generation: identification of a novel pathway involving ROCK-II activation by caspase-2. *Blood,* 108**,** 1868-76.

SCAFFIDI, P., MISTELI, T. & BIANCHI, M. E. 2002. Release of chromatin protein HMGB1 by necrotic cells triggers inflammation. *Nature,* 418**,** 191-195.

SCHACHTNER, H., LI, A., STEVENSON, D., CALAMINUS, S. D., THOMAS, S. G., WATSON, S. P., SIXT, M., WEDLICH-SOLDNER, R., STRATHDEE, D. & MACHESKY, L. M. 2012. Tissue inducible Lifeact expression allows visualization of actin dynamics in vivo and ex vivo. *Eur J Cell Biol,* 91**,** 923-9.

SCHACKMANN, R. C. J., VAN AMERSFOORT, M., HAARHUIS, J. H. I., VLUG, E. J., HALIM, V. A., ROODHART, J. M. L., VERMAAT, J. S., VOEST, E. E., VAN DER GROEP, P., VAN DIEST, P. J., JONKERS, J. & DERKSEN, P. W. B. 2011. Cytosolic p120-catenin regulates growth of metastatic lobular carcinoma through Rock1-mediated anoikis resistance. *Journal of Clinical Investigation,* 121**,** 3176-3188.

SCHILLER, H. B., HERMANN, M. R., POLLEUX, J., VIGNAUD, T., ZANIVAN, S., FRIEDEL, C. C., SUN, Z., RADUCANU, A., GOTTSCHALK, K. E., THERY, M., MANN, M. & FASSLER, R. 2013. beta1- and alphav-class integrins cooperate to regulate myosin II during rigidity sensing of fibronectin-based microenvironments. *Nat Cell Biol,* 15**,** 625-36.

SCHREIBER, R. D., OLD, L. J. & SMYTH, M. J. 2011. Cancer immunoediting: integrating immunity's roles in cancer suppression and promotion. *Science,* 331**,** 1565-70.

SCHWARZ, M., BUCHMANN, A. & BOCK, K. W. 1995. Role of cell proliferation at early stages of hepatocarcinogenesis. *Toxicol Lett,* 82-83**,** 27-32.

SCOTT, R. W. & OLSON, M. F. 2007. LIM kinases: function, regulation and association with human disease. *J Mol Med,* 85**,** 555-68.

SEBBAGH, M., HAMELIN, J., BERTOGLIO, J., SOLARY, E. & BREARD, J. 2005. Direct cleavage of ROCK II by granzyme B induces target cell membrane blebbing in a caspase-independent manner. *J Exp Med,* 201**,** 465-71.

SEBBAGH, M., RENVOIZE, C., HAMELIN, J., RICHE, N., BERTOGLIO, J., BREARD, J., RENVOIZÃ©, C., RICHÃ©, N. & BRÃ©ARD, J. 2001. Caspase-3-mediated cleavage of ROCK I induces MLC phosphorylation and apoptotic membrane blebbing. *Nature cell biology,* 3**,** 346-52.

SEGAWA, K., KURATA, S., YANAGIHASHI, Y., BRUMMELKAMP, T. R., MATSUDA, F. & NAGATA, S. 2014. Caspase-mediated cleavage of phospholipid flippase for apoptotic phosphatidylserine exposure. *Science,* 344**,** 1164-8.

SHI, J., WU, X., SURMA, M., VEMULA, S., ZHANG, L., YANG, Y., KAPUR, R. & WEI, L. 2013. Distinct roles for ROCK1 and ROCK2 in the regulation of cell detachment. *Cell Death Dis,* 4**,** e483.

SHI, J., ZHANG, L. & WEI, L. 2011. Rho-kinase in development and heart failure: Insights from genetic models. *Pediatric Cardiology,* 32**,** 297-304.

SHIMIZU, T., IHARA, K., MAESAKI, R., AMANO, M., KAIBUCHI, K. & HAKOSHIMA, T. 2003. Parallel coiled-coil association of the RhoA-binding domain in Rho-kinase. *J Biol Chem,* 278**,** 46046-51.

SHIMIZU, Y., THUMKEO, D., KEEL, J., ISHIZAKI, T., OSHIMA, H., OSHIMA, M., NODA, Y., MATSUMURA, F., TAKETO, M. M. & NARUMIYA, S. 2005. ROCK-I regulates closure of the eyelids and ventral body wall by inducing assembly of actomyosin bundles. *J Cell Biol,* 168**,** 941-53.

SHIRAO, S., KASHIWAGI, S., SATO, M., MIWA, S., NAKAO, F., KUROKAWA, T., TODOROKI-IKEDA, N., MOGAMI, K., MIZUKAMI, Y., KURIYAMA, S., HAZE, K., SUZUKI, M. & KOBAYASHI, S. 2002. Sphingosylphosphorylcholine is a novel messenger for Rho-kinase-mediated Ca2+ sensitization in the bovine cerebral artery: unimportant role for protein kinase C. *Circ Res,* 91**,** 112-119.

SIMS, G. P., ROWE, D. C., RIETDIJK, S. T., HERBST, R. & COYLE, A. J. 2010. HMGB1 and RAGE in inflammation and cancer. *Annu Rev Immunol,* 28**,** 367-88.

SIN, W. C., CHEN, X. Q., LEUNG, T. & LIM, L. 1998. RhoA-binding kinase alpha translocation is facilitated by the collapse of the vimentin intermediate filament network. *Mol Cell Biol,* 18**,** 6325-39.

SINNING, J. M., LOSCH, J., WALENTA, K., BÖHM, M., NICKENIG, G. & WERNER, N. 2011. Circulating CD31 +/Annexin V + microparticles correlate with cardiovascular outcomes. *European Heart Journal,* 32**,** 2034-2041.

SITIA, G., IANNACONE, M., MULLER, S., BIANCHI, M. E. & GUIDOTTI, L. G. 2007. Treatment with HMGB1 inhibitors diminishes CTL-induced liver disease in HBV transgenic mice. *J Leukoc Biol,* 81**,** 100-7.

SMITH, M. L., YELESWARAPU, L., LOCKER, J. & LOMBARDI, B. 1991. Expression of p53 mutant protein(s) in diethylnitrosamine-induced foci of enzyme-altered hepatocytes in male Fischer-344 rats. *Carcinogenesis,* 12**,** 1137-41.

SOMLYO, A. P. & SOMLYO, A. V. 1994. Signal transduction and regulation in smooth muscle. *Nature,* 372**,** 231-6.

SOMLYO, A. P. & SOMLYO, A. V. 2003. Ca2+ sensitivity of smooth muscle and nonmuscle myosin II: modulated by G proteins, kinases, and myosin phosphatase. *Physiol Rev,* 83**,** 1325-1358.

SOUCEK, L. & EVAN, G. I. 2010. The ups and downs of Myc biology. *Curr Opin Genet Dev,* 20**,** 91-5.

STROEKEN, P. J., ALVAREZ, B., VAN RHEENEN, J., WIJNANDS, Y. M., GEERTS, D., JALINK, K. & ROOS, E. 2006. Integrin cytoplasmic domain-associated protein-1 (ICAP-1) interacts with the ROCK-I kinase at the plasma membrane. *J Cell Physiol,* 208**,** 620-8.

STUART, L. M., TAKAHASHI, K., SHI, L., SAVILL, J. & EZEKOWITZ, R. A. 2005. Mannose-binding lectin-deficient mice display defective apoptotic cell clearance but no autoimmune phenotype. *J Immunol,* 174**,** 3220-6.

SU, H. P., NAKADA-TSUKUI, K., TOSELLO-TRAMPONT, A. C., LI, Y., BU, G., HENSON, P. M. & RAVICHANDRAN, K. S. 2002. Interaction of CED-6/GULP, an adapter protein involved in engulfment of apoptotic cells with CED-1 and CD91/low density lipoprotein receptor-related protein (LRP). *J Biol Chem,* 277**,** 11772-9.

SU, J. H., ANDERSON, A. J., CUMMINGS, B. J. & COTMAN, C. W. 1994. Immunohistochemical evidence for apoptosis in Alzheimer's disease. *Neuroreport,* 5**,** 2529-33.

SUGIMOTO, K., FUJII, S. & YAMASHITA, K. 1991. Expression of stress fibers in bullfrog mesothelial cells in response to tension. *Exp Cell Res,* 196**,** 353-61.

SUMI, T., MATSUMOTO, K. & NAKAMURA, T. 2001. Specific activation of LIM kinase 2 via phosphorylation of threonine 505 by ROCK, a Rho-dependent protein kinase. *J Biol Chem,* 276**,** 670-6.

SURMA, M., WEI, L. & SHI, J. 2011. Rho kinase as a therapeutic target in cardiovascular disease. *Future Cardiology,* 7**,** 657-671.

SUTTIE, A. W. 2006. Histopathology of the spleen. *Toxicol Pathol,* 34**,** 466-503.

SUZUKI, J., DENNING, D. P., IMANISHI, E., HORVITZ, H. R. & NAGATA, S. 2013. Xk-related protein 8 and CED-8 promote phosphatidylserine exposure in apoptotic cells. *Science,* 341**,** 403-6.

SUZUKI, J., UMEDA, M., SIMS, P. J. & NAGATA, S. 2010. Calcium-dependent phospholipid scrambling by TMEM16F. *Nature,* 468**,** 834-8.

SWANN, J. B. & SMYTH, M. J. 2007. Immune surveillance of tumors. *J Clin Invest,* 117**,** 1137-46.

SWARD, K., DREJA, K., SUSNJAR, M., HELLSTRAND, P., HARTSHORNE, D. J. & WALSH, M. P. 2000. Inhibition of Rho-associated kinase blocks agonist-induced Ca2+ sensitization of myosin phosphorylation and force in guinea-pig ileum. *J Physiol,* 522 Pt 1**,** 33-49.

TABAS, I. 2010. Macrophage death and defective inflammation resolution in atherosclerosis. *Nat Rev Immunol,* 10**,** 36-46.

TAKEDA, N., KONDO, M., ITO, S., ITO, Y., SHIMOKATA, K. & KUME, H. 2006. Role of RhoA inactivation in reduced cell proliferation of human airway smooth muscle by simvastatin. *Am J Respir Cell Mol Biol,* 35**,** 722-9.

TANAKA, H., YOSHIZAWA, H., YAMAGUCHI, Y., ITO, K., KAGAMU, H., SUZUKI, E., GEJYO, F., HAMADA, H. & ARAKAWA, M. 1999. Successful adoptive immunotherapy of murine poorly immunogenic tumor with specific effector cells generated from gene-modified tumor-primed lymph node cells. *J Immunol,* 162**,** 3574-82.

TANAKA, T., NISHIMURA, D., WU, R. C., AMANO, M., ISO, T., KEDES, L., NISHIDA, H., KAIBUCHI, K. & HAMAMORI, Y. 2006. Nuclear Rho kinase, ROCK2, targets p300 acetyltransferase. *J Biol Chem,* 281**,** 15320-9.

TENG, M. W., VESELY, M. D., DURET, H., MCLAUGHLIN, N., TOWNE, J. E., SCHREIBER, R. D. & SMYTH, M. J. 2012. Opposing roles for IL-23 and IL-12 in maintaining occult cancer in an equilibrium state. *Cancer Res,* 72**,** 3987-96.

THEOFILOPOULOS, A. N. & DIXON, F. J. 1985. Murine models of systemic lupus erythematosus. *Adv Immunol,* 37**,** 269-390.

THOMAS, L. B., GATES, D. J., RICHFIELD, E. K., O'BRIEN, T. F., SCHWEITZER, J. B. & STEINDLER, D. A. 1995. DNA end labeling (TUNEL) in Huntington's disease and other neuropathological conditions. *Exp Neurol,* 133**,** 265-72.

THORP, E., CUI, D., SCHRIJVERS, D. M., KURIAKOSE, G. & TABAS, I. 2008. Mertk receptor mutation reduces efferocytosis efficiency and promotes apoptotic cell accumulation and plaque necrosis in atherosclerotic lesions of apoe-/- mice. *Arterioscler Thromb Vasc Biol,* 28**,** 1421-8.

THUMKEO, D., KEEL, J., ISHIZAKI, T., HIROSE, M., NONOMURA, K., OSHIMA, H., OSHIMA, M., TAKETO, M. M. & NARUMIYA, S. 2003. Targeted disruption of the mouse rho-associated kinase 2 gene results in intrauterine growth retardation and fetal death. *Mol Cell Biol,* 23**,** 5043-55.

THUMKEO, D., SHIMIZU, Y., SAKAMOTO, S., YAMADA, S. & NARUMIYA, S. 2005. ROCK-I and ROCK-II cooperatively regulate closure of eyelid and ventral body wall in mouse embryo. *Genes Cells,* 10**,** 825-34.

TILG, H., WILMER, A., VOGEL, W., HEROLD, M., NOLCHEN, B., JUDMAIER, G. & HUBER, C. 1992. Serum levels of cytokines in chronic liver diseases. *Gastroenterology,* 103**,** 264-74.

TILLY, J. L., KOWALSKI, K. I., JOHNSON, A. L. & HSUEH, A. J. 1991. Involvement of apoptosis in ovarian follicular atresia and postovulatory regression. *Endocrinology,* 129**,** 2799-801.

TOGAWA, J., NAGASE, H., TANAKA, K., INAMORI, M., NAKAJIMA, A., UENO, N., SAITO, T. & SEKIHARA, H. 2002. Oral administration of lactoferrin reduces colitis in rats via modulation of the immune system and correction of cytokine imbalance. *J Gastroenterol Hepatol,* 17**,** 1291-8.

TOKUSHIGE, H., INATANI, M., NEMOTO, S., SAKAKI, H., KATAYAMA, K., UEHATA, M. & TANIHARA, H. 2007. Effects of topical administration of y-39983, a selective rho-associated protein kinase inhibitor, on ocular tissues in rabbits and monkeys. *Invest Ophthalmol Vis Sci,* 48**,** 3216-22.

TOTSUKAWA, G., YAMAKITA, Y., YAMASHIRO, S., HARTSHORNE, D. J., SASAKI, Y. & MATSUMURA, F. 2000. Distinct roles of ROCK (Rho-kinase) and MLCK in spatial regulation of MLC phosphorylation for assembly of stress fibers and focal adhesions in 3T3 fibroblasts. *J Cell Biol,* 150**,** 797-806.

TRIULZI, T., TAGLIABUE, E., BALSARI, A. & CASALINI, P. 2013. FOXP3 expression in tumor cells and implications for cancer progression. *J Cell Physiol,* 228**,** 30-5.

TRUMAN, L. A., FORD, C. A., PASIKOWSKA, M., POUND, J. D., WILKINSON, S. J., DUMITRIU, I. E., MELVILLE, L., MELROSE, L. A., OGDEN, C. A., NIBBS, R., GRAHAM, G., COMBADIERE, C. & GREGORY, C. D. 2008. CX3CL1/fractalkine is released from apoptotic lymphocytes to stimulate macrophage chemotaxis. *Blood,* 112**,** 5026-36.

TU, D., LI, Y., SONG, H. K., TOMS, A. V., GOULD, C. J., FICARRO, S. B., MARTO, J. A., GOODE, B. L. & ECK, M. J. 2011. Crystal structure of a coiled-coil domain from human ROCK I. *PLoS One,* 6**,** e18080.

UEHARA, T., POGRIBNY, I. P. & RUSYN, I. 2014. The DEN and CCl4 -Induced Mouse Model of Fibrosis and Inflammation-Associated Hepatocellular Carcinoma. *Curr Protoc Pharmacol,* 66**,** 14 30 1-14 30 10.

UEHATA, M., ISHIZAKI, T., SATOH, H., ONO, T., KAWAHARA, T., MORISHITA, T., TAMAKAWA, H., YAMAGAMI, K., INUI, J., MAEKAWA, M. & NARUMIYA, S. 1997. Calcium sensitization of smooth muscle mediated by a Rho-associated protein kinase in hypertension. *Nature,* 389**,** 990-4.

UNDERHILL, D. M. & GOODRIDGE, H. S. 2012. Information processing during phagocytosis. *Nat Rev Immunol,* 12**,** 492-502.

VANDENABEELE, P., GALLUZZI, L., VANDEN BERGHE, T. & KROEMER, G. 2010. Molecular mechanisms of necroptosis: an ordered cellular explosion. *Nat Rev Mol Cell Biol,* 11**,** 700-714.

VANDIVIER, R. W., RICHENS, T. R., HORSTMANN, S. A., DECATHELINEAU, A. M., GHOSH, M., REYNOLDS, S. D., XIAO, Y. Q., RICHES, D. W., PLUMB, J., VACHON, E., DOWNEY, G. P. & HENSON, P. M. 2009. Dysfunctional cystic fibrosis transmembrane conductance regulator inhibits phagocytosis of apoptotic cells with proinflammatory consequences. *Am J Physiol Lung Cell Mol Physiol,* 297**,** L677-86.

VARLEY, J. M. 2003. Germline TP53 mutations and Li-Fraumeni syndrome. *Hum Mutat,* 21**,** 313-20.

VERNA, L., WHYSNER, J. & WILLIAMS, G. M. 1996. N-nitrosodiethylamine mechanistic data and risk assessment: bioactivation, DNA-adduct formation, mutagenicity, and tumor initiation. *Pharmacol Ther,* 71**,** 57-81.

VESSELINOVITCH, S. D., KOKA, M., MIHAILOVICH, N. & RAO, K. V. 1984. Carcinogenicity of diethylnitrosamine in newborn, infant, and adult mice. *J Cancer Res Clin Oncol,* 108**,** 60-5.

VICENTE-MANZANARES, M., MA, X., ADELSTEIN, R. S. & HORWITZ, A. R. 2009. Non-muscle myosin II takes centre stage in cell adhesion and migration. *Nat Rev Mol Cell Biol,* 10**,** 778-90.

VIVIER, E., UGOLINI, S., BLAISE, D., CHABANNON, C. & BROSSAY, L. 2012. Targeting natural killer cells and natural killer T cells in cancer. *Nat Rev Immunol,* 12**,** 239-52.

VOLL, R. E., HERRMANN, M., ROTH, E. A., STACH, C., KALDEN, J. R. & GIRKONTAITE, I. 1997. Immunosuppressive effects of apoptotic cells. *Nature,* 390**,** 350-351.

VOUSDEN, K. H. & PRIVES, C. 2009. Blinded by the Light: The Growing Complexity of p53. *Cell,* 137**,** 413-431.

WANG, H., BLOOM, O., ZHANG, M., VISHNUBHAKAT, J. M., OMBRELLINO, M., CHE, J., FRAZIER, A., YANG, H., IVANOVA, S., BOROVIKOVA, L., MANOGUE, K. R., FAIST, E., ABRAHAM, E., ANDERSSON, J., ANDERSSON, U., MOLINA, P. E., ABUMRAD, N. N., SAMA, A. & TRACEY, K. J. 1999. HMG-1 as a late mediator of endotoxin lethality in mice. *Science,* 285**,** 248-51.

WANG, X., SUN, R., WEI, H. & TIAN, Z. 2013. High-mobility group box 1 (HMGB1)-Toll-like receptor (TLR)4-interleukin (IL)-23-IL-17A axis in drug-induced damage-associated lethal hepatitis: Interaction of gammadelta T cells with macrophages. *Hepatology,* 57**,** 373-84.

WARD, Y., YAP, S. F., RAVICHANDRAN, V., MATSUMURA, F., ITO, M., SPINELLI, B. & KELLY, K. 2002. The GTP binding proteins Gem and Rad are negative regulators of the Rho- Rho kinase pathway. *J Cell Biol,* 157**,** 291-302.

WATANABE, N., KATO, T., FUJITA, A., ISHIZAKI, T. & NARUMIYA, S. 1999. Cooperation between mDia1 and ROCK in Rho-induced actin reorganization. *Nat Cell Biol,* 1**,** 136-43.

WEI, L., ROBERTS, W., WANG, L., YAMADA, M., ZHANG, S., ZHAO, Z., RIVKEES, S. A., SCHWARTZ, R. J. & IMANAKA-YOSHIDA, K. 2001. Rho kinases play an obligatory role in vertebrate embryonic organogenesis. *Development,* 128**,** 2953-62.

WEN, W., LIU, W., YAN, J. & ZHANG, M. 2008. Structure Basis and Unconventional Lipid Membrane Binding Properties of the PH-C1 Tandem of Rho Kinases. *J. Biol. Chem.,* 283**,** 26263-26273.

WICKMAN, G., JULIAN, L. & OLSON, M. F. 2012. How apoptotic cells aid in the removal of their own cold dead bodies. *Cell death and differentiation,* 19**,** 735-742.

WICKMAN, G. R., JULIAN, L., MARDILOVICH, K., SCHUMACHER, S., MUNRO, J., RATH, N., ZANDER, S. A., MLECZAK, A., SUMPTON, D., MORRICE, N., BIENVENUT, W. V. & OLSON, M. F. 2013. Blebs produced by actin-myosin contraction during apoptosis release damage-associated molecular pattern proteins before secondary necrosis occurs. *Cell Death Differ,* 20**,** 1293-305.

WILKINSON, S., PATERSON, H. F. & MARSHALL, C. J. 2005. Cdc42-MRCK and Rho-ROCK signalling cooperate in myosin phosphorylation and cell invasion. *Nat Cell Biol,* 7**,** 255-61.

WILLIAMS, G. M., IATROPOULOS, M. J., WANG, C. X., ALI, N., RIVENSON, A., PETERSON, L. A., SCHULZ, C. & GEBHARDT, R. 1996. Diethylnitrosamine exposure-responses for DNA damage, centrilobular cytotoxicity, cell proliferation and carcinogenesis in rat liver exhibit some non-linearities. *Carcinogenesis,* 17**,** 2253-8.

WILSON, C. L., JURK, D., FULLARD, N., BANKS, P., PAGE, A., LULI, S., ELSHARKAWY, A. M., GIELING, R. G., CHAKRABORTY, J. B., FOX, C., RICHARDSON, C., CALLAGHAN, K., BLAIR, G. E., FOX, N., LAGNADO, A., PASSOS, J. F., MOORE, A. J., SMITH, G. R., TINIAKOS, D. G., MANN, J., OAKLEY, F. & MANN, D. A. 2015. NFkappaB1 is a suppressor of neutrophil-driven hepatocellular carcinoma. *Nat Commun,* 6**,** 6818.

WOLF, K., MAZO, I., LEUNG, H., ENGELKE, K., VON ANDRIAN, U. H., DERYUGINA, E. I., STRONGIN, A. Y., BROCKER, E.-B. & FRIEDL, P. 2003. Compensation mechanism in tumor cell migration: mesenchymal-amoeboid transition after blocking of pericellular proteolysis. *J. Cell Biol.,* 160**,** 267-277.

WOOD, W., TURMAINE, M., WEBER, R., CAMP, V., MAKI, R. A., MCKERCHER, S. R. & MARTIN, P. 2000. Mesenchymal cells engulf and clear apoptotic footplate cells in macrophageless PU.1 null mouse embryos. *Development,* 127**,** 5245-52.

WU, Y. C. & HORVITZ, H. R. 1998. C. elegans phagocytosis and cell-migration protein CED-5 is similar to human DOCK180. *Nature,* 392**,** 501-4.

WYCKOFF, J. B., PINNER, S. E., GSCHMEISSNER, S., CONDEELIS, J. S. & SAHAI, E. 2006. ROCK- and myosin-dependent matrix deformation enables protease-independent tumor-cell invasion in vivo. *Curr Biol,* 16**,** 1515-23.

WYLLIE, A. H., KERR, J. F. & CURRIE, A. R. 1980. Cell death: the significance of apoptosis. *Int Rev Cytol,* 68**,** 251-306.

XIANG, K., CHENG, L., LUO, Z., REN, J., TIAN, F., TANG, L., CHEN, T. & DAI, R. 2014. Glycyrrhizin suppresses the expressions of HMGB1 and relieves the severity of traumatic pancreatitis in rats. *PLoS One,* 9**,** e115982.

YAHIAOUI, L., VILLENEUVE, A., VALDERRAMA-CARVAJAL, H., BURKE, F. & FIXMAN, E. D. 2006. Endothelin-1 regulates proliferative responses, both alone and synergistically with PDGF, in rat tracheal smooth muscle cells. *Cell Physiol Biochem,* 17**,** 37-46.

YAMAGUCHI, H., KASA, M., AMANO, M., KAIBUCHI, K. & HAKOSHIMA, T. 2006. Molecular mechanism for the regulation of rho-kinase by dimerization and its inhibition by fasudil. *Structure,* 14**,** 589-600.

YANAGI, S., TSUDA, H., SAKAMOTO, M., NINOMIYA, Y. & ITO, N. 1984. Evaluation of a histologic classification of mouse liver tumors based on pyruvate kinase isozymes and status of host lipids. *J Natl Cancer Inst,* 73**,** 1311-7.

YANG, H., KIM, A., DAVID, T., PALMER, D., JIN, T., TIEN, J., HUANG, F., CHENG, T., COUGHLIN, S. R., JAN, Y. N. & JAN, L. Y. 2012. TMEM16F forms a

Ca2+-activated cation channel required for lipid scrambling in platelets during blood coagulation. *Cell,* 151**,** 111-22.

YASUI, Y., AMANO, M., NAGATA, K., INAGAKI, N., NAKAMURA, H., SAYA, H., KAIBUCHI, K. & INAGAKI, M. 1998. Roles of Rho-associated kinase in cytokinesis; mutations in Rho-associated kinase phosphorylation sites impair cytokinetic segregation of glial filaments. *J Cell Biol,* 143**,** 1249-58.

YOKOYAMA, T., GOTO, H., IZAWA, I., MIZUTANI, H. & INAGAKI, M. 2005. Aurora-B and Rho-kinase/ROCK, the two cleavage furrow kinases, independently regulate the progression of cytokinesis: possible existence of a novel cleavage furrow kinase phosphorylates ezrin/radixin/moesin (ERM). *Genes Cells,* 10**,** 127-37.

YONEDA, A., MULTHAUPT, H. A. & COUCHMAN, J. R. 2005. The Rho kinases I and II regulate different aspects of myosin II activity. *J Cell Biol,* 170**,** 443-453.

YONEDA, A., USHAKOV, D., MULTHAUPT, H. A. & COUCHMAN, J. R. 2007. Fibronectin matrix assembly requires distinct contributions from Rho kinases I and -II. *Mol Biol Cell,* 18**,** 66-75.

YUN, J. H., HENSON, P. M. & TUDER, R. M. 2008. Phagocytic clearance of apoptotic cells: role in lung disease. *Expert Rev Respir Med,* 2**,** 753-65.

ZHAI, C. L., ZHANG, M. Q., ZHANG, Y., XU, H. X., WANG, J. M., AN, G. P., WANG, Y. Y. & LI, L. 2012. Glycyrrhizin protects rat heart against ischemia-reperfusion injury through blockade of HMGB1-dependent phospho-JNK/Bax pathway. *Acta Pharmacol Sin,* 33**,** 1477-87.

ZHANG, J., WU, Y., WENG, Z., ZHOU, T., FENG, T. & LIN, Y. 2014. Glycyrrhizin protects brain against ischemia-reperfusion injury in mice through HMGB1-TLR4-IL-17A signaling pathway. *Brain Res,* 1582**,** 176-86.

ZHANG, S., TANG, Q., XU, F., XUE, Y., ZHEN, Z., DENG, Y., LIU, M., CHEN, J., LIU, S., QIU, M., LIAO, Z., LI, Z., LUO, D., SHI, F., ZHENG, Y. & BI, F. 2009. RhoA regulates G1-S progression of gastric cancer cells by modulation of multiple INK4 family tumor suppressors. *Mol Cancer Res,* 7**,** 570-80.

ZHANG, X. F., TAN, X., ZENG, G., MISSE, A., SINGH, S., KIM, Y., KLAUNIG, J. E. & MONGA, S. P. 2010. Conditional beta-catenin loss in mice promotes chemical hepatocarcinogenesis: role of oxidative stress and platelet-derived growth factor receptor alpha/phosphoinositide 3-kinase signaling. *Hepatology,* 52**,** 954-65.

ZHANG, Y. M., BO, J., TAFFET, G. E., CHANG, J., SHI, J., REDDY, A. K., MICHAEL, L. H., SCHNEIDER, M. D., ENTMAN, M. L., SCHWARTZ, R. J. & WEI, L. 2006. Targeted deletion of ROCK1 protects the heart against pressure overload by inhibiting reactive fibrosis. *Faseb J,* 20**,** 916-25.

ZHAO, Z. & RIVKEES, S. A. 2003. Rho-associated kinases play an essential role in cardiac morphogenesis and cardiomyocyte proliferation. *Dev Dyn,* 226**,** 24-32.

ZHOU, R. R., ZHAO, S. S., ZOU, M. X., ZHANG, P., ZHANG, B. X., DAI, X. H., LI, N., LIU, H. B., WANG, H. & FAN, X. G. 2011. HMGB1 cytoplasmic translocation in patients with acute liver failure. *BMC Gastroenterol,* 11**,** 21.

ZIHNI, C., MITSOPOULOS, C., TAVARES, I. A., BAUM, B., RIDLEY, A. J. & MORRIS, J. D. 2007. Prostate-derived sterile 20-like kinase 1-alpha induces apoptosis. JNK- and caspase-dependent nuclear localization is a requirement for membrane blebbing. *J Biol Chem,* 282**,** 6484-93.

ZIMMERMANN, H. W., SEIDLER, S., NATTERMANN, J., GASSLER, N., HELLERBRAND, C., ZERNECKE, A., TISCHENDORF, J. J., LUEDDE, T.,

WEISKIRCHEN, R., TRAUTWEIN, C. & TACKE, F. 2010. Functional contribution of elevated circulating and hepatic non-classical CD14CD16 monocytes to inflammation and human liver fibrosis. *PLoS One,* 5**,** e11049.

ZIMMERMANN, H. W., TRAUTWEIN, C. & TACKE, F. 2012. Functional role of monocytes and macrophages for the inflammatory response in acute liver injury. *Front Physiol,* 3**,** 56.

Appendices

Publications

WICKMAN, G. R., **JULIAN, L.**[*], MARDILOVICH, K., SCHUMACHER, S., MUNRO, J., RATH, N., ZANDER, S. A., MLECZAK, A., SUMPTON, D., MORRICE, N., BIENVENUT, W. V. & OLSON, M. F. 2013. Blebs produced by actin-myosin contraction during apoptosis release damage-associated molecular pattern proteins before secondary necrosis occurs. Cell Death Differ, 20, 1293-305. (* **co-first author**)

WICKMAN, G., **JULIAN, L**. & OLSON, M. F. 2012. How apoptotic cells aid in the removal of their own cold dead bodies. Cell death and differentiation, 19, 735-742.

JULIAN, L. & OLSON, M. F. 2014. Rho-associated coiled-coil containing kinases (ROCK): structure, regulation, and functions. Small GTPases, 5, e29846.

JULIAN, L. & OLSON, M. F. 2015. Apoptotic membrane dynamics in health and disease. Cell Health and Cytoskeleton, 7, 133-142.